

# Impact and Implications of Melting on the Preservation of Trace Elements in High-Alpine Snow and Glacier Ice

Inauguraldissertation  
der Philosophisch-naturwissenschaftlichen Fakultät  
der Universität Bern

vorgelegt von  
**Sven Erik Avak**  
aus Deutschland

Leiterin der Arbeit:  
Prof. Dr. Margit Schwikowski  
Departement für Chemie und Biochemie der Universität Bern  
Labor für Umweltchemie des Paul Scherrer Instituts

Originaldokument gespeichert auf dem Webserver der Universitätsbibliothek Bern



Dieses Werk ist unter einem  
Creative Commons Namensnennung-Keine kommerzielle Nutzung-Keine Bearbeitung 2.5  
Schweiz Lizenzvertrag lizenziert. Um die Lizenz anzusehen, gehen Sie bitte zu  
<http://creativecommons.org/licenses/by-nc-nd/2.5/ch/> oder schicken Sie einen Brief an  
Creative Commons, 171 Second Street, Suite 300, San Francisco, California 94105, USA.

### Urheberrechtlicher Hinweis

Dieses Dokument steht unter einer Lizenz der Creative Commons  
Namensnennung-Keine kommerzielle Nutzung-Keine Bearbeitung 2.5 Schweiz.  
<http://creativecommons.org/licenses/by-nc-nd/2.5/ch/>

Sie dürfen:



dieses Werk vervielfältigen, verbreiten und öffentlich zugänglich machen

Zu den folgenden Bedingungen:



**Namensnennung.** Sie müssen den Namen des Autors/Rechteinhabers in der von ihm festgelegten Weise nennen (wodurch aber nicht der Eindruck entstehen darf, Sie oder die Nutzung des Werkes durch Sie würden entlohnt).



**Keine kommerzielle Nutzung.** Dieses Werk darf nicht für kommerzielle Zwecke verwendet werden.



**Keine Bearbeitung.** Dieses Werk darf nicht bearbeitet oder in anderer Weise verändert werden.

Im Falle einer Verbreitung müssen Sie anderen die Lizenzbedingungen, unter welche dieses Werk fällt, mitteilen.

Jede der vorgenannten Bedingungen kann aufgehoben werden, sofern Sie die Einwilligung des Rechteinhabers dazu erhalten.

Diese Lizenz lässt die Urheberpersönlichkeitsrechte nach Schweizer Recht unberührt.

Eine ausführliche Fassung des Lizenzvertrags befindet sich unter  
<http://creativecommons.org/licenses/by-nc-nd/2.5/ch/legalcode.de>

# Impact and Implications of Melting on the Preservation of Trace Elements in High-Alpine Snow and Glacier Ice

Inauguraldissertation  
der Philosophisch-naturwissenschaftlichen Fakultät  
der Universität Bern

vorgelegt von  
**Sven Erik Avak**  
aus Deutschland

Leiterin der Arbeit:  
Prof. Dr. Margit Schwikowski  
Departement für Chemie und Biochemie der Universität Bern  
Labor für Umweltchemie des Paul Scherrer Instituts

Von der Philosophisch-naturwissenschaftlichen Fakultät angenommen.

Bern, den 31. Januar 2019

Der Dekan:  
Prof. Dr. Zoltan Balogh



*“Nothing has such power to broaden the mind as the ability to investigate systematically and truly all that comes under thy observation in life.”*  
– Marcus Aurelius Antoninus Augustus (121-180 AD)



# Summary

Cold high-Alpine glaciers are invaluable archives of past climate and atmospheric composition. Especially trace element records from high-Alpine ice cores and snow pits contain comprehensive information about paleo atmospheric changes. Monitoring past environmental pollution is particularly important for Europe, one of the world's most densely populated and most highly industrialized regions. Trace element records from different high-Alpine sites revealed that human activities have significantly impacted the composition of the atmosphere during the last 150 years. Unanswered questions still remain. For instance, the onset of European anthropogenic impact on the atmosphere, such as the impact from the earliest metal production in Western Europe interfering with natural background levels of trace elements from mineral dust deposition, has not been identified yet.

Due to the current global climate warming, particularly pronounced for mountain regions such as the European Alps, many glaciers even at high altitudes are increasingly in danger to significantly suffer from melting. Apart from severe socioeconomic impacts caused by glacial melting, as Alpine glaciers are the major fresh water resource in Europe, meltwater percolation has been shown to substantially alter the information stored in these environmental archives. To further use trace element records as paleo atmospheric archives to investigate the open research questions, the influence of melting on the preservation of trace elements in snow and ice needs to be thoroughly understood. Only little and ambiguous information is available on meltwater-induced relocation of trace elements so far. The behavior of atmospheric impurities during meltwater percolation is assumed to be strongly dependent on their location in the ice microstructure. This spatial distribution of impurities at a grain scale is likely to be determined by rearrangement processes during snow metamorphism. However, information on the micro scale distribution of trace elements in Alpine snow and glacier ice and on the corresponding role of snow metamorphism is not yet available.

In this thesis, part of the interdisciplinary “Microscale Distribution of Impurities in Snow and Glacier Ice (MiSo)” project, the behavior of trace elements during melting of high-Alpine snow and glacier ice was extensively investigated to assess their potential as reconstruction proxies in melt-affected ice core and snow pit records. Particular attention was dedicated to understand the underlying causes and mechanisms leading to the observed trace element behavior during melting, including the spatial distribution of trace elements in high-Alpine glacier ice and rearrangement processes during snow metamorphism.

To examine the impact of melting on the preservation of trace elements of natural and anthropogenic origin, a 50 m segment of an ice core from upper Grenzgletscher, Switzerland, was analyzed for 35 trace elements using discrete inductively coupled plasma mass spectrometry. This segment included a 16 m section affected by meltwater percolation in the firn part. A fractionation depending on water solubility and location at the grain scale was observed. Ba, Ca, Cd, Co, Mg, Mn, Na, Ni, Sr, and Zn revealed significant concentration depletion, while Ag, Al, Bi, Cu, Cs, Fe, Li, Mo, Pb, Rb, Sb, Th, Tl, U, V, W, Zr, and the rare-earth elements (Ce, Eu, La, Nd, Pr, Sc, Sm, Yb) were well preserved. Trace elements likely to originate from insoluble minerals were found to be mostly preserved, even though typically enriched on grain surfaces. Immobility with meltwater percolation is a result of their insolubility in water. Trace elements linked to water-soluble particles revealed a variable meltwater-mobility. While trace elements occurring in ultra-low concentrations tend to be preserved due to incorporation into the ice lattice, abundant trace elements are prone to meltwater-induced relocation due to exceeded solubility limits in ice and consequent segregation to grain surfaces. The size of the corresponding ions was found to have a negligible effect. For ice cores from high-Alpine sites partially affected by melting, records of Ag, Al, Bi, Cu, Cs, Fe, Li, Mo, Pb, Rb, Sb, Th, Tl, U, V, W, Zr, and the rare-earth elements are proposed to be still applicable as robust environmental proxies.

In collaboration with the Swiss Snow and Avalanche Research Institute, the impact of melting on the preservation of trace elements in snow was studied by conducting an extensive snow pit campaign at the Weissfluhjoch test site, Switzerland, with regular sampling from January to June 2017, to monitor the behavior of trace elements during melting of the snow pack. Comparison of snow pit profiles representing dry (insignificant occurrence of melting) and wet conditions (snow pack heavily soaked with meltwater) revealed a preferential loss of certain trace elements depending on their presumed microscopic location and their water solubility. The obtained elution behavior matched the findings from the upper Grenzgletscher ice core. Variable mobility was observed for trace elements originating from water-soluble particles, where low abundant trace elements were preferably retained. Concentration-independent preservation was visible for water-insoluble trace elements, owing to their meltwater immobility. Precipitation at the two 180 km distant high-Alpine sites upper Grenzgletscher and Weissfluhjoch is characteristic for Central European atmospheric aerosol composition. As the large majority of investigated trace elements revealed a consistent behavior with meltwater percolation at those two sites, the proposed applicability of trace elements as reconstruction proxies in melt-affected ice core and snow pit records is therefore most likely representative for the entire Alpine region.

The redistribution of six major ions (ammonium, calcium, chloride, fluoride, sodium, sulfate) and 35 trace elements during artificial and natural snow metamorphism was extensively investigated in another collaboration with the Swiss Snow and Avalanche



Research Institute. For this, artificial and natural snow samples were exposed to a controlled temperature gradient of  $40 \text{ K m}^{-1}$  in the laboratory for up to 90 days. Simultaneously, the distribution of the same atmospheric impurities was studied in samples taken from different depths of the snow pack at the Weissfluhjoch test site, each corresponding to a distinct exposure time of a natural temperature gradient. Initial snow structures, monitored by X-ray micro-tomography, and impurity distribution, determined by elution experiments, varied strongly between the different snow samples. However, with progressing snow metamorphism, snow structures became similar and ions exhibiting a high solubility in ice (ammonium, fluoride, chloride) were gradually buried in the ice interiors, whereas calcium, sodium, and sulfate were enriched at ice crystal surfaces. The redistribution of atmospheric impurities during snow metamorphism was shown to be strongly dependent on the temperature gradient, the exposure time, and the chemical composition. The observed preferred incorporation of certain species into the ice interior during snow metamorphism is correlated with their persistence during meltwater percolation. The elution experiments allowed investigation of water-soluble major ions only, whereas results for the trace elements could not be interpreted due to non-quantitative dissolubility of trace elements in the deployed eluent (ultra-pure water).

An analytical method for the direct *in situ* analysis of trace elements at a sub-millimeter resolution in high-Alpine glacier ice was developed in collaboration with the Institute of Geochemistry and Petrology at ETH Zurich. This method is based on laser ablation inductively coupled plasma mass spectrometry. The development process comprised the construction and the consistent further development of a cooled sample holder, featuring an automatic coolant leakage detection system and compatibility to a commercially available laser ablation system, as well as choice of the optimal cooling medium, customization of the pre-existing laser ablation hardware and software, and the development of additional equipment for both sample preparation and handling. In addition to this, a measurement procedure for high-Alpine glacier ice was established, involving the determination of appropriate laser ablation parameters and setting up a procedure for signal intensity quantification. The availability of an internal standard in ice was evaluated and an approach to prepare matrix-matched ice standards from multi-element standard solutions for external calibration was established. The acidity of the multi-element solutions and the storage time of the ice standard after preparation were found to have the most significant impact on the calibration. Preliminary measurements of high-Alpine glacier ice samples from upper Gletscher demonstrated that samples exhibiting an overwhelming mineral dust abundance do not provide evidence for a linkage between micro-scale distribution of trace elements and the grain boundary network. Such a dispersion of atmospheric contaminants in the ice matrix has also very recently been reported for layers with high impurity enrichment in deep ice from Antarctica and Greenland.

Future work should involve *in situ* analysis of high-Alpine glacier ice exhibiting ultra-low levels of trace elements to minimize the influence of dust particles on the fractionation of trace elements at a grain scale and to further directly corroborate the indirect assessment of trace element location in the firn part of the ice core from upper Gletscher. This requires further background suppression of the developed micro analytical method. The proposed applicability of trace elements as reconstruction proxies in melt-affected high-Alpine ice core and snow pit records should be reviewed for other regions with a different overall trace element composition, as high-mountain glaciers worldwide are increasingly affected by melting. For instance, the presence of water-insoluble trace elements, less prone to meltwater-induced relocation, is favored in glacier ice where higher mineral dust content prevails. Additionally, the impact of melting on the preservation of other reconstruction proxies, such as mercury or black carbon, should be investigated to possibly expand the set of rather “meltwater-persistent” proxies.

# Contents

<b>Summary</b>	<b>iii</b>
<b>1 Introduction</b>	<b>1</b>
1.1 High-Alpine ice cores and snow pits as archives of past atmospheric pollution . . . . .	1
1.2 Trace elements as environmental proxies in high-Alpine ice cores and snow pits . . . . .	3
1.3 Climate warming in the high-Alpine region . . . . .	5
1.4 Post-depositional alteration of ice core and snow pit records by melting	6
1.5 Snow metamorphism and the location of impurities . . . . .	7
1.6 Objectives and outline of the thesis . . . . .	8
Bibliography . . . . .	9
<b>2 Study sites and analytical methods</b>	<b>15</b>
2.1 Study sites . . . . .	15
2.1.1 Upper Grenzgletscher . . . . .	15
2.1.2 Weissfluhjoch test site . . . . .	17
2.2 Trace element analysis . . . . .	19
2.2.1 Inductively coupled plasma sector field mass spectrometry . .	19
Bibliography . . . . .	22
<b>3 Impact and implications of meltwater percolation on trace element records observed in a high-Alpine ice core</b>	<b>25</b>
Abstract . . . . .	26
3.1 Introduction . . . . .	26
3.2 Materials and methods . . . . .	28
3.2.1 Ice core characteristics, detection of meltwater percolation, and dating . . . . .	28
3.2.2 Sample preparation and trace element analysis . . . . .	28
3.2.3 Data evaluation . . . . .	29
3.3 Results and discussion . . . . .	30
3.3.1 Data presentation and characterization . . . . .	30
3.3.2 Quantification of concentration depletion in the meltwater-influenced section . . . . .	33
3.3.3 Causes for preferential elution of TEs . . . . .	33
3.3.4 Incorporation of TEs into glacier ice . . . . .	35

3.3.5	Implications . . . . .	38
3.4	Conclusions . . . . .	40
	Acknowledgments . . . . .	41
	Bibliography . . . . .	41
<b>4</b>	<b>Melt-induced fractionation of major ions and trace elements in an Alpine snow pack</b>	<b>47</b>
	Abstract . . . . .	48
4.1	Introduction . . . . .	48
4.2	Materials and methods . . . . .	50
4.2.1	Study site . . . . .	50
4.2.2	Snow pit sampling . . . . .	50
4.2.3	Major ion, water stable isotope, and trace element analysis . .	52
4.2.4	Data evaluation . . . . .	53
4.3	Results and discussion . . . . .	54
4.3.1	Major ions . . . . .	54
4.3.2	Trace elements . . . . .	57
4.4	Conclusions . . . . .	62
	Acknowledgments . . . . .	63
	Bibliography . . . . .	63
<b>5</b>	<b>Redistribution of major ions and trace elements during snow metamorphism</b>	<b>69</b>
5.1	Microscale rearrangement of ammonium induced by snow metamorphism . . . . .	69
	Abstract . . . . .	70
5.1.1	Introduction . . . . .	70
5.1.2	Methods . . . . .	72
5.1.3	Results . . . . .	77
5.1.4	Discussion . . . . .	83
5.1.5	Conclusion . . . . .	89
	Acknowledgments . . . . .	90
	Bibliography . . . . .	90
5.2	Elution experiments of trace elements . . . . .	94
5.2.1	Introduction . . . . .	94
5.2.2	Materials and methods . . . . .	94
5.2.3	Results . . . . .	95
5.2.4	Discussion . . . . .	97
5.2.5	Conclusion . . . . .	99
	Bibliography . . . . .	99
<b>6</b>	<b>Development of a method for <i>in situ</i> trace element analysis with high spatial resolution of high-Alpine glacier ice</b>	<b>101</b>
	Abstract . . . . .	102

6.1	Introduction . . . . .	102
6.1.1	Impurity location in glacier ice . . . . .	102
6.1.2	Laser Ablation ICP-MS . . . . .	103
6.1.3	Overview of different cryocells . . . . .	104
6.1.4	Applications of cryocell LA-ICP-MS to ice core analysis . . . . .	106
6.1.5	Motivation for this method development . . . . .	106
6.2	Materials and methods . . . . .	107
6.2.1	Instrumentation . . . . .	107
6.2.2	Sample preparation and processing . . . . .	108
6.3	Results and discussion . . . . .	108
6.3.1	Development of the cryocell . . . . .	108
6.3.2	Development of additional experimental hardware . . . . .	116
6.3.3	Development of a calibration procedure . . . . .	118
6.3.4	Pilot study for final method assessment . . . . .	126
6.4	Conclusion . . . . .	133
	Acknowledgments . . . . .	133
	Bibliography . . . . .	133
<b>7</b>	<b>Conclusion and outlook</b>	<b>139</b>
	<b>List of abbreviations and symbols</b>	<b>141</b>
	<b>List of figures</b>	<b>147</b>
	<b>List of tables</b>	<b>149</b>
	<b>Acknowledgments</b>	<b>151</b>
	<b>Declaration of consent</b>	<b>153</b>
	<b>Curriculum vitae</b>	<b>155</b>



# 1 Introduction

## 1.1 High-Alpine ice cores and snow pits as archives of past atmospheric pollution

Glaciers are located in the polar and high-mountain regions of the world. They are formed by the continuous accumulation of snow, that first transforms into firn, through a process called snow metamorphism, and by further compaction of the overlying snow and firn layers to ice. Snow metamorphism is mainly driven by natural temperature gradients in the snow cover. The high vapor pressure of snow causes sublimation of warmer ice surfaces and subsequent deposition of the water vapor on colder surfaces, leading to the structural transformation of snow.

Due to its porous structure, snow deposited on a glacier surface contains not yet entrapped atmospheric air. As snow metamorphism proceeds and the pressure by the overlying layers increases, the porous space is reduced until ice with bubbles, in which ancient air is archived, is ultimately formed. Additionally, atmospheric aerosols and gases are transported to the surface of a glacier, either by wet deposition, due to their precedent scavenging by snowflakes, or by dry deposition, due to gravity and diffusion, resulting likewise in their preservation in glacier ice. Glaciers can therefore serve as invaluable paleo atmospheric archives. Cold glaciers, where the ice temperature is below the pressure melting point, that feature insignificant lateral ice flow and year-round precipitation deposition in the form of snow, are ideally suited for the retrieval of ice cores. Analyzing ice cores then allows reconstruction of atmospheric transport and circulation, volcanic activities, solar variability, temperature, precipitation, moisture sources, natural and anthropogenic air pollution, vegetation changes, or greenhouse gas concentrations [Thompson, 2009; Raynaud and Parrenin, 2009]. While ice cores retrieved from polar regions provide essential information to understand the Earth's climate dynamics (e.g., Augustin et al. [2004]), ice cores from high-mountain glaciers allow, due to their locations in the mid- and low-latitudes, reconstruction of past climate and changes in atmospheric composition for the world's areas where the majority of mankind lives.

In Europe, one of the most densely populated and highly industrialized regions globally, instrumental data on the atmosphere is, even though it is probably the most comprehensive data set worldwide, only available for the last decades. In contrast, ice cores from high-Alpine glaciers can provide paleo atmospheric information on decadal to millennial time scales [Jenk et al., 2009]. Snow pits and shallow ice

cores from high-Alpine glaciers are valuable to trace back the most recent changes of European climate and atmospheric composition [Gabrieli *et al.*, 2011a].

Ice core records have mainly been recovered from four suitable sites in the European Alps:

- Fiescherhorn saddle (3900 m a.s.l.), located in the northern European Alps (Bernese Alps)
- Colle Gnifetti saddle (4450 m a.s.l.) and upper Grenzgletscher (4200 m a.s.l.), both located in the Monte Rose massif in the southern European Alps (Valais Alps)
- Col du Dôme saddle (4250 m a.s.l.), located in the Mont Blanc massif in the western European Alps (Graian Alps)
- Glacier Alto dell'Ortles (3859 m a.s.l.), located in the eastern European Alps (Ortler Alps)

Records from these high-Alpine sites not only allowed to reconstruct European climate variability such as regional signatures of the Medieval Climate Optimum (950-1250 AD), the Little Ice Age (1450-1850 AD), or the recent warming [Bohleber *et al.*, 2013, 2018], but are, due to their proximity to emission sources, in particular appropriate to track back past natural and anthropogenic air pollution, and to assess the human impact on the atmosphere. Concentration records of ammonium, mainly released by agriculture due to the use of fertilizers [Schwikowski *et al.*, 1999; Döscher *et al.*, 1996], nitrate, primarily emitted by traffic [Döscher *et al.*, 1995; Wagenbach *et al.*, 1988; Preunkert *et al.*, 2003], sulfate, typical for fossil fuel burning [Döscher *et al.*, 1995; Schwikowski *et al.*, 1999; Preunkert *et al.*, 2001], and black carbon, which is for the most recent time period a product of incomplete fossil fuel combustion [Lavanchy *et al.*, 1999; Thevenon *et al.*, 2009; Sigl *et al.*, 2018], revealed the strong impact of Western European industry and society on the atmosphere over the last decades. While atmospheric ammonium and nitrate emissions generally remain on a high level, sulfate and black carbon emissions decreased towards the end of the 20<sup>th</sup> century because of stricter environmental policies and the implementation of cleaner technologies [Engardt *et al.*, 2017]. Temporal variations of European biogenic and anthropogenic emissions of organic pollutants were also reconstructed from high-Alpine records [Pavlova *et al.*, 2015; Müller-Tautges *et al.*, 2016; Gabrieli *et al.*, 2010; Kirchgeorg *et al.*, 2013]. Historic variations of mineral dust emissions to the atmosphere, mainly originating from the Saharan desert, were investigated by Wagenbach and Geis [1989], Wagenbach *et al.* [1996], and Bohleber *et al.* [2018]. Concentration records of chloride, representing input of marine sea salt aerosols, were obtained by Eichler *et al.* [2000] and Legrand [2002].



## 1.2 Trace elements as environmental proxies in high-Alpine ice cores and snow pits

Paleo atmospheric pollution information from ice core or snow pit records is generally obtained by chemical analysis of the atmospheric contaminants that initially reached the surface of a glacier by wet or dry deposition, and were preserved over time [Gabrielli and Vallelonga, 2015]. Among the different sorts of tracers relevant for reconstructing the various forms of natural and anthropogenic pollution to the atmosphere, so-called proxies, trace elements (TEs) are particularly important. The term “trace element” refers to a terminology by IUPAC indicating that the abundance of an element in a system i.e., the specimen does not exceed 100 parts per million (ppm) equivalent to e.g.,  $100 \text{ mg kg}^{-1}$  [Morrison *et al.*, 1979]. Abundances of TEs in high-Alpine glaciers and snow packs are generally extremely low with concentrations ranging from a few nanograms per liter to the low milligram per liter level.

TE concentration records from high-Alpine ice cores or snow pits are able to yield diverse information. Among the most commonly analyzed TEs in ice cores and snow pits from high-Alpine sites (Figure 1.1), the majority (Al, Ba, Bi, Ca, Cs, Fe, Li, Mg, Mn, Na, Rb, Sr, Th, Tl, U, W, Zr, and the REEs e.g., Ce, Eu, La, Nd, Pr, Sc, Sm, Yb) reaches the surface of a glacier as mineral dust [Gabrielli *et al.*, 2008; Gabrieli *et al.*, 2011a], predominantly originating from the Saharan desert [Wagenbach and Geis, 1989]. Na has been shown to not only reflect geogenic sources, but can also be of marine sea salt origin [Eichler *et al.*, 2004]. Anthropogenic pollution to the atmosphere is generally reflected by enhanced concentrations of Ag, Cd, Co, Cu, Mo, Ni, Pb, Sb, V, and Zn [Van de Velde *et al.*, 1999, 2000; Barbante *et al.*, 2004; Schwikowski *et al.*, 2004; Gabrielli *et al.*, 2008; Gabrieli *et al.*, 2011a]. Bi, Cd, Pb, Sb, Tl, and Zn can be, although never shown for high-Alpine ice core records so far, also representative for aerosol input coming from volcanism [Kaspari *et al.*, 2009; Kellerhals *et al.*, 2010; Gabrielli *et al.*, 2014; Nho *et al.*, 1996].

Paleo atmospheric TE records from high-Alpine glaciers are confined to only a very few studies from Colle Gnifetti, Col du Dôme, and Alto dell’Ortles. Figure 1.2 shows an example of a paleo atmospheric reconstruction using an ice core recovered from Colle Gnifetti. Historical changes in Western European atmospheric Pb pollution were reconstructed for the time period 1650-2000 based on the Pb ice core concentration record [Schwikowski *et al.*, 2004]. Pb is a heavy metal mainly emitted to the atmosphere by mining activities, metal production, coal combustion, or the use of leaded gasoline, and can therefore be used as a proxy reflecting industrial development. The record shows that industrialization in Western Europe started around 1880 and Pb emissions peaked in the 1970s due to the introduction and widespread use of leaded gasoline. Stricter air pollution control in Western Europe led to a significant decrease of Pb emissions, nevertheless they are still elevated compared to the natural, pre-industrial (1650-1850) variation of Pb.

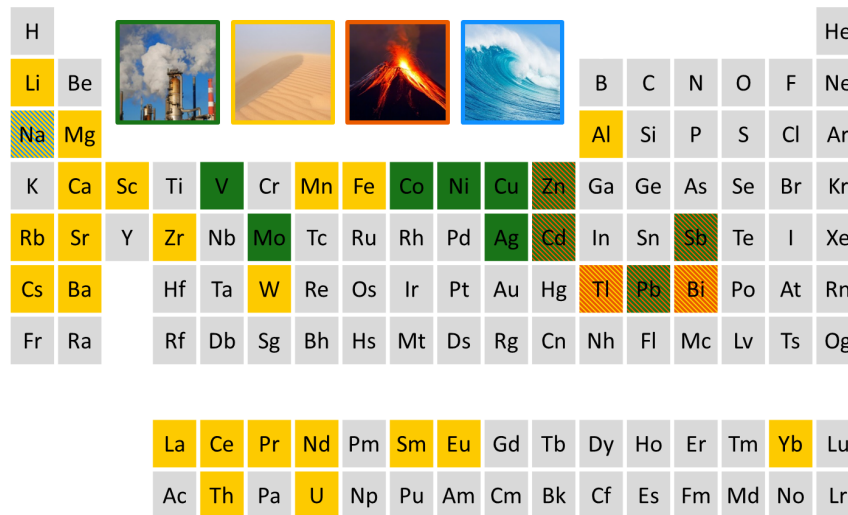


**Figure 1.1:** Periodic table showing the most common trace elements analyzed in high-Alpine ice core and snow pit records and their predominant sources. Sources, shown as pictograms with their corresponding color code, can be of anthropogenic (green), mineral dust (yellow), volcanic (red), and/or marine origin (blue).

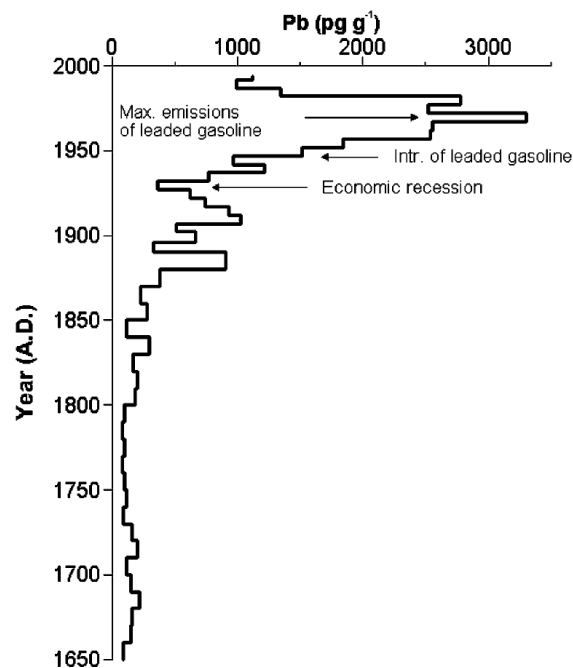


**Figure 1.2:** Paleo concentration record of Pb from Colle Gnifetti, Switzerland, showing Western European pre-industrial (1650-1850) and industrial (1850-2000) Pb emissions to the atmosphere (from *Schwikowski et al. [2004]*).

The influence on the atmosphere by human activities in Western Europe during the last centuries is also reflected in records of other heavy metals from Colle Gnifetti [Barbante *et al.*, 2004; Gabrieli *et al.*, 2011b], Col du Dôme [Van de Velde *et al.*, 1999, 2000], and for the most recent time period in snow pit records from Alto dell’Ortles [Gabrieli *et al.*, 2011a]. Apart from the necessity to continue monitoring natural and human-caused air pollution using TE records from high-Alpine glaciers, past atmospheric TE emissions have not yet been fully understood. Although there are high-Alpine TE records from Colle Gnifetti and Alto dell’Ortles reaching even further back in time and spanning the last 2000-3000 years [Gabrieli and Barbante, 2014; More *et al.*, 2017; Bertò, 2017], the question whether there is evidence that early human impact on the atmosphere in Western Europe started with the Roman Empire or even earlier, could not be unambiguously resolved so far. Other research questions, such as the occurrence of TEs related to volcanism or the elemental composition of the particulate component of mineral dust preserved in high-Alpine glaciers remain largely unclear, impeding a precise source apportionment to refine the reconstruction of past dust transport.

## 1.3 Climate warming in the high-Alpine region

To establish a reliable reconstruction of past climate and atmospheric composition from high-Alpine ice cores and snow pits, it is necessary to ensure that a drilling and sampling site, respectively, is chosen, where post-depositional melting processes did not occur or are negligible. Meltwater percolation has been shown to substantially disturb and alter the preservation of proxies, impeding or even making paleo atmospheric reconstructions impossible (Section 1.4). Therefore, ice cores and snow pits from cold glaciers have been used as paleo atmospheric archives [Zhang *et al.*, 2015]. However, the current global temperature increase [Marcott *et al.*, 2013] causes the climate of high-mountain environments to change even more rapidly [Pepin *et al.*, 2015]. As a result, even high-mountain glaciers globally will become poly-thermal or temperate (ice temperature at pressure melting point) and will increasingly suffer from melting in the highest accumulation areas. A recent modeling study by Huss *et al.* [2017] revealed that high-mountain glaciers, in particular in the European Alps (Figure 1.3), will due to a continuing strong negative mass balance [Huss *et al.*, 2015], significantly retreat and many will be vanished by the end of the century. The glaciers’ equilibrium line, where accumulation (i.e., mass gain) is equivalent to ablation (i.e., mass loss), is predicted to increase by several hundred meters in elevation. Apart from significant consequences on both economy and society, potential drilling and sampling sites for high-Alpine ice cores and snow pits, respectively, where no melting occurred, will be more and more difficult to find.

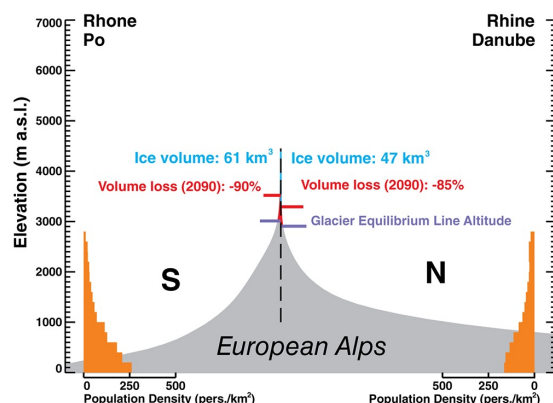


**Figure 1.3:** Cumulative land surface hypsometry of the European Alps, separated by the north-south weather divide. Glacier ice volume and elevations of glacier equilibrium lines (blue horizontal lines) at present are shown together with the modeled future ice volume, indicating massive potential loss of glaciated areas (red), and significant increase in elevation of the equilibrium lines (red horizontal lines; from *Huss et al.* [2017]).

## 1.4 Post-depositional alteration of ice core and snow pit records by melting

If glaciers are used in the future as environmental archives of past natural and anthropogenic emissions to the atmosphere under the unfavorable conditions of (increased) melting, it is exceedingly crucial to understand in detail how meltwater percolation affects the preservation of proxies. Several studies have already examined the impact of melting on the fate of different kinds of reconstruction proxies in snow and glacier ice. The signal of the stable oxygen isotope ratio ( $\delta^{18}\text{O}$ ), used as a proxy for temperature, has been shown to be smoothed by meltwater percolation making it unemployable for climate reconstructions [*Thompson et al.*, 1993]. Major ion records, also important reconstruction proxies of past atmospheric composition and air pollution (Section 1.1), are eluted with varying efficiencies from melt-affected glaciers and snow packs [*Eichler et al.*, 2001; *Li et al.*, 2006; *Ginot et al.*, 2010]. Melting can also release organic pollutants from glaciers [*Pavlova et al.*, 2015; *Müller-Tautges et al.*, 2016] and bias the signal of black carbon [*Osmond et al.*, 2018].

However, little is known on the effect of melting on the preservation of TEs. A systematic investigation clarifying to what extent TEs are suitable as reconstruction tracers in melt-affected ice core and snow pit records, in particular from the Alpine region, is lacking. TEs were reported to be eluted from a snow-firn pack in the Central Asian Tian Shan Mountains after meltwater percolation during summer [*Zhongqin et al.*, 2007]. On the contrary, TE records both of crustal and anthropogenic origin did not seem to be substantially altered by significant summer melting

in a high-Alpine snow pit from Alto dell'Ortles glacier [Gabrieli *et al.*, 2011a]. More recently, Wong *et al.* [2013] artificially infiltrated Greenland snow pits with meltwater and compared them to pristine snow pits by focusing on the concentration records of a limited set of 12 TEs, typical for mineral dust. The seasonality of the signals was observed to be generally well preserved, with some records lower in concentrations, while particle-bound TEs, such as the rare-earth elements, remained relatively immobile during meltwater percolation.

The behavior of atmospheric contaminants preserved in glaciers during meltwater percolation is likely to correlate with their location in the ice crystal lattice, as suggested for the major ions by Eichler *et al.* [2001]. Meltwater percolation in high-Alpine firn revealed that major ions located on grain surfaces were removed by meltwater, whereas those previously incorporated into the grain interiors were more protected from meltwater-induced relocation and therefore preserved. The fate of TEs in poly-thermal and temperate glaciers is likely to be location-dependent, too. However, information on TE distribution at a grain scale in glacier ice are rare and in the case of high-Alpine snow and glacier ice not available. Della Lunga *et al.* [2014] analyzed the spatial distribution of TEs in layers enriched with impurities (cloudy bands) and in layers with low abundance of impurities (clear bands) of deep Greenland ice. While TEs were observed to be enriched both at grain boundaries and junctions in clear bands, no correlation between TE distribution and the grain boundary net was visible in cloudy bands. Due to the age represented by the investigated samples (>84,000 years before present), no information on the microscopic location of anthropogenic related TEs was obtained.

## 1.5 Snow metamorphism and the location of impurities

Even though it is reasonable to assume that the preservation of atmospheric impurities in glaciers during melting depends on their microscopic location, it is not yet known how impurities are actually incorporated into snow, firn, and ultimately in glacier ice. A separation of  $\text{Na}^+$  and  $\text{Cl}^-$  during meltwater percolation in high-Alpine firn revealed evidence that the final embedding of impurities in snow cannot solely be driven by atmospheric scavenging processes or precipitation formation, as NaCl must have initially been deposited as sea salt particle [Eichler *et al.*, 2001]. Instead, post-depositional rearrangement processes during snow metamorphism are likely to affect the spatial distribution of impurities in snow, firn, and ice. Pinzer *et al.* [2012] showed that snow undergoes substantial transformation cycles during snow metamorphism, where water vapor fluxes lead to a mass turnover of up to 60% of the entire ice mass, and result in drastic micro-structural changes (Figure 1.4). Those micro-structural changes may significantly affect the distribution of atmospheric impurities in snow and consequently also determine their fate during meltwater per-

colation.

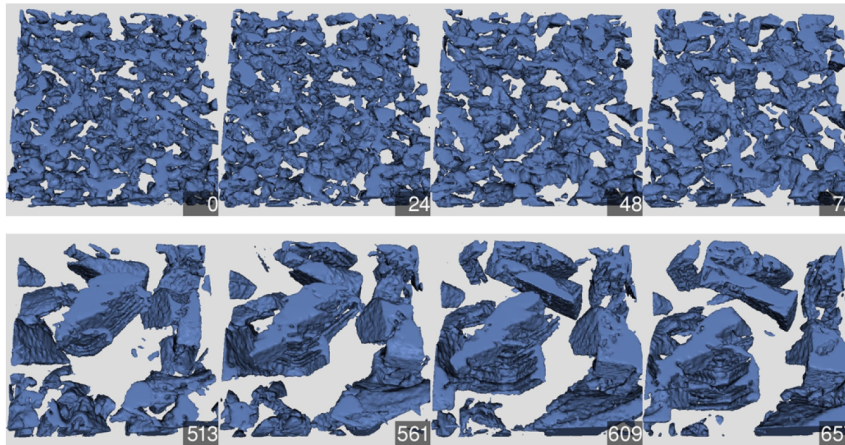


**Figure 1.4:** Structural evolution of snow during snow metamorphism observed by *in situ* time-lapse X-ray micro-tomography. Numbers in the lower right corner of the individual pictures indicate the periods (in hours) during which a temperature gradient, to mimic snow metamorphism, was applied (from *Pinzer et al.* [2012]).

## 1.6 Objectives and outline of the thesis

This thesis is part of the interdisciplinary “Microscale Distribution of Impurities in Snow and Glacier Ice (MiSo)” project between the Laboratory of Environmental Chemistry of the Paul Scherrer Institute and the Snow Physics research group of the WSL Institute of Snow and Avalanche Research SLF. The project is dedicated to investigate the impact of the physical micro-environment of impurities in snow on their re-distribution during metamorphism, chemical reactivity, and transfer to ice core archives.

To tackle the open research needs addressed above, this thesis includes:

1. An extensive investigation of the influence of meltwater percolation on the preservation of TEs in both a high-Alpine glacier and snow pack, to assess their potential as reconstruction proxies in ice core and snow pit records affected by melting, and to indirectly infer their microscopic location in the ice lattice.
2. A field- and laboratory-based study to examine the influence of snow metamorphism on the post-depositional spatial redistribution of different atmospheric impurities.
3. The development of an analytical method for spatially resolved TE analysis of high-Alpine glacier ice to directly inspect TE locations at a grain scale.

The thesis is structured as follows:

Chapter 2 gives an overview on the study sites, the field campaigns, and the analytical methods employed during this thesis.

Chapter 3 is dedicated to examine how melting impacts the preservation of TEs in glaciers, in order assess their potential as environmental proxies in high-Alpine ice cores affected by melting. This was accomplished by acquiring concentration profiles of 35 TEs reflecting a 50 m segment of the ice core from upper Grenzgletscher, Switzerland, including a section in the firn part affected by meltwater percolation. The outcome of this study allowed to infer guidelines for future TE-based atmospheric pollution reconstructions using melt-affected ice core records from high-Alpine glaciers. Moreover, an indirect assessment of TE location in the ice lattice was accomplished.

The impact of melting on the preservation of TEs in snow is addressed in depth in Chapter 4. Therefore, a snow pit campaign, with regular sampling from January to June 2017, was conducted at the Weissfluhjoch test site, Switzerland, to monitor the behavior of TEs during the melting of the snow pack. This allowed to evaluate the potential of melt-affected TE snow pit records from high-Alpine regions to reconstruct recent natural and anthropogenic atmospheric pollution. Additionally, the geographical representativeness of the findings described in Chapter 3 was examined.

Chapter 5 is devoted to a study extensively investigating the influence of snow metamorphism on the spatial redistribution of different snow impurities to explain their varying elution behavior during meltwater percolation, and the relation to their microscopic location in snow.

Chapter 6 ultimately describes the development and a preliminary application of a method, based on laser ablation inductively coupled plasma mass spectrometry, for the direct *in situ* analysis of TEs in glacier ice at a sub-millimeter resolution. This technique will enable a better understanding of the microscopic distribution at a grain scale of TEs in high-Alpine glacier ice.

A conclusion and an outlook of the thesis are provided in Chapter 7.

## Bibliography

- Augustin, L., et al., Eight glacial cycles from an Antarctic ice core, *Nature*, 429(6992), 623–628, doi:10.1038/nature02599, 2004.
- Barbante, C., et al., Historical Record of European Emissions of Heavy Metals to the Atmosphere Since the 1650s from Alpine Snow/Ice Cores Drilled near Monte Rosa, *Environmental Science & Technology*, 38(15), 4085–4090, doi:10.1021/es049759r, 2004.
- Bertò, M., Aerosol deposition, trace elements and black carbon, over the highest glacier of the Eastern European Alps (Mt. Ortles, 3905 m) during the last 3000 years: environmental and climatic impacts, Ph.D. thesis, Università Ca' Foscari Venice, 2017.

- Bohleber, P., D. Wagenbach, W. Schöner, and R. Böhm, To what extent do water isotope records from low accumulation Alpine ice cores reproduce instrumental temperature series?, *Tellus B: Chemical and Physical Meteorology*, *65*(1), 20,148, doi:10.3402/tellusb.v65i0.20148, 2013.
- Bohleber, P., T. Erhardt, N. Spaulding, H. Hoffmann, H. Fischer, and P. Mayewski, Temperature and mineral dust variability recorded in two low-accumulation Alpine ice cores over the last millennium, *Climate of the Past*, *14*(1), 21–37, doi:10.5194/cp-14-21-2018, 2018.
- Della Lunga, D., W. Müller, S. O. Rasmussen, and A. Svensson, Location of cation impurities in NGRIP deep ice revealed by cryo-cell UV-laser-ablation ICPMS, *Journal of Glaciology*, *60*(223), 970–988, doi:10.3189/2014JoG13J199, 2014.
- Döscher, A., H. W. Gäggeler, U. Schotterer, and M. Schwikowski, A130 years deposition record of sulfate, nitrate and chloride from a high-alpine glacier, *Water, Air, & Soil Pollution*, *85*(2), 603–609, doi:10.1007/BF00476895, 1995.
- Döscher, A., H. W. Gäggeler, U. Schotterer, and M. Schwikowski, A historical record of ammonium concentrations from a glacier in the Alps, *Geophysical Research Letters*, *23*(20), 2741–2744, doi:10.1029/96GL02615, 1996.
- Eichler, A., M. Schwikowski, and H. W. Gäggeler, An Alpine ice-core record of anthropogenic HF and HCl emissions, *Geophysical Research Letters*, *27*(19), 3225–3228, doi:10.1029/2000GL012006, 2000.
- Eichler, A., M. Schwikowski, and H. W. Gäggeler, Meltwater-induced relocation of chemical species in Alpine firn, *Tellus B: Chemical and Physical Meteorology*, *53*(2), 192–203, doi:10.3402/tellusb.v53i2.16575, 2001.
- Eichler, A., M. Schwikowski, M. Furger, U. Schotterer, and H. W. Gäggeler, Sources and distribution of trace species in Alpine precipitation inferred from two 60-year ice core paleorecords, *Atmospheric Chemistry and Physics Discussions*, *4*(1), 71–108, doi:10.5194/acpd-4-71-2004, 2004.
- Engardt, M., D. Simpson, M. Schwikowski, and L. Granat, Deposition of sulphur and nitrogen in Europe 1900-2050. Model calculations and comparison to historical observations, *Tellus B: Chemical and Physical Meteorology*, *69*(1), 1328,945, doi:10.1080/16000889.2017.1328945, 2017.
- Gabrieli, J., and C. Barbante, The Alps in the age of the Anthropocene: the impact of human activities on the cryosphere recorded in the Colle Gnifetti glacier, *Rendiconti Lincei*, *25*(1), 71–83, doi:10.1007/s12210-014-0292-2, 2014.
- Gabrieli, J., et al., Post 17th-Century Changes of European PAH Emissions Recorded in High-Altitude Alpine Snow and Ice, *Environmental Science & Technology*, *44*(9), 3260–3266, doi:10.1021/es903365s, 2010.
- Gabrieli, J., et al., Impact of Po Valley emissions on the highest glacier of the Eastern European Alps, *Atmospheric Chemistry and Physics*, *11*(15), 8087–8102, doi:10.5194/acp-11-8087-2011, 2011a.
- Gabrieli, J., et al., Contamination of Alpine snow and ice at Colle Gnifetti, Swiss/Italian Alps, from nuclear weapons tests, *Atmospheric Environment*, *45*(3), 587–593, doi:10.1016/j.atmosenv.2010.10.039, 2011b.
- Gabrieli, P., and P. Vallelonga, Contaminant Records in Ice Cores, in *Environmental Contaminants. Developments in Paleoenvironmental Research, vol 18.*, edited by J. M. Blais, M. R. Rosen, and J. P. Smol, pp. 393–430, Springer, Dordrecht, doi:10.1007/978-94-017-9541-8\_14, 2015.
- Gabrieli, P., G. Cozzi, S. Torcini, P. Cescon, and C. Barbante, Trace elements in winter snow of the Dolomites (Italy): A statistical study of natural and anthropogenic contributions, *Chemosphere*, *72*(10), 1504–1509, doi:10.1016/j.chemosphere.2008.04.076, 2008.



- Gabrielli, P., D. Hardy, N. Kehrwald, M. Davis, G. Cozzi, C. Turetta, C. Barbante, and L. Thompson, Deglaciated areas of Kilimanjaro as a source of volcanic trace elements deposited on the ice cap during the late Holocene, *Quaternary Science Reviews*, *93*, 1–10, doi:10.1016/j.quascirev.2014.03.007, 2014.
- Ginot, P., U. Schotterer, W. Stichler, M. A. Godoi, B. Francou, and M. Schwikowski, Influence of the Tungurahua eruption on the ice core records of Chimborazo, Ecuador, *The Cryosphere*, *4*(4), 561–568, doi:10.5194/tc-4-561-2010, 2010.
- Huss, M., L. Dhulst, and A. Bauder, New long-term mass-balance series for the Swiss Alps, *Journal of Glaciology*, *61*(227), 551–562, doi:10.3189/2015JoG15J015, 2015.
- Huss, M., et al., Toward mountains without permanent snow and ice, *Earth's Future*, *5*(5), 418–435, doi:10.1002/2016EF000514, 2017.
- Jenk, T. M., et al., A novel radiocarbon dating technique applied to an ice core from the Alps indicating late Pleistocene ages, *Journal of Geophysical Research*, *114*(D14), D14,305, doi:10.1029/2009JD011860, 2009.
- Kaspari, S., P. A. Mayewski, M. Handley, S. Kang, S. Hou, S. Sneed, K. Maasch, and D. Qin, A High-Resolution Record of Atmospheric Dust Composition and Variability since A.D. 1650 from a Mount Everest Ice Core, *Journal of Climate*, *22*(14), 3910–3925, doi:10.1175/2009JCLI2518.1, 2009.
- Kellerhals, T., L. Tobler, S. Brüttsch, M. Sigl, L. Wacker, H. W. Gäggeler, and M. Schwikowski, Thallium as a Tracer for Preindustrial Volcanic Eruptions in an Ice Core Record from Illimani, Bolivia, *Environmental Science & Technology*, *44*(3), 888–893, doi:10.1021/es902492n, 2010.
- Kirchgeorg, T., et al., Temporal variations of perfluoroalkyl substances and polybrominated diphenyl ethers in alpine snow, *Environmental Pollution*, *178*, 367–374, doi:10.1016/j.envpol.2013.03.043, 2013.
- Lavanchy, V. M. H., H. W. Gäggeler, U. Schotterer, M. Schwikowski, and U. Baltensperger, Historical record of carbonaceous particle concentrations from a European high-alpine glacier (Colle Gnifetti, Switzerland), *Journal of Geophysical Research: Atmospheres*, *104*(D17), 21,227–21,236, doi:10.1029/1999JD900408, 1999.
- Legrand, M., Seasonally resolved Alpine and Greenland ice core records of anthropogenic HCl emissions over the 20th century, *Journal of Geophysical Research*, *107*(D12), 4139, doi:10.1029/2001JD001165, 2002.
- Li, Z., R. Edwards, E. Mosley-Thompson, F. Wang, Z. Dong, X. You, H. Li, C. Li, and Y. Zhu, Seasonal variability of ionic concentrations in surface snow and elution processes in snow-firn packs at the PGPI site on Ürümqi glacier No. 1, eastern Tien Shan, China, *Annals of Glaciology*, *43*, 250–256, doi:10.3189/172756406781812069, 2006.
- Marcott, S. A., J. D. Shakun, P. U. Clark, and A. C. Mix, A Reconstruction of Regional and Global Temperature for the Past 11,300 Years, *Science*, *339*(6124), 1198–1201, doi:10.1126/science.1228026, 2013.
- More, A. F., et al., Next-generation ice core technology reveals true minimum natural levels of lead (Pb) in the atmosphere: Insights from the Black Death, *GeoHealth*, *1*(4), 211–219, doi:10.1002/2017GH000064, 2017.
- Morrison, G. H., K. L. Cheng, and M. Grasserbauer, General Aspects of Trace Analytical Methods-IV. Recommendations for Nomenclature, Standard Procedures and Reporting of Experimental Data for Surface Analysis Techniques, *Pure and Applied Chemistry*, *51*(11), 2243–2250, doi:10.1351/pac197951112243, 1979.

- Müller-Tautges, C., A. Eichler, M. Schwikowski, G. B. Pezzatti, M. Conedera, and T. Hoffmann, Historic records of organic compounds from a high Alpine glacier: influences of biomass burning, anthropogenic emissions, and dust transport, *Atmospheric Chemistry and Physics*, 16(2), 1029–1043, doi:10.5194/acp-16-1029-2016, 2016.
- Nho, E.-Y., M.-F. Le Cloarec, B. Ardouin, and W. Tjetjep, Source strength assessment of volcanic trace elements emitted from the Indonesian arc, *Journal of Volcanology and Geothermal Research*, 74(1-2), 121–129, doi:10.1016/S0377-0273(96)00051-0, 1996.
- Osmont, D., I. A. Wendl, L. Schmidely, M. Sigl, C. P. Vega, E. Isaksson, and M. Schwikowski, An 800-year high-resolution black carbon ice core record from Lomonosovfonna, Svalbard, *Atmospheric Chemistry and Physics*, 18(17), 12,777–12,795, doi:10.5194/acp-18-12777-2018, 2018.
- Pavlova, P. A., T. M. Jenk, P. Schmid, C. Bogdal, C. Steinlin, and M. Schwikowski, Polychlorinated Biphenyls in a Temperate Alpine Glacier: 1. Effect of Percolating Meltwater on their Distribution in Glacier Ice, *Environmental Science & Technology*, 49(24), 14,085–14,091, doi:10.1021/acs.est.5b03303, 2015.
- Pepin, N., et al., Elevation-dependent warming in mountain regions of the world, *Nature Climate Change*, 5(5), 424–430, doi:10.1038/nclimate2563, 2015.
- Pinzer, B. R., M. Schneebeli, and T. U. Kaempfer, Vapor flux and recrystallization during dry snow metamorphism under a steady temperature gradient as observed by time-lapse microtomography, *The Cryosphere*, 6(5), 1141–1155, doi:10.5194/tc-6-1141-2012, 2012.
- Preunkert, S., M. Legrand, and D. Wagenbach, Sulfate trends in a Col du Dôme (French Alps) ice core: A record of anthropogenic sulfate levels in the European midtroposphere over the twentieth century, *Journal of Geophysical Research: Atmospheres*, 106(D23), 31,991–32,004, doi:10.1029/2001JD000792, 2001.
- Preunkert, S., D. Wagenbach, and M. Legrand, A seasonally resolved alpine ice core record of nitrate: Comparison with anthropogenic inventories and estimation of preindustrial emissions of NO in Europe, *Journal of Geophysical Research: Atmospheres*, 108(D21), doi:10.1029/2003JD003475, 2003.
- Raynaud, D., and F. Parrenin, Ice Cores, Antarctica And Greenland, in *Encyclopedia of Paleoclimatology and Ancient Environments*, edited by V. Gornitz, pp. 453–457, Springer, Dordrecht, doi:10.1007/978-1-4020-4411-3\_110, 2009.
- Schwikowski, M., S. Brütsch, H. W. Gäggeler, and U. Schotterer, A high-resolution air chemistry record from an Alpine ice core: Fiescherhorn glacier, Swiss Alps, *Journal of Geophysical Research: Atmospheres*, 104(D11), 13,709–13,719, doi:10.1029/1998JD100112, 1999.
- Schwikowski, M., et al., Post-17th-Century Changes of European Lead Emissions Recorded in High-Altitude Alpine Snow and Ice, *Environmental Science & Technology*, 38(4), 957–964, doi:10.1021/es034715o, 2004.
- Sigl, M., N. J. Abram, J. Gabrieli, T. M. Jenk, D. Osmont, and M. Schwikowski, 19th century glacier retreat in the Alps preceded the emergence of industrial black carbon deposition on high-alpine glaciers, *The Cryosphere*, 12(10), 3311–3331, doi:10.5194/tc-12-3311-2018, 2018.
- Thevenon, F., F. S. Anselmetti, S. M. Bernasconi, and M. Schwikowski, Mineral dust and elemental black carbon records from an Alpine ice core (Colle Gnifetti glacier) over the last millennium, *Journal of Geophysical Research*, 114(D17), D17,102, doi:10.1029/2008JD011490, 2009.
- Thompson, L., E. Mosley-Thompson, M. Davis, P. Lin, T. Yao, M. Dyurgerov, and J. Dai, "Recent warming": ice core evidence from tropical ice cores with emphasis on Central Asia, *Global and Planetary Change*, 7(1-3), 145–156, doi:10.1016/0921-8181(93)90046-Q, 1993.

- Thompson, L. G., Ice Cores, Mountain Glaciers, in *Encyclopedia of Paleoclimatology and Ancient Environments*, edited by V. Gornitz, pp. 457–463, Springer, Dordrecht, doi:10.1007/978-1-4020-4411-3\_111, 2009.
- Van de Velde, K., C. Ferrari, C. Barbante, I. Moret, T. Bellomi, S. Hong, and C. Boutron, A 200 Year Record of Atmospheric Cobalt, Chromium, Molybdenum, and Antimony in High Altitude Alpine Firn and Ice, *Environmental Science & Technology*, 33(20), 3495–3501, doi:10.1021/es990066y, 1999.
- Van de Velde, K., C. F. Boutron, C. P. Ferrari, A.-L. Moreau, R. J. Delmas, C. Barbante, T. Bellomi, G. Capodaglio, and P. Cescon, A two hundred years record of atmospheric cadmium, copper and zinc concentrations in high altitude snow and ice from the French-Italian Alps, *Geophysical Research Letters*, 27(2), 249–252, doi:10.1029/1999GL010786, 2000.
- Wagenbach, D., and K. Geis, The Mineral Dust Record in a High Altitude Alpine Glacier (Colle Gnifetti, Swiss Alps), in *Paleoclimatology and Paleometeorology: Modern and Past Patterns of Global Atmospheric Transport*, pp. 543–564, Springer Netherlands, Dordrecht, doi:10.1007/978-94-009-0995-3\_23, 1989.
- Wagenbach, D., K. Münnich, U. Schotterer, and H. Oeschger, The Anthropogenic Impact on Snow Chemistry at Colle Gnifetti, Swiss Alps, *Annals of Glaciology*, 10, 183–187, doi:10.3189/S0260305500004407, 1988.
- Wagenbach, D., S. Preunkert, J. Schäfer, W. Jung, and L. Tomadin, Northward Transport of Saharan Dust Recorded in a Deep Alpine Ice Core, in *The Impact of Desert Dust Across the Mediterranean*, edited by S. Chester and R. Guerzoni, pp. 291–300, Springer Netherlands, Dordrecht, doi:10.1007/978-94-017-3354-0\_29, 1996.
- Wong, G. J., R. L. Hawley, E. R. Lutz, and E. C. Osterberg, Trace-element and physical response to melt percolation in Summit (Greenland) snow, *Annals of Glaciology*, 54(63), 52–62, doi:10.3189/2013AoG63A602, 2013.
- Zhang, Q., S. Kang, P. Gabrielli, M. Loewen, and M. Schwikowski, Vanishing High Mountain Glacial Archives: Challenges and Perspectives, *Environmental Science & Technology*, 49(16), 9499–9500, doi:10.1021/acs.est.5b03066, 2015.
- Zhongqin, L., L. Chuanjin, L. Yuefang, W. Feiteng, and L. Huilin, Preliminary results from measurements of selected trace metals in the snow-firn pack on Ürümqi glacier No. 1, eastern Tien Shan, China, *Journal of Glaciology*, 53(182), 368–373, doi:10.3189/002214307783258486, 2007.



## 2 Study sites and analytical methods

### 2.1 Study sites

Upper Grenzglatscher and the Weissfluhjoch test site, both located in the Swiss Alps (Figure 2.1), were chosen as suitable study sites by providing unique characteristics to accomplish the research objectives of this thesis.

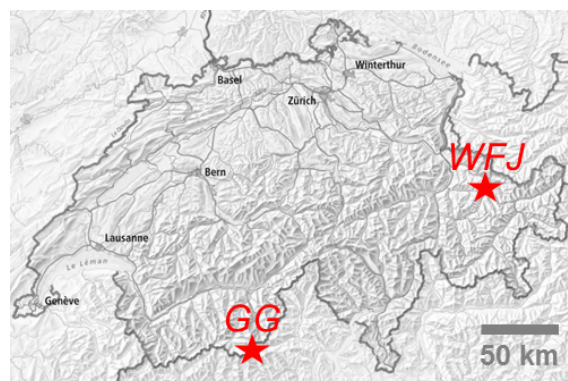


**Figure 2.1:** Location of the two study sites of this thesis in Switzerland. Upper Grenzglatscher (GG) is located in the Southern Swiss Alps close to the Swiss-Italian border, whereas the Weissfluhjoch test site (WFJ) is located in the Northern Swiss Alps in the eastern part of Switzerland (map adapted from <https://map.geo.admin.ch>).

#### 2.1.1 Upper Grenzglatscher

The Grenzglatscher is a valley glacier of 1-1.5 km width and approximately 8 km length in the canton of Valais in the south-western part of Switzerland close to the Swiss-Italian border (Figure 2.1). It is surrounded by the summits of Dufourspitze (4634 m a.s.l.), Zumsteinspitze (4562 m a.s.l.), Signalkuppe (4554 m a.s.l.), all part of Monte Rosa, and Lyskamm (4527 m a.s.l.), and flows towards the north-west, before it used to merge into the Gorner Glacier (Figure 2.2).

In October 1994, a 125 m long ice core was retrieved from upper Grenzglatscher at an altitude of 4200 m a.s.l. ( $45^{\circ}55'28''$  N,  $7^{\circ}52'3''$  E). The age-depth relationship

of this ice core was established by applying a multi-proxy approach [Eichler *et al.*, 2000b]. Annual layer counting of the strongly seasonal varying signals of  $\text{NH}_4^+$  and  $\delta^{18}\text{O}$  was combined with reference horizons from Saharan dust falls (1947, 1977, 1990), atmospheric nuclear weapons tests in the 1950s and 60s, and the 1986 Chernobyl reactor accident [Eichler *et al.*, 2000b]. Nuclear dating with  $^{210}\text{Pb}$  and fitting a simple kinematic ice flow model through the data supported the obtained chronology. The ice core was found to cover the time period of 1937-94, with a dating uncertainty of  $<1$  year for the period 1970-94 and  $\pm 2$  years for the time period 1937-69. The mean annual accumulation rate was determined to be 2.7 m w.eq. and corresponds to precipitation rates at the 50 km distant meteorological station, Col du Grand St Bernard (2469 m a.s.l.), suggesting that a year-round precipitation record is preserved at upper Grenzletscher.

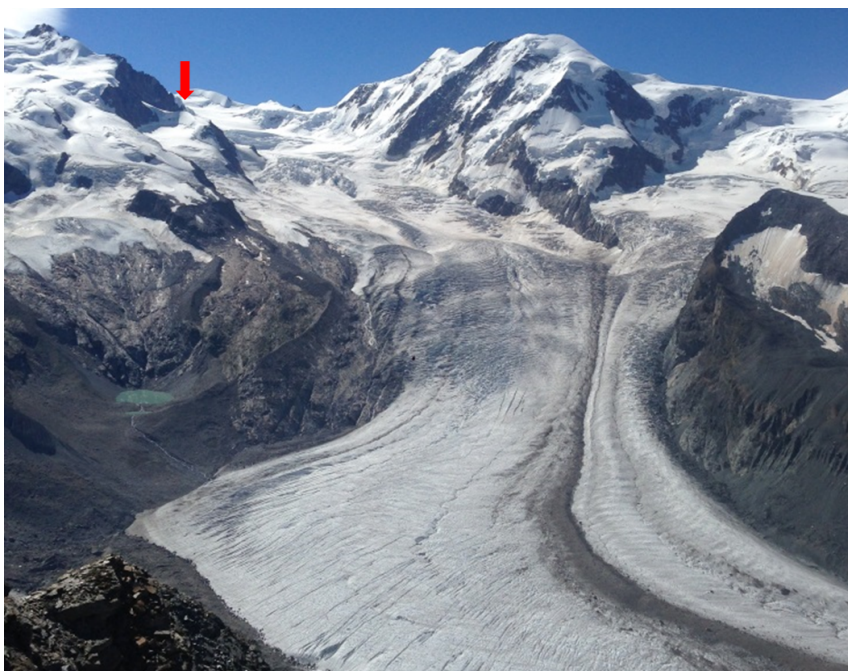


**Figure 2.2:** View of the Grenzletscher, a valley glacier located between the western part of Monte Rosa to the left and the summit of Liskamm to the right in the Southern Swiss Alps. The red arrow indicates the upper area of the glacier, where, at an altitude of 4200 m a.s.l., the 125 m ice core was retrieved in October 1994 (Photo: Sven Avak).

The ice core from upper Grenzletscher has been subject to various studies. It served as archive to reconstruct sources and transport of HF and HCl [Eichler *et al.*, 2000a], temperature and precipitation for the Alpine region [Mariani *et al.*, 2014], emissions and melt-induced relocation of polychlorinated biphenyls [Pavlova *et al.*, 2015], and most recently, historical changes of atmospheric organic dicarbonyl and long-chain dicarboxylic acid emissions [Müller-Tautges *et al.*, 2016]. Additionally, the ice core from upper Grenzletscher provides a very unique feature. Even though borehole

temperatures were continuously below the freezing point, a local temperature maximum of  $-1\text{ }^{\circ}\text{C}$  at a depth of 18 m w.eq. was observed, and later explained by a lateral inflow of meltwater at 11-12 m w.eq. due to a crevasse system in the glacier (Figure 2.3, *Eichler et al.* [2001]). Meltwater percolated through the underlying firn layers, before draining at the firn-ice transition at 24 m w.eq. Significant disturbance of certain major ions was observed in this 13 m w.eq. section affected by meltwater percolation, while the rest of the ice core revealed a well preserved chemical stratigraphy [*Eichler et al.*, 2001]. This allowed to investigate leaching effects caused by melting on the major ion composition in high-Alpine firn. While  $\text{Cl}^-$ ,  $\text{F}^-$ ,  $\text{NO}_3^-$ , and  $\text{NH}_4^+$  revealed a preserved seasonal variability, concentration records of  $\text{SO}_4^{2-}$ ,  $\text{K}^+$ ,  $\text{Na}^+$ ,  $\text{Ca}^{2+}$ , and  $\text{Mg}^{2+}$  were substantially depleted.

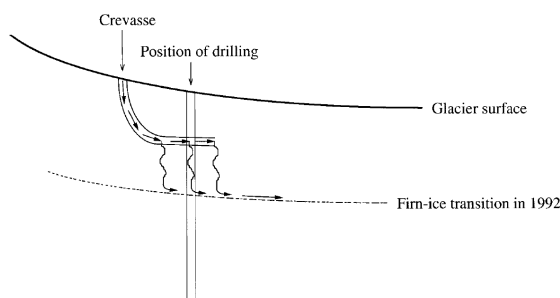


**Figure 2.3:** Scheme showing the suggested flow of meltwater at the drilling site of upper Grenzgletscher. Meltwater was fed by a crevasse system in the glacier, subsequently percolated through the underlying firn layers, and drained at the firn-ice transition (from *Eichler et al.* [2001]).

In this thesis, a 50 m segment of this ice core, including the meltwater-affected section, was investigated to assess the impact of meltwater percolation on the preservation of TEs in high-Alpine glaciers.

### 2.1.2 Weissfluhjoch test site

The Alpine Weissfluhjoch test site (2536 m a.s.l.,  $46^{\circ}49'47''$  N,  $9^{\circ}48'33''$  E) of the Swiss WSL Institute of Snow and Avalanche Research (SLF) is located in the Eastern Alps of Switzerland above the city of Davos, canton of Grisons (Figure 2.1). Due to its flat area (ca. 100 x 100 m) surrounded by slopes exposed to avalanches (Figure 2.4), this site has been serving for snow and avalanche research since 1936 and is very well characterized due to a vast number of studies, mainly addressing avalanche formation, snow characterization, snow mechanics, snow metamorphism, as well as the development and implementation of novel snow measurement techniques [*Marty and Meister*, 2012]. While it is usually snow free in summer, most of the precipitation in winter falls as snow and several parameters, such as snow height, air and snow surface temperature, snow pack density, or snow classifications, are continuously being monitored at a high resolution throughout the cold

season.

Although it is located in a unique topographic situation, where strong winds causing significant perturbations of the snow stratigraphy are exceptional and a uniform spatial snow deposition prevails [Baltensperger *et al.*, 1993], making the Weissfluhjoch test site also a very suitable location to investigate the chemical composition of atmospheric aerosols in the snow pack, only two studies are available. Baltensperger *et al.* [1993] compared continuous surface snow measurements of major ions ( $\text{SO}_4^{2-}$ ,  $\text{NO}_3^-$ ,  $\text{Cl}^-$ ,  $\text{NH}_4^+$ ), stable isotopes ( $\delta^{18}\text{O}$ ,  $\delta\text{D}$ ), and radioactive tracers ( $^{10}\text{Be}$ ,  $^{36}\text{Cl}$ ,  $^{210}\text{Pb}$ ), performed from January to March 1988, to a snow pit taken end of March. It was shown that the chemical stratigraphy of the snow pit reflects the snow deposition during the winter. Concentrations of environmentally relevant chemical species ( $\text{SO}_4^{2-}$ ,  $\text{NO}_3^-$ ,  $\text{Cl}^-$ ,  $\text{K}^+$ ,  $\text{Na}^+$ ,  $\text{NH}_4^+$ ,  $\text{Ca}^{2+}$ ,  $\text{Mg}^{2+}$ ) in the snow pack at the Weissfluhjoch test site were also reported by Schwikowski *et al.* [1997]. The vertical distribution of ionic species in the snow profile was found to correlate with their seasonal variability in deposition and their different emissions sources.



**Figure 2.4:** View of the Weissfluhjoch test site of the WSL Institute for Snow and Avalanche Research SLF at an elevation of 2536 m a.s.l. in the Plessur Alps, Switzerland (Photo: Sven Avak).

In view of the excellent conditions provided by the Alpine Weissfluhjoch test site, an extensive snow pit study was accomplished in this thesis to monitor the behavior of TEs during melting of the snow pack. Five snow pits were taken in winter, spring, and early summer 2017 on January 25<sup>th</sup>, February 22<sup>nd</sup>, March 21<sup>st</sup>, April 17<sup>th</sup>, and June 1<sup>st</sup>. This snow pit campaign was parallel to an extensive series of snow



pack measurements conducted by the SLF during the entire winter season 2016/17, granting access to high-resolution density data for the individual snow pits. Special precautions, such as the wearing of sterile clean room overalls, face masks, and ultra-clean plastic gloves, had to be taken during the snow pit samplings, as snow is very sensitive to contamination at an ultra-trace level (Figure 2.5).



**Figure 2.5:** Special precautions, such as wearing clean room overalls, face masks, and ultra-clean plastic gloves, were taken during the snow pit samplings to avoid contamination of the samples (Photo: Sven Avak).

## 2.2 Trace element analysis

Concentrations of the various TEs preserved in high-Alpine glacier ice and snow (Figure 1.1) are usually in the nano- to milligrams per liter range, requiring a highly sensitive analytical method capable for multi-elemental detection. For this purpose, inductively coupled plasma mass spectrometry (ICP-MS) is an appropriate technique, as it provides detection limits in the low parts per trillion (ppt) range and allows detection of isotopes of more than 70 elements ranging from  ${}^7\text{Li}$  to  ${}^{238}\text{U}$  [Thomas, 2004].

### 2.2.1 Inductively coupled plasma sector field mass spectrometry

In this thesis, an ICP sector-field (SF) MS as shown in Figure 2.6 was employed. The principle of function is the following [Gross, 2011]: The core part consists of a coil (torch), where a fluctuating electromagnetic field heats up a stream of argon, creating a toroidal plasma. The dry sample aerosol, produced by an upstream

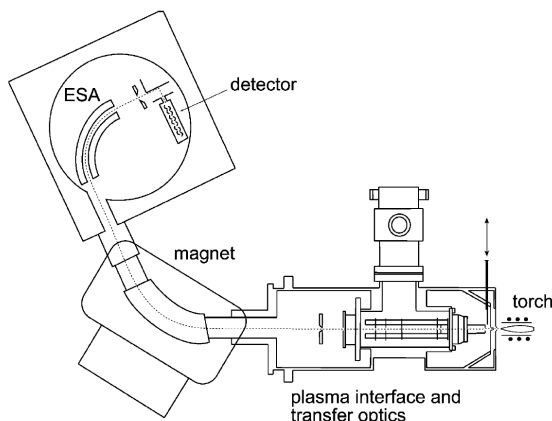


**Figure 2.6:** Scheme of a double-focusing ICP-SF-MS with inverse Nier-Johnson geometry. “Inverse” implies that the electrostatic analyzer (ESA) is positioned after the magnetic analyzer (from *Gäbler* [2002]).

nebulizer (in case of the setup used in this thesis), is introduced into the argon plasma (ca. 10'000 K). The latter serves as ion source by vaporizing, atomizing, and ionizing the introduced sample aerosol. The ions are guided through the first pumping stage, where a sampler cone followed by a voltage-carrying skimmer cone ensure that uncharged atoms are pumped off. After subsequent focusing to an ion beam, acceleration in an electric field to a velocity  $v$  by applying a potential  $U$  (up to 10 kV), the ions are transferred by a second differentially pumped interface to the sector-field mass analyzer. The latter usually consists of a separate magnetic and an electrostatic analyzer (so-called double-focusing design). If the magnetic analyzer is positioned before the electrostatic analyzer, which is the case for the ICP-SF-MS used in this thesis, it is referred to as “inverse Nier-Johnson geometry”. The electromagnetic analyzer acts as key part of the entire analyzer, where the ions are separated according to their mass-to-charge ratio ( $m/z$ ).

The electromagnetic analyzer works as follows [*Gross*, 2011]: A constant magnetic field  $B$  (ca. 1 T) exerts a force on an ion of mass  $m$ , traveling at a velocity  $v$  and bearing a charge  $q$ , resulting into its deflection along a circular path with radius  $r$ . As  $B$  can be assumed to be perpendicular to the ion’s translational motion, the relationship between the Lorentz force  $F_L$  and the centripetal force  $F_C$  is therefore defined by the scalar equilibrium:

$$F_L = q \cdot v \cdot B = \frac{m \cdot v^2}{r} = F_C \quad (2.1)$$

Rearrangement of Equation 2.1 gives the radius  $r$  of the ion’s circular motion:

$$r = \frac{m \cdot v}{q \cdot B} \quad (2.2)$$

Equation 2.2 shows that  $r$  is dependent on the ion’s momentum  $mv$ , which again is dependent on the ion’s charge  $q$ . Due to the acceleration of the ion beam in the

transfer optics, the potential energy  $E_{pot}$  of an ion is converted into kinetic energy  $E_{kin}$ :

$$E_{kin} = \frac{1}{2} \cdot m \cdot v^2 = q \cdot U = E_{pot} \quad (2.3)$$

The velocity  $v$  of an ion can be obtained by rearranging Equation 2.3:

$$v = \sqrt{\frac{2 \cdot q \cdot U}{m}} \quad (2.4)$$

Substitution of  $v$  from Equation 2.4 in Equation 2.2 yields:

$$r^2 = \frac{m \cdot 2 \cdot U}{q \cdot B^2} \quad (2.5)$$

The mass-to-charge ratio can finally be obtained by rearranging Equation 2.5:

$$\frac{m}{q} = \frac{r^2 \cdot B^2}{2 \cdot U} \quad (2.6)$$

Alternatively, as  $q = z \cdot e$ , where  $e$  is the constant elementary charge and  $z$  the charge number, Equation 2.6 can be expressed as:

$$\frac{m}{z} = \frac{r^2 \cdot B^2}{2 \cdot U} \quad (2.7)$$

Equation 2.7 shows that the radius of deflection  $r$  is dependent on the mass-to-charge ratio  $m/z$  of the ion, the acceleration potential  $U$ , and the magnetic field  $B$ . As  $z = 1$ , an ion of higher mass is less deflected than an ion of lower mass, indicating that the ions have distinct trajectories when they enter the electrostatic analyzer, where they are sorted according to their kinetic energy, before reaching the detector in a trajectory of radius  $r$ . Using Equation 2.7 and knowing  $r$ ,  $B$ ,  $U$ , and  $z$ , the mass  $m$  of an ion i.e., an isotope can be determined.

ICP-SF-MS has been adapted and well established for the analysis of TEs in high-Alpine ice cores at PSI [Döring *et al.*, 1997; Knüsel *et al.*, 2003; Kellerhals *et al.*, 2010; Eichler *et al.*, 2012, 2014, 2015, 2017]. The extremely low concentrations of TEs in high-Alpine glaciers and snow packs do not only require elemental analysis with low detection limits, but also demand thorough sample decontamination and measures to prevent sample contamination, respectively. If not stated otherwise, sample preparation steps, measurement, and evaluation procedures for the discrete snow and ice core samples of this thesis were performed as described in detail by Knüsel [2003] and Kellerhals [2008]. In this thesis, an Element 2 ICP-SF-MS (Thermo Fisher Scientific, Bremen, Germany) was used to determine concentrations, either in low (LR) or medium resolution (MR), of  $^7\text{Li}$  (LR & MR),  $^{23}\text{Na}$ ,  $^{24}\text{Mg}$ ,  $^{27}\text{Al}$ ,  $^{44}\text{Ca}$ ,  $^{45}\text{Sc}$ ,  $^{51}\text{V}$ ,  $^{55}\text{Mn}$ ,  $^{56}\text{Fe}$ ,  $^{59}\text{Co}$  (all MR),  $^{60}\text{Ni}$ ,  $^{63}\text{Cu}$ ,  $^{66}\text{Zn}$  (all LR & MR),  $^{85}\text{Rb}$ ,  $^{88}\text{Sr}$ ,  $^{90}\text{Zr}$ ,  $^{95}\text{Mo}$ ,  $^{109}\text{Ag}$ ,  $^{111}\text{Cd}$ ,  $^{121}\text{Sb}$ ,  $^{133}\text{Cs}$ ,  $^{138}\text{Ba}$ ,  $^{139}\text{La}$ ,  $^{140}\text{Ce}$ ,  $^{141}\text{Pr}$ ,  $^{146}\text{Nd}$ ,  $^{147}\text{Sm}$ ,  $^{153}\text{Eu}$ ,  $^{172}\text{Yb}$ ,  $^{182}\text{W}$ ,  $^{205}\text{Tl}$ ,  $^{206}\text{Pb}$ ,  $^{207}\text{Pb}$ ,  $^{208}\text{Pb}$ ,  $^{209}\text{Bi}$ ,  $^{232}\text{Th}$ , and  $^{238}\text{U}$  (all LR).

### 2.2.1.1 Laser ablation ICP-MS

Coupling laser ablation (LA) to ICP-MS allows for the direct sampling on a microscopic scale from the surface of solids. As schematically shown in Figure 2.7, a laser serves as key component by emitting a pulsed beam which is focused onto the surface of a sample, located inside a gas-tight ablation chamber. This results in the release of small particles (so-called “ablation”). The sample aerosol is then directly transported by a carrier gas to the ICP-MS for subsequent elemental analysis as described above. This technique has been widely used to investigate concentrations or isotope ratios of elements in archeology, biology, chemistry forensics, geology, medicine, metallurgy, and environmental and material science [Durrant and Ward, 2005; Günther and Hattendorf, 2005; Koch and Günther, 2011; Lobo et al., 2018]. The LA-ICP-MS system used in this thesis, consisted of a Resonetics Resolution S155 LA system (Australian Scientific Instruments, Fyshwick, Australia), equipped with a 193 nm ArF excimer gas laser, coupled to an Element XR ICP-SF-MS (Thermo Fisher Scientific, Bremen, Germany) and was located at the Institute of Geochemistry and Petrology, ETH Zurich. Further technical details and applications for frozen sample analysis are extensively described in Chapter 6.

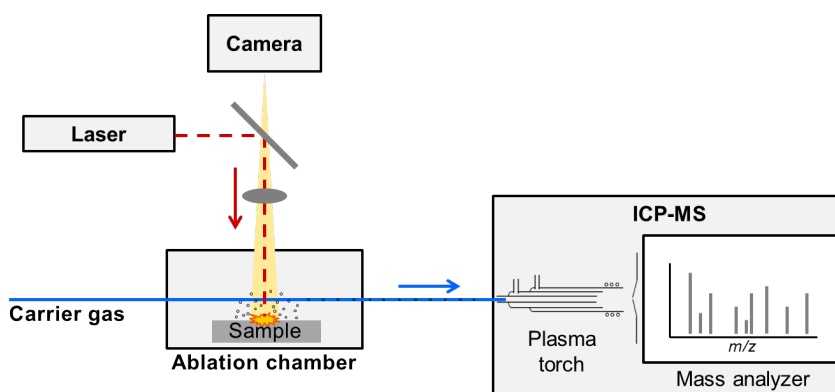


Figure 2.7: Schematic of LA-ICP-MS.

## Bibliography

- Baltensperger, U., M. Schwikowski, H. Gäggeler, D. Jost, J. Beer, U. Siegenthaler, D. Wagenbach, H. Hofmann, and H. Synal, Transfer of atmospheric constituents into an alpine snow field, *Atmospheric Environment. Part A. General Topics*, 27(12), 1881–1890, doi:10.1016/0960-1686(93)90293-8, 1993.
- Döring, T., M. Schwikowski, and H. W. Gäggeler, Determination of lead concentrations and isotope ratios in recent snow samples from high alpine sites with a double focusing ICP-MS, *Fresenius' Journal of Analytical Chemistry*, 359(4-5), 382–384, doi:10.1007/s002160050592, 1997.
- Durrant, S. F., and N. I. Ward, Recent biological and environmental applications of laser ablation inductively coupled plasma mass spectrometry (LA-ICP-MS), *Journal of Analytical Atomic Spectrometry*, 20(9), 821, doi:10.1039/b502206a, 2005.

- Eichler, A., M. Schwikowski, and H. W. Gäggeler, An Alpine ice-core record of anthropogenic HF and HCl emissions, *Geophysical Research Letters*, 27(19), 3225–3228, doi:10.1029/2000GL012006, 2000a.
- Eichler, A., M. Schwikowski, H. W. Gäggeler, V. Furrer, H.-A. Synal, J. Beer, M. Saurer, and M. Funk, Glaciochemical dating of an ice core from upper Grenzgletscher (4200 m a.s.l.), *Journal of Glaciology*, 46(154), 507–515, doi:10.3189/172756500781833098, 2000b.
- Eichler, A., M. Schwikowski, and H. W. Gäggeler, Meltwater-induced relocation of chemical species in Alpine firn, *Tellus B: Chemical and Physical Meteorology*, 53(2), 192–203, doi:10.3402/tellusb.v53i2.16575, 2001.
- Eichler, A., L. Tobler, S. Eyrikh, G. Gramlich, N. Malygina, T. Papina, and M. Schwikowski, Three Centuries of Eastern European and Altai Lead Emissions Recorded in a Belukha Ice Core, *Environmental Science & Technology*, 46(8), 4323–4330, doi:10.1021/es2039954, 2012.
- Eichler, A., L. Tobler, S. Eyrikh, N. Malygina, T. Papina, and M. Schwikowski, Ice-Core Based Assessment of Historical Anthropogenic Heavy Metal (Cd, Cu, Sb, Zn) Emissions in the Soviet Union, *Environmental Science & Technology*, 48(5), 2635–2642, doi:10.1021/es404861n, 2014.
- Eichler, A., G. Gramlich, T. Kellerhals, L. Tobler, and M. Schwikowski, Pb pollution from leaded gasoline in South America in the context of a 2000-year metallurgical history, *Science Advances*, 1(2), e1400196, doi:10.1126/sciadv.1400196, 2015.
- Eichler, A., G. Gramlich, T. Kellerhals, L. Tobler, T. Rehren, and M. Schwikowski, Ice-core evidence of earliest extensive copper metallurgy in the Andes 2700 years ago, *Scientific Reports*, 7(1), 41,855, doi:10.1038/srep41855, 2017.
- Gäbler, H.-E., Applications of magnetic sector ICP-MS in geochemistry, *Journal of Geochemical Exploration*, 75(1-3), 1–15, doi:10.1016/S0375-6742(01)00197-2, 2002.
- Gross, J. H., *Mass Spectrometry*, Springer Berlin Heidelberg, Berlin, Heidelberg, doi:10.1007/978-3-642-10711-5, 2011.
- Günther, D., and B. Hattendorf, Solid sample analysis using laser ablation inductively coupled plasma mass spectrometry, *TrAC Trends in Analytical Chemistry*, 24(3), 255–265, doi:10.1016/j.trac.2004.11.017, 2005.
- Kellerhals, T., Holocene climate fluctuations in tropical South America deduced from an Illimani ice core, Ph.D. thesis, University of Bern, 2008.
- Kellerhals, T., L. Tobler, S. Brütsch, M. Sigl, L. Wacker, H. W. Gäggeler, and M. Schwikowski, Thallium as a Tracer for Preindustrial Volcanic Eruptions in an Ice Core Record from Illimani, Bolivia, *Environmental Science & Technology*, 44(3), 888–893, doi:10.1021/es902492n, 2010.
- Knüsel, S., Continuous Trace-Element Analysis and Identification of Climate Signals using an Ice Core from Nevado Illimani, Bolivia, Ph.D. thesis, University of Bern, 2003.
- Knüsel, S., D. E. Piguet, M. Schwikowski, and H. W. Gäggeler, Accuracy of Continuous Ice-Core Trace-Element Analysis by Inductively Coupled Plasma Sector Field Mass Spectrometry, *Environmental Science & Technology*, 37(10), 2267–2273, doi:10.1021/es026452o, 2003.
- Koch, J., and D. Günther, Review of the State-of-the-Art of Laser Ablation Inductively Coupled Plasma Mass Spectrometry, *Applied Spectroscopy*, 65(5), 155–162, doi:10.1366/11-06255, 2011.
- Lobo, L., R. Pereiro, and B. Fernández, Opportunities and challenges of isotopic analysis by laser ablation ICP-MS in biological studies, *TrAC Trends in Analytical Chemistry*, 105, 380–390, doi:10.1016/j.trac.2018.05.020, 2018.
- Mariani, I., A. Eichler, T. M. Jenk, S. Brönnimann, R. Auchmann, M. C. Leuenberger, and M. Schwikowski, Temperature and precipitation signal in two Alpine ice cores over the period 1961–2001, *Climate of the Past*, 10(3), 1093–1108, doi:10.5194/cp-10-1093-2014, 2014.

- Marty, C., and R. Meister, Long-term snow and weather observations at Weissfluhjoch and its relation to other high-altitude observatories in the Alps, *Theoretical and Applied Climatology*, *110*(4), 573–583, doi:10.1007/s00704-012-0584-3, 2012.
- Müller-Tautges, C., A. Eichler, M. Schwikowski, G. B. Pezzatti, M. Conedera, and T. Hoffmann, Historic records of organic compounds from a high Alpine glacier: influences of biomass burning, anthropogenic emissions, and dust transport, *Atmospheric Chemistry and Physics*, *16*(2), 1029–1043, doi:10.5194/acp-16-1029-2016, 2016.
- Pavlova, P. A., T. M. Jenk, P. Schmid, C. Bogdal, C. Steinlin, and M. Schwikowski, Polychlorinated Biphenyls in a Temperate Alpine Glacier: 1. Effect of Percolating Meltwater on their Distribution in Glacier Ice, *Environmental Science & Technology*, *49*(24), 14,085–14,091, doi:10.1021/acs.est.5b03303, 2015.
- Schwikowski, M., et al., Intercomparison of snow sampling and analysis within the alpine-wide snowpack investigation (SNOSP), *Water, Air, & Soil Pollution*, *93*(1-4), 67–91, doi:10.1007/BF02404748, 1997.
- Thomas, R., *Practical Guide to ICP-MS*, Marcel Dekker, Inc., New York, Basel, 2004.

# 3 Impact and implications of meltwater percolation on trace element records observed in a high-Alpine ice core

Sven Erik Avak<sup>a,b,c</sup>, Margit Schwikowski<sup>a,b,c</sup>, and Anja Eichler<sup>a,c,\*</sup>

<sup>a</sup>Laboratory of Environmental Chemistry, Paul Scherrer Institute, Villigen PSI, 5232, Switzerland

<sup>b</sup>Department of Chemistry and Biochemistry, University of Bern, Bern, 3012, Switzerland

<sup>c</sup>Oeschger Centre for Climate Change Research, University of Bern, Bern, 3012, Switzerland

\*Corresponding author

*Manuscript published in  
Journal of Glaciology, 64(248), 877–886, 2018*

## Abstract

Past atmospheric pollution can be reconstructed from ice core trace element records retrieved from mountain glaciers. However, the current global temperature increase can result in post-depositional melt processes, significantly altering the originally stored information. Here, we present a comprehensive study on the behavior of 35 trace elements (TEs) during meltwater percolation in a high-Alpine ice core segment from upper Grenzgletscher, Switzerland. Some TEs revealed significant concentration depletion, whereas others were well preserved depending on their water solubility and location at the grain scale. TEs present in insoluble minerals, typically enriched at grain boundaries, were found to be mostly preserved because their insolubility in water results in immobility with meltwater percolation. Water-soluble TEs revealed a variable meltwater-mobility. Whereas ultra-TEs tend to be preserved, likely due to incorporation into the ice lattice, abundant TEs are prone to relocation from grain-boundary regions. We propose that at Alpine sites, Ag, Al, Bi, Cu, Cs, Fe, Li, Mo, Pb, Rb, Sb, Th, Tl, U, V, W, Zr, and the rare-earth elements may still be applicable as robust environmental proxies even if partial melting occurred, whereas Ba, Ca, Cd, Co, Mg, Mn, Na, Ni, Sr, and Zn are prone to significant depletion.

## 3.1 Introduction

High-mountain glacier ice cores serve as invaluable environmental archives for the reconstruction of past climate and atmospheric composition. Due to their close proximity, ice core records retrieved from high-altitude glaciers and ice caps often allow to track environmental changes in the most densely populated and industrialized regions in the world. Environmental paleo records from ice cores are generally obtained through the chemical analysis of the entrapped atmospheric air, and the impurities which were transported as wet or dry deposition to the surface of a glacier and preserved in the ice over time. Among the ensemble of impurities used as reconstruction proxies, trace elements (TEs) play a substantial role. TE concentration records from high-altitude ice cores can provide a wide range of regional and global scale information such as for example on volcanism [Kaspari *et al.*, 2009b; Kellerhals *et al.*, 2010; Gabrielli *et al.*, 2014], sources and variations of atmospheric mineral dust [Kaspari *et al.*, 2009a], and in particular, historical changes of the various forms of atmospheric anthropogenic pollution [Correia *et al.*, 2003; Hong *et al.*, 2004; Schwikowski *et al.*, 2004; Barbante *et al.*, 2004; Gabrieli *et al.*, 2011; Lee *et al.*, 2011; Eichler *et al.*, 2014, 2015, 2017; Uglietti *et al.*, 2015; Grigholm *et al.*, 2016; Eyrikh *et al.*, 2017; Beaudon *et al.*, 2017; Sierra-Hernández *et al.*, 2018].

For reconstructing past climatic and environmental changes, the use of pristine ice cores, where the multiple proxy information has not been disturbed by post-depositional processes such as melting, infiltration, and refreezing, is advantageous



to ensure a reliable reconstruction [Zhang *et al.*, 2015]. For this reason, ice cores from high-altitude cold glaciers, which do not experience significant meltwater percolation between different annual layers, are the preferred objects of investigation. However, potential drilling sites are more and more difficult to find as many high-mountain glaciers worldwide are retreating or are in danger of melting [Zemp *et al.*, 2009; Huss *et al.*, 2017] due to the current global temperature increase [Marcott *et al.*, 2013]. To continue using ice cores from high-altitude areas as environmental archives in the future, it is crucial to understand to what extent proxy information in ice core records is altered by post-depositional melting processes.

Several studies have been addressing this issue. In the case of the stable oxygen isotope ratio ( $\delta^{18}\text{O}$ ) the annual signal can be smoothed due to meltwater percolation making any reconstruction of past temperature impossible [Thompson *et al.*, 1993]. The major ion record can also be dramatically disturbed as detected in a 16 m section of an ice core from upper Grenzgletscher, Swiss Alps (Note: the same ice core investigated here; Eichler *et al.* [2001]). Concentration records of some major ions in this core were well preserved, but others were depleted to values close to the detection limit due to relocation with percolating meltwater. An elution sequence was postulated to explain the preferential removal of certain ionic species. Pavlova *et al.* [2015] showed that partial melting and refreezing, a process frequently occurring in temperate glaciers, can even result in relocation and release of persistent organic pollutants, substances with low water solubility. However, the influence of meltwater percolation on TE records still remains largely unclear as there has been no systematic investigation so far. Wong *et al.* [2013] focused on 12 TEs associated with insoluble dust and observed that artificial meltwater infiltration in Greenland snow pits lowered TE concentrations, but in spite of that, the TE seasonality was still conserved. They concluded that especially particle bound rare-earth elements (REEs) are relatively immobile with meltwater percolation. In another study, profiles of both crustal and anthropogenic originating TEs of a snow pit from Mt. Ortles glacier, Italian Alps, did not seem to be notably altered even though significant melt events occurred during summer [Gabrieli *et al.*, 2011].

Here, we discuss the behavior of 35 TEs in a 50 m segment of an ice core from upper Grenzgletscher, Switzerland. At the center of this segment, a 16 m section is located that was affected by meltwater percolation induced by a lateral meltwater inflow, presumably originating from a crevasse system. This core section consisted of firn at the time of infiltration [Eichler *et al.*, 2001]. This unique setting allows comparing the affected, and unaffected TE profiles above and below to characterize the impact of melting processes. Particular attention is given to providing an approach for explaining the observed TE patterns, and how the outcome of this study may contribute to the future interpretation of TE ice core records disturbed by meltwater percolation events.

## 3.2 Materials and methods

### 3.2.1 Ice core characteristics, detection of meltwater percolation, and dating

The 50 m ice core segment investigated in this study was part of a 125 m long ice core recovered from upper Grenzgletscher, Monte Rosa massif, southern Swiss Alps (4200 m a.s.l.; 45°55'28" N, 7°52'3" E) in October 1994 [Eichler *et al.*, 2000a, b, 2001; Müller-Tautges *et al.*, 2016]. Continuous negative borehole temperatures indicated that the upper Grenzgletscher consists of cold firn and ice down to a depth of 125 m. The borehole temperature profile also revealed an unusual local temperature maximum of  $-1$  °C at a depth of 28 m (18 m w.eq.) [Eichler *et al.*, 2000b]. This maximum was attributed to a lateral inflow of meltwater at 19-20 m (11-12 m w.eq.) presumably due to a crevasse system in the glacier, subsequent percolation through the underlying firn layers, partial refreezing, and drainage along the former firn/ice transition located at 35 m (24 m w.eq.) at the time of the drilling [Eichler *et al.*, 2001]. Refreezing of meltwater generally leads to an increased ice temperature due to the release of latent heat [Schwikowski *et al.*, 2013].

The age-depth relationship of the ice core was established by combining annual layer counting of signals with strong seasonal variations ( $\text{NH}_4^+$  and  $\delta^{18}\text{O}$ ) together with reference horizons from Saharan dust falls (1947, 1977, and 1990), atmospheric nuclear weapons tests (1950s and 60s), and the 1986 Chernobyl reactor accident [Eichler *et al.*, 2000b]. The obtained timescale was supported by nuclear dating with  $^{210}\text{Pb}$  and fitting a simple kinematic ice flow model through the data. The 125 m long ice core covered the time period of 1937-94 with a dating uncertainty of  $<1$  year for the period 1970-94 and  $\pm 2$  years for the period 1937-69.

The determined mean annual accumulation rate at the drilling site was 2.7 m w.eq. Comparison of annual accumulation rates at the upper Grenzgletscher site and annual precipitation rates at the 50 km distant weather station, Col du Grand St Bernard (2469 m a.s.l.; Eichler *et al.* [2000b]; Mariani *et al.* [2014]), indicates that the upper Grenzgletscher retains an all-year precipitation record. This is in contrast to the nearby Colle Gnifetti saddle (1 km away) with strong wind erosion especially during winter [Döscher *et al.*, 1995].

### 3.2.2 Sample preparation and trace element analysis

The ice core sections were stored in polyethylene tubes at  $-20$  °C until sample preparation. The segment between 2.2 and 52.2 m, corresponding to the time period 1980-93, was analyzed for this study. This includes the section affected by meltwater percolation between 19 and 35 m. This section consisted of firn when meltwater infiltration occurred [Eichler *et al.*, 2001]. The segments 13.3-14.7 m (within the year 1991) and 43.4-44.4 m (within the year 1982) could not be sampled as there

was no ice remaining after previous analyses.

To remove possible contamination caused by the drilling procedure, previous sample preparation, or storage, the outer surface of the ice core sections was removed with a band saw, fitted with a Teflon-coated saw guide and tabletop, at  $-20\text{ }^{\circ}\text{C}$  in the cold room at the Paul Scherrer Institute. In total, 550 samples with a cross-section of  $1.6\text{ x }1.6\text{ cm}$  and lengths ranging from 4 to 15 cm (average of 8.3 cm) were cut resulting in an average sampling resolution of 41 samples per year. Ice samples from a core depth below 20.0 m were rinsed with ultra-pure water (18 M  $\Omega\text{ cm}$  quality, Milli-Q<sup>®</sup> Element system, Merck Millipore, Burlington MA, USA) under a class 100 laminar flow clean bench to remove the outer  $\sim 0.2\text{ cm}$  containing potential contamination from the stainless steel saw blade and/or the handling. Firn samples above this depth were decontaminated by scraping all faces ( $0.3\text{ cm}$ ) with a ceramic knife (Boker USA, Lakewood CO, USA) since rinsing was not possible due to high porosity (density  $<0.7\text{ g cm}^{-3}$ ). This decontamination procedure has been well established for discrete TE analysis [Eichler *et al.*, 2012]. All decontaminated samples were transferred into polypropylene tubes (Sarstedt, Nümbrecht, Germany), which were cleaned five times with ultra-pure water and once with 0.2 M  $\text{HNO}_3$ , prepared from ultra-pure  $\text{HNO}_3$  (Optima<sup>™</sup>, Fisher Chemical, Loughborough, UK) beforehand.

The samples were acidified with concentrated ultra-pure  $\text{HNO}_3$  to 0.2 M, melted at room temperature, and analyzed using discrete inductively coupled plasma sector field mass spectrometry (ICP-SF-MS, Element 2, Thermo Fisher Scientific, Bremen, Germany). Concentrations, either in low (LR) or medium resolution (MR), of  $^7\text{Li}$  (LR & MR),  $^{23}\text{Na}$ ,  $^{24}\text{Mg}$ ,  $^{27}\text{Al}$ ,  $^{44}\text{Ca}$ ,  $^{45}\text{Sc}$ ,  $^{51}\text{V}$ ,  $^{55}\text{Mn}$ ,  $^{56}\text{Fe}$ ,  $^{59}\text{Co}$  (all MR),  $^{60}\text{Ni}$ ,  $^{63}\text{Cu}$ ,  $^{66}\text{Zn}$  (all LR & MR),  $^{85}\text{Rb}$ ,  $^{88}\text{Sr}$ ,  $^{90}\text{Zr}$ ,  $^{95}\text{Mo}$ ,  $^{109}\text{Ag}$ ,  $^{111}\text{Cd}$ ,  $^{121}\text{Sb}$ ,  $^{133}\text{Cs}$ ,  $^{138}\text{Ba}$ ,  $^{139}\text{La}$ ,  $^{140}\text{Ce}$ ,  $^{141}\text{Pr}$ ,  $^{146}\text{Nd}$ ,  $^{147}\text{Sm}$ ,  $^{153}\text{Eu}$ ,  $^{172}\text{Yb}$ ,  $^{182}\text{W}$ ,  $^{205}\text{Tl}$ ,  $^{206}\text{Pb}$ ,  $^{207}\text{Pb}$ ,  $^{208}\text{Pb}$ ,  $^{209}\text{Bi}$ ,  $^{232}\text{Th}$ , and  $^{238}\text{U}$  (all LR) were determined. A microconcentric nebulizer (apex Q, Elemental Scientific, Omaha NE, USA) together with an autosampler (CETAC ASX-260, Teledyne Cetac, Omaha NE, USA) was used for sample introduction.  $^{103}\text{Rh}$  served as the internal standard to correct for intensity variations during sample introduction, and for plasma fluctuations. External calibration with seven different liquid calibration standards was used for quantification. Concentrations of each element in the calibration standards were adapted to account for their different concentrations in glacier ice. Correlation coefficients for linear regressions of the calibration curves were consistently higher than 0.999. This calibration procedure has been successfully employed in previous studies [Knüsel *et al.*, 2003; Eichler *et al.*, 2012, 2014, 2015, 2017].

### 3.2.3 Data evaluation

Raw data were evaluated following the method described by Knüsel *et al.* [2003]. Concentrations were blank-corrected by subtracting a procedural blank (Table 3.1). Procedural blank concentrations were determined by analyzing 8 cm long ice sticks of frozen ultra-pure water. These sticks were prepared like the ice core samples and

were either decontaminated with ultra-pure water or a ceramic knife as described above. The instrumental detection limit was defined as  $3\sigma$  of the measurement blank consisting of 22 measurements of ultra-pure water (Table 3.1). Concentrations below the detection limit were substituted with half the value of the detection limit. A reduced data set consisting of equidistant data points was created out of the blank-corrected data set for each TE by calculating average concentration values for each month within the time period 1980-93 covered by the investigated ice core segment, assuming homogeneous precipitation distribution throughout the year (or equal binning).

## 3.3 Results and discussion

### 3.3.1 Data presentation and characterization

Ice core concentration records of selected TEs (Ag, Cd, Cs, Eu, Na, Pb, Tl) covering the period 1980-93 are shown in Figure 3.1. The entire ice core was previously analyzed for the main soluble inorganic cations and anions using ion chromatography (IC) [Eichler *et al.*, 2000b, 2001]. Thus, concentrations of Na, Mg, and Ca have been determined by two independent analytical methods and can, therefore, be used to assess the reproducibility and representativeness of the data. Our measurements of Ca, Na, and Mg concentrations agree well with the concentration records obtained by IC. For example, the  $\text{Na}^+$  and the Na concentration profiles (Figure 3.1) reveal a strong correspondence between each other ( $R^2 = 0.81$ ) despite different sampling and analytical methods, and the long-term storage between the two studies.

In general, concentration records of all 35 TEs reveal a very distinct seasonal pattern with high summer and low winter concentrations. This seasonality, typical for high-Alpine sites, is the result of stronger convection in summer allowing polluted air masses from the planetary boundary layer to reach the high-altitude sites of the Alps, while in winter, they are decoupled from the underlying air masses [Baltensperger *et al.*, 1997]. The pronounced seasonal variability is also visible in the record of water stable isotopes ( $\delta^{18}\text{O}$ ), in line with temperature data from the nearby weather station Col du Grand St. Bernard (Eichler *et al.* [2001]; Mariani *et al.* [2014], Figure 3.1). Depending on the identifiability of the seasonal pattern within the meltwater-affected period 1985-89, the investigated 35 TEs were split into two groups. TEs of group 1, including Ag, Al, Bi, Ce, Cs, Cu, Eu, Fe, La, Li, Mo, Nd, Pb, Pr, Rb, Sb, Sc, Sm, Tl, Th, U, V, W, Yb, and Zr, keep their seasonal concentration pattern. Group 2 TEs, comprising Ba, Ca, Cd, Co, Mg, Mn, Na, Ni, Sr, and Zn, are significantly depleted and no seasonality can be identified. This is exemplarily shown in Figure 3.1 with Ag, Cs, Eu, Tl, Pb for group 1 TEs and Cd, Na representing group 2 TEs.

These observed anomalies within the time period 1985-89 coincide with the observations of ion fractionation made by Eichler *et al.* [2001]. In their study, they

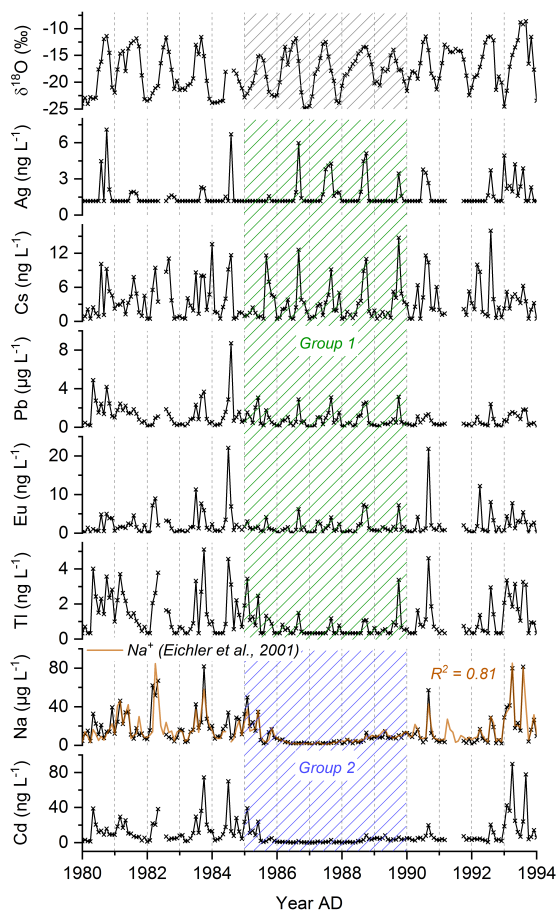


**Figure 3.1:** Monthly mean concentration records of Ag, Cs, Pb, Eu, Tl, Na, and Cd representing group 1 and 2 TEs and covering the period 1980-93 corresponding to the ice core segment from upper Grenzletscher analyzed and discussed in this study. For comparison, the  $\delta^{18}\text{O}$  and the  $\text{Na}^+$  records reported by *Eichler et al.* [2001] are shown. The shaded area (1985-89) indicates the section affected by meltwater percolation.

postulated that meltwater percolated through the firn layers at the time of infiltration, primarily along the grain surfaces, removing impurities by drainage at the firn/ice transition. We suggest that the same process caused the disturbed and depleted concentration profiles of some TEs. Apparently, TEs were removed with different efficiencies; while some were almost completely depleted, others were not affected or only affected to a minor degree.

**Table 3.1:** Detection limits (DLs), procedural blank concentrations<sup>1</sup> of the discrete ICP-SF-MS analysis, concentration ratios between the mean concentration of the meltwater-affected section and the unaffected sections, mean concentrations within the unaffected part of the ice core segment (time periods 1980-84 and 1990-92)<sup>2</sup>, ionic radii in aqueous solution<sup>3</sup>, and hydrated radii<sup>4</sup> of the investigated TEs. Where more than one oxidation state is stated, the mean of the respective radii is listed.

TE	DL (ng L <sup>-1</sup> )	Procedural blank ultra-pure water <sup>5</sup> (ng L <sup>-1</sup> )	Procedural blank ceramic knife <sup>6</sup> (ng L <sup>-1</sup> )	Concen- tration ratio	Mean concentration in unaffected part (ng L <sup>-1</sup> )	Ionic radius in aqueous solution (pm)	Hy- drated radius <sup>7</sup> (pm)
Ag	2.3	<DL	<DL	1.2±0.23	1.5±0.11	115 (Ag <sup>+</sup> )	341
Al	206	394±406	<DL	0.69±0.22	18700±2800	53 (Al <sup>3+</sup> )	475
Ba	5.2	<DL	15±5.9	0.25±0.08	583±88	136 (Ba <sup>2+</sup> )	404
Bi	1.7	<DL	<DL	0.98±0.35	2.6±0.42	102 (Bi <sup>3+</sup> )	-
Ca	642	958±1020	2400±760	0.08±0.02	136000±24200	100 (Ca <sup>2+</sup> )	412
Cd	0.42	<DL	<DL	0.11±0.04	11±1.4	95 (Cd <sup>2+</sup> )	426
Ce	0.07	0.22±0.27	0.25±0.16	0.71±0.27	89±15	101 (Ce <sup>3+</sup> )	452
Co	0.33	<DL	<DL	0.21±0.06	21±2.8	70 (Co <sup>2+/3+</sup> )	423
Cs	0.90	<DL	<DL	0.77±0.21	3.7±0.38	170 (Cs <sup>+</sup> )	329
Cu	13	<DL	20±0.53	0.71±0.19	111±12	73 (Cu <sup>2+</sup> )	419
Eu	0.21	<DL	<DL	0.60±0.23	2.5±0.41	95 (Eu <sup>3+</sup> )	465
Fe	351	<DL	636±598	0.75±0.22	11300±1430	72 (Fe <sup>2+/3+</sup> )	442.5
La	0.09	0.11±0.16	0.14±0.05	0.71±0.28	40±6.7	105 (La <sup>3+</sup> )	452
Li	11	<DL	<DL	0.54±0.12	18±1.8	69 (Li <sup>+</sup> )	382
Mg	77	89±68	355±109	0.26±0.10	15900±3800	72 (Mg <sup>2+</sup> )	428
Mn	2.7	<DL	7.1±2.2	0.13±0.04	1250±171	83 (Mn <sup>2+</sup> )	438
Mo	2.5	<DL	<DL	0.60±0.17	8.0±0.79	-	-
Na	446	<DL	1030±651	0.22±0.05	16400±1650	102 (Na <sup>+</sup> )	358
Nd	0.06	0.09±0.11	0.08±0.06	0.67±0.26	49±8.3	99 (Nd <sup>3+</sup> )	461
Ni	3.8	4.4±7.7	6.1±6.1	0.21±0.06	77±6.6	69 (Ni <sup>2+</sup> )	404
Pb	48	<DL	<DL	0.73±0.22	1080±139	118 (Pb <sup>2+</sup> )	401
Pr	0.07	<DL	<DL	0.69±0.27	12±2.0	100 (Pr <sup>3+</sup> )	461
Rb	1.5	<DL	<DL	0.49±0.13	46±4.9	149 (Rb <sup>+</sup> )	329
Sb	1.6	<DL	<DL	0.79±0.23	7.8±0.77	77 (Sb <sup>3+</sup> )	-
Sc	0.51	<DL	<DL	0.65±0.21	3.0±0.41	75 (Sc <sup>3+</sup> )	-
Sm	0.07	<DL	<DL	0.65±0.25	10±1.8	96 (Sm <sup>3+</sup> )	462
Sr	5.5	6.6±9.0	5.8±1.5	0.18±0.06	599±90	113 (Sr <sup>2+</sup> )	412
Th	1.1	<DL	<DL	0.59±0.20	5.0±0.63	100 (Th <sup>4+</sup> )	-
Tl	0.68	<DL	<DL	0.38±0.07	1.3±0.13	150 (Tl <sup>+</sup> )	330
U	0.03	0.04±0.06	<DL	0.62±0.19	3.8±0.50	101 (U <sup>3+/4+</sup> )	-
V	2.8	<DL	<DL	0.47±0.14	110±11	72 (V <sup>2+/3+</sup> )	-
W	1.7	<DL	<DL	0.98±0.25	1.4±0.13	-	-
Yb	0.05	<DL	<DL	0.61±0.22	2.4±0.40	87 (Yb <sup>3+</sup> )	475
Zn	67	74±62	76±31	0.26±0.07	868±108	75 (Zn <sup>2+</sup> )	430
Zr	10	<DL	<DL	0.57±0.12	12±1.5	72 (Zr <sup>4+</sup> )	-

<sup>1</sup> Errors given correspond to  $1\sigma$ .

<sup>2</sup> Standard errors are given.

<sup>3</sup> Values from *Marcus* [2015].

<sup>4</sup> Values from *Nightingale* [1959] or *David et al.* [2001].

<sup>5</sup> Procedural blank including decontamination by rinsing samples with ultra-pure water.

<sup>6</sup> Procedural blank including decontamination by scraping all sample faces with a ceramic knife.

<sup>7</sup> Given values refer to the same oxidation state as for the ionic radius in aqueous solution.

### 3.3.2 Quantification of concentration depletion in the meltwater-influenced section

To quantify and directly compare the different behavior of the 35 TEs, a ratio between the mean concentration of the meltwater-affected section (1986-88) and the unaffected sections (1980-84 and 1990-92) was calculated for each TE (Table 3.1). The transition periods, corresponding to the years 1985 and 1989, and the year 1993 were not included in this analysis. The latter showed exceptional elevated summer values for many TEs compared with the previous years. The closer the concentration ratio for a certain TE is to one, the less affected the record in the meltwater-influenced section is. Correspondingly, the closer the ratio is to zero, the more affected the record is. In addition to the influence of meltwater percolation, the concentration ratio can be impacted by changes in atmospheric TE emissions or by changes in the transport of TEs from the emission sources to the high-Alpine sites. For example, the Pb concentration record reveals preserved seasonal variations, but also shows an overall slight decreasing trend (Figure 3.1), which is due to declining anthropogenic Pb emissions since the 1970s [Schwikowski *et al.*, 2004]. Regarding possible changes in transport, the similar seasonal cycles of Cs concentrations during the period 1980-93 indicate a nearly constant dustinput to this high-Alpine site. Thus, we assume that among those three factors that can have an influence on the concentration ratio, meltwater-induced relocation processes are dominant and outweigh possible changes in emissions or transport dynamics, especially, on such a short timescale as discussed here. All TEs had ratios between zero and one, except for Ag ( $1.22 \pm 0.23$ ) (Table 3.1). Concentrations of Ag are to a large extent below the detection limit (Figure 3.1, Table 3.1) and the annual summer maxima within the meltwater-influenced section are more pronounced probably due to elevated emissions in the period 1985-89.

A rank of preservation was established by arranging all TEs in ascending order according to their concentration ratio. This qualitatively shows the relative degree of impact of meltwater percolation on the different TEs within the affected section. The rank of preservation plotted against the concentration ratio (Figure 3.2) demonstrates the impact observed for the 35 TEs and their distinct fractionation after meltwater percolation. Ca shows the strongest depletion, whereas Ag is the least depleted. Group 1 TEs possess a ratio between  $0.38 \pm 0.07$  (Tl) and  $1.22 \pm 0.23$  (Ag) occupying ranks of preservation 1-25, while group 2 TEs have ratios between  $0.08 \pm 0.02$  (Ca) and  $0.26 \pm 0.07$  (Zn), corresponding to the ranks 26-35. The steady decline of the concentration ratios indicates a preferential elution of TEs after meltwater percolation.

### 3.3.3 Causes for preferential elution of TEs

A fractionation of water-soluble major ions was already observed by Eichler *et al.* [2001] within the section of this ice core that consisted of firn when meltwater per-

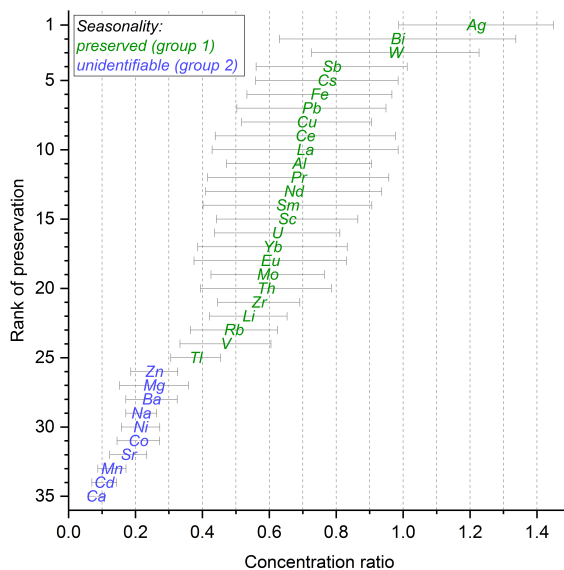


**Figure 3.2:** Rank of preservation plotted against the concentration ratio for each TE. The concentration ratio is defined as the ratio between the mean concentration of the meltwater-affected section (1986-88) and the unaffected sections (1980-84 and 1990-92). Colour coding of the symbols indicates whether a TE kept its seasonal concentration pattern (group 1) or shows a significant depletion and no seasonality can be identified (group 2) within the section affected by meltwater percolation.

colation occurred.  $K^+$ ,  $Na^+$ ,  $Mg^{2+}$ ,  $Ca^{2+}$ , and  $SO_4^{2-}$  were substantially depleted, whereas  $NH_4^+$ ,  $F^-$ ,  $Cl^-$ , and  $NO_3^-$  showed a well-preserved seasonality. A separation of  $Na^+$  and  $Cl^-$  of the initial deposited sea salt aerosol particle supported their conclusion that the different leaching efficiencies were not predominantly caused by precipitation formation or atmospheric scavenging processes. Rather, the different efficiencies were the result of post-depositional rearrangement processes during snow metamorphism causing a redistribution of chemical species according to their solubility in ice. The incorporation of  $NH_4^+$ ,  $F^-$ ,  $Cl^-$ , and  $NO_3^-$  into the ice lattice led to their relative immobility with meltwater percolation. On the contrary,  $K^+$ ,  $Na^+$ ,  $Mg^{2+}$ ,  $Ca^{2+}$ , and  $SO_4^{2-}$ , which have lower solubility in ice, were excluded to grain boundaries where they were more prone to being removed. The assumption that meltwater only percolated along grain surfaces in the firn layers and did not affect the interior of the crystals is corroborated by the completely preserved  $\delta^{18}O$  record (Eichler *et al.* [2001], Figure 3.1).

We assume that post-depositional snow metamorphism significantly affects the spatial distribution of TEs in snow, firn, and ice. Snow metamorphism involves water vapor fluxes which can lead to a mass turnover of up to 60% of the entire ice mass per day inducing changes in the snow microstructure [Pinzer *et al.*, 2012]. During snow metamorphism, initially deposited snowflakes are transformed by continuous sublimation/evaporation and subsequent condensation processes into firn grains, since



larger grains grow at the expense of smaller ones [Davis, 1991]. The rearrangement of TEs within the ice structure during grain growth depends on two properties: (1) the water solubility of the TE or its compounds (e.g. water-insoluble dust particles vs. soluble sea salt aerosols) and (2) their solubility in ice. These factors determine their incorporation in glacier ice and are discussed in the following section considering also the major sources of the investigated TEs.

#### 3.3.4 Incorporation of TEs into glacier ice

Among the set of 35 TEs discussed in this study, the majority are of geogenic origin deposited with mineral dust: Al, Ba, Bi, Ca, Cs, Fe, Li, Mg, Mn, Na, Rb, Sr, Th, Tl, U, W, Zr, and the REEs (Ce, Eu, La, Nd, Pr, Sc, Sm, Yb) [Gabrielli *et al.*, 2008; Gabrieli *et al.*, 2011]. About two-thirds of the mineral dust at the nearby Colle Gnifetti site originate from the Saharan desert [Wagenbach and Geis, 1989]. In Alpine ice cores, Na does not only reflect contributions from mineral dust but also contributions from marine sea salt aerosols [Eichler *et al.*, 2004]. Anthropogenic atmospheric pollution is represented by elevated concentrations of Ag, Cd, Co, Cu, Mo, Ni, Pb, Sb, V, and Zn at alpine sites [Van de Velde *et al.*, 1999, 2000; Barbante *et al.*, 2004; Schwikowski *et al.*, 2004; Gabrielli *et al.*, 2008; Gabrieli *et al.*, 2011]. Nevertheless, those TEs can also be, to a minor extent, of mineral dust origin. In addition, Bi, Cd, and Tl can be tracers for volcanism [Kaspari *et al.*, 2009a; Kellerhals *et al.*, 2010; Gabrielli *et al.*, 2014].

In the atmosphere, aerosol particles comprising TEs can be incorporated into the core of snow crystals by acting as ice nuclei as it is known for mineral dust aerosols [Szyrmer and Zawadzki, 1997]. Accumulation of supercooled water droplets onto ice crystal surfaces (riming) or direct impaction of aerosol particles on snow crystals usually results in the enrichment of impurities at the edges of the crystal [Mosimann *et al.*, 1994; Pruppacher and Klett, 2010]. As explained above, we suggest that these processes play a minor role in determining the final location of TEs in ice. The location is predominantly determined by the effect of snow metamorphism.

##### 3.3.4.1 Water-insoluble TEs

Al, Fe, Zr, and the REEs likely originated from water-insoluble mineral dust as particles containing these TEs typically reveal a water solubility of <10% [Greaves *et al.*, 1994; Birmili *et al.*, 2006; Hsu *et al.*, 2010; Li *et al.*, 2015]. Those particles are most likely enriched at grain boundaries during snow metamorphism, even if initially deposited as condensation nuclei in the snow grain interior. Such an enrichment of Fe and Al was shown for clear bands in Greenland ice [Della Lunga *et al.*, 2014]. Although enriched on grain surfaces, their insolubility in water results in immobility with meltwater, explaining the retention of their seasonality within the section affected by meltwater percolation (Figure 3.2). This interpretation is in agreement with the work performed by Wong *et al.* [2013], where artificial meltwater

infiltration in Greenland snow pack showed that, in particular, REEs are relatively immobile during meltwater percolation, and tend to keep their seasonally varying signal.

### 3.3.4.2 Partially water-soluble TEs

Compounds exhibiting low water solubility like terrestrial Ba, Ca, or Mg sulphate and carbonate salts are present as ions below their solubility limit. Compounds featuring high water solubility like salts of alkali metals (Cs, Na, Li, Rb) predominantly occur as ions in snow and ice. These ions can be either incorporated into the ice lattice or segregated to grain boundaries during snow metamorphism.

Ions might be incorporated into the ice lattice following two different mechanisms. First, they can substitute water molecules located on lattice sites as suggested for  $\text{NH}_4^+$ ,  $\text{F}^-$ ,  $\text{Cl}^-$ , and  $\text{NO}_3^-$  [Zaromb and Brill, 1956; Eichler *et al.*, 2001; Petrenko and Whitworth, 2002]. To be incorporated into the ice lattice site without significant additional strain, chemical impurities need to be of similar size and type as the oxygen atom of the water molecule to be substituted [Wolff, 1996]. The more similar in size dopants are compared to that of a water molecule (diameter 2.75 Å), the more likely is substitution on lattice sites [Hobbs, 1974]. Second, impurities can also occupy interstitial sites as proposed for  $\text{K}^+$  regarding the incorporation of KOH in the ice lattice [Petrenko and Whitworth, 2002]. Hexagonal ice  $\text{I}_h$  possesses two kinds of interstices denoted as capped trigonal (Tc) and uncapped trigonal site (Tu). The Tu site (Figure 3.3), which features a distance between its center and the edges of 2.95 Å, has been shown to be a more stable host for interstitial species such as water molecules [Itoh *et al.*, 1996].

Hereafter, we discuss factors possibly influencing whether TEs associated with (low) water-soluble compounds are incorporated into the ice lattice or segregated to grain boundaries. Our analysis reveals that the concentration and the atomic mass of TEs appear to have a major effect whereas TE size does not seem to play a role.

**Influence of trace element size** For examining the influence of atomic size on the two possible ways of incorporation in ice (occupation of Tu interstitial space or a lattice site), we assumed that TEs originating from (low) water-soluble compounds are present as ions. Accordingly, we investigated the relationship between the concentration ratios of the TEs and the corresponding ionic radii in aqueous solution as well as the hydrated ionic radii (Table 3.1, Figure 3.3). No significant correlation ( $R^2 < 0.05$ ) was found either between the hydrated or the ionic radii in aqueous solution and the concentration ratio, even after removing Al, Fe, Zr, and the REEs primarily not present as ions but insoluble particles (Figure 3.3). There is also no evident dependency between the concentration ratio and the distribution of the ionic radii in aqueous solution around the radius of a water molecule; TEs having a similar ionic radius as the water molecule such as Ba, Rb, Tl do not have the highest concentration ratios. Except for Cs, Rb, and Tl, all other TEs have smaller ionic

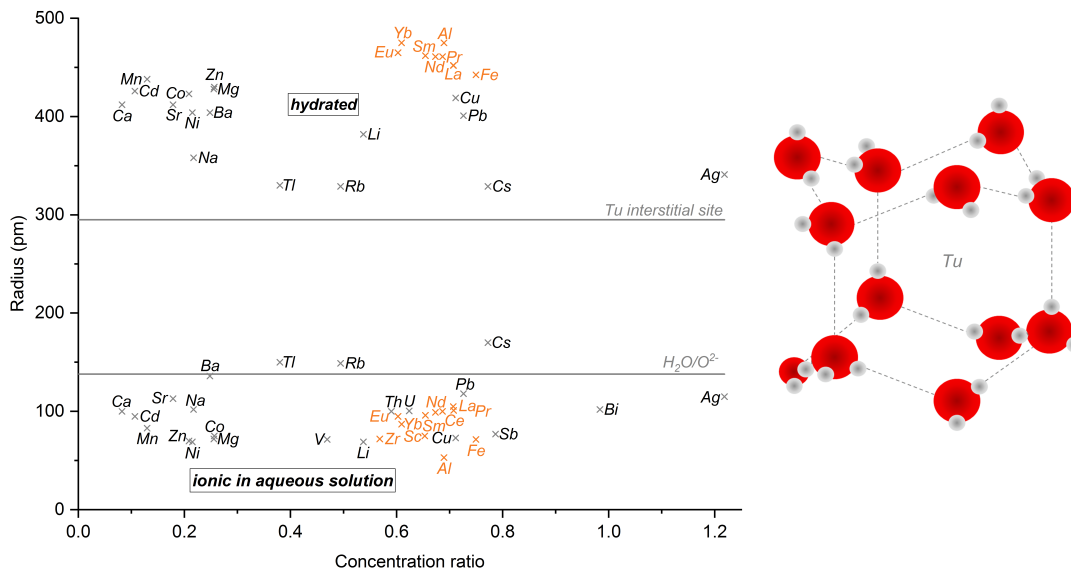


**Figure 3.3:** Left: Hydrated and ionic radii in aqueous solution (Table 3.1) plotted against the concentration ratio of the corresponding TEs. Data points shown in orange represent TEs which are most likely not present as ions but rather as insoluble compounds. The radius of a water molecule, and the distance between the center and the edges of the uncapped trigonal (Tu) interstitial site in ice  $I_h$ , likely to host interstitials, are depicted as horizontal lines. Right: Sketch of the Tu site (adapted from *Itoh et al.* [1996]). Oxygen and hydrogen atoms are shown as red and gray spheres, respectively.

radii than that of the water molecule suggesting that they could substitute water molecules on lattice sites. Concerning a possible occupation of the Tu interstitial site, it appears that the ionic radii are invariably smaller than the distance between the center and the edges of the Tu interstitial site. This means that all TEs could be incorporated interstitially if present as ions. In contrast, hydrated ionic radii of all TEs are significantly larger than the radius of the Tu site implying that incorporation with a hydration shell is unlikely. Our results suggest that although almost all TEs could substitute a water molecule or be interstitially incorporated into the ice lattice if present as ions, the size of TEs is not the controlling factor affecting their preservation in the presence of meltwater.

**Influence of trace element concentrations and atomic mass** One fundamental property of a TE in glacier ice is the average concentration it exhibits; this generally reflects the corresponding atmospheric concentration levels [*Kaspari et al.*, 2009b]. Concentrations of TEs can be largely site-specific, such as mineral dust related TEs [*Beaudon et al.*, 2017]. Here, the mean concentrations of each TE within the two unaffected parts of the ice core segment (1980-84 and 1990-92, Table 3.1) were assumed to be representative of an ice core segment where no meltwater percolation

took place. This assumption is justified because mean TE concentrations in ice cores from the nearby Colle Gnifetti saddle [Barbante *et al.*, 2004; Schwikowski *et al.*, 2004; Gabrieli, 2008], the Dôme de Goûter, Mont Blanc Massif [Barbante *et al.*, 1999] and from a snow pit from Alto dell’Ortles glacier located in the Eastern European Alps [Gabrieli *et al.*, 2011] are largely within the same orders of magnitude. Nevertheless, it should be noted that these reported mean concentrations do not cover exactly the same time period.

Figure 3.4 shows the mean concentration for each TE (logarithmic scale) plotted against the respective concentration ratio together with an exponential fit. A significant negative correlation ( $R^2 = 0.25$ ) was observed indicating that TEs occurring in low concentration tend to have higher concentration ratios whereas TEs with higher concentrations are mostly associated with low concentration ratios. This trend becomes even more pronounced if the TEs associated with insoluble particles (Al, Fe, Zr, REEs) are excluded ( $R^2 = 0.41$ ). Based on these results, we suggest that atmospheric concentration levels are a major driving force determining whether TEs originating from (low) soluble compounds are incorporated into the ice lattice or segregated to the grain surfaces. Abundant TEs such as Ca, Mg, Mn, Na, or Zn are likely to be segregated to the grain boundaries, since their concentrations exceed solubility limits in ice, and are thus prone to relocation by meltwater. TEs present in ultra-trace amounts including Ag, Bi, Cs, Sb, or W tend to be incorporated into the ice lattice as indicated by a strong preservation of these TEs in the meltwater-affected section.

A significant correlation coefficient of  $R^2 = 0.18$  was obtained for a linear fit between the atomic mass of the measured isotopes and the concentration ratio (Figure 3.4). The fact that heavier TEs tend to be related to higher concentration ratios is presumably linked to the dependence between the average concentration in ice and the atomic mass. The average concentration in glacier ice serves as an indicator for the atmospheric concentration level, which is by itself connected to the overall abundance of a TE. Abundant TEs significantly contributing to the composition of the Earth’s crust generally possess lower masses compared with the ones with higher masses that are rarer [Allègre *et al.*, 2001]. Like the mean concentration, the correlation becomes stronger ( $R^2 = 0.24$ ) if TEs related to insoluble particles are excluded.

Our analysis showed that TEs originating from (low) water-soluble compounds present in ultra-trace amounts and characterized by large atomic masses tend to be preserved, while no influence regarding the size of TEs could be identified. TEs related to mineral dust particles are likely to be enriched at grain boundaries, but resistant to meltwater percolation due to water insolubility.

### 3.3.5 Implications

This study advances the understanding of TE preservation patterns in ice cores from glaciers partially affected by melting. This is necessary for evaluating the potential

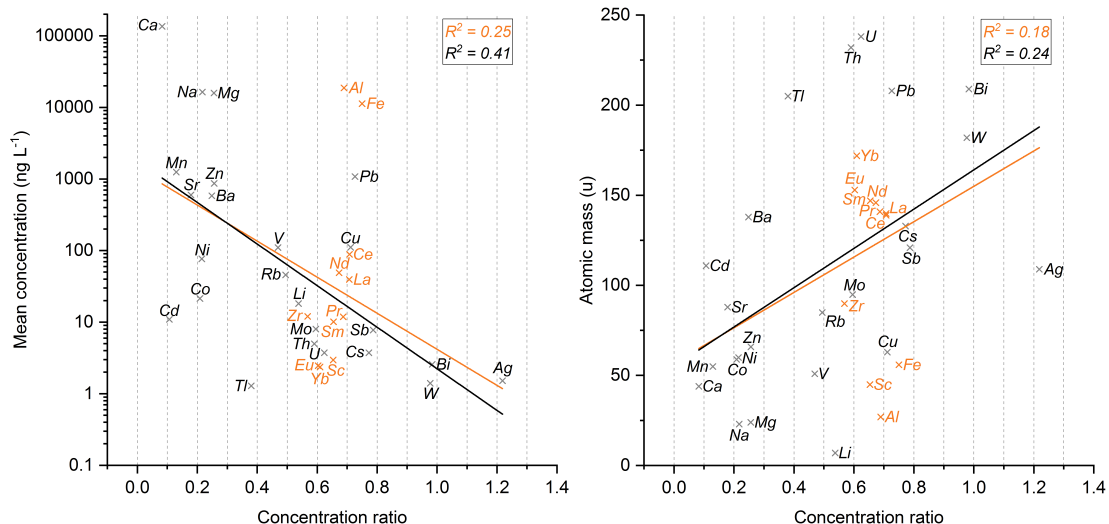


**Figure 3.4:** Left: Mean concentration within the unaffected part of the ice core segment (logarithmic axis, time periods 1980-84 and 1990-92, Table 3.1) plotted against the concentration ratio of each TE. Right: Atomic mass of the measured isotopes (data from *Bruno and Svoronos [2017]*) plotted against the concentration ratio of each TE. The orange lines represent an exponential (left) and a linear fit (right), respectively including all 35 TEs (corresponding correlation coefficients in orange). The black lines represent the fit excluding Al, Fe, Zr, and the REEs (corresponding correlation coefficients in black).

of TEs as environmental proxies, especially for future interpretation of paleo atmospheric TE ice core records from high-mountain glaciers. High-mountain glaciers are increasingly prone to melt processes even in the highest accumulation areas [*Zhang et al., 2015*].

Among the set of TEs contained in mineral dust, Al, Bi, Cs, Fe, Li, Rb, Th, Tl, U, W, Zr, and the REEs (Ce, Eu, La, Nd, Pr, Sc, Sm, Yb) stand out at the investigated high-Alpine site due to their resistance to mobilization by meltwater percolation (Figs 1, 2). Ba, Ca, Mg, Mn, Na, and Sr, however, showed concentration records heavily impacted by meltwater percolation (Figure 3.1 and Figure 3.2), and are therefore not recommended to be used as mineral dust proxies in cases where meltwater formation occurred.

Within the group of TEs representative of anthropogenic atmospheric pollution, Cd, Co, Ni, and Zn were significantly depleted in the section affected by meltwater, thereby their seasonal variation could not be identified anymore (group 2, Figure 3.1 and Figure 3.2). These TEs are commonly emitted to the atmosphere due to human activities such as metallurgic processes or fuel combustion [*Pacyna and Pacyna, 2001*]. In contrast, Ag, Cu, Mo, Pb, Sb, and V exhibited an exceptional robustness regarding post-depositional melting processes (group 1, Figure 3.1 and Figure 3.2). In this group, Pb has been extensively used as a proxy for metal smelting, mining

activities, coal combustion and use of leaded gasoline in ice cores [Huo *et al.*, 1999; McConnell *et al.*, 2002; Schwikowski *et al.*, 2004; Shotyk *et al.*, 2005; Li *et al.*, 2006; Osterberg *et al.*, 2008; Lee *et al.*, 2011; Eichler *et al.*, 2012]. Based on these observations, we suggest that Ag, Cu, Mo, Pb, Sb, and V could still serve as tracers to reconstruct and estimate the impact of human emissions to the atmosphere [Galloway *et al.*, 1982] from melt-affected ice core archives. However, Cd, Co, Ni, and Zn records should be interpreted with caution due to probable meltwater mobility. Regarding volcanism, in addition to the previously mentioned Pb and Sb, Bi and Tl tend to be reliable proxies in melt-affected ice core records. Also, volcanic ejection material is often enriched in Cd and Zn [Nho *et al.*, 1996], but as discussed above, the use of Cd and Zn as tracers is not recommended.

Group 1 TEs, with their pronounced and less affected seasonal concentration variability, could also serve as markers for annual layer counting to establish the chronology of ice cores affected by post-depositional melt processes.

Our study demonstrates that many TEs are still valuable environmental proxies even if partial melting occurs at high-Alpine sites. One should note that our results are not rigorously transferable to ice core archives from other locations. Our findings show that the preservation of TEs during melting is determined by their concentrations and the dust mineralogy. Both parameters are site-specific. For instance, TE concentrations in ice cores from the remote Greenland and Antarctic ice sheets [Candelone *et al.*, 1995; Vallelonga *et al.*, 2003] can be up to three orders of magnitude lower compared with Alpine sites. According to our findings, the low concentrations at these sites could generally favor preservation of TEs during melting. In contrast, higher TE concentrations occur in ice cores from the Tibetan Plateau, especially for mineral dust related TEs [Beaudon *et al.*, 2017; Sierra-Hernández *et al.*, 2018]. At these sites, concentration records of (low) water-soluble mineral dust related TEs assigned to group 1 in our study could be significantly disturbed by meltwater percolation. Contrariwise, higher mineral dust loading favors the presence of water-insoluble particles, less prone to meltwater relocation.

### 3.4 Conclusions

The analysis of 35 TEs in a 50 m ice core segment from upper Grenzgletscher is presented here. This segment of the ice core comprised a 16 m section that consisted of firn when an inflow and percolation of meltwater occurred. The special setting of sections unaffected by meltwater above and below this melt-affected section in the studied ice core segment provided good references for characterizing the TE response to post-depositional melting processes at high-Alpine sites.

Some TEs revealed significant concentration depletion due to meltwater-induced relocation, whereas others were well preserved depending on their water solubility and location at the grain scale. TEs linked to insoluble particles, typically enriched at grain boundaries, were found to be mostly preserved, because their insolubility in

water results in immobility with meltwater percolation. In the case of TEs present as (low) soluble compounds, variable mobility with meltwater was observed presumably due to a different microscopic location in the ice structure. We suggest that for those TEs, the concentration present is the major driving force determining their incorporation into the ice lattice or segregation to the grain surfaces. The size of the corresponding ions has a negligible effect. Further studies, preferably using direct *in situ* techniques, are needed to corroborate this indirect assessment of TE location in ice.

Based on their immobility with meltwater percolation, we propose that Ag, Al, Bi, Cu, Cs, Fe, Li, Mo, Pb, Rb, Sb, Th, Tl, U, V, W, Zr, and the REEs (Ce, Eu, La, Nd, Pr, Sc, Sm, Yb) may still be applicable as robust environmental proxies in ice cores from Alpine glaciers partially affected by melting. In contrast, concentration records of Ba, Ca, Cd, Co, Mg, Mn, Na, Ni, Sr, and Zn are prone to significant depletion.

Site-specific variations in TE concentrations and mineralogy are likely to modify our established classification. Thus, TE response to post-depositional melting processes may vary between remote sites and heavily polluted regions.

## Acknowledgments

Funding by the Swiss National Science Foundation (SNSF, Grant No. 155999) is gratefully acknowledged. We also thank Leonhard Tobler for introducing SEA to the ICP-MS analysis and Jacinta Edebeli for improving the English of the manuscript. We greatly appreciate the detailed comments and suggestions of the two anonymous referees. They helped to improve the clarity of the manuscript.

## Bibliography

- Allègre, C., G. Manhès, and É. Lewin, Chemical composition of the Earth and the volatility control on planetary genetics, *Earth and Planetary Science Letters*, 185(1-2), 49–69, doi:10.1016/S0012-821X(00)00359-9, 2001.
- Baltensperger, U., H. W. Gäggeler, D. T. Jost, M. Lugauer, M. Schwikowski, E. Weingartner, and P. Seibert, Aerosol climatology at the high-alpine site Jungfraujoch, Switzerland, *Journal of Geophysical Research: Atmospheres*, 102(D16), 19,707–19,715, doi:10.1029/97JD00928, 1997.
- Barbante, C., G. Cozzi, G. Capodaglio, K. van de Velde, C. Ferrari, C. Boutron, and P. Cescon, Trace element determination in alpine snow and ice by double focusing inductively coupled plasma mass spectrometry with microconcentric nebulization, *Journal of Analytical Atomic Spectrometry*, 14(9), 1433–1438, doi:10.1039/a901949i, 1999.
- Barbante, C., et al., Historical Record of European Emissions of Heavy Metals to the Atmosphere Since the 1650s from Alpine Snow/Ice Cores Drilled near Monte Rosa, *Environmental Science & Technology*, 38(15), 4085–4090, doi:10.1021/es049759r, 2004.
- Beaudon, E., P. Gabrielli, M. R. Sierra-Hernández, A. Wegner, and L. G. Thompson, Central Tibetan Plateau atmospheric trace metals contamination: A 500-year record

- from the Puruogangri ice core, *Science of The Total Environment*, 601-602, 1349–1363, doi:10.1016/j.scitotenv.2017.05.195, 2017.
- Birmili, W., A. G. Allen, F. Bary, and R. M. Harrison, Trace Metal Concentrations and Water Solubility in Size-Fractionated Atmospheric Particles and Influence of Road Traffic, *Environmental Science & Technology*, 40(4), 1144–1153, doi:10.1021/es0486925, 2006.
- Bruno, T. J., and P. D. Svoronos, Atomic Masses and Abundances, in *CRC Handbook of Chemistry and Physics, 98th Edition*, edited by J. R. Rumble, CRC Press/Taylor & Francis, Boca Raton, FL, 2017.
- Candelone, J.-P., S. Hong, C. Pellone, and C. F. Boutron, Post-Industrial Revolution changes in large-scale atmospheric pollution of the northern hemisphere by heavy metals as documented in central Greenland snow and ice, *Journal of Geophysical Research*, 100(D8), 16,605, doi:10.1029/95JD00989, 1995.
- Correia, A., R. Freydier, R. J. Delmas, J. C. Simões, J.-D. Taupin, B. Dupré, and P. Artaxo, Trace elements in South America aerosol during 20th century inferred from a Nevado Illimani ice core, Eastern Bolivian Andes (6350 m asl), *Atmospheric Chemistry and Physics*, 3(5), 1337–1352, doi:10.5194/acp-3-1337-2003, 2003.
- David, F., V. Vokhmin, and G. Ionova, Water characteristics depend on the ionic environment. Thermodynamics and modelisation of the aquo ions, *Journal of Molecular Liquids*, 90(1-3), 45–62, doi:10.1016/S0167-7322(01)00106-4, 2001.
- Davis, R. E., Links Between Snowpack Physics and Snowpack Chemistry, in *Seasonal Snowpacks*, pp. 115–138, Springer Berlin Heidelberg, Berlin, Heidelberg, doi:10.1007/978-3-642-75112-7\_5, 1991.
- Della Lunga, D., W. Müller, S. O. Rasmussen, and A. Svensson, Location of cation impurities in NGRIP deep ice revealed by cryo-cell UV-laser-ablation ICPMS, *Journal of Glaciology*, 60(223), 970–988, doi:10.3189/2014JoG13J199, 2014.
- Döscher, A., H. W. Gäggeler, U. Schotterer, and M. Schwikowski, A130 years deposition record of sulfate, nitrate and chloride from a high-alpine glacier, *Water, Air, & Soil Pollution*, 85(2), 603–609, doi:10.1007/BF00476895, 1995.
- Eichler, A., M. Schwikowski, and H. W. Gäggeler, An Alpine ice-core record of anthropogenic HF and HCl emissions, *Geophysical Research Letters*, 27(19), 3225–3228, doi:10.1029/2000GL012006, 2000a.
- Eichler, A., M. Schwikowski, H. W. Gäggeler, V. Furrer, H.-A. Synal, J. Beer, M. Saurer, and M. Funk, Glaciochemical dating of an ice core from upper Grenzgletscher (4200 m a.s.l.), *Journal of Glaciology*, 46(154), 507–515, doi:10.3189/172756500781833098, 2000b.
- Eichler, A., M. Schwikowski, and H. W. Gäggeler, Meltwater-induced relocation of chemical species in Alpine firn, *Tellus B: Chemical and Physical Meteorology*, 53(2), 192–203, doi:10.3402/tellusb.v53i2.16575, 2001.
- Eichler, A., M. Schwikowski, M. Furger, U. Schotterer, and H. W. Gäggeler, Sources and distribution of trace species in Alpine precipitation inferred from two 60-year ice core paleorecords, *Atmospheric Chemistry and Physics Discussions*, 4(1), 71–108, doi:10.5194/acpd-4-71-2004, 2004.
- Eichler, A., L. Tobler, S. Eyrikh, G. Gramlich, N. Malygina, T. Papina, and M. Schwikowski, Three Centuries of Eastern European and Altai Lead Emissions Recorded in a Belukha Ice Core, *Environmental Science & Technology*, 46(8), 4323–4330, doi:10.1021/es2039954, 2012.
- Eichler, A., L. Tobler, S. Eyrikh, N. Malygina, T. Papina, and M. Schwikowski, Ice-Core Based Assessment of Historical Anthropogenic Heavy Metal (Cd, Cu, Sb, Zn) Emissions in the Soviet Union, *Environmental Science & Technology*, 48(5), 2635–2642, doi:10.1021/es404861n, 2014.



- Eichler, A., G. Gramlich, T. Kellerhals, L. Tobler, and M. Schwikowski, Pb pollution from leaded gasoline in South America in the context of a 2000-year metallurgical history, *Science Advances*, 1(2), e1400196, doi:10.1126/sciadv.1400196, 2015.
- Eichler, A., G. Gramlich, T. Kellerhals, L. Tobler, T. Rehren, and M. Schwikowski, Ice-core evidence of earliest extensive copper metallurgy in the Andes 2700 years ago, *Scientific Reports*, 7, 41,855, doi:10.1038/srep41855, 2017.
- Eyrikh, S., A. Eichler, L. Tobler, N. Malygina, T. Papina, and M. Schwikowski, A 320 Year Ice-Core Record of Atmospheric Hg Pollution in the Altai, Central Asia, *Environmental Science & Technology*, 51(20), 11,597–11,606, doi:10.1021/acs.est.7b03140, 2017.
- Gabrieli, J., Trace elements and polycyclic aromatic hydrocarbons (PAHs) in snow and ice sampled at Colle Gnifetti, Monte Rosa (4450 m), during the past 10,000 years: environmental and climatic implications, Ph.D. thesis, University Ca' Foscari of Venice, Italy, 2008.
- Gabrieli, J., et al., Impact of Po Valley emissions on the highest glacier of the Eastern European Alps, *Atmospheric Chemistry and Physics*, 11(15), 8087–8102, doi:10.5194/acp-11-8087-2011, 2011.
- Gabrielli, P., G. Cozzi, S. Torcini, P. Cescon, and C. Barbante, Trace elements in winter snow of the Dolomites (Italy): A statistical study of natural and anthropogenic contributions, *Chemosphere*, 72(10), 1504–1509, doi:10.1016/j.chemosphere.2008.04.076, 2008.
- Gabrielli, P., D. Hardy, N. Kehrwald, M. Davis, G. Cozzi, C. Turetta, C. Barbante, and L. Thompson, Deglaciated areas of Kilimanjaro as a source of volcanic trace elements deposited on the ice cap during the late Holocene, *Quaternary Science Reviews*, 93, 1–10, doi:10.1016/j.quascirev.2014.03.007, 2014.
- Galloway, J. N., J. Thornton, S. A. Norton, H. L. Volchok, and R. A. McLean, Trace metals in atmospheric deposition: A review and assessment, *Atmospheric Environment (1967)*, 16(7), 1677–1700, doi:10.1016/0004-6981(82)90262-1, 1982.
- Greaves, M., P. Statham, and H. Elderfield, Rare earth element mobilization from marine atmospheric dust into seawater, *Marine Chemistry*, 46(3), 255–260, doi:10.1016/0304-4203(94)90081-7, 1994.
- Grigholm, B., et al., Mid-twentieth century increases in anthropogenic Pb, Cd and Cu in central Asia set in hemispheric perspective using Tien Shan ice core, *Atmospheric Environment*, 131, 17–28, doi:10.1016/j.atmosenv.2016.01.030, 2016.
- Hobbs, P. V., *Ice Physics*, Oxford University Press, Oxford, 1974.
- Hong, S., et al., Atmospheric heavy metals in tropical South America during the past 22 000 years recorded in a high altitude ice core from Sajama, Bolivia, *J. Environ. Monit.*, 6(4), 322–326, doi:10.1039/B314251E, 2004.
- Hsu, S.-C., et al., Sources, solubility, and dry deposition of aerosol trace elements over the East China Sea, *Marine Chemistry*, 120, 116–127, doi:10.1016/j.marchem.2008.10.003, 2010.
- Huo, W., T. Yao, and Y. Li, Increasing atmospheric pollution revealed by Pb record of a 7 000-m ice core, *Chinese Science Bulletin*, 44(14), 1309–1312, doi:10.1007/BF02885851, 1999.
- Huss, M., et al., Toward mountains without permanent snow and ice, *Earth's Future*, 5(5), 418–435, doi:10.1002/2016EF000514, 2017.
- Itoh, H., K. Kawamura, T. Hondoh, and S. Mae, Molecular dynamics studies of self-interstitials in ice Ih, *The Journal of Chemical Physics*, 105(6), 2408–2413, doi:10.1063/1.472108, 1996.
- Kaspari, S., P. A. Mayewski, M. Handley, S. Kang, S. Hou, S. Sneed, K. Maasch, and D. Qin, A High-Resolution Record of Atmospheric Dust Composition and Variability since A.D. 1650 from a Mount Everest Ice Core, *Journal of Climate*, 22(14), 3910–3925, doi:10.1175/2009JCLI2518.1, 2009a.

- Kaspari, S., P. A. Mayewski, M. Handley, E. Osterberg, S. Kang, S. Sneed, S. Hou, and D. Qin, Recent increases in atmospheric concentrations of Bi, U, Cs, S and Ca from a 350-year Mount Everest ice core record, *Journal of Geophysical Research*, *114*, D04,302, doi:10.1029/2008JD011088, 2009b.
- Kellerhals, T., L. Tobler, S. Brüttsch, M. Sigl, L. Wacker, H. W. Gäggeler, and M. Schwikowski, Thallium as a Tracer for Preindustrial Volcanic Eruptions in an Ice Core Record from Illimani, Bolivia, *Environmental Science & Technology*, *44*(3), 888–893, doi:10.1021/es902492n, 2010.
- Knüsel, S., D. E. Piguët, M. Schwikowski, and H. W. Gäggeler, Accuracy of Continuous Ice-Core Trace-Element Analysis by Inductively Coupled Plasma Sector Field Mass Spectrometry, *Environmental Science & Technology*, *37*(10), 2267–2273, doi:10.1021/es026452o, 2003.
- Lee, K., S. D. Hur, S. Hou, L. J. Burn-Nunes, S. Hong, C. Barbante, C. F. Boutron, and K. J. Rosman, Isotopic signatures for natural versus anthropogenic Pb in high-altitude Mt. Everest ice cores during the past 800 years, *Science of The Total Environment*, *412-413*, 194–202, doi:10.1016/j.scitotenv.2011.10.002, 2011.
- Li, T., Y. Wang, W. J. Li, J. M. Chen, T. Wang, and W. X. Wang, Concentrations and solubility of trace elements in fine particles at a mountain site, southern China: regional sources and cloud processing, *Atmospheric Chemistry and Physics*, *15*(15), 8987–9002, doi:10.5194/acp-15-8987-2015, 2015.
- Li, Z., T. Yao, L. Tian, B. Xu, and Y. Li, Atmospheric Pb variations in Central Asia since 1955 from Muztagata ice core record, eastern Pamirs, *Chinese Science Bulletin*, *51*(16), 1996–2000, doi:10.1007/s11434-006-2061-9, 2006.
- Marcott, S. A., J. D. Shakun, P. U. Clark, and A. C. Mix, A Reconstruction of Regional and Global Temperature for the Past 11,300 Years, *Science (New York, N.Y.)*, *339*(6124), 1198–1201, doi:10.1126/science.1228026, 2013.
- Marcus, Y., Ions and their Properties, in *Ions in Solution and their Solvation*, pp. 10–62, John Wiley & Sons, Inc, Hoboken, NJ, doi:10.1002/9781118892336, 2015.
- Mariani, I., A. Eichler, T. M. Jenk, S. Brönnimann, R. Auchmann, M. C. Leuenberger, and M. Schwikowski, Temperature and precipitation signal in two Alpine ice cores over the period 1961–2001, *Climate of the Past*, *10*(3), 1093–1108, doi:10.5194/cp-10-1093-2014, 2014.
- McConnell, J. R., G. W. Lamorey, and M. A. Hutterli, A 250-year high-resolution record of Pb flux and crustal enrichment in central Greenland, *Geophysical Research Letters*, *29*(23), doi:10.1029/2002GL016016, 2002.
- Mosimann, L., E. Weingartner, and A. Waldvogel, An Analysis of Accreted Drop Sizes and Mass on Rimed Snow Crystals, *Journal of the Atmospheric Sciences*, *51*(11), 1548–1558, doi:10.1175/1520-0469(1994)051<1548:AAOADS>2.0.CO;2, 1994.
- Müller-Tautges, C., A. Eichler, M. Schwikowski, G. B. Pezzatti, M. Conedera, and T. Hoffmann, Historic records of organic compounds from a high Alpine glacier: influences of biomass burning, anthropogenic emissions, and dust transport, *Atmospheric Chemistry and Physics*, *16*(2), 1029–1043, doi:10.5194/acp-16-1029-2016, 2016.
- Nho, E.-Y., M.-F. Le Cloarec, B. Ardouin, and W. Tjetjep, Source strength assessment of volcanic trace elements emitted from the Indonesian arc, *Journal of Volcanology and Geothermal Research*, *74*(1-2), 121–129, doi:10.1016/S0377-0273(96)00051-0, 1996.
- Nightingale, E. R., Phenomenological Theory of Ion Solvation. Effective Radii of Hydrated Ions, *The Journal of Physical Chemistry*, *63*(9), 1381–1387, doi:10.1021/j150579a011, 1959.
- Osterberg, E., et al., Ice core record of rising lead pollution in the North Pacific atmosphere, *Geophysical Research Letters*, *35*(L05810), doi:10.1029/2007GL032680, 2008.

- Pacyna, J. M., and E. G. Pacyna, An assessment of global and regional emissions of trace metals to the atmosphere from anthropogenic sources worldwide, *Environmental Reviews*, 9(4), 269–298, doi:10.1139/a01-012, 2001.
- Pavlova, P. A., T. M. Jenk, P. Schmid, C. Bogdal, C. Steinlin, and M. Schwikowski, Polychlorinated Biphenyls in a Temperate Alpine Glacier: 1. Effect of Percolating Meltwater on their Distribution in Glacier Ice, *Environmental Science & Technology*, 49(24), 14,085–14,091, doi:10.1021/acs.est.5b03303, 2015.
- Petrenko, V. F., and R. W. Whitworth, *Physics of Ice*, Oxford University Press, Oxford, doi:10.1093/acprof:oso/9780198518945.001.0001, 2002.
- Pinzer, B. R., M. Schneebeli, and T. U. Kaempfer, Vapor flux and recrystallization during dry snow metamorphism under a steady temperature gradient as observed by time-lapse microtomography, *The Cryosphere*, 6(5), 1141–1155, doi:10.5194/tc-6-1141-2012, 2012.
- Pruppacher, H., and J. Klett, *Microphysics of Clouds and Precipitation*, *Atmospheric and Oceanographic Sciences Library*, vol. 18, Springer Netherlands, Dordrecht, doi:10.1007/978-0-306-48100-0, 2010.
- Schwikowski, M., M. Schläppi, P. Santibañez, A. Rivera, and G. Casassa, Net accumulation rates derived from ice core stable isotope records of Pío XI glacier, Southern Patagonia Icefield, *The Cryosphere*, 7(5), 1635–1644, doi:10.5194/tc-7-1635-2013, 2013.
- Schwikowski, M., et al., Post-17th-Century Changes of European Lead Emissions Recorded in High-Altitude Alpine Snow and Ice, *Environmental Science & Technology*, 38(4), 957–964, doi:10.1021/es034715o, 2004.
- Shotyk, W., J. Zheng, M. Krachler, C. Zdanowicz, R. Koerner, and D. Fisher, Predominance of industrial Pb in recent snow (1994–2004) and ice (1842–1996) from Devon Island, Arctic Canada, *Geophysical Research Letters*, 32(L21814), doi:10.1029/2005GL023860, 2005.
- Sierra-Hernández, M. R., P. Gabrielli, E. Beaudon, A. Wegner, and L. G. Thompson, Atmospheric depositions of natural and anthropogenic trace elements on the Guliya ice cap (northwestern Tibetan Plateau) during the last 340 years, *Atmospheric Environment*, 176, 91–102, doi:10.1016/j.atmosenv.2017.11.040, 2018.
- Szyrmer, W., and I. Zawadzki, Biogenic and Anthropogenic Sources of Ice-Forming Nuclei: A Review, *Bulletin of the American Meteorological Society*, 78(2), 209–228, doi:10.1175/1520-0477(1997)078<0209:BAASOI>2.0.CO;2, 1997.
- Thompson, L., E. Mosley-Thompson, M. Davis, P. Lin, T. Yao, M. Dyurgerov, and J. Dai, “Recent warming”: ice core evidence from tropical ice cores with emphasis on Central Asia, *Global and Planetary Change*, 7(1-3), 145–156, doi:10.1016/0921-8181(93)90046-Q, 1993.
- Uglietti, C., P. Gabrielli, C. A. Cooke, P. Vallelonga, and L. G. Thompson, Widespread pollution of the South American atmosphere predates the industrial revolution by 240 y, *Proceedings of the National Academy of Sciences*, 112(8), 2349–2354, doi:10.1073/pnas.1421119112, 2015.
- Vallelonga, P., J.-P. Candelone, K. Van de Velde, M. Curran, V. Morgan, and K. Rosman, Lead, Ba and Bi in Antarctic Law Dome ice corresponding to the 1815 AD Tambora eruption: an assessment of emission sources using Pb isotopes, *Earth and Planetary Science Letters*, 211(3-4), 329–341, doi:10.1016/S0012-821X(03)00208-5, 2003.
- Van de Velde, K., C. Ferrari, C. Barbante, I. Moret, T. Bellomi, S. Hong, and C. Boutron, A 200 Year Record of Atmospheric Cobalt, Chromium, Molybdenum, and Antimony in High Altitude Alpine Firn and Ice, *Environmental Science & Technology*, 33(20), 3495–3501, doi:10.1021/es990066y, 1999.

- Van de Velde, K., C. F. Boutron, C. P. Ferrari, A.-L. Moreau, R. J. Delmas, C. Barbante, T. Bellomi, G. Capodaglio, and P. Cescon, A two hundred years record of atmospheric cadmium, copper and zinc concentrations in high altitude snow and ice from the French-Italian Alps, *Geophysical Research Letters*, 27(2), 249–252, doi:10.1029/1999GL010786, 2000.
- Wagenbach, D., and K. Geis, The Mineral Dust Record in a High Altitude Alpine Glacier (Colle Gnifetti, Swiss Alps), in *Paleoclimatology and Paleometeorology: Modern and Past Patterns of Global Atmospheric Transport*, pp. 543–564, Springer Netherlands, Dordrecht, doi:10.1007/978-94-009-0995-3\_23, 1989.
- Wolff, E. W., Location, Movement and Reactions of Impurities in Solid Ice, in *Chemical Exchange Between the Atmosphere and Polar Snow*, pp. 541–560, Springer Berlin Heidelberg, Berlin, Heidelberg, doi:10.1007/978-3-642-61171-1\_23, 1996.
- Wong, G. J., R. L. Hawley, E. R. Lutz, and E. C. Osterberg, Trace-element and physical response to melt percolation in Summit (Greenland) snow, *Annals of Glaciology*, 54(63), 52–62, doi:10.3189/2013AoG63A602, 2013.
- Zaromb, S., and R. Brill, Solid Solutions of Ice and NH<sub>4</sub>F and Their Dielectric Properties, *The Journal of Chemical Physics*, 24(4), 895–902, doi:10.1063/1.1742629, 1956.
- Zemp, M., M. Hoelzle, and W. Haeberli, Six decades of glacier mass-balance observations: a review of the worldwide monitoring network, *Annals of Glaciology*, 50(50), 101–111, doi:10.3189/172756409787769591, 2009.
- Zhang, Q., S. Kang, P. Gabrielli, M. Loewen, and M. Schwikowski, Vanishing High Mountain Glacial Archives: Challenges and Perspectives, *Environmental Science & Technology*, 49(16), 9499–9500, doi:10.1021/acs.est.5b03066, 2015.

# 4 Melt-induced fractionation of major ions and trace elements in an Alpine snow pack

Sven Erik Avak<sup>a,b,c</sup>, Jürg Christian Trachsel<sup>d,e</sup>, Jacinta Edebeli<sup>a,e</sup>, Sabina Brütsch<sup>a</sup>, Thorsten Bartels-Rausch<sup>a</sup>, Martin Schneebeli<sup>d</sup>, Margit Schwikowski<sup>a,b,c</sup>, and Anja Eichler<sup>a,c,\*</sup>

<sup>a</sup>Laboratory of Environmental Chemistry, Paul Scherrer Institute, Villigen PSI, 5232, Switzerland

<sup>b</sup>Department of Chemistry and Biochemistry, University of Bern, Bern, 3012, Switzerland

<sup>c</sup>Oeschger Centre for Climate Change Research, University of Bern, Bern, 3012, Switzerland

<sup>d</sup>WSL-Institute for Snow and Avalanche Research SLF, Davos Dorf, 7260, Switzerland

<sup>e</sup>Department of Environmental Systems Science, ETH Zurich, Zurich, 8006, Switzerland

\*Corresponding author

*Manuscript to be submitted to  
Journal of Geophysical Research: Atmospheres*

## Abstract

Understanding the impact of melting on the preservation of atmospheric contaminants in high-Alpine snow and glacier ice is crucial for future reconstruction of past atmospheric conditions. However, detailed studies investigating melt-related changes on proxy information are rare. Here, we present a series of five snow pit measurements of 6 major ions and 34 trace elements at Weissfluhjoch, Switzerland, conducted between January and June 2017. Atmospheric pollutants were preserved during the cold season while melting towards summer resulted in preferential loss of certain species from the snow pack or enrichment in the bottom-most part. Decreasing mobilization of major ions with meltwater in the order of  $\text{SO}_4^{2-} \sim \text{Ca}^{2+} \sim \text{NO}_3^- > \text{Na}^+ \sim \text{Cl}^- > \text{NH}_4^+$  is related to their increasing solubility in ice, leading to a stronger embedding in crystal interiors during snow metamorphism. Microscopic location-dependent preservation was also observed for trace elements related to water-soluble particles where low abundance favored incorporation. Trace elements originating from water-insoluble particles were generally well preserved due to immobility with meltwater.  $\text{NH}_4^+$ , Ce, Eu, La, Mo, Nd, Pb, Pr, Sb, Sc, Sm, U, and W particularly withstand melt-induced relocation and may still serve as tracers to reconstruct past natural and anthropogenic atmospheric emissions from melt-affected snow pit and ice core records. The obtained elution behavior matches the findings from another high-Alpine site at upper Grenzgletscher for major ions and the large majority of investigated trace elements, indicating that the observed species dependent preservation from melting snow and ice are representative for the Alpine region.

## 4.1 Introduction

Major ions (MIs) and trace elements (TEs) serve as important proxies for reconstructing past atmospheric pollution from high-Alpine snow pits [Gabrieli *et al.*, 2011; Greilinger *et al.*, 2016; Hiltbrunner *et al.*, 2005; Kuhn *et al.*, 1998; Kutuzov *et al.*, 2013] and ice cores [Döscher *et al.*, 1996; Eichler *et al.*, 2000; Preunkert *et al.*, 2000; Schwikowski *et al.*, 1999, 2004]. However, post-depositional melting induced by climate warming can significantly alter concentration records of atmospheric contaminants from high-altitude glaciers and snow packs as shown for MIs, organic pollutants, or water stable isotopes [Eichler *et al.*, 2001; Herreros *et al.*, 2009; Kang *et al.*, 2008; Müller-Tautges *et al.*, 2016; Pavlova *et al.*, 2015; Sinclair and MacDonell, 2016; You *et al.*, 2015]. As glaciers, which have served as environmental archives to assess the natural and anthropogenic impact on the atmosphere, are progressively in danger to be affected by melting [Zhang *et al.*, 2015], there is an increasing need to understand the impact of melting on the preservation of various environmental proxies in these archives. Investigation of the fate of MIs during melting of snow packs and glacier ice has been the subject of several studies [Eichler

*et al.*, 2001; *Ginot et al.*, 2010; *Kang et al.*, 2008; *Lee et al.*, 2008; *Li et al.*, 2006; *Virkkunen et al.*, 2007; *Wang et al.*, 2018; *Zong-xing et al.*, 2015]. Preferential elution of certain ions relative to others has been observed, and is strongly dependent on the respective location of the snow pack. As a common feature,  $\text{SO}_4^{2-}$  is generally significantly depleted with melting, while  $\text{NH}_4^+$  appears to be preserved despite meltwater percolation.

In the majority of these studies, either melting had strongly affected the MI records making the initial conditions before melting occurred unknown, or a direct comparison of concentration records before and after melting occurred to quantify the degree of depletion has not been performed. The effect of melting on the fate of TEs in snow has still not been well characterized. To the best of our knowledge, only a few studies have addressed the influence of melting on TE concentration records in snow pits. *Wong et al.* [2013] artificially infiltrated meltwater into Greenland snow pits to investigate melt effects on 12 different TE records. In their study, *Wong et al.* [2013] observed that mineral dust particle-bound TEs remained immobile during meltwater percolation resulting in the preservation of their seasonal chemical signal. On the contrary, *Zhongqin et al.* [2007] reported from the analyses of snow-firn pits taken in the Central Asian Tian Shan Mountains that meltwater percolation during the summer may have eluted the five selected TEs, Al, Cd, Fe, Pb, and Zn, from the snow-firn pack. From the analysis of a meltwater-affected firn part of an Alpine ice core, we could recently show that meltwater percolation led to preferential loss of certain TEs [*Avak et al.*, 2018]. TEs associated with water-insoluble particles and low-abundant water-soluble TEs remained largely immobile with meltwater. As we also proposed a geographical site-specificity for the preferential elution of TEs [*Avak et al.*, 2018], it remains unclear how representative these findings are for the Alpine region.

The high-Alpine snow test site at Weissfluhjoch, Switzerland, is well-suited for weather observations and snow pack measurements. This site has been used for numerous studies focusing on snow characterization, snow mechanics, snow metamorphism, and the development of measurement methods since 1936 [*Marty and Meister*, 2012]. So far, studies investigating the chemical composition of atmospheric aerosols contained in the snow pack at Weissfluhjoch focused on MIs and water stable isotopes. *Baltensperger et al.* [1993] have compared consecutive measurements of surface snow sampled from January to March 1988 to that from a snow pit taken at the end of March at Weissfluhjoch. The snow pit samples were found to be representative of deposition during the winter. Snow pit sampling, sample handling procedures, and chemical analysis of MIs were further refined by *Schwikowski et al.* [1997]. In addition, the seasonal variability in deposition and the different emission sources of impurities were reflected in the vertical distribution of MIs in the snow pack [*Schwikowski et al.*, 1997].

Here, we present the first study monitoring the post-depositional fate of an extensive set of environmentally relevant atmospheric contaminants in the high-Alpine snow pack at Weissfluhjoch, Switzerland. We monitored six MIs and 34 TEs during an entire winter/spring season and investigated their behavior during melting of the

snow pack. Five snow pits sampled in the first half of the year, 2017, from January to June allowed capturing both the initial, undisturbed records of atmospheric contaminants in the snow pack and the records after melting has occurred during the warmer season. Impurity profiles reflecting dry conditions (without significant melting) were compared with profiles reflecting wet conditions (snow pack heavily soaked with meltwater) to systematically investigate the impact of melting on the preservation of atmospheric tracers in high-Alpine snow.

## 4.2 Materials and methods

### 4.2.1 Study site

Five snow pit samplings were conducted at the high-Alpine snow test site of the Swiss Institute for Snow and Avalanche Research (SLF), Weissfluhjoch (WFJ), Plessur Alps, Eastern Switzerland (2536 m a.s.l., 46°49'47" N 9°48'33" E) at regular time intervals in the winter, spring, and early summer seasons in 2017 on January 25<sup>th</sup>, February 22<sup>nd</sup>, March 21<sup>st</sup>, April 17<sup>th</sup>, and June 1<sup>st</sup>. Earlier snow sampling studies suggest uniform spatial snow deposition and insignificant perturbations of the snow stratigraphy due to strong winds at this site [Baltensperger *et al.*, 1993; Schwikowski *et al.*, 1997]. Samples were obtained from the snow pits either one day before or after the weekly density measurements with 3 cm resolution, which were part of an extensive series of snow pack measurements conducted by the SLF during the winter seasons [Calonne *et al.*, 2016]. The snow height during the samplings were 87 cm (Jan 25<sup>th</sup>), 126 cm (Feb 22<sup>nd</sup>), 185 cm (Mar 21<sup>st</sup>), 166 cm (Apr 17<sup>th</sup>), and 83 cm (Jun 1<sup>st</sup>, Figure 4.1). Continuous snow surface and air temperature measurements by an automated weather station indicated that dry conditions, where no significant melting occurred, prevailed for the first three sampling dates (Figure 4.1). Partial melting was already identifiable in the snow pit on the fourth sampling date (Figure 4.2). The snow pack was entirely soaked with meltwater on the fifth sampling date due to a preceding period of several days with air temperatures above 0 °C (Figure 4.1).

### 4.2.2 Snow pit sampling

As snow is particularly sensitive to contamination on a trace amount level, precautions were taken during sampling. Sterile clean room overalls (Tyvek<sup>®</sup> IsoClean<sup>®</sup>, DuPont, Wilmington DE, United States), particulate respirator face masks (3M, Maplewood MN, United States), and ultra-clean plastic gloves (Semadeni, Ostermundigen, Switzerland) were worn during the sampling (Figure 4.3a). All tools were carefully rinsed with ultra-pure water (18 M  $\Omega$  cm quality, arium<sup>®</sup> pro, Sartorius, Göttingen, Germany) prior to use. Snow pits were sampled with a vertical



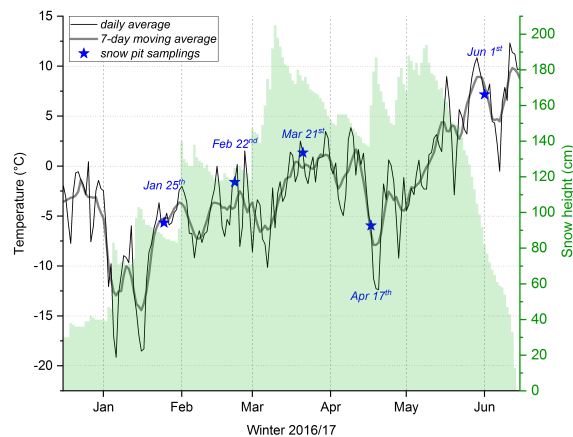


**Figure 4.1:** Continuous air temperature and daily snow heights at the Weissfluhjoch test site, Swiss Alps, during the winter season of 2016/17. Snow pit samplings were conducted both in the cold season where dry conditions without significant melting prevailed, and in the warm season, where severe melting of the snow pack occurred.



**Figure 4.2:** During the sampling of April 17<sup>th</sup> the snow pack was partly soaked with meltwater.

resolution of 6 cm down to the soil by pushing a custom-built rectangular (15 x 24 cm) sampler made from polycarbonate (Figure 4.3b) into the pit wall. To allow for sufficient sample volume, the snow was filled into 50 mL polypropylene (PP) vials (Sarstedt, Nümbrecht, Germany) by pushing them twice with the opening facing downwards into the snow (Figure 4.3c). Separate vials were used for MI, water stable isotope (WSI), and TE analysis (Figure 3d). PP vials were pre-cleaned five times with ultra-pure water (18 M  $\Omega$  cm quality, arium<sup>®</sup> pro, Sartorius, Göttingen,

Germany) for MI and WSI samples. For TE samples, the tubes were cleaned five times with ultra-pure water (18 M  $\Omega$  cm quality, Milli-Q<sup>®</sup> Element, Merck Millipore, Burlington MA, United States) plus once with 0.2 M HNO<sub>3</sub> prepared from ultra-pure HNO<sub>3</sub> (Optima<sup>™</sup>, Fisher Chemical, Loughborough, United Kingdom). Samples for TE analysis were taken from the snow overlying the front part of the sampler to prevent possible cross contamination of the vials used for MI sampling with HNO<sub>3</sub> (Figure 4.3d).

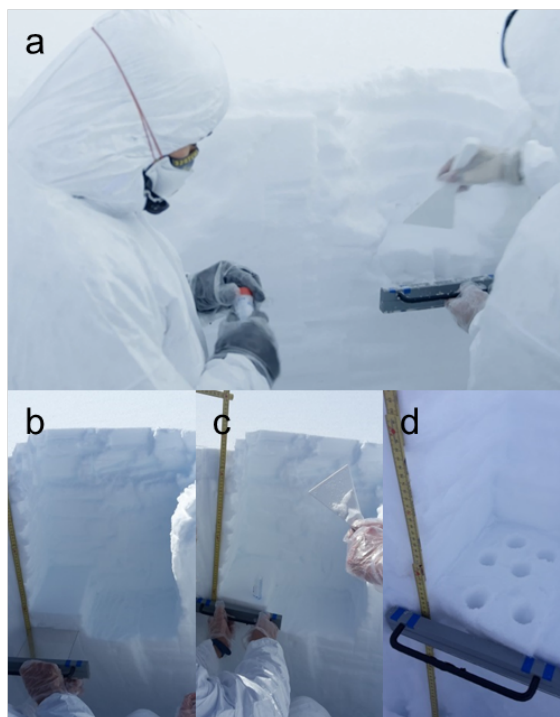


**Figure 4.3:** a) Clean room overalls, particulate respirator face masks, and ultra-clean plastic gloves were worn during the snow pit sampling to avoid contamination. b) A rectangular sampler made from polycarbonate was pushed into the pit wall to vertically sample the profile in continuous increments of 6 cm. c) 50 mL polypropylene vials were filled with snow by pushing them twice with the opening facing downwards into the snow. d) Samples for TE, MI, and WSI analysis were taken separately from the front backwards.

### 4.2.3 Major ion, water stable isotope, and trace element analysis

A total of 324 samples for MI, WSI and TE analysis were kept frozen at  $-20$  °C until analysis at the Paul Scherrer Institute.

MIIs ( $\text{Na}^+$ ,  $\text{NH}_4^+$ ,  $\text{Ca}^{2+}$ ,  $\text{Cl}^-$ ,  $\text{NO}_3^-$ , and  $\text{SO}_4^{2-}$ ) present in the snow pit samples were analyzed after melting at room temperature using ion chromatography (IC, 850 Professional IC equipped with a 872 Extension Module Liquid Handling and a 858 Pro-

fessional Sample Processor auto sampler, Metrohm, Herisau, Switzerland). Cations were separated using a Metrosep C4 column (Metrohm) and 2.8 mM HNO<sub>3</sub> as eluent at a flow rate of 1 mL min<sup>-1</sup>. Anions were separated using a Metrosep A Supp 10 column (Metrohm) and were eluted stepwise using first, a 1.5 mM Na<sub>2</sub>CO<sub>3</sub>/0.3 mM NaHCO<sub>3</sub> (1:1 mixture) eluent, then an 8 mM Na<sub>2</sub>CO<sub>3</sub>/1.7 mM NaHCO<sub>3</sub> (1:1 mixture) eluent at a flow rate of 0.9 mL min<sup>-1</sup>. Possible instrumental drifts were monitored by measuring an in-house standard after every 20<sup>th</sup> sample. The precision of the method was ~5%. WSI samples were melted at room temperature and 1 mL aliquots were analyzed for δD and δ<sup>18</sup>O using a wavelength-scanned cavity ring down spectrometer (WS-CRDS, L2130-i Analyzer, Picarro, Santa Clara CA, United States). Samples were injected into the vaporizer (A0211, Picarro, Santa Clara CA, United States) using a PAL HTC-xt autosampler (LEAP Technologies, Carrboro NC, United States). Three in-house standards were measured after every tenth sample for calibration and to monitor instrumental drifts. The measurement uncertainty was <0.1‰ for δ<sup>18</sup>O and <0.5‰ for δD.

Snow pit samples for TE analysis were acidified with concentrated ultra-pure HNO<sub>3</sub> to 0.2 M, melted at room temperature, and analyzed using discrete inductively coupled plasma sector field mass spectrometry (ICP-SF-MS, Element 2, Thermo Fisher Scientific, Bremen, Germany). Concentrations, either in low (LR) or medium resolution (MR), of <sup>7</sup>Li (LR & MR), <sup>23</sup>Na, <sup>24</sup>Mg, <sup>27</sup>Al, <sup>44</sup>Ca, <sup>45</sup>Sc, <sup>51</sup>V, <sup>55</sup>Mn, <sup>56</sup>Fe, <sup>59</sup>Co (all MR), <sup>60</sup>Ni, <sup>63</sup>Cu, <sup>66</sup>Zn (all LR & MR), <sup>85</sup>Rb, <sup>88</sup>Sr, <sup>90</sup>Zr, <sup>95</sup>Mo, <sup>109</sup>Ag, <sup>111</sup>Cd, <sup>121</sup>Sb, <sup>133</sup>Cs, <sup>138</sup>Ba, <sup>139</sup>La, <sup>140</sup>Ce, <sup>141</sup>Pr, <sup>146</sup>Nd, <sup>147</sup>Sm, <sup>153</sup>Eu, <sup>172</sup>Yb, <sup>182</sup>W, <sup>205</sup>Tl, <sup>206</sup>Pb, <sup>207</sup>Pb, <sup>208</sup>Pb, <sup>209</sup>Bi, <sup>232</sup>Th, and <sup>238</sup>U (all LR) were determined. A micro concentric nebulizer (apex Q, Elemental Scientific, Omaha NE, United States) together with an auto sampler (CETAC ASX-260, Teledyne Cetac, Omaha NE, United States) were used for sample introduction. <sup>103</sup>Rh served as internal standard to correct for intensity variations during sample introduction, and for plasma fluctuations. External calibration with seven different liquid calibration standards was used for quantification. Concentrations of each element in the calibration standards were adapted to account for their different concentrations in snow and glacier ice. Correlation coefficients for linear regressions of the calibration curves were >0.999. This calibration procedure has been successfully employed in previous studies [Eichler *et al.*, 2012, 2014, 2015, 2017; Knüsel *et al.*, 2003].

#### 4.2.4 Data evaluation

IC raw data was processed using the MagIC Net 3.2 software (Metrohm, Herisau, Switzerland). Sample concentrations were not blank-corrected as the concentrations of the blank, determined by analyzing ultra-pure water, were below the detection limit (DL). Sample concentrations below the DL were substituted with half the value of the DL. ICP-MS raw data was evaluated following the method described by Knüsel *et al.* [2003]. Concentrations were blank-corrected by subtracting a measurement blank consisting of four measurements of ultra-pure water. The instrumental DL

was defined as  $3\sigma$  of the measurement blank and concentrations below the DL were substituted with half of the value of the DL.  $^{109}\text{Ag}$  was excluded from the data set for further evaluation and discussion as concentrations of all samples were below the DL.

Total depths of the snow profiles were converted to water equivalents (w.eq.). As Apr 17<sup>th</sup> had the largest snow depth, the profiles on Jan 25<sup>th</sup>, Feb 22<sup>nd</sup>, Mar 21<sup>st</sup>, and Jun 1<sup>st</sup> were aligned relative to the profile on Apr 17<sup>th</sup>, with 0 cm w.eq. being the surface. All five profiles cover the depth interval 45-65 cm w.eq. The profiles on Feb 22<sup>nd</sup>, Mar 21<sup>st</sup>, Apr 17<sup>th</sup>, and Jun 1<sup>st</sup> cover 36-65 cm w.eq., the profiles on Feb 22<sup>nd</sup>, Mar 21<sup>st</sup>, and Apr 17<sup>th</sup> cover 30-65 cm w.eq., and the profiles on Mar 21<sup>st</sup> and Apr 17<sup>th</sup> cover 5-65 cm w.eq. The sample at the base of each snow pit was omitted from all chemical profiles to exclude a possible influence of the soil at WFJ. The uppermost (surface) samples of the snow pit from June 1<sup>st</sup> were not taken into consideration for all chemical profiles as the respective TE sample revealed highly elevated values ( $>\text{mean}+1.5\sigma$ ) for many TEs.

## 4.3 Results and discussion

### 4.3.1 Major ions

#### 4.3.1.1 Comparison of the five MI concentration profiles

The chemical profiles of selected MIs ( $\text{NH}_4^+$ ,  $\text{Cl}^-$ ,  $\text{Ca}^{2+}$ ) and the  $\delta^{18}\text{O}$  records in the five snow pits are shown in Figure 4.4. The general patterns of these profiles, reflecting the winter and spring periods, show a strong correspondence in the respective overlapping parts. Apart from possible changes caused by melting (Apr 17<sup>th</sup>), slight concentration differences in the profiles can be attributed to the spatial variability of contaminants within the snow pack as the locations of the individual snow pit samplings at WFJ were several meters (up to 20 m) apart. The resemblance between the four winter and spring snow pits is also visible for the corresponding  $\delta^{18}\text{O}$  profiles which support the depth assignment of the different snow pits.

The chemical profiles of  $\text{NH}_4^+$ ,  $\text{Cl}^-$ , and  $\text{Ca}^{2+}$  are exemplary for the different emission sources of MIs in Alpine snow and ice. The depths 0-30 cm w.eq. (Mar 21<sup>st</sup> and Apr 17<sup>th</sup>) indicate precipitation occurring in the spring after Feb 22<sup>nd</sup>, while 30-65 cm w.eq. represent winter precipitation. The  $\text{NH}_4^+$  springtime concentrations (Mar 21<sup>st</sup> and Apr 17<sup>th</sup>) are roughly three times higher than wintertime concentrations.  $\text{NH}_4^+$  detected in snow pits and ice cores from high-Alpine sites is generally of anthropogenic origin [Döscher *et al.*, 1996; Gabrieli *et al.*, 2011].  $\text{NH}_4^+$  also shows a pronounced maximum towards summer due to enhanced emissions from agricultural activities, and stronger convection [Baltensperger *et al.*, 1997]. Higher concentrations of  $\text{NH}_4^+$  in the springtime snowfall compared to wintertime snowfall at WFJ were also observed by Schwikowski *et al.* [1997].  $\text{Ca}^{2+}$  and  $\text{Cl}^-$ , unlike  $\text{NH}_4^+$ , have higher

concentrations in the wintertime snow than in the spring. At Alpine sites,  $\text{Ca}^{2+}$  and  $\text{Cl}^-$  are indicative of the input from mineral dust [Bohleber *et al.*, 2018] and marine sea salt aerosols [Eichler *et al.*, 2004], respectively.

After several weeks with temperatures above  $0^\circ\text{C}$ , the snow pack was entirely soaked with meltwater (and rainwater) at the beginning of the summer (Jun 1<sup>st</sup>; Figure 1). The respective  $\delta^{18}\text{O}$  profile reveals a strong smoothing compared to the previous profiles, indicative of strong melting [Thompson *et al.*, 1993]. The MI profiles of Jun 1<sup>st</sup> compared to those of the first three sampling dates are either almost unaltered ( $\text{NH}_4^+$ ), depleted ( $\text{Na}^+$ ,  $\text{Cl}^-$ ), or strongly depleted ( $\text{Ca}^{2+}$ ,  $\text{NO}_3^-$ ,  $\text{SO}_4^{2-}$ ), most likely due to different elution behavior of the investigated ions with meltwater [Eichler *et al.*, 2001].

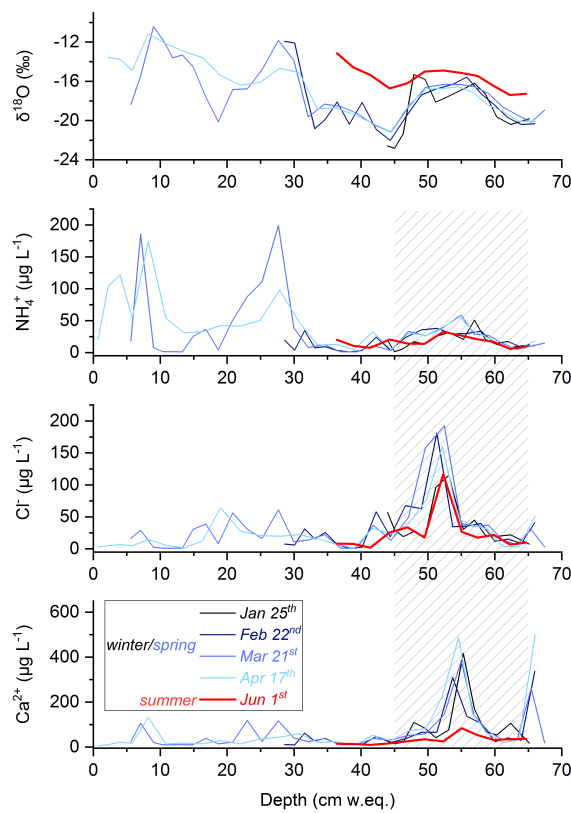


**Figure 4.4:** Concentration profiles of  $\text{NH}_4^+$ ,  $\text{Cl}^-$ , and  $\text{Ca}^{2+}$  of the five snow pits taken at the Weissfluhjoch test site during winter/spring (black/blue curves) and early summer (red curve). For comparison, the corresponding  $\delta^{18}\text{O}$  records are shown. Profile depths were aligned to the one of April 17<sup>th</sup>. The shaded area indicates the depth interval (45–65 cm w.eq.) used for calculation of the concentration ratio and determining an elution sequence.

### 4.3.1.2 Preferential elution of MIs: Elution sequence and discussion

To quantify and compare the apparent preferential elution of MIs, a concentration ratio  $c_{\text{wet}}/c_{\text{dry}}$  for the overlapping depth (45-65 cm w.eq.) was calculated for each MI (Table 4.1).  $c_{\text{wet}}$  corresponds to the integrated MI concentration for the wet profile of Jun 1<sup>st</sup>, whereas  $c_{\text{dry}}$  represents the mean of the integrated concentration profiles during dry (no significant melting) periods (Jan 25<sup>th</sup>, Feb 22<sup>nd</sup>, Mar 21<sup>st</sup>). The profiles on Apr 17<sup>th</sup> were not included as the snow pack was neither completely dry nor entirely soaked (Figure 4.2). Corresponding to the concentration ratio, an elution sequence was established:  $\text{NH}_4^+ < \text{Cl}^- \sim \text{Na}^+ < \text{NO}_3^- \sim \text{Ca}^{2+} \sim \text{SO}_4^{2-}$ , where  $\text{NH}_4^+$  is the least mobile ion and  $\text{SO}_4^{2-}$ , the most mobile ion. Similar elution sequences have been reported by *Eichler et al.* [2001], *Li et al.* [2006], *Ginot et al.* [2010], and recently by *Zong-xing et al.* [2015], who observed a particularly pronounced leaching of  $\text{SO}_4^{2-}$  and  $\text{Ca}^{2+}$ , while  $\text{NH}_4^+$  and  $\text{Cl}^-$  were retained in melting firn and snow packs.

Elution sequences of MIs can also be determined through laboratory studies [*Cragin et al.*, 1996; *Tranter et al.*, 1992; *Tsiouris et al.*, 1985]. We recently performed an elution experiment where, for the first time, homogenous impurity-doped artificial snow was exposed to well-defined snow metamorphism conditions prior to leaching with 0 °C ultra-pure water. This experiment was conducted to determine enrichment differences of MIs between snow grain interiors and surfaces after metamorphism [*Trachsel et al.*, 2017]. Snow undergoes drastic structural transformation cycles during metamorphism [*Pinzer et al.*, 2012], which may significantly influence impurity redistribution. Our elution sequence here agrees well with the findings from the aforementioned elution experiment (Figure 4.5).  $\text{Ca}^{2+}$  and  $\text{SO}_4^{2-}$  were enriched on the snow grain surfaces with snow metamorphism; this may explain their availability for mobilization with meltwater.

MIs having a higher solubility in ice such as  $\text{NH}_4^+$  and  $\text{Cl}^-$  [*Feibelman*, 2007; *Hobbs*, 1974], also showed less mobility most likely due to incorporation into the crystal interior by substitution of water molecules located on lattice sites [*Petrenko and Whitworth*, 2002; *Zaromb and Brill*, 1956]. This is also supported by previous location studies of salts in ice. *Mulvaney et al.* [1988] used a combination of scanning electron microscopy (SEM) and energy-dispersive X-ray micro analysis (EDXMA) to show that  $\text{H}_2\text{SO}_4$  concentrations at triple junctions are several orders of magnitude higher compared to grain interiors in polar ice from Antarctica. Similar observations for  $\text{H}_2\text{SO}_4$  and  $\text{HNO}_3$  using Raman spectroscopy were reported by *Fukazawa et al.* [1998]. Accumulation of  $\text{MgSO}_4$  at grain boundaries in Greenland GISP2 ice could be revealed by low-vacuum SEM-EDX [*Baker et al.*, 2003]. The varying elution behavior of MIs observed in the snow pit of Jun 1<sup>st</sup> with  $\text{NO}_3^-$ ,  $\text{Ca}^{2+}$  and  $\text{SO}_4^{2-}$  being most heavily depleted can therefore be explained by their microscopic locations on grain surfaces, exposing them to relocation during melting.

Our findings show that the atmospheric composition of MIs is well preserved in the snow pack at WFJ during the cold season. Melting during the warm season leads to preferential leaching of MIs depending on their microscopic location in/on the ice

grain. The loss of MIs is particularly significant for  $\text{Ca}^{2+}$  and  $\text{SO}_4^{2-}$ . In contrast, the strong persistence of  $\text{NH}_4^+$  emphasizes that  $\text{NH}_4^+$  can still serve as environmental tracer for the interpretation of snow pit and ice core records affected by melting.

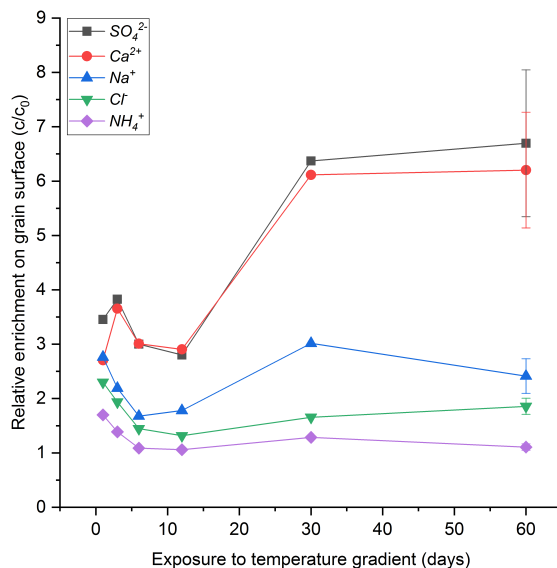


**Figure 4.5:** Time evolution of relative snow grain surface and interior accumulation of  $\text{Na}^+$ ,  $\text{NH}_4^+$ ,  $\text{Ca}^{2+}$ ,  $\text{Cl}^-$ , and  $\text{SO}_4^{2-}$  determined by leaching artificial snow, homogeneously doped with known concentrations of MIs and exposed for different time periods to a temperature gradient mimicking snow metamorphism, with  $0^\circ\text{C}$  ultra-pure water (adapted from *Trachsel et al.* [2017]).

## 4.3.2 Trace elements

### 4.3.2.1 TE concentration profiles

Concentrations of selected TEs (Co, Fe, Ce, Sb, Ca, Sr) in the snow pits on Jan 25<sup>th</sup>, Feb 22<sup>nd</sup>, Mar 21<sup>st</sup>, Apr 17<sup>th</sup>, and Jun 1<sup>st</sup> are shown in Figure 4.6. The general pattern of the profiles of the first four snow pits (Jan to Apr) agree well in the overlapping depths. As for the MI profiles, misalignment in peaks can be attributed to small-scale spatial variability of impurities in the snow pack. The reproducibility of chemical profiles revealing concentrations on an ultra-trace level (e.g. Ce and Sb) from different sampling campaigns demonstrates that significant contamination during the snow pit samplings did not occur.

The 34 TEs discussed within the scope of this work can be either of geogenic origin or emitted by anthropogenic sources. At high-Alpine sites, Al, Ba, Bi, Ca, Cs, Fe, Li, Mg, Mn, Na, Rb, Sr, Th, Tl, U, W, Zr, and the REEs (Ce, Eu, La, Nd, Pr, Sc, Sm, Yb) are mainly deposited with mineral dust [*Gabrieli et al.*, 2011; *Gabrielli et al.*, 2008] whereas Ag, Cd, Co, Cu, Mo, Ni, Pb, Sb, V, and Zn in Alpine

**Table 4.1:** Classification<sup>1</sup>, concentration ratio, and mean concentration of the dry snow pits (Jan 25<sup>th</sup>, Feb 22<sup>nd</sup>, Mar 21<sup>st</sup>) of MIs and TEs investigated in this study.

	Classification	Concentration ratio	Mean concentration (ng L <sup>-1</sup> )
Na <sup>+</sup>	-	0.62±0.45	17000±2840
NH <sub>4</sub> <sup>+</sup>	-	0.77±0.27	26300±4580
Ca <sup>2+</sup>	-	0.37±0.18	71500±11400
Cl <sup>-</sup>	-	0.64±0.43	34000±4980
NO <sub>3</sub> <sup>-</sup>	-	0.37±0.11	249000±21200
SO <sub>4</sub> <sup>2-</sup>	-	0.36±0.10	57300±5330
Al	i.b.s.	-	4870±792
Ba	Group 2	0.39±0.26	262±67
Bi	Group 2	0.50±0.28	4.5±0.91
Ca	Group 2	0.46±0.24	110000±21400
Cd	Group 2	0.55±0.23	1.9±0.26
Ce	Group 1	1.5±1.1	14±2.9
Co	i.b.s.	-	24±4.5
Cs	i.b.s.	-	2.1±0.33
Cu	i.b.s.	-	48±5.6
Eu	Group 1	1.1±0.79	0.51±0.10
Fe	i.b.s.	-	5990±1180
La	Group 1	1.5±1.1	6.1±1.2
Li	i.b.s.	-	6.1±0.90
Mg	i.b.s.	-	37000±6600
Mn	i.b.s.	-	612±110
Mo	Group 1	1.1±0.59	3.1±0.46
Na	Group 2	0.50±0.32	15900±2620
Nd	Group 1	1.2±0.92	7.7±1.7
Ni	i.b.s.	-	101±22
Pb	Group 1	0.84±0.36	180±15
Pr	Group 1	1.1±0.84	1.8±0.38
Rb	i.b.s.	-	15±2.1
Sb	Group 1	0.88±0.36	9.1±1.2
Sc	Group 1	1.5±1.4	1.8±0.41
Sm	Group 1	1.2±0.88	2.0±0.46
Sr	Group 2	0.37±0.21	270±55
Th	Group 2	0.45±0.30	1.4±0.25
Tl	i.b.s.	-	0.39±0.04
U	Group 1	1.5±0.99	2.3±0.64
V	i.b.s.	-	19±2.5
W	Group 1	1.2±0.69	0.54±0.07
Yb	i.b.s.	-	0.63±0.13
Zn	Group 2	0.47±0.36	2780±463
Zr	Group 2	0.13±0.08	5.4±0.75

<sup>1</sup> TEs were classified depending on whether the profile of the snow pit of Jun 1<sup>st</sup> showed a strong enrichment from the soil below 55 cm w.eq. (i.b.s./influenced by soil), an unbiased profile pattern compared to the dry condition profiles (group 1), or a heavily depleted concentration curve (group 2).



snow and ice are characteristic of anthropogenic atmospheric pollution [Barbante *et al.*, 2004; Gabrieli *et al.*, 2011; Gabrielli *et al.*, 2008; Schwikowski *et al.*, 2004; Van de Velde *et al.*, 1999, 2000]. The chemical profiles of Ca, Ce, Fe, and Sr (Figure 4.6) are representative of TEs originating from mineral dust particles and show an enrichment in the depths reflecting winter precipitation (30-65 cm w.eq.) where dry conditions prevailed (Jan 25<sup>th</sup>, Feb 22<sup>nd</sup>, Mar 21<sup>st</sup>). As explained above for NH<sub>4</sub><sup>+</sup>, TEs indicative of anthropogenic influence such as Sb (Figure 4.6), are enriched in depths reflecting spring precipitation deposited after Feb 22<sup>nd</sup> (0-30 cm w.eq.).

Corresponding to the concentration profiles on Jun 1<sup>st</sup>, the 34 investigated TEs can be divided into three groups (Table 4.1). TEs categorized as group 1 (Ce, Eu, La, Mo, Nd, Pb, Pr, Sb, Sc, Sm, U, W) revealed an almost unbiased profile pattern between 45 and 65 cm w.eq. compared to the dry condition profiles (e.g. Ce, Sb, Figure 4.6). This indicates that group 1 TEs were not affected by melting. Group 2 TEs (Ba, Bi, Ca, Cd, Na, Sr, Th, Zn, Zr) were strongly depleted on Jun 1<sup>st</sup> compared to winter and springtime records (as shown for Ca and Sr in Figure 4.6). TEs denoted as “i.b.s.” (influenced by soil) Al, Co, Cs, Cu, Fe, Li, Mg, Mn, Ni, Rb, Tl, V, Yb exhibit a strong enrichment below 55 cm w.eq. close to the soil (see e.g. Co and Fe, Figure 4.6). The bottom of the snow pack on Jun 1st was heavily soaked with meltwater, probably enriched with impurities not of atmospheric origin, but from the soil at WFJ. The strong increase in concentration below 55 cm w.eq. for “i.b.s.” TEs is likely to be caused by this influence of the soil. “i.b.s.” TEs were therefore not included in further evaluation and discussion due to this artifact, which does not allow exclusive assessment of the impact of melting on the atmospheric composition preserved in the snow pack. The different preservation of group 1 and 2 TEs is, however, related to varying elution behavior during melting.

#### 4.3.2.2 Different preservation of TEs from melting snow

A quantitative classification of fractionation during melting of the snow pack (group 1 and 2) was performed by calculating a concentration ratio  $c_{\text{wet}}/c_{\text{dry}}$  for each TE in the overlapping depths (see above, Table 4.1). The highest concentration ratio was obtained for La indicative of its well preserved concentration record on Jun 1<sup>st</sup>, whereas the concentration profile of Zr is most severely affected by melting, having the lowest concentration ratio. Concentration ratios of TEs classified as group 1 range between  $1.5 \pm 1.1$  (La) and  $0.84 \pm 0.36$  (Pb); concentration ratios of group 2 TEs range between  $0.55 \pm 0.23$  (Cd) and  $0.13 \pm 0.08$  (Zr). Arranging the concentration ratios according to size and plotting this rank against the ratio indicates that each TE belonging to group 1 and 2 was differently preserved in the snow pack during melting (Figure 4.7).

Elements of group 1 with observed concentration ratios  $>0.7$  (Ce, Eu, La, Mo, Nd, Pb, Pr, Sb, Sc, Sm, U, W), well preserved at WFJ, are in excellent agreement with findings made in our previous study from another Alpine site (Avak *et al.*

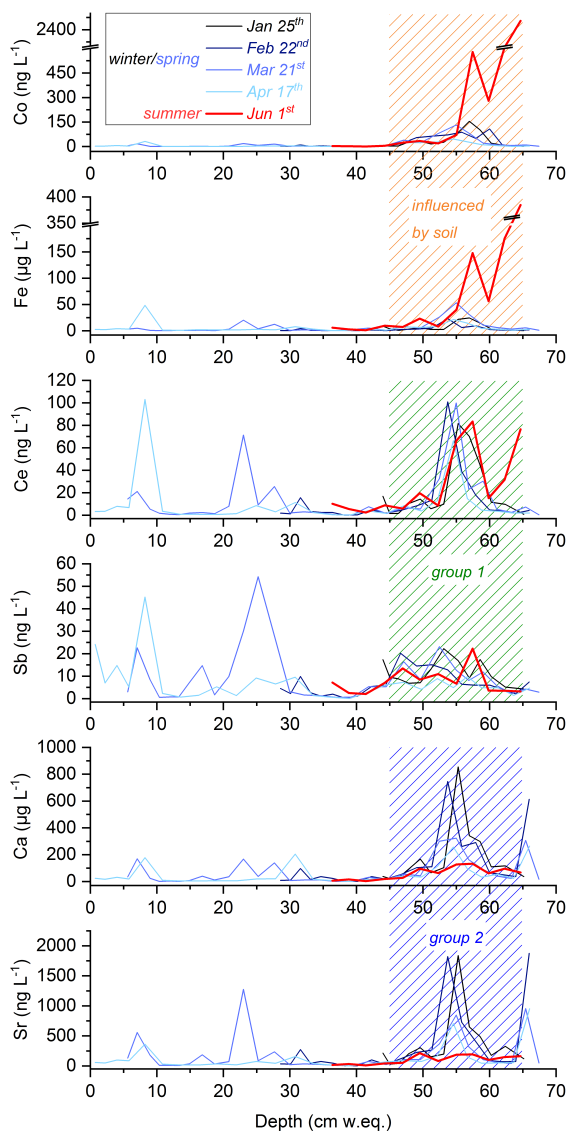


**Figure 4.6:** Concentration profiles of Co, Fe, Ce, Sb, Ca and Sr of the five snow pits taken at the Weissfluhjoch test site between winter/spring (black/blue curves) and early summer (red curve). Profile depths were aligned to the one of April 17<sup>th</sup>. The shaded area indicates the depth interval (45-65 cm w.eq.) used for calculation of the concentration ratio. TEs were classified as “i.b.s.”, respectively allocated to group 1 or 3 according to the pattern in the profile of Jun 1<sup>st</sup>.

[2018], Figure 4.7). At this  $\sim 180$  km distant site, meltwater percolation led to post-depositional disturbance of a 16 m firn section of a high-Alpine ice core from the upper Grenzletscher (GG, Monte Rosa massif, southern Swiss Alps, 4200 m a.s.l., 45°55'28" N 7°52'3" E). Preferential elution of TEs led to significant concentration depletion in the records of Ba, Ca, Cd, Co, Mg, Mn, Na, Ni, Sr, and Zn, whereas the seasonality in the Al, Bi, Ce, Cs, Cu, Eu, Fe, La, Li, Mo, Nd, Pb, Pr, Rb,

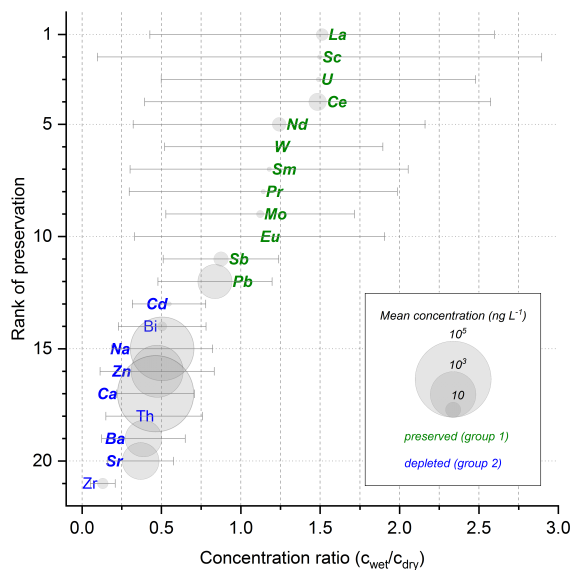


**Figure 4.7:** Rank of preservation plotted against the concentration ratio  $c_{wet}/c_{dry}$  in the overlapping part (45-65 cm w.eq. depth) for each TE classified into group 1 (retained concentration profile) or 2 (depleted concentration profile).  $c_{wet}$  corresponds to the integrated TE concentration of the wet profile (Jun 1<sup>st</sup>), whereas  $c_{dry}$  represents the mean of the integrated concentration profiles during dry conditions (Jan 25<sup>th</sup>, Feb 22<sup>nd</sup>, Mar 21<sup>st</sup>). Symbols in bold indicate a similar behavior as observed during meltwater percolation in high-Alpine firn reported by *Avak et al.* [2018]. Circle sizes represent the mean concentrations in the dry snow pits where no melting occurred and demonstrate that TEs present in low concentrations tend to be preserved.

Sb, Sc, Sm, Tl, Th, U, V, W, Yb, and Zr records was well preserved [*Avak et al.*, 2018]. The different behavior of TEs during meltwater percolation was related to their varying water solubility and location at the grain scale. TEs mainly present in water-insoluble mineral dust particles at the GG site (Al, Fe, Zr, and the REEs) were enriched on grain surfaces and mostly preserved, since their insolubility in water resulted in immobility with meltwater. TEs likely present in water-soluble compounds (Ba, Bi, Ca, Cd, Co, Cs, Cu, Li, Mg, Mn, Mo, Na, Ni, Pb, Rb, Sb, Sr, Tl, Th, U, V, W, Zn) revealed variable mobility with meltwater presumably due to the different microscopic location of the ions in the ice structure. For those rather water-soluble TEs, the atmospheric concentration at the GG site was found to be primarily decisive determining either incorporation into the ice lattice during snow metamorphism or segregation to grain surfaces because of exceeded solubility limits in ice.

In correspondence with the GG study and the work reported by *Wong et al.* [2013], also at WFJ, records of investigated TEs present as water-insoluble mineral dust particles (rare-earth elements (REEs): Ce, Eu, La, Nd, Pr, Sc, Sm) are well preserved most probably due to their immobility with meltwater. There is also strong agree-

ment in the behavior of rather water-soluble TEs between GG and WFJ, showing a dependency on the concentration level. While TEs present in ultra-trace amounts tend to be preserved, more abundant TEs were preferentially eluted (Figure 4.7). The only three TEs revealing a different behavior between the two sites are Bi, Th and Zr, which still show a preservation of the seasonality at GG, but significant depletion at WFJ. One explanation could be a higher proportion of the water-soluble fraction of Bi, Th and Zr deposited during winter at WFJ, favoring higher meltwater mobility. Another possible reason is differing concentrations. However, Th and Zr concentrations are not significantly different between the two sites. Only the higher Bi concentrations at WFJ could explain stronger melt-induced relocation.

These findings in the preservation of TEs corroborate our previous hypothesis [Avak *et al.*, 2018] that for Alpine areas, Ce, Eu, La, Mo, Nd, Pb, Pr, Sb, Sc, Sm, U and W may still be used as robust environmental proxies both in melt-affected ice cores and snow pits, whereas chemical profiles of Ba, Ca, Cd, Na, Zn, and Sr are prone to be depleted by melting. Records of Bi, Th and Zr behaved differently at the two Alpine sites. The potential of TEs classified as “i.b.s.” here and previously found to be preserved (Al, Cs, Cu, Fe, Li, Rb, Tl, V, Yb) or depleted (Co, Mg, Mn, Ni) in firn [Avak *et al.*, 2018] could not be further corroborated because of influence of the soil in the presence of meltwater.

## 4.4 Conclusions

The analysis of five snow pits sampled during the winter/spring season of 2017 at WFJ is presented here. Comparison of impurity profiles representing dry and wet conditions allowed observing the fate of atmospheric contaminants during melting of the snow pack. While the atmospheric composition is well preserved during the winter, melting in the spring and early summer causes a preferential loss of certain MIs and TEs depending on their microscopic location. The microscopic location is defined by redistribution processes occurring during snow metamorphism. In the case of MIs,  $\text{NH}_4^+$  was retained probably due to incorporation into the ice lattice.  $\text{Ca}^{2+}$  and  $\text{SO}_4^{2-}$  concentrations were significantly depleted; this can be explained by their predominant occurrence on snow grain surfaces. Variable mobility was also observed for TEs originating from water-soluble particles where low abundant TEs were preferably retained. Preservation of water-insoluble TEs such as REEs is concentration-independent due to their general immobility with meltwater.

Based on our observations, we propose that  $\text{NH}_4^+$ , TEs deposited as water-insoluble particles, and TEs of water-soluble particles occurring in low concentrations may still be applicable as environmental proxies in snow pits and ice cores affected by melting.  $\text{NH}_4^+$  and 18 out of 21 investigated TEs revealed a consistent behavior with meltwater percolation at two Alpine sites, WFJ and GG, which are 180 km apart. This indicates that this proposition is particularly valid for the Alpine region. Corroborating the existence of meltwater-resistant proxies is particularly relevant as

many high-mountain glaciers worldwide, which provide avenues for assessing natural and anthropogenic impact on the atmosphere, are increasingly affected by melting.

## Acknowledgments

The authors would like to thank Philipp Baumann and Matthias Jaggi (both from SLF) for support during the sampling campaigns of February 22<sup>nd</sup> and June 1<sup>st</sup>, respectively. Funding was provided by the Swiss National Science Foundation (SNSF) under Grant No. 155999.

## Bibliography

- Avak, S. E., M. Schwikowski, and A. Eichler, Impact and implications of meltwater percolation on trace element records observed in a high-Alpine ice core, *Journal of Glaciology*, 64(248), 877–886, doi:10.1017/jog.2018.74, 2018.
- Baker, I., D. Cullen, and D. Iliescu, The microstructural location of impurities in ice, *Canadian Journal of Physics*, 81(1-2), 1–9, doi:10.1139/p03-030, 2003.
- Baltensperger, U., M. Schwikowski, H. Gäggeler, D. Jost, J. Beer, U. Siegenthaler, D. Wagenbach, H. Hofmann, and H. Synal, Transfer of atmospheric constituents into an alpine snow field, *Atmospheric Environment. Part A. General Topics*, 27(12), 1881–1890, doi:10.1016/0960-1686(93)90293-8, 1993.
- Baltensperger, U., H. W. Gäggeler, D. T. Jost, M. Lugauer, M. Schwikowski, E. Weingartner, and P. Seibert, Aerosol climatology at the high-alpine site Jungfrauoch, Switzerland, *Journal of Geophysical Research: Atmospheres*, 102(D16), 19,707–19,715, doi:10.1029/97JD00928, 1997.
- Barbante, C., et al., Historical Record of European Emissions of Heavy Metals to the Atmosphere Since the 1650s from Alpine Snow/Ice Cores Drilled near Monte Rosa, *Environmental Science & Technology*, 38(15), 4085–4090, doi:10.1021/es049759r, 2004.
- Bohleber, P., T. Erhardt, N. Spaulding, H. Hoffmann, H. Fischer, and P. Mayewski, Temperature and mineral dust variability recorded in two low-accumulation Alpine ice cores over the last millennium, *Climate of the Past*, 14(1), 21–37, doi:10.5194/cp-14-21-2018, 2018.
- Calonne, N., C. Cetti, C. Fierz, A. Van Herwijnen, M. Jaggi, H. Löwe, M. Matzl, L. Schmid, and M. Schneebeli, A unique time series of daily and weekly snowpack measurements at Weissfluhjoch, Davos, Switzerland, in *International snow science workshop proceedings 2016. International snow science workshop, ISSW 2016, Breckenridge, CO, USA, October 2-7*, pp. 684–689, 2016.
- Cragin, J. H., A. D. Hewitt, and S. C. Colbeck, Grain-scale mechanisms influencing the elution of ions from snow, *Atmospheric Environment*, 30(1), 119–127, doi:10.1016/1352-2310(95)00232-N, 1996.
- Döscher, A., H. W. Gäggeler, U. Schotterer, and M. Schwikowski, A historical record of ammonium concentrations from a glacier in the Alps, *Geophysical Research Letters*, 23(20), 2741–2744, doi:10.1029/96GL02615, 1996.
- Eichler, A., M. Schwikowski, and H. W. Gäggeler, An Alpine ice-core record of anthropogenic HF and HCl emissions, *Geophysical Research Letters*, 27(19), 3225–3228, doi:10.1029/2000GL012006, 2000.

- Eichler, A., M. Schwikowski, and H. W. Gäggeler, Meltwater-induced relocation of chemical species in Alpine firn, *Tellus B: Chemical and Physical Meteorology*, 53(2), 192–203, doi:10.3402/tellusb.v53i2.16575, 2001.
- Eichler, A., M. Schwikowski, M. Furger, U. Schotterer, and H. W. Gäggeler, Sources and distribution of trace species in Alpine precipitation inferred from two 60-year ice core paleorecords, *Atmospheric Chemistry and Physics Discussions*, 4(1), 71–108, doi:10.5194/acpd-4-71-2004, 2004.
- Eichler, A., L. Tobler, S. Eyrikh, G. Gramlich, N. Malygina, T. Papina, and M. Schwikowski, Three Centuries of Eastern European and Altai Lead Emissions Recorded in a Belukha Ice Core, *Environmental Science & Technology*, 46(8), 4323–4330, doi:10.1021/es2039954, 2012.
- Eichler, A., L. Tobler, S. Eyrikh, N. Malygina, T. Papina, and M. Schwikowski, Ice-Core Based Assessment of Historical Anthropogenic Heavy Metal (Cd, Cu, Sb, Zn) Emissions in the Soviet Union, *Environmental Science & Technology*, 48(5), 2635–2642, doi:10.1021/es404861n, 2014.
- Eichler, A., G. Gramlich, T. Kellerhals, L. Tobler, and M. Schwikowski, Pb pollution from leaded gasoline in South America in the context of a 2000-year metallurgical history, *Science Advances*, 1(2), e1400,196, doi:10.1126/sciadv.1400196, 2015.
- Eichler, A., G. Gramlich, T. Kellerhals, L. Tobler, T. Rehren, and M. Schwikowski, Ice-core evidence of earliest extensive copper metallurgy in the Andes 2700 years ago, *Scientific Reports*, 7(1), 41,855, doi:10.1038/srep41855, 2017.
- Feibelman, P. J., Substitutional NaCl hydration in ice, *Physical Review B*, 75(21), 214,113, doi:10.1103/PhysRevB.75.214113, 2007.
- Fukazawa, H., K. Sugiyama, S. Mae, H. Narita, and T. Hondoh, Acid ions at triple junction of Antarctic ice observed by Raman scattering, *Geophysical Research Letters*, 25(15), 2845–2848, doi:10.1029/98GL02178, 1998.
- Gabrieli, J., et al., Impact of Po Valley emissions on the highest glacier of the Eastern European Alps, *Atmospheric Chemistry and Physics*, 11(15), 8087–8102, doi:10.5194/acp-11-8087-2011, 2011.
- Gabrielli, P., G. Cozzi, S. Torcini, P. Cescon, and C. Barbante, Trace elements in winter snow of the Dolomites (Italy): A statistical study of natural and anthropogenic contributions, *Chemosphere*, 72(10), 1504–1509, doi:10.1016/j.chemosphere.2008.04.076, 2008.
- Ginot, P., U. Schotterer, W. Stichler, M. A. Godoi, B. Francou, and M. Schwikowski, Influence of the Tungurahua eruption on the ice core records of Chimborazo, Ecuador, *The Cryosphere*, 4(4), 561–568, doi:10.5194/tc-4-561-2010, 2010.
- Greilinger, M., W. Schöner, W. Winiwarter, and A. Kasper-Giebl, Temporal changes of inorganic ion deposition in the seasonal snow cover for the Austrian Alps (1983–2014), *Atmospheric Environment*, 132, 141–152, doi:10.1016/j.atmosenv.2016.02.040, 2016.
- Herrerros, J., I. Moreno, J.-D. Taupin, P. Ginot, N. Patris, M. De Angelis, M.-P. Ledru, F. Delachaux, and U. Schotterer, Environmental records from temperate glacier ice on Nevado Coropuna saddle, southern Peru, *Advances in Geosciences*, 22, 27–34, doi:10.5194/adgeo-22-27-2009, 2009.
- Hiltbrunner, E., M. Schwikowski, and C. Körner, Inorganic nitrogen storage in alpine snow pack in the Central Alps (Switzerland), *Atmospheric Environment*, 39(12), 2249–2259, doi:10.1016/j.atmosenv.2004.12.037, 2005.
- Hobbs, P. V., *Ice Physics*, Oxford University Press, Oxford, 1974.
- Kang, S., J. Huang, and Y. Xu, Changes in ionic concentrations and  $\delta^{18}\text{O}$  in the snowpack of Zhadang glacier, Nyainqentanglha mountain, southern Tibetan Plateau, *Annals of Glaciology*, 49(October 2006), 127–134, doi:10.3189/172756408787814708, 2008.

- Knüsel, S., D. E. Piguet, M. Schwikowski, and H. W. Gäggeler, Accuracy of Continuous Ice-Core Trace-Element Analysis by Inductively Coupled Plasma Sector Field Mass Spectrometry, *Environmental Science & Technology*, 37(10), 2267–2273, doi:10.1021/es026452o, 2003.
- Kuhn, M., J. Haslhofer, U. Nickus, and H. Schellander, Seasonal development of ion concentration in a high alpine snow pack, *Atmospheric Environment*, 32(23), 4041–4051, doi:10.1016/S1352-2310(97)00216-1, 1998.
- Kutuzov, S., M. Shahgedanova, V. Mikhaleiko, P. Ginot, I. Lavrentiev, and S. Kemp, High-resolution provenance of desert dust deposited on Mt. Elbrus, Caucasus in 2009–2012 using snow pit and firn core records, *The Cryosphere*, 7(5), 1481–1498, doi:10.5194/tc-7-1481-2013, 2013.
- Lee, J., V. E. Nez, X. Feng, J. W. Kirchner, R. Osterhuber, and C. E. Renshaw, A study of solute redistribution and transport in seasonal snowpack using natural and artificial tracers, *Journal of Hydrology*, 357(3–4), 243–254, doi:10.1016/j.jhydrol.2008.05.004, 2008.
- Li, Z., R. Edwards, E. Mosley-Thompson, F. Wang, Z. Dong, X. You, H. Li, C. Li, and Y. Zhu, Seasonal variability of ionic concentrations in surface snow and elution processes in snowfirn packs at the PGPI site on Ürümqi glacier No. 1, eastern Tien Shan, China, *Annals of Glaciology*, 43, 250–256, doi:10.3189/172756406781812069, 2006.
- Marty, C., and R. Meister, Long-term snow and weather observations at Weissfluhjoch and its relation to other high-altitude observatories in the Alps, *Theoretical and Applied Climatology*, 110(4), 573–583, doi:10.1007/s00704-012-0584-3, 2012.
- Müller-Tautges, C., A. Eichler, M. Schwikowski, G. B. Pezzatti, M. Conedera, and T. Hoffmann, Historic records of organic compounds from a high Alpine glacier: influences of biomass burning, anthropogenic emissions, and dust transport, *Atmospheric Chemistry and Physics*, 16(2), 1029–1043, doi:10.5194/acp-16-1029-2016, 2016.
- Mulvaney, R., E. W. Wolff, and K. Oates, Sulphuric acid at grain boundaries in Antarctic ice, *Nature*, 331(6153), 247–249, doi:10.1038/331247a0, 1988.
- Pavlova, P. A., T. M. Jenk, P. Schmid, C. Bogdal, C. Steinlin, and M. Schwikowski, Polychlorinated Biphenyls in a Temperate Alpine Glacier: 1. Effect of Percolating Meltwater on their Distribution in Glacier Ice, *Environmental Science & Technology*, 49(24), 14,085–14,091, doi:10.1021/acs.est.5b03303, 2015.
- Petrenko, V. F., and R. W. Whitworth, *Physics of Ice*, Oxford University Press, doi:10.1093/acprof:oso/9780198518945.001.0001, 2002.
- Pinzer, B. R., M. Schneebeli, and T. U. Kaempfer, Vapor flux and recrystallization during dry snow metamorphism under a steady temperature gradient as observed by time-lapse microtomography, *The Cryosphere*, 6(5), 1141–1155, doi:10.5194/tc-6-1141-2012, 2012.
- Preunkert, S., D. Wagenbach, M. Legrand, and C. Vincent, Col du Dôme (Mt Blanc Massif, French Alps) suitability for ice-core studies in relation with past atmospheric chemistry over Europe, *Tellus B: Chemical and Physical Meteorology*, 52(3), 993–1012, doi:10.3402/tellusb.v52i3.17081, 2000.
- Schwikowski, M., S. Brütsch, H. W. Gäggeler, and U. Schotterer, A high-resolution air chemistry record from an Alpine ice core: Fiescherhorn glacier, Swiss Alps, *Journal of Geophysical Research: Atmospheres*, 104(D11), 13,709–13,719, doi:10.1029/1998JD100112, 1999.
- Schwikowski, M., et al., Intercomparison of snow sampling and analysis within the alpine-wide snowpack investigation (SNOSP), *Water, Air, & Soil Pollution*, 93(1–4), 67–91, doi:10.1007/BF02404748, 1997.

- Schwikowski, M., et al., Post-17th-Century Changes of European Lead Emissions Recorded in High-Altitude Alpine Snow and Ice, *Environmental Science & Technology*, 38(4), 957–964, doi:10.1021/es034715o, 2004.
- Sinclair, K. E., and S. MacDonell, Seasonal evolution of penitente glaciochemistry at Tapado Glacier, Northern Chile, *Hydrological Processes*, 30(2), 176–186, doi:10.1002/hyp.10531, 2016.
- Thompson, L., E. Mosley-Thompson, M. Davis, P. Lin, T. Yao, M. Dyurgerov, and J. Dai, "Recent warming": ice core evidence from tropical ice cores with emphasis on Central Asia, *Global and Planetary Change*, 7(1-3), 145–156, doi:10.1016/0921-8181(93)90046-Q, 1993.
- Trachsel, J. C., M. Schneebeli, S. E. Avak, A. Eichler, J. Edebeli, and T. Bartels-Rausch, MISO: More than a Japanese Seasoning, in *Annual Report 2016 of the Laboratory of Environmental Chemistry*, p. 15, Villigen PSI, 2017.
- Tranter, M., S. Tsiouris, T. D. Davies, and H. G. Jones, A laboratory investigation of the leaching of solute from snowpack by rainfall, *Hydrological Processes*, 6(2), 169–178, doi:10.1002/hyp.3360060205, 1992.
- Tsiouris, S., C. E. Vincent, T. D. Davies, and P. Brimblecombe, The Elution of Ions Through Field and Laboratory Snowpacks, *Annals of Glaciology*, 7, 196–201, doi:10.3189/S0260305500006169, 1985.
- Van de Velde, K., C. Ferrari, C. Barbante, I. Moret, T. Bellomi, S. Hong, and C. Boutron, A 200 Year Record of Atmospheric Cobalt, Chromium, Molybdenum, and Antimony in High Altitude Alpine Firn and Ice, *Environmental Science & Technology*, 33(20), 3495–3501, doi:10.1021/es990066y, 1999.
- Van de Velde, K., C. F. Boutron, C. P. Ferrari, A.-L. Moreau, R. J. Delmas, C. Barbante, T. Bellomi, G. Capodaglio, and P. Cescon, A two hundred years record of atmospheric cadmium, copper and zinc concentrations in high altitude snow and ice from the French-Italian Alps, *Geophysical Research Letters*, 27(2), 249–252, doi:10.1029/1999GL010786, 2000.
- Virkkunen, K., J. Moore, E. Isaksson, V. Pohjola, P. Perämäki, A. Grinsted, and T. Kekonen, Warm summers and ion concentrations in snow: comparison of present day with Medieval Warm Epoch from snow pits and an ice core from Lomonosovfonna, Svalbard, *Journal of Glaciology*, 53(183), 623–634, doi:10.3189/002214307784409388, 2007.
- Wang, S., X. Shi, W. Cao, and T. Pu, Seasonal Variability and Evolution of Glaciochemistry at An Alpine Temperate Glacier on the Southeastern Tibetan Plateau, *Water*, 10(2), 114, doi:10.3390/w10020114, 2018.
- Wong, G. J., R. L. Hawley, E. R. Lutz, and E. C. Osterberg, Trace-element and physical response to melt percolation in Summit (Greenland) snow, *Annals of Glaciology*, 54(63), 52–62, doi:10.3189/2013AoG63A602, 2013.
- You, X., Z. Li, R. Edwards, and L. Wang, The transport of chemical components in homogeneous snowpacks on Urumqi Glacier No. 1, eastern Tianshan Mountains, Central Asia, *Journal of Arid Land*, 7(5), 612–622, doi:10.1007/s40333-015-0131-z, 2015.
- Zaromb, S., and R. Brill, Solid Solutions of Ice and NH<sub>4</sub>F and Their Dielectric Properties, *The Journal of Chemical Physics*, 24(4), 895–902, doi:10.1063/1.1742629, 1956.
- Zhang, Q., S. Kang, P. Gabrielli, M. Loewen, and M. Schwikowski, Vanishing High Mountain Glacial Archives: Challenges and Perspectives, *Environmental Science & Technology*, 49(16), 9499–9500, doi:10.1021/acs.est.5b03066, 2015.
- Zhongqin, L., L. Chuanjin, L. Yuefang, W. Feiteng, and L. Huilin, Preliminary results from measurements of selected trace metals in the snow-firn pack on Ürümqi glacier No. 1, eastern Tien Shan, China, *Journal of Glaciology*, 53(182), 368–373, doi:10.3189/002214307783258486, 2007.



Zong-xing, L., et al., The evolution and environmental significance of glaciochemistry during the ablation period in the north of Tibetan Plateau, China, *Quaternary International*, 374, 93–109, doi:10.1016/j.quaint.2014.06.071, 2015.



# 5 Redistribution of major ions and trace elements during snow metamorphism

## 5.1 Microscale rearrangement of ammonium induced by snow metamorphism

Jürg Christian Trachsel<sup>a,b</sup>, Sven Erik Avak<sup>c,d,e</sup>, Jacinta Edebeli<sup>b,c</sup>, Sabina Brütsch<sup>c</sup>, Thorsten Bartels-Rausch<sup>c</sup>, Martin Schneebeli<sup>a</sup>, and Anja Eichler<sup>c,e,\*</sup>

<sup>a</sup>WSL-Institute for Snow and Avalanche Research SLF, Davos Dorf, 7260, Switzerland

<sup>b</sup>Department of Environmental Systems Science, ETH Zurich, Zurich, 8006, Switzerland

<sup>c</sup>Laboratory of Environmental Chemistry, Paul Scherrer Institute, Villigen PSI, 5232, Switzerland

<sup>d</sup>Department of Chemistry and Biochemistry, University of Bern, Bern, 3012, Switzerland

<sup>e</sup>Oeschger Centre for Climate Change Research, University of Bern, Bern, 3012, Switzerland

\*Corresponding author

*Manuscript in preparation for  
The Cryosphere*

## Abstract

The fate of different chemical impurities during snow metamorphism has significant consequences on snow and atmospheric chemistry and on reconstructing past atmospheric pollution from ice core records. Although ammonium ( $\text{NH}_4^+$ ) is a fundamental proxy especially for biogenic, forest fire, and anthropogenic emissions, the redistribution during snow metamorphism affecting its potential post-depositional relocation and snow chemical reactivity is not understood so far. In this study we investigate the rearrangement of  $\text{NH}_4^+$  and five other major ions ( $\text{Ca}^{2+}$ ,  $\text{Cl}^-$ ,  $\text{F}^-$ ,  $\text{Na}^+$  and  $\text{SO}_4^{2-}$ ) in artificial and natural snow samples aged at a controlled temperature gradient for up to three months. In parallel, ion distribution in samples, taken from different depths of a natural snow pack at the Weissfluhjoch (Swiss Alps) that had undergone natural snow metamorphism, was studied. Initial snow structures (monitored with micro-computed tomography) and ion distribution (studied in elution experiments) varied strongly between the different snow samples. However, with progressing snow metamorphism snow structures became similar and ions with a high solubility in ice ( $\text{NH}_4^+$ ,  $\text{F}^-$ , and  $\text{Cl}^-$ ) were gradually buried in the ice interior, whereas  $\text{Ca}^{2+}$ ,  $\text{SO}_4^{2-}$  (and  $\text{Na}^+$ ) rather enriched at ice crystal surfaces. Our results show that the redistribution during snow metamorphism is strongly dependent on the temperature gradient, exposure time and chemical composition. The observed preferred incorporation of  $\text{NH}_4^+$  into ice interior during snow metamorphism suggests that this ion is less prone to post-depositional processes including meltwater percolation. Furthermore, our results imply that  $\text{NH}_4^+$  does not dominate snow chemical reactivity within an altered snow layer contrary to other species located at ice crystal surfaces such as  $\text{Ca}^{2+}$  and  $\text{SO}_4^{2-}$ .

### 5.1.1 Introduction

Ice cores recovered from cold glaciers are invaluable archives of past climate and atmospheric composition, covering up to 800,000 years [Augustin *et al.*, 2004] Among the countless impurities trapped in the ice, major ions provide precious information about past changes of anthropogenic pollution, atmospheric transport, forest fires, and of temperature changes [Eichler *et al.*, 2011; Kaspari *et al.*, 2007; Kellerhals *et al.*, 2010; Legrand and Mayewski, 1997; Thompson *et al.*, 2013]. During snowfall, atmospheric constituents such as aerosol particles and gases are scavenged and deposited by wet and/or dry deposition. After deposition in polar or high-altitude regions, snow is successive transformed into firn and glacier ice, leading to a final embedding of chemical impurities including major ions. However, the ice-core concentration records of major ions are not only determined by their initial atmospheric concentrations. Post-depositional processes can strongly alter the originally deposited signal. Such processes include wind erosion [Dansgaard, 1973; Lorius *et al.*, 1969], re-emission of volatile compounds from the snow surface [Röthlisberger *et al.*, 2002], sublimation [Stichler *et al.*, 2001], migration within the snow and firn

layer [Saltzman, 1995; Wolff, 1996], and relocation during melt-water percolation [Eichler *et al.*, 2001; Li *et al.*, 2006]. To use major ion records in ice cores as proxies for paleo atmospheric composition, post-depositional processes need to be understood.

The process of snow metamorphism strongly influences the embedding and location of chemical species within snow, firn, and glacier ice, determines their availability for post-depositional relocation, and has significant consequences on snow and atmospheric chemistry. Snow is a fully connected porous ice structure. During isothermal metamorphism, the structures with a higher curvature disappear, leading to a reduction in specific surface area. During temperature gradient metamorphism, the relatively warmer ice surface sublimates and becomes deposited on the cold side of a structure. This leads to a complete recrystallization of the original snow structure. Studies of snow exposed to a temperature gradient have shown, that dry metamorphism leads to substantial restructuring of the snow pack, i.e. to a mass turnover of the entire ice mass of up to 60% per day at a gradient of  $\sim 50 \text{ K m}^{-1}$  [Pinzer *et al.*, 2012; Pinzer and Schneebeli, 2009].

The sublimation and re-deposition of the ice phase affect the location of the embedded impurities. In particular, species that were deposited on the crystal surface can become embedded into the ice interior and vice versa. Furthermore, if volatile substances are present on the crystal surface, they are exposed to vertical water vapor fluxes. Although physical changes during snow metamorphism are well studied, very little is known about concurrent rearrangement of chemical species including major ions. Cragin *et al.* [1996] investigated the effect of snow metamorphism on the redistribution of the three major ions  $\text{Cl}^-$ ,  $\text{NO}_3^-$ ,  $\text{SO}_4^{2-}$ . By rinsing deionized water through a column of snow aged for 1-8 weeks they observed an increasingly preferential elution of  $\text{SO}_4^{2-}$  compared to  $\text{Cl}^-$  and  $\text{NO}_3^-$ . This observation was explained with an enhanced incorporation of  $\text{Cl}^-$  and  $\text{NO}_3^-$  into the ice interior and an exclusion of  $\text{SO}_4^{2-}$  to the ice crystal surface during snow metamorphism. The observed preferential elution of  $\text{SO}_4^{2-}$  compared to  $\text{NO}_3^-$  and  $\text{Cl}^-$  is in good agreement with field and laboratory investigations studying the elution of major ions through snow packs and firn/ice cores affected by melting [Brimblecombe *et al.*, 1985, 1987; Eichler *et al.*, 2001]. A consistent elution sequence of  $\text{SO}_4^{2-} > \text{NO}_3^- > \text{Cl}^-$  was found in most of the studies. A higher solubility of  $\text{Cl}^-$  compared to  $\text{SO}_4^{2-}$  in ice was used to explain its preferred incorporation into the ice matrix and thus, its less preferential removal with meltwater (see e.g. Eichler *et al.* [2001]).

To the best of our knowledge, no studies on the rearrangement of ammonium ( $\text{NH}_4^+$ ) and other cations during snow metamorphism are available, so far.  $\text{NH}_3$  is the most abundant alkaline gas in the atmosphere. Consequently,  $\text{NH}_3/\text{NH}_4^+$  concentrations in the air and snow strongly determine the uptake of acid species. A relocation of  $\text{NH}_4^+$  during snow metamorphism might thus significantly change pH and buffer capacity within the snow microstructure, with direct consequences for air-ice chemical exchanges and chemical reactivity [Bartels-Rausch *et al.*, 2014]. In ice cores, among the major ions,  $\text{NH}_4^+$  is an essential proxy for biogenic, forest fire, and anthropogenic agricultural emissions [Döscher *et al.*, 1996; Eichler *et al.*, 2009, 2011; Fuhrer *et al.*,

1996; Kellerhals *et al.*, 2010] and widely used to date ice cores by counting annual layers due to the strong seasonal variability [Führer *et al.*, 1993]. The majority of previous studies point to a good preservation of  $\text{NH}_4^+$  concentration records even in areas strongly affected by melting (Alps [Eichler *et al.*, 2001]; South America [Ginot *et al.*, 2010]; Tian Shan [Li *et al.*, 2006], Svalbard [Virkkunen *et al.*, 2007]).  $\text{NH}_4^+$  was often found at the end of elution sequences, as observed e.g. at the Ürümqi glacier No.1:  $\text{SO}_4^{2-} > \text{Ca}^{2+} > \text{Na}^+ > \text{NO}_3^- > \text{Cl}^- > \text{K}^+ > \text{Mg}^{2+} > \text{NH}_4^+$  [Li *et al.*, 2006]. Another study, however, led to contradicting results. Brimblecombe *et al.* [1985], observed an elution order of  $\text{SO}_4^{2-} > \text{NO}_3^- > \text{NH}_4^+ > \text{K}^+ > \text{Ca}^{2+} > \text{Mg}^{2+} > \text{Na}^+ > \text{Cl}^-$  in a field study from a Scottish snow pack, pointing to a higher mobility of  $\text{NH}_4^+$ . Together these studies have shown that  $\text{NH}_4^+$  is in most regions one of the least mobile ions with respect to meltwater percolation. However, the rearrangement of  $\text{NH}_4^+$  during snow metamorphism and its effect on the location at the microscopic scale, determining its post-depositional mobility and snow chemical reactivity, has never been investigated and is not understood, so far.

In this work, we studied the redistribution of six major ions  $\text{NH}_4^+$ ,  $\text{Ca}^{2+}$ ,  $\text{Cl}^-$ ,  $\text{F}^-$ ,  $\text{Na}^+$ , and  $\text{SO}_4^{2-}$  during snow metamorphism with a series of elution experiments. Artificial metamorphism was performed in the laboratory by exposing artificial and natural snow samples to a defined temperature gradient for up to three months. The snow structures of the samples were monitored using computer tomography. Elution experiments with ultra-pure water were performed to detect either the accumulation of the ions on the surface of the ice crystals or their inclusion in the ice interior. The surfaces of the artificial and natural snow crystals and thus the interface between ice and air, is referred to as “ice surface” in the following. For comparison, snow samples were stored at isothermal conditions during a three months period to clarify, whether the ion redistribution is driven by the temperature gradient or by the storage time. Additionally, we investigated structural differences and ion distribution in samples, taken from different depths of a natural snow pack that had undergone natural snow metamorphism. This setting allowed for the first time to extensively investigate the micro scale redistribution of  $\text{NH}_4^+$  with respect to other major ions during snow metamorphism and its driving forces.

## 5.1.2 Methods

### 5.1.2.1 Preparation of artificial and natural snow samples

**Preparation of artificial snow** Artificial snow was produced in the form of shock-frozen droplets. Solutions containing defined concentrations of the major ions were sprayed into a cryogenic container filled with liquid nitrogen. This method of snow production has already been successfully applied in other studies [Bartels-Rausch *et al.*, 2013]. The resulting ice droplets had diameters between 100 and 1000  $\mu\text{m}$ . Samples were prepared by sieving the snow to a fraction of 300-600  $\mu\text{m}$  in diameter. In the cold room at  $-20^\circ\text{C}$  about 60 g of the snow samples were filled in

**Table 5.1:** Comparison of the different bulk concentrations  $c_0$  in ppb.

	days	$\text{NH}_4^+$	$\text{Ca}^{2+}$	$\text{Cl}^-$	$\text{F}^-$	$\text{Na}^+$	$\text{NO}_3^-$	$\text{SO}_4^{2-}$
artificial snow	-	381±10	548±42	1003±25	851±55	1013±57	-	1024±30
natural snow	-	1029±5	99±7	52±4	8±0.2	18±2	1838±47	939±6
	0	1029±5	99±7	52±4	8±0.2	18±2	1838±47	939±6
natural snow pack	30	138±8	27±4	25±4	<0.5	10±1	218±12	83±9
	60	11±1	22±1	44±1	<0.5	18±1	257±8	36±1
	90	14±1	157±5	19±2	0.58±0.02	17±0.4	196±10	104±4

pre-cleaned 160 mL polypropylene (PP) containers. The bottom of each container was already covered with 40 g frozen ultra-pure water, to prevent the formation of an air gap at the bottom of the snow sample caused by the vapor flux during the aging. The containers were stored isothermally at  $-20^\circ\text{C}$  until the beginning of the metamorphism experiment. The bulk concentrations  $c_0$  of the different major ions in the sieved snow samples were determined in triplicate analyses using ion chromatography (IC). Concentrations varied between  $\sim 380$  and 1000 ppb (Table 5.1).

**Sampling of natural snow at Weissfluhjoch** After a major snowfall event on April 4<sup>th</sup>, 2017, we collected 20 kg of fresh snow from the Weissfluhjoch site (WFJ) in the Swiss Alps above Davos (2536 m a.s.l.). The snow was filled into a plastic box with a Teflon shovel. Both box and tools were pre-cleaned with ultra-pure water (Milli-Q, 18 M  $\Omega$  cm quality). The plastic box was sealed and placed in an insulated container which allowed to keep the snow frozen during the transport. In the laboratory at  $-20^\circ\text{C}$ , the snow was stirred with a Teflon rod to obtain a homogeneous snow sample. Bulk concentrations  $c_0$  of the different major ions in the WFJ snow samples determined in triplicate analyses by IC are given in Table 5.1. The natural snow samples were filled in 160 mL PP containers (as described above) and isothermally stored at  $-20^\circ\text{C}$  until the beginning of the metamorphism experiment.

### 5.1.2.2 Artificial and natural snow metamorphism

In total we examined three different combinations of snow type and metamorphism:

1. Artificial snow exposed to a laboratory-controlled temperature gradient,
2. natural snow exposed to a laboratory-controlled temperature gradient, and
3. natural snow from different depths of a snow pit at WFJ, that was exposed to natural metamorphism.

The combinations are listed in Table 5.2.

**Artificial metamorphism experiment in the laboratory** The 160 mL PP containers with the different snow samples were mounted into a metamorphism box

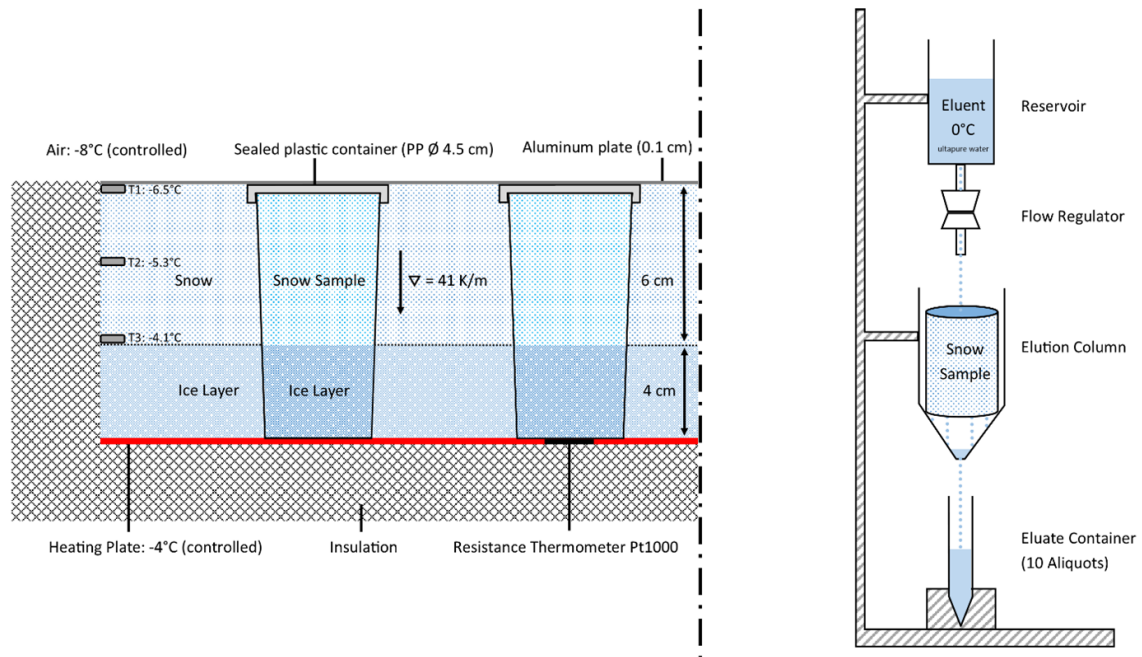


**Figure 5.1:** Left: Scheme of the metamorphism box containing 2 sample containers. In total there was space for up to 28 containers. Right: Scheme of the elution setup. This setup was installed in the laboratory at  $0^{\circ}\text{C}$ , a total of three elutions could be run simultaneously.

(Figure 5.1) and exposed for a period of 1-90 days to a well-defined temperature gradient. The metamorphism box (outside dimensions  $140 \times 70 \times 60 \text{ cm}$ ) offered space for up to 28 containers. The box was filled with a 4 cm ice layer covered with 6 cm of snow accordingly to the sample containers. On top of the surface, a thin aluminum plate prohibited sublimation of the filled snow. The bottom of the ice layer was heated to  $4^{\circ}\text{C}$  through a heating plate while the laboratory temperature was held at  $-8^{\circ}\text{C}$ . Effective temperatures at the top and bottom of the 6 cm thick snow samples were  $-6.5^{\circ}\text{C}$  and  $-4.1^{\circ}\text{C}$ , respectively, corresponding to a temperature gradient of  $40 \text{ K m}^{-1}$ . The snow samples were stored in the metamorphism box for 0, 3, 6, 12, 30, 60, and 90 days, respectively. At the end of each storage cycle, the corresponding containers were removed and prepared for the elution experiments. In order to keep the conditions steady throughout the experiment, empty spaces from removed containers were filled up with snow-filled dummy containers.

In addition to the snow samples aged at the defined temperature gradient in the metamorphism box, we stored samples of artificial and natural snow at isothermal conditions ( $-20^{\circ}\text{C}$ ) for a 90 days period. Samples were stored inside a multilayer box out of steel plates (1 cm thick) and Styrofoam (2 and 5 cm thick) according to *Löwe et al.* [2011] to maintain a homogeneous temperature of  $-20^{\circ}\text{C}$ . In Table 5.2 an overview of all used containers is given: For the artificial snow we used two containers for the 0, 6, 12, and 30-day batch (one for the elution experiment +



**Table 5.2:** Combinations of metamorphism type and snow examined in this study.

Metamorphism time (days)		0	3	6	12	30	60	90	90 isotherm
Metamorphism	Samples	number of sample containers: Elution/CT							
controlled (Lab)	artificial snow	1/1	-/-	1/1	1/1	1/1	3/1	-/-	-/1
controlled (Lab)	natural snow	3/1	3/1	3/1	3/1	3/1	3/1	3/1	1/1
natural	natural snow pack	3/1	-/-	-/-	-/-	3/1	3/1	3/1	-/-

one for monitoring structural changes using CT), 4 containers for the 60-day batch (triplicate elution + CT), and 1 container (CT) for the 90-day isothermal sample. For the natural snow we used 4 containers for each 0, 3, 6, 12, 30, 60, 90 day-batch (triplicate elution + CT), and 2 containers (elution + CT) for the 90-day isothermal batch. As initial state “Day 0” we define all states up to and including 24 hours of metamorphism.

**Natural metamorphism: Samples of natural snow from a WFJ snow pit** On April 4<sup>th</sup>, 2017 we sampled four times 1 kg of snow from the surface and three different depths of a snow pit at the field site WFJ. Each sample corresponded to a snowfall in January, February, March, and April 2017 and an age of three, two, one and zero month, respectively. This snow was filled into pre-cleaned plastic boxes and transported frozen to the cold lab. In the laboratory at  $-20$  °C, the snow was stirred with a Teflon rod and four times 60 g of each sample was filled into 160 mL PP containers (Table 5.2, triplicate elution + CT sample). Bulk concentrations  $c_0$  of the different major ions in the snow pit samples are given in Table 5.1. The containers were isothermally stored at  $-20$  °C until the beginning of the elution. These samples never went into the metamorphism box, as they were already exposed to a natural temperature gradient in the snow pack at WFJ.

The age of the snow in the snow profile was determined based on the density evolution. At the field site WFJ daily characterization of the snow pack was performed, including also density measurements with the Snow Micro Penetrometer SMP [Calonne *et al.*]. These measurements allowed to monitor the density evolution within the snow pack and to determine the age and depth of particular snow layers.

### 5.1.2.3 Elution experiments

All snow samples were tempered at a laboratory temperature of  $-0.2$  °C for 2 hours prior to the elution experiment. Then the snow sample was extracted by removing the ice bottom using a ceramic knife and transferred into the elution column. The elution was performed in a 10 cm long plastic column with a diameter of 6 cm (Figure 5.1). The sample was rinsed with an eluent of ultra-pure water (0 °C). The eluent flow was set to  $140$  mL  $h^{-1}$  with the help of a drop regulator. After a specific

saturation time, the eluate started to drip out at the outflow of the column and was collected in 15 mL PP vials (Sarstedt, Nümbrecht, Germany). We collected 10 aliquots for each elution experiment: the first 4 with a volume of 3 mL, the second 4 with 6 mL, and finally 2 aliquots with 12 mL volume. During the experiment the surface temperature was continuously monitored by an infrared thermometer and thermo-loggers to be stable at  $-0.5 \pm 0.5$  °C. After the collection of the 10 aliquots, the remaining snow sample in the elution column was allowed to melt at room temperature. Two aliquots were collected in 50 mL PP vials (Sarstedt, Nümbrecht, Germany).

#### 5.1.2.4 Vertical distribution of ions after temperature gradient storage

To investigate the vertical distribution of the ion concentration within one sample, we split the CT samples of the natural snow batch (0, 3, 6, 12, 60, 90, and 90 days isothermal, Table 5.2) into two parts: One part was used to determine the microstructure in the CT (see below). The second part was used to analyze the vertical distribution of the ions. The 6 cm snow samples were vertically cut into five  $\sim 1.2$  cm slices. The potentially contaminated surface of these slices was removed with a pre-cleaned ceramic knife and the decontaminated samples stored in 50 mL PP containers at  $-20$  °C until IC analysis.

#### 5.1.2.5 Ion chromatography

Concentrations of the major cations  $\text{Ca}^{2+}$ ,  $\text{Na}^+$ ,  $\text{NH}_4^+$ , and anions  $\text{Cl}^-$ ,  $\text{F}^-$ ,  $\text{SO}_4^{2-}$  in the different elution and snow samples were determined using ion chromatography (IC). A Metrohm (Herisau, Switzerland) 850 Professional IC combined with an 872 Extension Module and an 858 Professional Sample Processor autosampler was used for the analyses. Detection limits were 10, 1, 0.5, 0.5, 0.5, and 5 ppb for  $\text{Ca}^{2+}$ ,  $\text{Cl}^-$ ,  $\text{F}^-$ ,  $\text{Na}^+$ ,  $\text{NH}_4^+$ , and  $\text{SO}_4^{2-}$ , respectively.

#### 5.1.2.6 X-ray micro-tomography (CT)

For the structural analyses, one sample of each batch (Table 5.2) was scanned in the microCT. The snow sample was extracted from the container by removing the ice bottom, cut into a 1.5 x 1.5 x 6 cm column and mounted into a sample holder (diameter 2 cm). The X-ray computed tomography scanner (Scanco microCT 40) was operated at a temperature of  $-20$  °C and had a resolution of 10  $\mu\text{m}$ . The reconstructed CT images were filtered with a Gaussian filter (support 2 voxels, standard deviation 1 voxel) and the threshold for segmentation was applied according to *Hagenmuller et al.* [2014]. Structural parameters of the segmented ice structure were extracted with the software tools of the CT device (Image Processing Language, Scanco Medical). The specific surface area (SSA) was calculated by triangulation

of the ice-air interface [Kerbrat *et al.*, 2008]. Although the volume of snow in the sample holder was comparatively small, it was a hundred times larger than the representative elementary volume [Kaempfer *et al.*, 2005].

## 5.1.3 Results

### 5.1.3.1 Structural development of artificial and natural snow during metamorphism

**Temperature gradient metamorphism** The microCT images in Figure 5.2 show the different snow samples obtained during our study, demonstrating how snow underwent drastic structural changes during snow metamorphism.

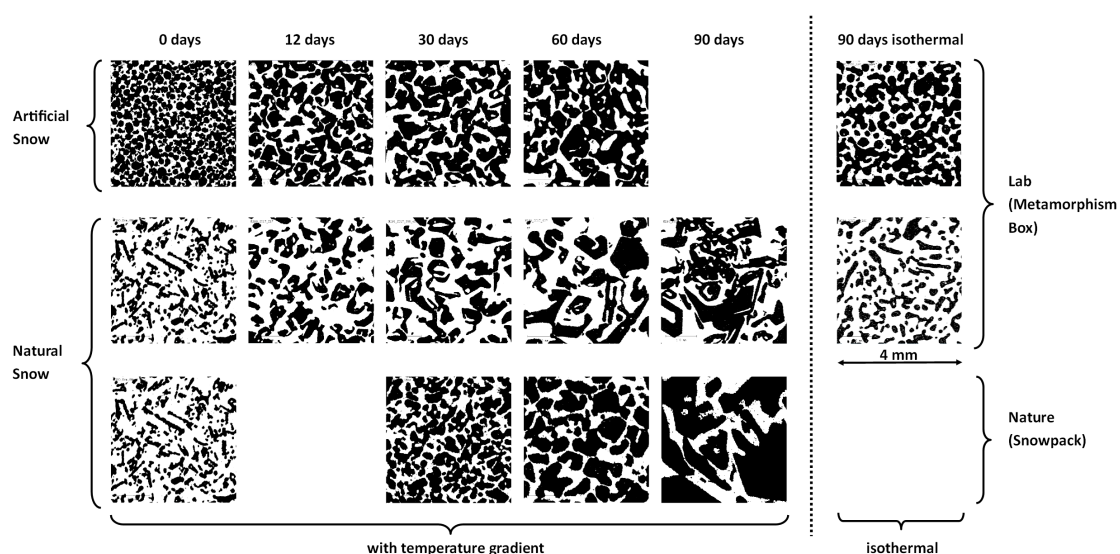


**Figure 5.2:** Structural development of the snow samples during metamorphism imaged by microCT. Solid ice is black colored, interstitial air white colored. Cross-sections are shown for artificial snow (upper row) and natural snow (middle row) after 0, 6, 12, 30, 60, and 90 days of storage under an artificial gradient of  $40 \text{ K m}^{-1}$  and 90 days isothermal storage at  $-20 \text{ }^\circ\text{C}$ . In the lower row cross-sections of 0, 30, 60, and 90 day old snow from different depths of the snow pit at WFJ are shown. These four samples originate from four different snowfall events.

The initial structure of the two types of snow differed strongly: In artificial snow, the individual spheres of homogeneous diameter are partially recognizable. The natural snow shows the typical characteristics of fresh snow with dendritic branching (see Figure 5.2 and Figure 5.3, first column). In both types, the bonds between the individual particles are still little developed, so that the shape of the original crystals can be presumed. Already after 12 days of storage time at a gradient of  $40 \text{ K m}^{-1}$ , the differences between the two types of snow were much smaller. A significant

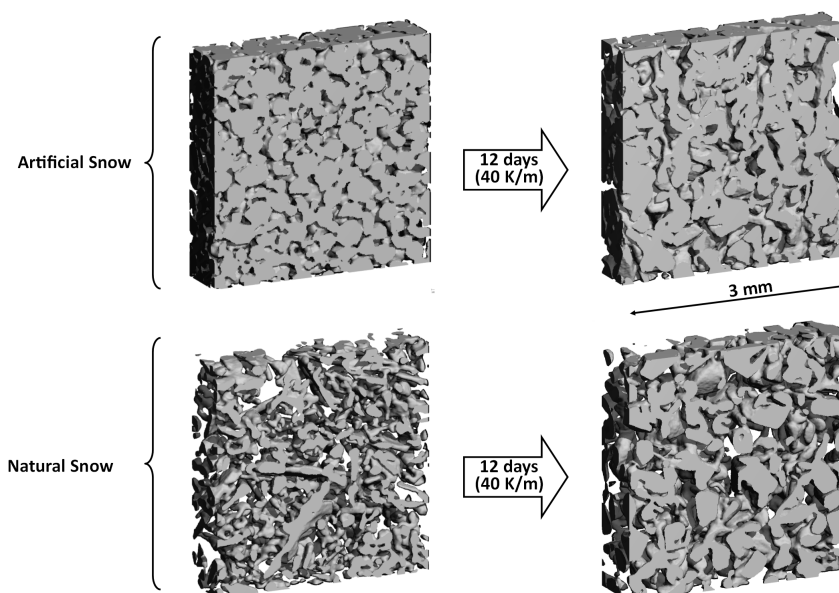


**Figure 5.3:** Qualitative evolution (3D microstructure) of artificial and natural snow under an artificial temperature gradient of  $40 \text{ K m}^{-1}$  imaged by microCT after 0 days (left) and 12 days (right). The dimensions of the observed sub-volume of the measured field of view are  $3 \times 3 \times 0.5 \text{ mm}$ .

coarsening of the structure could be observed and a fully connected porous ice structure had grown out of both the spheres and the fresh snow. The reduction of the SSA during this recrystallization is clearly visible. With increasing storage time, the coarsening is further strengthened (Figure 5.2, third to fifth column). Although the snow from the snow pit originates from three different snowfall events, it shows the same behavior as the snow exposed to an artificial temperature gradient. The 90-day natural snow pack sample has transformed most compared to the initial state at day 0 (Figure 5.2, last row).

The development of the specific surface area (SSA) of the individual snow samples during the metamorphism experiment is shown in Figure 5.4. At the beginning, the different snow types show the respective highest SSA. During storage under temperature gradient, the SSA of all snow samples decreased. For natural snow, the initial decrease in SSA was most pronounced. It decreased by a factor of 2.2 from  $27.0 \text{ m}^2 \text{ kg}^{-1}$  to  $12.2 \text{ m}^2 \text{ kg}^{-1}$  within 30 days. The initial decrease was less pronounced for artificial snow, showing a decline from  $15.9 \text{ m}^2 \text{ kg}^{-1}$  to  $12.2 \text{ m}^2 \text{ kg}^{-1}$  during the first month. After 12 days the artificial and the natural snow showed a comparable SSA within the uncertainty of  $\sim 10\%$ . From this moment on, the development of the respective SSA proceeded in parallel.

The snow samples taken from the WFJ profile showed a similar SSA decrease during the first 30 days compared to the natural snow aged in the laboratory at  $40 \text{ K m}^{-1}$  (Figure 5.4). Afterwards, the SSA of the WFJ snow pit samples decreased below the levels of the samples exposed to artificial metamorphism.

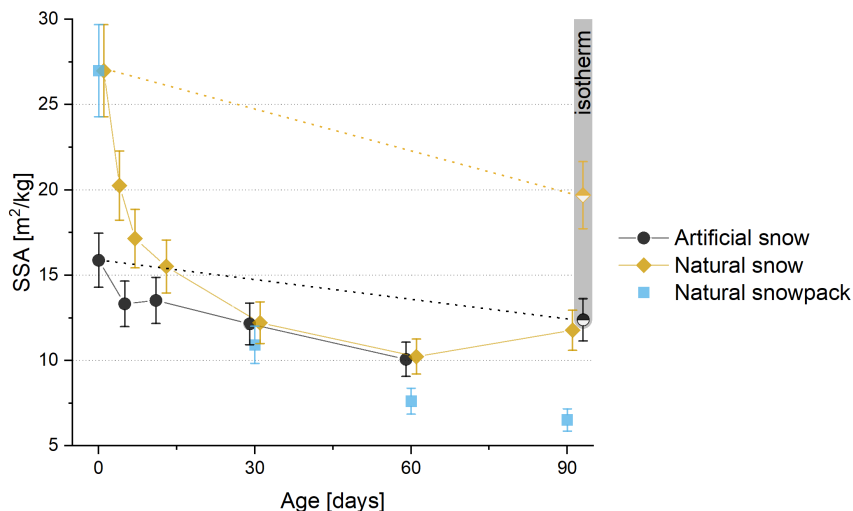


**Figure 5.4:** SSA evolution of natural (yellow diamonds) and artificial snow (black dots) aged at the artificial temperature gradient of  $40 \text{ K m}^{-1}$ ; the blue squares represent SSA changes in 0, 30, 60, and 90-day old snow from different depths of the snow pit at WFJ. These four samples originate from four different snowfall events.

**Isothermal metamorphism** The two samples isothermally stored at  $-20 \text{ }^\circ\text{C}$  for 90 days behaved differently: Both artificial and natural snow have undergone much less change without a temperature gradient. The fine edged structures of the natural snow were rounded, but the individual crystals were still recognizable. For artificial snow, the decrease in SSA after 90 days to  $12.4 \text{ m}^2 \text{ kg}^{-1}$  was  $\sim 22\%$ , which corresponds to an aging time of  $\sim 30$  days at a gradient of  $40 \text{ K m}^{-1}$ . The SSA of natural snow after 90 days isothermal storage decreased to  $19.7 \text{ m}^2 \text{ kg}^{-1}$  at the same time. This decrease of  $\sim 27\%$  corresponds to an aging time of  $\sim 3$  days at a gradient of  $40 \text{ K m}^{-1}$ .

### 5.1.3.2 Redistribution of ammonium and other major ions during snow metamorphism

**Elution experiments** Results for the elution of WFJ snow samples exposed to artificial metamorphism for 0 and 30 days are shown in Figure 5.5a and b, respectively. Concentrations of the six investigated major ions decreased between the 1<sup>st</sup> and 10<sup>th</sup> eluate aliquot (as exemplarily shown for  $\text{NH}_4^+$  and  $\text{Ca}^{2+}$ ). We assume that the concentration  $c_s$  of the 1<sup>st</sup> aliquot represents the composition of the ice surface (Figure 5.5a and b, left gray bars). Additionally, major ion concentrations  $c_i$  in the residual sample after the elution characterize conditions in the ice interior (Figure 5.5a and b, right gray bars). Concentrations in the ten aliquots and the residual samples were normalized to the bulk concentrations  $c_{\text{Bulk}}$  of the original snow sample, to allow comparability between the different ions. By comparing the

elution results for the samples aged for 0 and 30 days (Figure 5.5a and b) it is obvious that strong chemical fractionation had occurred:  $\text{Ca}^{2+}$  was stronger enriched at the ice surfaces after 30 days, explaining its higher concentrations in the first eluate. On the contrary,  $\text{NH}_4^+$  concentration at the ice surfaces did not significantly change between day 0 and 30, whereas it increased in the ice interior compared to  $\text{Ca}^{2+}$ .

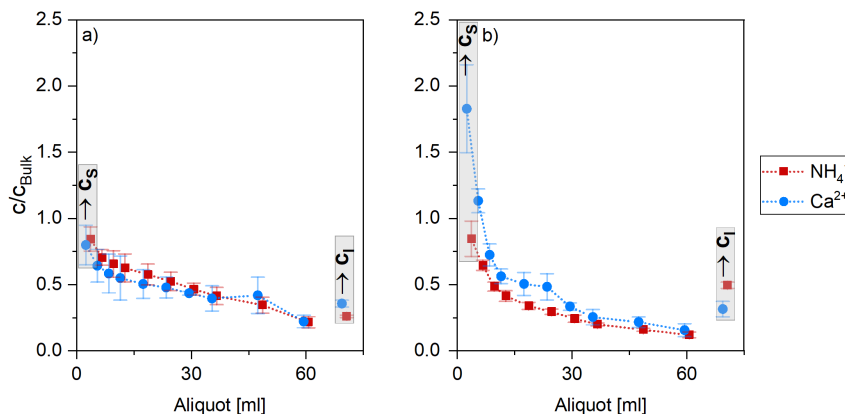


**Figure 5.5:** Comparison of the  $\text{NH}_4^+$  (red) and  $\text{Ca}^{2+}$  concentration (blue) in the 10 different aliquots and the molten residual snow during the elution of natural snow at (a) 0 day and (b) 30 days storage time. The concentration of the first eluate corresponds to the composition at the ice surface ( $c_s$ ). The concentration of the molten residual snow sample represents conditions in the ice interior ( $c_i$ ).

**Temporal changes of ion concentrations at ice surface and ice interior** For the investigation of the chemical fractionation of the six major ions during snow metamorphism, we analyzed the temporal trends of the normalized ion concentrations  $c_s/c_{\text{Bulk}}$  in the first eluate (Figure 5.6a-c) and  $c_i/c_{\text{Bulk}}$  in the molten residual sample (Figure 5.6d-f). Depending on the different snow types we observed varying chemical fractionation with time:

- *Artificial metamorphism, artificial snow (Figure 5.6a and d)*  
There was a continuous enrichment of  $\text{NH}_4^+$ ,  $\text{Cl}^-$ ,  $\text{F}^-$ ,  $\text{Na}^+$  concentrations in the ice interior during the two months of aging.  $\text{NH}_4^+$  and  $\text{Cl}^-$  showed the strongest increase. At the ice surfaces concentrations of all ions basically decreased during the first 12 days, then  $\text{SO}_4^{2-}$  and  $\text{Ca}^{2+}$  showed over two months the strongest enrichment.
- *Artificial metamorphism, natural snow (Figure 5.6b and e)*  
There was a continuous enrichment of  $\text{F}^-$ ,  $\text{NH}_4^+$ ,  $\text{Cl}^-$ ,  $\text{SO}_4^{2-}$  in the ice interior during the first month.  $\text{NH}_4^+$  and  $\text{F}^-$  showed the strongest increase. Between one and three months the concentration was rather stable. The concentration of  $\text{Na}^+$  and  $\text{Ca}^{2+}$  stayed almost constant with time. At the ice surfaces, we observed declining concentrations of all major ions during the first 12 days,

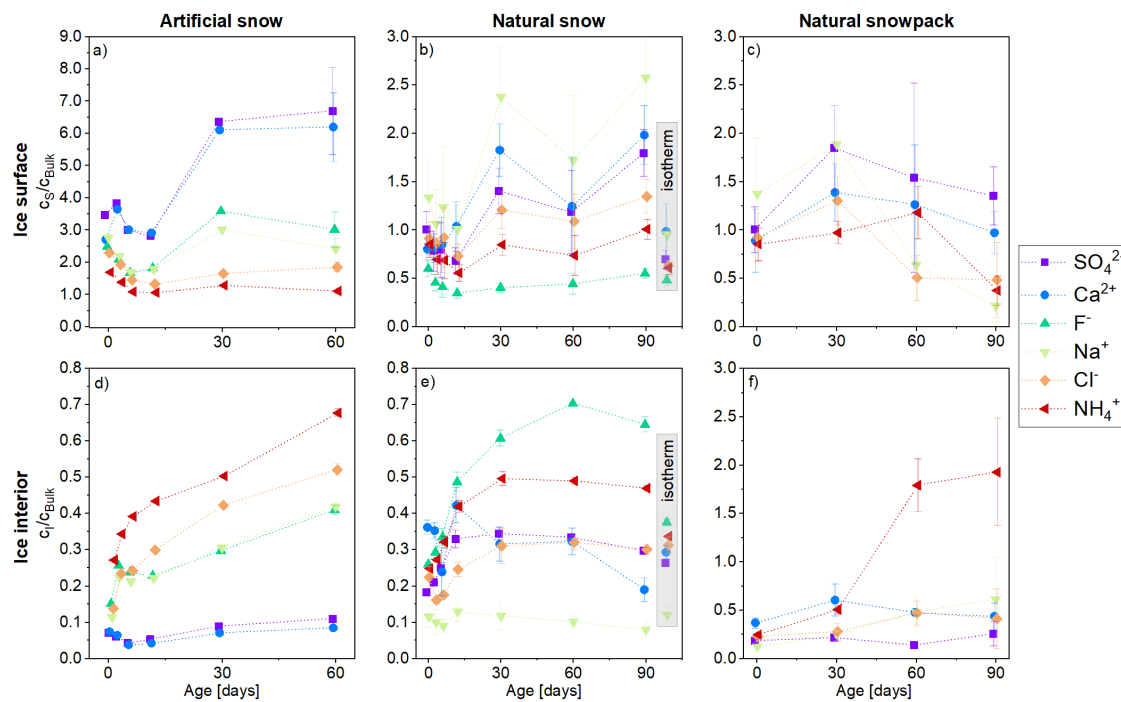


**Figure 5.6:** Temporal evolution of normalized ion concentrations  $c_S/c_{\text{Bulk}}$  at ice surfaces (a-c) and  $c_I/c_{\text{Bulk}}$  in the ice interior (d-f). a,d: artificial metamorphism, artificial snow. b,e: artificial metamorphism, natural snow. c,f: natural metamorphism, natural snow pack. Data points within the gray bars (b,e) represent a sample isothermal stored for 90 days at  $-20\text{ }^\circ\text{C}$ .

followed by increasing values most pronounced for  $\text{Na}^+$  and  $\text{Ca}^{2+}$  during the first month. Then the concentration remained stable.

- *Natural metamorphism, WFJ snow pit (Figure 5.6c and f)*

In the ice interior, we determined a continuous enrichment of  $\text{NH}_4^+$ , whereas the concentrations of  $\text{Cl}^-$ ,  $\text{SO}_4^{2-}$ ,  $\text{Na}^+$ , and  $\text{Ca}^{2+}$  did change less. The concentration of  $\text{F}^-$  was below the detection limit. At the ice surfaces we observed in tendency highest concentrations for all ions after 30 days. After 90 days the concentrations of  $\text{SO}_4^{2-}$  and  $\text{Ca}^{2+}$  were enriched the most. Note: the four different snow samples (0, 30, 60, 90 days) resulted from four different precipitation events and the metamorphism proceeded under unknown conditions.

### Temporal changes in ion concentrations at grain boundaries and interior under isotherm conditions

The results of the elution of the isothermally stored reference samples showed that fractionation of the ions without temperature gradient was much less pronounced compared to the same age with gradient (Figure 5.6b and e). Chemical fractionation after 90 days of isothermal storage only corresponds to the change of  $\sim 6$ -12 days with temperature gradient.

**Enrichment of  $\text{NH}_4^+$  in the ice interior (gradient/isotherm)** To qualitatively compare the enrichment of  $\text{NH}_4^+$  compared to the other ions in the ice interior, we investigated the ratio of the normalized ion concentration  $c_I(\text{ion})/c_{\text{Bulk}}(\text{ion})$  to the normalized  $\text{NH}_4^+$  concentration  $c_I(\text{NH}_4^+)/c_{\text{Bulk}}(\text{NH}_4^+)$  (Figure 5.7).

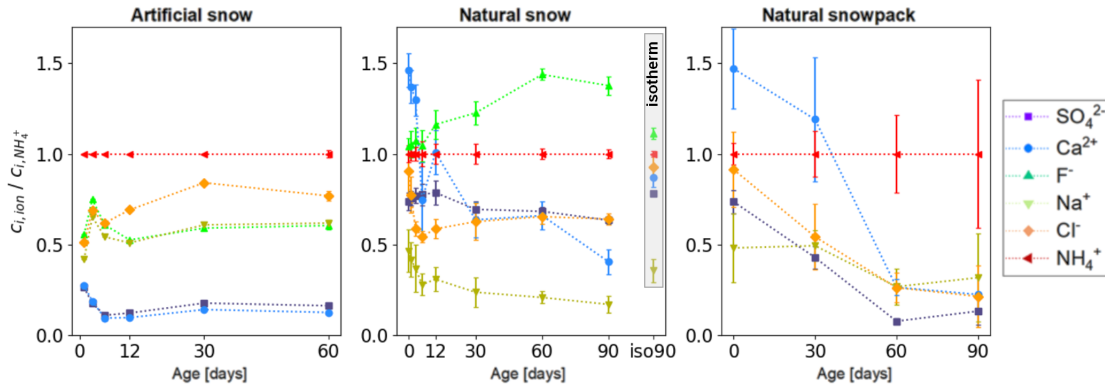


**Figure 5.7:** Concentration records of the individual ions in relation to  $\text{NH}_4^+$  within the ice interior. Shown are results for artificial metamorphism/ artificial snow (left), artificial metamorphism/ natural snow (middle), natural metamorphism/ natural snow pack (right). Data points within the gray bar (natural snow) represent a sample isothermally stored for 90 days at  $-20\text{ }^\circ\text{C}$ .

- *Artificial metamorphism, artificial snow (Figure 5.7 left)*  
 $\text{NH}_4^+$  was strongest enriched compared to all other ions during the whole experiment.  $\text{Ca}^{2+}$  and  $\text{SO}_4^{2-}$  were found to be most depleted from the beginning on. The enrichment sequence did not distinctly change with time.
- *Artificial metamorphism, WFJ snow (Figure 5.7 middle)*  
 $\text{Ca}^{2+}$  concentrations were higher compared to all other ions in the beginning. With time, a gradual decrease in the  $\text{Ca}^{2+}$  concentrations occurred. From day  $\sim 12$  on,  $\text{Ca}^{2+}$  concentrations were smaller than  $\text{NH}_4^+$  and  $\text{F}^-$  concentrations. Whereas in the beginning  $\text{NH}_4^+$  and  $\text{F}^-$  concentrations were similar, a gradual increase in  $\text{F}^-$  compared to  $\text{NH}_4^+$  concentrations occurred.  $\text{Na}^+$  concentrations were smallest during the whole experiment. Fractionation of the ions in the samples stored isothermally for 90 days was much less pronounced compared to the same age with gradient. Observed changes correspond to a gradient storage of 6-12 days.
- *Natural metamorphism, WFJ snow (Figure 5.7 right)*  
 $\text{F}^-$  concentrations were below detection limit for all samples.  $\text{Ca}^{2+}$  concentrations were higher compared to all other ions in the beginning. Only between 30 and 60 days  $\text{Ca}^{2+}$  concentrations dropped below  $\text{NH}_4^+$  levels and after 60 days  $\text{NH}_4^+$  was strongest enriched.



**Vertical distribution of ions after temperature gradient storage** The comparison of the concentrations of the ions within the five parts ( $\sim 1.2$  cm) of the vertically split snow samples did not show any significant differences. No vertical gradient was formed during the different stages of snow metamorphism.

## 5.1.4 Discussion

### 5.1.4.1 Structural change under temperature gradient

Within temperature metamorphism, the gradient is the initiating driving force for the migration of the water vapor in the interstices of the ice [Sokratov *et al.*, 2001]. The flux is moving from the warmer end to the colder end of the snow [Adams and Brown, 1983]. If the vapor flux hits a crystal, it is deposited on its colder side. This causes the crystal to grow in the opposite direction to the flux [Adams and Miller, 2003]. At the same time, sublimation takes place on the warmer side of the crystal. This provides new vapor to supply the closest adjacent crystal [Pinzer *et al.*, 2012]. Thus, a directed vapor flux from crystal to crystal is created without a continuous flow-through from the bottom to the top. Over time, these local rearrangements completely renew and transform the structure of the original ice crystals. This rebuild is accompanied by a decrease in SSA [Chen and Baker, 2010]. Smaller structures are eliminated during this relocation because their lifetime is shorter than the one of larger structures due to the fact that smaller structures sublimate faster than larger ones. Pinzer *et al.* [2012] showed a characteristic residence time of 2-3 days for an ice volume at a gradient of  $50 \text{ K m}^{-1}$ . Accordingly, during our storage period of 90 days, the entire ice structure was continuously sublimated and rebuilt up to 40 times.

Figure 3 shows, that the initial SSA decrease for artificial snow was much less pronounced compared to natural snow. The rounded structures of the artificial droplets hardly had any fine crystals that would have significantly altered the SSA due to their rapid degradation. The absence of small structures in artificial snow results on the one hand of the production-related round shape and on the other hand on the subsequent sieving. Natural snow, however, contained these fine structures and therefore showed a much larger initial surface area than the artificial droplets. Within the first 30 days the SSA of natural snow decreased by a factor of 2.2 from  $27.0 \text{ m}^2 \text{ kg}^{-1}$  to  $12.2 \text{ m}^2 \text{ kg}^{-1}$ , whereas that of artificial snow dropped only by a factor of 1.3 from  $27.0 \text{ m}^2 \text{ kg}^{-1}$  to  $12.2 \text{ m}^2 \text{ kg}^{-1}$ . After 12 days, the SSA of natural and artificial snow showed similar values. The development of the SSA in our experiments corresponds to results of other studies on dry metamorphism [Pinzer *et al.*, 2012].

The samples taken directly from the different depths of the WFJ snow pit originated from different snowfall events and had been exposed to varying temperature gradients in the field. Within a natural snow pack often a diurnal cycle is visible. The radiation at night cools the snow surface and the gradient increases. The warming

by the sun during the day leads to an increase of the snow surface temperature and it can even cause a reversed gradient. The SSA after 60 and 90 days of natural metamorphism was lower compared to that of the laboratory study. Since temperature gradients smaller than  $40 \text{ K m}^{-1}$  have been observed in the Alpine snow cover at WFJ during winter, this lower value is probably the result of stable growth of the crystals during medium temperature gradients. Unstable crystal growth has been proposed to occur at very high temperature gradients of  $\sim 50 \text{ K m}^{-1}$  [Pinzer *et al.*, 2012]. However, this process is poorly understood and needs further studies.

The structural development in Figure 5.2 reveals how an anisotropic structure is successively formed from the isotropic starting material: On day 0 the single globules in artificial snow and the fine dendritic branches in natural snow were visible. After 12 days the metamorphism had formed a cluster-like structure. The resulting structures differ no longer between artificial and natural snow.

#### 5.1.4.2 Structural changes under isothermal conditions

After isothermal storage of 90 days, the natural snow showed only a small change and therefore a higher SSA compared to the sample exposed to a gradient of  $40 \text{ K m}^{-1}$  for the same time. The SSA in the isothermal sample corresponds roughly to the value of the natural snow stored for only  $\sim 3$  days within the gradient. This can be explained by the lower recrystallization rate: During the metamorphism without a gradient, surface energy is minimized by reducing the area of the surface [Löwe *et al.*, 2011]. The convex ends of the tiny ice branches have the highest curvature and the highest surface tension [Colbeck, 1980]. There, ice is sublimated and re-deposited to adjacent concave cavities [Flin *et al.*, 2004]. Dendritic snow crystals are thus progressively rounded off. The flux due to the curvature is significantly smaller than the one due to the temperature gradient and therefore, this process is much slower [Sokratov and Maeno, 1997].

For artificial snow, the structural changes were even less pronounced. The comparison of Figure 5.2 (last row) confirms that the structure is still isotropic: After 90 days of isothermal storage, the original structure of the artificial snow was still visible. Only the bonding between the original particles increases. In natural snow, the single crystals were generally preserved and visible. However, these crystals were visibly rounded, as the edged contours had disappeared due to the optimization of the surface energy [Löwe *et al.*, 2011].

Initial snow structures and SSA widely varied between natural and artificial snow. After  $\sim 12$  days of artificial aging, however, these original differences vanished, and both types of snow showed similar structural and SSA changes during metamorphism induced by the temperature gradient. Physical changes after 2-3 months of natural snow metamorphism inside the WFJ snow pack were even more advanced, demonstrating a more stable crystal growth at this site.

The comparison of the physical development of the different snow samples in our study shows how much the structure changes during temperature-induced artificial

and natural snow metamorphism. The strong transformation in which the entire ice structure is altered forms the basis of our hypothesis that metamorphism has an effect on the distribution of the chemical species contained in snow.

#### 5.1.4.3 Rearrangement of major ions during snow metamorphism

During the three months of metamorphism, we observed a strong fractionation of the major ions between ice interior and ice surfaces, detected in the normalized concentration records  $c_I$  and  $c_S$  of the elution experiments, respectively (Figure 5.6). The interpretation of the results of the elution experiments is based on the following assumptions:

- The ions, located on the ice surfaces are instantly dissolved by the eluent (ultra-pure water).
- The exchange between ice surface and interior (diffusion in ice) is much slower than the dissolution in water at the surface. Thus, the ions present in the ice are preserved during elution.
- Elution with 0 °C water at 0 °C room temperature does not melt the crystals.

For artificial and natural snow samples the change in concentrations during the three months of artificial metamorphism was not linear and can be split into two phases:

- Phase 1) During the first 12 days of the experiment, a decrease at the ice surface ( $c_S$ ) occurred in the concentrations of almost all ions (Figure 5.6a and b).
- Phase 2) After 12 days until 3 months there was a strong fractionation of the ions: Whereas in general  $\text{NH}_4^+$ ,  $\text{Cl}^-$ ,  $\text{F}^-$  were gradually enriched in the ice interior, an exclusion of  $\text{SO}_4^{2-}$  and  $\text{Ca}^{2+}$  to the ice surface took place.

For WFJ snow samples that had undergone natural metamorphism, the most significant feature is a strong enrichment of  $\text{NH}_4^+$  compared to other ions in the ice interior after one month (Figure 5.6f). Due to the high heterogeneity of the different samples from the WFJ snow pack (indicated by the large error bars, Figure 5.6c) significant concentration trends could not be observed at the ice surface. However, similar to the samples experiencing artificial metamorphism,  $\text{SO}_4^{2-}$  and  $\text{Ca}^{2+}$  were enriched compared to the other ions after 60 days.

**Initial ion location in the snow structure** *Artificial snow:* The artificial snow was produced by shock-freezing a solution of the six ions  $\text{Ca}^{2+}$ ,  $\text{Na}^+$ ,  $\text{NH}_4^+$ ,  $\text{Cl}^-$ ,  $\text{F}^-$ , and  $\text{SO}_4^{2-}$ . Concentrations were chosen in such a way that solubility limits for the formation of potential water-insoluble components ( $\text{CaSO}_4$ ,  $\text{CaF}_2$ ) were not exceeded and all species were present as ions. Already at the beginning before the start of the metamorphism experiment, there was a strong fractionation of the ions in the shock frozen droplets.  $\text{NH}_4^+$  concentrations (day 0) were enhanced in the ice lattice

( $c_I$ , Figure 5.6d and Figure 5.7) and depleted at the ice surface ( $c_S$ , Figure 5.6a) compared to the other five ions. Obviously, the high solubility of  $\text{NH}_4^+$  in ice (see below) determines already its segregation during the process of shock-freezing.

*Natural snow:* In natural snow, the initial position of an ion in the snow structure is determined by scavenging processes in the atmosphere. Aerosol particles containing major ions can be incorporated in the snow crystal matrix, by acting as ice nuclei. On the other hand, direct impaction of aerosol particles on snow crystals or accumulation of supercooled water droplets onto ice crystal surfaces (riming) leads to the enrichment of these species at the edges of the crystal [Mosimann *et al.*, 1994; Pruppacher and Klett, 2010]. Contrary to the artificial snow, where  $\text{NH}_4^+$  was already initially enriched in the ice lattice, enhanced  $\text{Ca}^{2+}$  concentrations were observed in the ice interior for the natural snow (Figure 5.6 and Figure 5.7). This finding is in good agreement with the fact that mineral dust particles preferably act as ice nuclei [Szyrmer and Zawadzki, 1997]. Concentrations of the six investigated ions in the natural snow were well below solubility limits for potential water insoluble components (such as  $\text{CaSO}_4$ ) and we propose that all were present as ions in the snow structure.

### **General decreasing surface concentrations $c_S$ during the first 12 days – SSA changes**

The general decrease in concentration of all ions at the surface ( $c_S$ ) in the first 12 days was concurrent with a reduction of the SSA (Figure 5.4). This SSA decrease reduces the active area, where chemical exchange processes can take place. The SSA decline of natural snow during the first 12 days was much more pronounced for the natural snow and less distinct for the artificial snow (see above). Thus, we would expect a much stronger decrease in the  $c_S$  of the natural snow based only on SSA changes. However, changes in  $c_S$  of the two snow types were rather similar (decrease factors of  $\sim 1.2$ -2 between day 0 and 12, see Figure 5.6a and b). This discrepancy can be explained by an additional influence of the permeability of the snow samples. Natural snow revealed a lower density ( $\sim 0.4 \text{ g cm}^{-3}$ ) compared to artificial snow ( $\sim 0.6 \text{ g cm}^{-3}$ ) during the initial 12 days. The lower density of the natural snow led to a smaller residence time of the eluent in the snow sample (higher permeability) and thus, less uptake of ions from the ice surface, counteracting the effect of a higher active surface.

A second possible approach to explain the decrease of  $c_S$  during the first 12 days is the covering of the surface with clean ice. The temperature-induced water vapor flux sublimates clean water and deposits layer by layer on adjacent crystals (see above). This also coats the ions lying on the surface and prevents them from being mobilized during elution. With this approach, however, it remains unexplained, why this effect was no longer recognizable after 12 days.

### **Ion fraction between 12 days and 3 months – solubility in ice**

In the second phase starting from day  $\sim 12$ , despite a constant or further decreased SSA, there was a significant enrichment of the ions  $\text{SO}_4^{2-}$ ,  $\text{Ca}^{2+}$ , (and  $\text{Na}^+$ ) compared to the

other ions at the ice surface. At the same time,  $\text{NH}_4^+$ ,  $\text{Cl}^-$ , and  $\text{F}^-$  concentrations preferably increased in the ice interior. We relate this different behavior to a varying solubility of the ions in ice. High solubilities are known for  $\text{NH}_4^+$  and  $\text{F}^-$ . Since atomic radii of N and F are comparable to that of an O atom,  $\text{NH}_4^+$  and  $\text{F}^-$  are most probably substitutionally incorporated, replacing water molecules in the ice lattice up to  $\sim 10^{-2}$  mol l $^{-1}$  [Pruppacher and Klett, 2010]. For  $\text{Cl}^-$  a maximum solubility of  $9 \cdot 10^{-5}$  mol l $^{-1}$  and interstitial incorporation into the ice structure was proposed by Thibert and Dominé [1998]. Data on the solubility of  $\text{Na}^+$ ,  $\text{Ca}^{2+}$ , and  $\text{SO}_4^{2-}$  in ice is lacking, maximum solubilities in the order of  $10^{-7}$  mol l $^{-1}$  have been suggested [Eichler et al., 2001]. Thus, the low solubility of the latter three ions in ice favors their segregation at the ice surface with time, whereas the higher solubility of  $\text{NH}_4^+$ ,  $\text{F}^-$ , and  $\text{Cl}^-$  explains their incorporation into the ice interior.

Besides solubility in ice, varying volatility of chemical species may play a role in their redistribution during snow metamorphism. This was tested by investigating vertical concentration gradients in the snow samples at different metamorphism stages. No vertical gradients were found throughout the duration of the experiment. Thus, we conclude that there is no transport of potential volatile species with the vapor flux at scales above  $\sim 1.2$  cm and solubility in ice is the driving factor explaining ion fractionation during snow metamorphism.

**$\text{NH}_4^+$  enrichment in the ice interior** For the qualitative comparison of the  $\text{NH}_4^+$  incorporation into the ice compared to that of the other five ions, we formed enrichment sequences based on the ratio of the normalized ion concentration to the normalized  $\text{NH}_4^+$  concentration in the ice interior (Figure 5.7). We obtained the following enrichment sequences (enrichment in inner samples after 90 days) for the three different experiments:

1. Artificial metamorphism/ artificial snow:  
 $\text{NH}_4^+ > \text{Cl}^- > \text{F}^- \sim \text{Na}^+ > \text{SO}_4^{2-} \sim \text{Ca}^{2+}$
2. Artificial metamorphism/ WFJ snow:  
 $\text{F}^- > \text{NH}_4^+ > \text{Cl}^- \sim \text{SO}_4^{2-} \sim \text{Ca}^{2+} > \text{Na}^+$
3. Natural metamorphism/ WFJ snow:  
 $\text{NH}_4^+ > \text{Cl}^- \sim \text{Na}^+ > \text{SO}_4^{2-} \sim \text{Ca}^{2+}$  ( $\text{F}^-$  below detection limit)

After 90 days  $\text{NH}_4^+$  was in two of the three experiments (1, 3) the ion, strongest enriched in the ice interior. Only for the WFJ snow samples exposed to artificial metamorphism (2) we observed a more favorable incorporation of  $\text{F}^-$  compared to  $\text{NH}_4^+$ ,  $\text{SO}_4^{2-}$ ,  $\text{Ca}^{2+}$  (and  $\text{Na}^+$ ) were the ions less preferential located in the interior and were in all experiments strongly rejected to the ice surface.

For the experiment 1 the enrichment sequence did not significantly change with time.  $\text{NH}_4^+$  was strongest enriched already in the initial artificial droplets (Figure 5.7), suggesting a separation accordingly to different solubilities already during the shock-freezing process, becoming more pronounced with time. This is different for the experiments 2 and 3 based on natural snow (Figure 5.7). Here,  $\text{Ca}^{2+}$  was initially

more favorable located in the interior part due to its supposed occurrence in the ice nuclei. With increasing metamorphism time, the  $\text{Ca}^{2+}$  ion migrated to the surface, whereas  $\text{F}^-$  and  $\text{NH}_4^+$  got stronger enriched in the ice lattice accordingly to their higher solubility.

The differences in the obtained enrichment sequences 1, 2, and 3 are most probably due to varying chemical composition. We assume that the absolute concentration differences play a major role, as has been observed for trace elements [Avak *et al.*, 2018]. For example,  $\text{F}^-$  concentrations in the artificial snow are two orders of magnitude higher compared to the WFJ snow (Table 5.1). At higher concentrations solubility limits might have already been exceeded, explaining the less favorable  $\text{F}^-$  incorporation in the ice interior in 1 compared to 2. More difficult to explain is the stronger enrichment of  $\text{Na}^+$  at the ice surface in 2 compared to 1 even if  $\text{Na}^+$  concentrations in the artificial snow 1 were significantly higher. One possible reason is the exceptional high  $\text{NO}_3^-$  concentration in the WFJ snow. Incorporation of the abundant  $\text{NO}_3^-$  into the ice interior during metamorphism could lead to fewer available lattice sites for  $\text{Na}^+$ .

Besides the chemical composition, the rearrangement of  $\text{NH}_4^+$  and the other ions during snow metamorphism was found to be strongly dependent on the applied temperature gradient. Fractionation was much less pronounced under isothermal conditions (Figure 5.6b, Figure 5.7). The rearrangement of the major ions after 90 days of isotherm storage corresponded to the change after  $\sim 6$ -12 days with a temperature gradient of  $40 \text{ K m}^{-1}$ .

#### 5.1.4.4 Comparison with published elution sequences

As mentioned above, there are to the best of our knowledge no data published investigating the relocation of  $\text{NH}_4^+$  together with other major ions during snow metamorphism. Indirect data about ion location at the micrometer scale at different stages of snow metamorphism, however, can be inferred from elution studies of natural snow packs or melt-affected firn and glacier ice. The relocation of chemical species with meltwater is strongly dependent on their actual position in the snow structure. Major ions mainly located at the ice surface are preferably leached with meltwater, whereas others revealing a high solubility in ice are less prone to relocation. A compilation of published elution sequences is shown in Table 5.3. This compilation contains only sites, where  $\text{NH}_4^+$  was studied together with other major ions. Furthermore, for better clarity the sequences above contain only the six major ions investigated in our study, even though further ions are published in some of the works. The compilation shows that in all elution studies (except one)  $\text{SO}_4^{2-}$  and  $\text{Ca}^{2+}$  are the most mobile ions with respect to meltwater percolation. This is in agreement with our work, demonstrating that these two ions are gradually enriched at the ice surface during snow metamorphism. All studies point to either  $\text{NH}_4^+$  or  $\text{Cl}^-$  as the least mobile ions, again in good correspondence with our findings that these species are preferably incorporated into the ice interior due to their high sol-

**Table 5.3:** Compilation of published elution sequences.

	Location	Sequence
<i>Brimblecombe et al.</i> [1985]	Scotland	$\text{SO}_4^{2-} > \text{NH}_4^+ > \text{Ca}^{2+} > \text{Na}^+ > \text{Cl}^-$
<i>Eichler et al.</i> [2001]	Swiss Alps	$\text{SO}_4^{2-} > \text{Ca}^{2+} > \text{Na}^+ > \text{NH}_4^+ \sim \text{F}^- > \text{Cl}^-$
<i>Li et al.</i> [2006]	Tian Shan	$\text{SO}_4^{2-} > \text{Ca}^{2+} > \text{Na}^+ > \text{Cl}^- > \text{NH}_4^+$
<i>Virkkunen et al.</i> [2007]	Svalbard	$\text{SO}_4^{2-} \sim \text{Ca}^{2+} > \text{Na}^+ \sim \text{Cl}^- > \text{NH}_4^+$
<i>Ginot et al.</i> [2010]	Ecuador	$\text{SO}_4^{2-} > \text{Ca}^{2+} > \text{F}^- > \text{Na}^+ > \text{Cl}^- > \text{NH}_4^+$
<i>You et al.</i> [2015]	Tian Shan	$\text{SO}_4^{2-} > \text{Ca}^{2+} \sim \text{Na}^+ > \text{Cl}^- > \text{NH}_4^+$
<i>Wang et al.</i> [2018]	Yunnan, China	$\text{Ca}^{2+} > \text{SO}_4^{2-} > \text{NH}_4^+ > \text{Na}^+ > \text{Cl}^-$

ubility in ice. Obvious differences between the published elution sequences can be explained by varying chemical composition and concentrations, but certainly also by the different aging stages and temperature gradients of the investigated snow pack.

### 5.1.5 Conclusion

In this study we investigated the redistribution of  $\text{NH}_4^+$  and five other major ions ( $\text{Ca}^{2+}$ ,  $\text{Na}^+$ ,  $\text{Cl}^-$ ,  $\text{F}^-$ , and  $\text{SO}_4^{2-}$ ) during snow metamorphism and its driving forces. Different artificial and natural snow samples were aged using a controlled temperature gradient of  $40 \text{ K m}^{-1}$  for up to three months, while structural and chemical changes were monitored in detail. Additionally, we studied samples, taken from different depths of a natural snow pack that had undergone natural snow metamorphism. The snow structures of the samples were monitored using computer tomography and elution experiments with ultra-pure water were performed to detect either the accumulation of the ions on the surface of the ice or their inclusion in the ice interior.

Initial snow structures and SSA widely varied between natural and artificial snow. After  $\sim 12$  days of artificial aging, however, these original differences vanished and both types of snow showed similar structural and SSA changes during metamorphism induced by the temperature gradient.

The strong altering of the snow structure during snow metamorphism caused a rearrangement of chemical species between ice surface and interior. For snow samples aged using an artificial temperature gradient of  $40 \text{ K m}^{-1}$  chemical fractionation occurred in two phases: During the first  $\sim 12$  days of the snow metamorphism concentrations of all ions decreased at the ice surface mainly due to a reduction of the SSA. After 12 days until 3 months  $\text{NH}_4^+$ ,  $\text{Cl}^-$ , and  $\text{F}^-$  concentrations were gradually enriched in the interior of the ice, whereas an exclusion of  $\text{SO}_4^{2-}$  and  $\text{Ca}^{2+}$  to the ice surface took place. A high solubility in ice was found to be the main driving force for preferred incorporation in the ice interior. Snow samples of the WFJ snow pit aged for 0-3 months under a natural temperature gradient confirm these findings with a gradual burying of  $\text{NH}_4^+$  in the interior of the ice and strongest enrichment of  $\text{Ca}^{2+}$  and  $\text{SO}_4^{2-}$  at the ice surface after 90 days.

Distinct differences in the temporal  $\text{NH}_4^+$  distribution were observed between natu-

ral and artificial snow samples. The sequence determined for the preferential enrichment of  $\text{NH}_4^+$  compared to the other five major ions in the ice interior did not significantly change with time for artificial snow.  $\text{NH}_4^+$  was strongest enriched already in the initial artificial droplets, suggesting a separation accordingly to different solubilities already during the shock-freezing process, becoming more pronounced with time. This was different during the metamorphism of natural snow. Here, initial ion fractionation could be related to their positioning during atmospheric scavenging processes with a high  $\text{Ca}^{2+}$  concentration at the interior of the ice due to its supposed occurrence in the ice nuclei.  $\text{NH}_4^+$  and  $\text{F}^-$  showed a stronger enrichment in the ice interior compared to  $\text{Ca}^{2+}$  with increasing metamorphism time, according to their higher solubility.

We found a strong dependence of the structural changes and the rearrangement of  $\text{NH}_4^+$  and the other ions during snow metamorphism on the applied temperature gradient. SSA decrease and fractionation was much less pronounced under isothermal conditions. Our results showed that chemical rearrangement of the major ions after 90 days of isotherm storage corresponded to the changes after 6-12 days with a temperature gradient of  $40 \text{ K m}^{-1}$ .

Based on our results it is possible to unambiguously relate observed elution sequences from natural snow packs and melt-affected firn and glacier ice to rearrangement processes during snow metamorphism. The segregation of  $\text{Ca}^{2+}$  and  $\text{SO}_4^{2-}$  to the ice crystal surface explains their efficient removal with meltwater detected at almost all study sites. However, incorporation of  $\text{NH}_4^+$ ,  $\text{F}^-$ , and  $\text{Cl}^-$  into the interior of the ice is responsible for their observed general good preservation during melting. Differences between our results and (within) the observed elution sequences from field studies can be explained by varying chemical composition and concentrations, and/or different aging stages and temperature gradients within the investigated snow packs. The observed preferred gradual burial of  $\text{NH}_4^+$  into the interior of the ice during snow metamorphism compared to many other species implies that this ion is much less prone to post-depositional processes like migration, sublimation, or meltwater relocation in snow and firn. Furthermore, our results suggest that  $\text{NH}_4^+$  does not dominate snow chemical reactivity within an altered snow layer contrary to other species located at ice surfaces such as  $\text{Ca}^{2+}$  and  $\text{SO}_4^{2-}$ .

## Acknowledgments

We are grateful for the technical assistance of Matthias Jaggi (SLF) during the experiments in the SLF cold lab (metamorphism box, elution experiments and microCT scans). Further we would like to thank Mario Birrer (PSI) for his help during the production of artificial snow. Funding was provided by the Swiss National Science Foundation (SNSF) under Grant No. 155999.



## Bibliography

- Adams, E. E., and R. L. Brown, Metamorphism of Dry Snow as a Result of Temperature Gradient and Vapor Density Differences, *Annals of Glaciology*, 4, 3–9, doi:10.1017/S0260305500005140, 1983.
- Adams, E. E., and D. A. Miller, Ice crystals grown from vapor onto an orientated substrate: application to snow depth-hoar development and gas inclusions in lake ice, *Journal of Glaciology*, 49(164), 8–12, doi:10.3189/172756503781830953, 2003.
- Augustin, L., et al., Eight glacial cycles from an Antarctic ice core, *Nature*, 429(6992), 623–628, doi:10.1038/nature02599, 2004.
- Avak, S. E., M. Schwikowski, and A. Eichler, Impact and implications of meltwater percolation on trace element records observed in a high-Alpine ice core, *Journal of Glaciology*, 64(248), 877–886, doi:10.1017/jog.2018.74, 2018.
- Bartels-Rausch, T., S. N. Wren, S. Schreiber, F. Riche, M. Schneebeli, and M. Ammann, Diffusion of volatile organics through porous snow: impact of surface adsorption and grain boundaries, *Atmospheric Chemistry and Physics*, 13(14), 6727–6739, doi:10.5194/acp-13-6727-2013, 2013.
- Bartels-Rausch, T., et al., A review of air-ice chemical and physical interactions (AICI): liquids, quasi-liquids, and solids in snow, *Atmospheric Chemistry and Physics*, 14(3), 1587–1633, doi:10.5194/acp-14-1587-2014, 2014.
- Brimblecombe, P., M. Tranter, P. Abrahams, I. Blackwood, T. Davies, and C. Vincent, Relocation and Preferential Elution of Acidic Solute through the Snowpack of a Small, Remote, High-Altitude Scottish Catchment, *Annals of Glaciology*, 7, 141–147, doi:10.3189/S0260305500006066, 1985.
- Brimblecombe, P., S. Clegg, T. Davies, D. Shooter, and M. Tranter, Observations of the preferential loss of major ions from melting snow and laboratory ice, *Water Research*, 21(10), 1279–1286, doi:10.1016/0043-1354(87)90181-3, 1987.
- Calonne, N., B. Richter, H. Löwe, J. Cetti, C., A. van Herwijnen, C. Fierz, M. Jaggi, and M. Schneebeli, The RHOSSA campaign: Monitoring the seasonal evolution of an alpine snowpack up to daily resolution, *in preparation*.
- Chen, S., and I. Baker, Evolution of individual snowflakes during metamorphism, *Journal of Geophysical Research*, 115(D21), D21,114, doi:10.1029/2010JD014132, 2010.
- Colbeck, S. C., Thermodynamics of snow metamorphism due to variations in curvature, *Journal of Glaciology*, 26(94), 291–301, doi:10.1017/S0022143000010832, 1980.
- Cragin, J. H., A. D. Hewitt, and S. C. Colbeck, Grain-scale mechanisms influencing the elution of ions from snow, *Atmospheric Environment*, 30(1), 119–127, doi:10.1016/1352-2310(95)00232-N, 1996.
- Dansgaard, W., *Stable Isotope Glaciology. Meddelelser om Grønland*, 1–53 pp., C.A. Reitzel, København, 1973.
- Döscher, A., H. W. Gäggeler, U. Schotterer, and M. Schwikowski, A historical record of ammonium concentrations from a glacier in the Alps, *Geophysical Research Letters*, 23(20), 2741–2744, doi:10.1029/96GL02615, 1996.
- Eichler, A., M. Schwikowski, and H. W. Gäggeler, Meltwater-induced relocation of chemical species in Alpine firn, *Tellus B: Chemical and Physical Meteorology*, 53(2), 192–203, doi:10.3402/tellusb.v53i2.16575, 2001.
- Eichler, A., S. Brütsch, S. Olivier, T. Papina, and M. Schwikowski, A 750 year ice core record of past biogenic emissions from Siberian boreal forests, *Geophysical Research Letters*, 36(18), L18,813, doi:10.1029/2009GL038807, 2009.

- Eichler, A., W. Tinner, S. Brütsch, S. Olivier, T. Papina, and M. Schwikowski, An ice-core based history of Siberian forest fires since AD 1250, *Quaternary Science Reviews*, 30(9-10), 1027–1034, doi:10.1016/j.quascirev.2011.02.007, 2011.
- Flin, F., J.-B. Brzoska, B. Lesaffre, C. Coléou, and R. A. Pieritz, Three-dimensional geometric measurements of snow microstructural evolution under isothermal conditions, *Annals of Glaciology*, 38, 39–44, doi:10.3189/172756404781814942, 2004.
- Fuhrer, K., A. Neftel, M. Anklin, and V. Maggi, Continuous measurements of hydrogen peroxide, formaldehyde, calcium and ammonium concentrations along the new grip ice core from summit, Central Greenland, *Atmospheric Environment. Part A. General Topics*, 27(12), 1873–1880, doi:10.1016/0960-1686(93)90292-7, 1993.
- Fuhrer, K., A. Neftel, M. Anklin, T. Staffelbach, and M. Legrand, High-resolution ammonium ice core record covering a complete glacial-interglacial cycle, *Journal of Geophysical Research: Atmospheres*, 101(D2), 4147–4164, doi:10.1029/95JD02903, 1996.
- Ginot, P., U. Schotterer, W. Stichler, M. A. Godoi, B. Francou, and M. Schwikowski, Influence of the Tungurahua eruption on the ice core records of Chimborazo, Ecuador, *The Cryosphere*, 4(4), 561–568, doi:10.5194/tc-4-561-2010, 2010.
- Hagenmuller, P., T. C. Theile, and M. Schneebeli, Numerical simulation of microstructural damage and tensile strength of snow, *Geophysical Research Letters*, 41(1), 86–89, doi:10.1002/2013GL058078, 2014.
- Kaempfer, T. U., M. Schneebeli, and S. A. Sokratov, A microstructural approach to model heat transfer in snow, *Geophysical Research Letters*, 32(21), L21,503, doi:10.1029/2005GL023873, 2005.
- Kaspari, S., et al., Reduction in northward incursions of the South Asian monsoon since 1400 AD inferred from a Mt. Everest ice core, *Geophysical Research Letters*, 34(16), doi:10.1029/2007GL030440, 2007.
- Kellerhals, T., S. Brütsch, M. Sigl, S. Knüsel, H. W. Gäggeler, and M. Schwikowski, Ammonium concentration in ice cores: A new proxy for regional temperature reconstruction?, *Journal of Geophysical Research*, 115(D16), D16,123, doi:10.1029/2009JD012603, 2010.
- Kerbrat, M., B. Pinzer, T. Huthwelker, H. W. Gäggeler, M. Ammann, and M. Schneebeli, Measuring the specific surface area of snow with X-ray tomography and gas adsorption: comparison and implications for surface smoothness, *Atmospheric Chemistry and Physics*, 8(5), 1261–1275, doi:10.5194/acp-8-1261-2008, 2008.
- Legrand, M., and P. Mayewski, Glaciochemistry of polar ice cores: A review, *Reviews of Geophysics*, 35(3), 219–243, doi:10.1029/96RG03527, 1997.
- Li, Z., R. Edwards, E. Mosley-Thompson, F. Wang, Z. Dong, X. You, H. Li, C. Li, and Y. Zhu, Seasonal variability of ionic concentrations in surface snow and elution processes in snow-firn packs at the PGPI site on Ürümqi glacier No. 1, eastern Tien Shan, China, *Annals of Glaciology*, 43, 250–256, doi:10.3189/172756406781812069, 2006.
- Lorius, C., L. Merlivat, and R. Hagemann, Variation in the mean deuterium content of precipitations in Antarctica, *Journal of Geophysical Research*, 74(28), 7027–7031, doi:10.1029/JC074i028p07027, 1969.
- Löwe, H., J. Spiegel, and M. Schneebeli, Interfacial and structural relaxations of snow under isothermal conditions, *Journal of Glaciology*, 57(203), 499–510, doi:10.3189/002214311796905569, 2011.
- Mosimann, L., E. Weingartner, and A. Waldvogel, An Analysis of Accreted Drop Sizes and Mass on Rimed Snow Crystals, *Journal of the Atmospheric Sciences*, 51(11), 1548–1558, doi:10.1175/1520-0469(1994)051<1548:AAOADS>2.0.CO;2, 1994.

- Pinzer, B. R., and M. Schneebeli, Snow metamorphism under alternating temperature gradients: Morphology and recrystallization in surface snow, *Geophysical Research Letters*, *36*(23), L23,503, doi:10.1029/2009GL039618, 2009.
- Pinzer, B. R., M. Schneebeli, and T. U. Kaempfer, Vapor flux and recrystallization during dry snow metamorphism under a steady temperature gradient as observed by time-lapse microtomography, *The Cryosphere*, *6*(5), 1141–1155, doi:10.5194/tc-6-1141-2012, 2012.
- Pruppacher, H., and J. Klett, *Microphysics of Clouds and Precipitation, Atmospheric and Oceanographic Sciences Library*, vol. 18, Springer Netherlands, Dordrecht, doi:10.1007/978-0-306-48100-0, 2010.
- Röthlisberger, R., et al., Nitrate in Greenland and Antarctic ice cores: a detailed description of post-depositional processes, *Annals of Glaciology*, *35*, 209–216, doi:10.3189/172756402781817220, 2002.
- Saltzman, E. S., Ocean/Atmosphere Cycling of Dimethylsulfide, in *Ice Core Studies of Global Biogeochemical Cycles*, pp. 65–89, Springer Berlin Heidelberg, Berlin, Heidelberg, doi:10.1007/978-3-642-51172-1\_4, 1995.
- Sokratov, S. A., and N. Maeno, *Heat and mass transport in snow under a temperature gradient*, 49–54 pp., Balkema, Rotterdam, 1997.
- Sokratov, S. A., A. Sato, and Y. Kamata, Water vapor in the pore space of snow, *Annals of Glaciology*, *32*, 51–58, doi:10.3189/172756401781819111, 2001.
- Stichler, W., U. Schotterer, K. Fröhlich, P. Ginot, C. Kull, H. Gäggeler, and B. Pouyaud, Influence of sublimation on stable isotope records recovered from high-altitude glaciers in the tropical Andes, *Journal of Geophysical Research: Atmospheres*, *106*(D19), 22,613–22,620, doi:10.1029/2001JD900179, 2001.
- Szyrmer, W., and I. Zawadzki, Biogenic and Anthropogenic Sources of Ice-Forming Nuclei: A Review, *Bulletin of the American Meteorological Society*, *78*(2), 209–228, doi:10.1175/1520-0477(1997)078<0209:BAASOI>2.0.CO;2, 1997.
- Thibert, E., and F. Dominé, Thermodynamics and Kinetics of the Solid Solution of HNO<sub>3</sub> in Ice, *The Journal of Physical Chemistry B*, *102*(22), 4432–4439, doi:10.1021/jp980569a, 1998.
- Thompson, L. G., E. Mosley-Thompson, M. E. Davis, V. S. Zagorodnov, I. M. Howat, V. N. Mikhailenko, and P.-N. Lin, Annually Resolved Ice Core Records of Tropical Climate Variability over the Past 1800 Years, *Science*, *340*(6135), 945–950, doi:10.1126/science.1234210, 2013.
- Virkkunen, K., J. Moore, E. Isaksson, V. Pohjola, P. Perämäki, A. Grinsted, and T. Kekonen, Warm summers and ion concentrations in snow: comparison of present day with Medieval Warm Epoch from snow pits and an ice core from Lomonosovfonna, Svalbard, *Journal of Glaciology*, *53*(183), 623–634, doi:10.3189/002214307784409388, 2007.
- Wang, S., X. Shi, W. Cao, and T. Pu, Seasonal Variability and Evolution of Glaciochemistry at An Alpine Temperate Glacier on the Southeastern Tibetan Plateau, *Water*, *10*(2), 114, doi:10.3390/w10020114, 2018.
- Wolff, E. W., Location, Movement and Reactions of Impurities in Solid Ice, in *Chemical Exchange Between the Atmosphere and Polar Snow*, pp. 541–560, Springer Berlin Heidelberg, Berlin, Heidelberg, doi:10.1007/978-3-642-61171-1\_23, 1996.
- You, X., Z. Li, R. Edwards, and L. Wang, The transport of chemical components in homogeneous snowpacks on Urumqi Glacier No. 1, eastern Tianshan Mountains, Central Asia, *Journal of Arid Land*, *7*(5), 612–622, doi:10.1007/s40333-015-0131-z, 2015.

## 5.2 Elution experiments of trace elements

### 5.2.1 Introduction

To extend the understanding of the influence of snow metamorphism on the redistribution of other impurities than major ions, elution experiments were also performed for 35 trace elements (TEs; Ag, Al, Ba, Bi, Ca, Ce, Cd, Co, Cs, Cu, Eu, Fe, La, Li, Mg, Mn, Mo, Na, Nd, Ni, Pb, Pr, Rb, Sb, Sc, Sm, Sr, Th, Tl, U, V, W, Yb, Zn, Zr). Elution experiments investigating the spatial distribution of TEs in snow have not been reported so far. The elution experiments carried out for the TEs focused on two of the three previously described types (Section 5.1.2.2):

- Newly fallen snow from the Weissfluhjoch test site subsequently exposed for 0, 3, 6, 12, 30, 60, or 90 days to a laboratory-controlled temperature gradient of  $40 \text{ K m}^{-1}$  (type 2).
- Snow from different depths of the snow pack at Weissfluhjoch, reflecting different exposure times (0, 30, 60, and 90 days) to a natural temperature gradient (type 3).

### 5.2.2 Materials and methods

Snow sampling at the Weissfluhjoch test site, homogenization of the snow and filling of the 160 mL PP containers at  $-20 \text{ }^\circ\text{C}$ , exposure to the artificial temperature gradient in the metamorphism box at SLF, respectively isothermal storage at  $-20 \text{ }^\circ\text{C}$  for the samples from the snow pack, was carried out together with the preparation of the major ion samples. The design of the elution experiments was identical as described above for the major ions and they were concurrently performed under the same conditions (Figure 5.1). The only difference is that 15 mL PP vials used to collect the ten aliquots (4x 3 mL, 4x 6 mL, and 2x 12 mL per batch) of the eluate and the 50 mL vials to collect the remaining snow sample in the elution column (2x  $\sim 45$  mL per batch) were pre-cleaned by five times rinsing with ultra-pure water (18 M  $\Omega$  cm quality, Milli-Q<sup>®</sup> Element, Merck Millipore, Burlington MA, United States), plus onetime rinsing with 0.2 M  $\text{HNO}_3$  prepared from ultra-pure  $\text{HNO}_3$  (Optima<sup>™</sup>, Fisher Chemical, Loughborough, United Kingdom). Samples were kept frozen at  $-20 \text{ }^\circ\text{C}$  until analysis. A total of 588 samples, including samples representing  $c_{\text{Bulk}}$  analogous to the major ions, was acidified with concentrated ultra-pure  $\text{HNO}_3$  to 0.2 M, melted at room temperature, analyzed using discrete inductively coupled plasma sector field mass spectrometry (ICP-SF-MS, Element 2, Thermo Fisher Scientific, Bremen, Germany), and evaluated as described in Chapter 4. On average, 13% of the measurement values were below the instrumental detection limit, which was defined as  $3 \sigma$  of the measurement blank consisting of 7 measurements of ultra-pure water.

### 5.2.3 Results

In general, TEs revealed, as for the major ions, a decrease in concentration with increasing volume of collected eluate aliquots for all the individual batches of the two performed types of elution experiment. This trend was even observed for TEs occurring in the ultra-low concentration ranges such as Cs (Figure 5.8). The 9<sup>th</sup> and 10<sup>th</sup> aliquots of collected eluate were usually close or below the instrumental detection limit. The remaining snow samples in the elution column generally showed a higher concentration compared to the 9<sup>th</sup> and 10<sup>th</sup> aliquots of collected eluate (Figure 5.8).

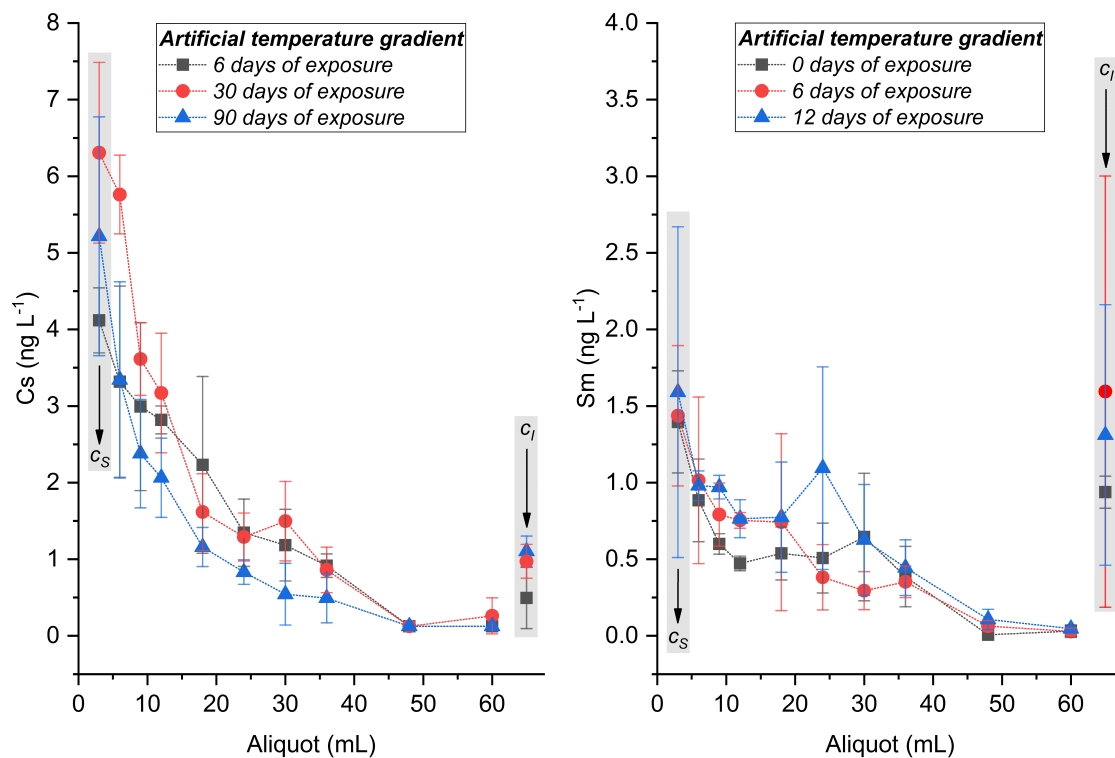


**Figure 5.8:** Exemplary elution curves of Cs and Sm for different artificial temperature gradient exposure times.  $c_s$  represents the concentration on the ice (crystal) surfaces and  $c_i$  represents the concentration of the ice (crystal) interiors.

Depending on the temporal evolution of the  $c_s$  concentrations, corresponding to the concentrations of the 1<sup>st</sup> aliquots of each batch and representing the composition of the ice surfaces after respective temperature gradient exposure, TEs were qualitatively categorized (Figure 5.9).

#### 5.2.3.1 Artificial metamorphism of natural snow

Two distinct patterns of the  $c_s$  concentration profile were identified for natural snow exposed for different time periods to the artificial temperature gradient (type 2,

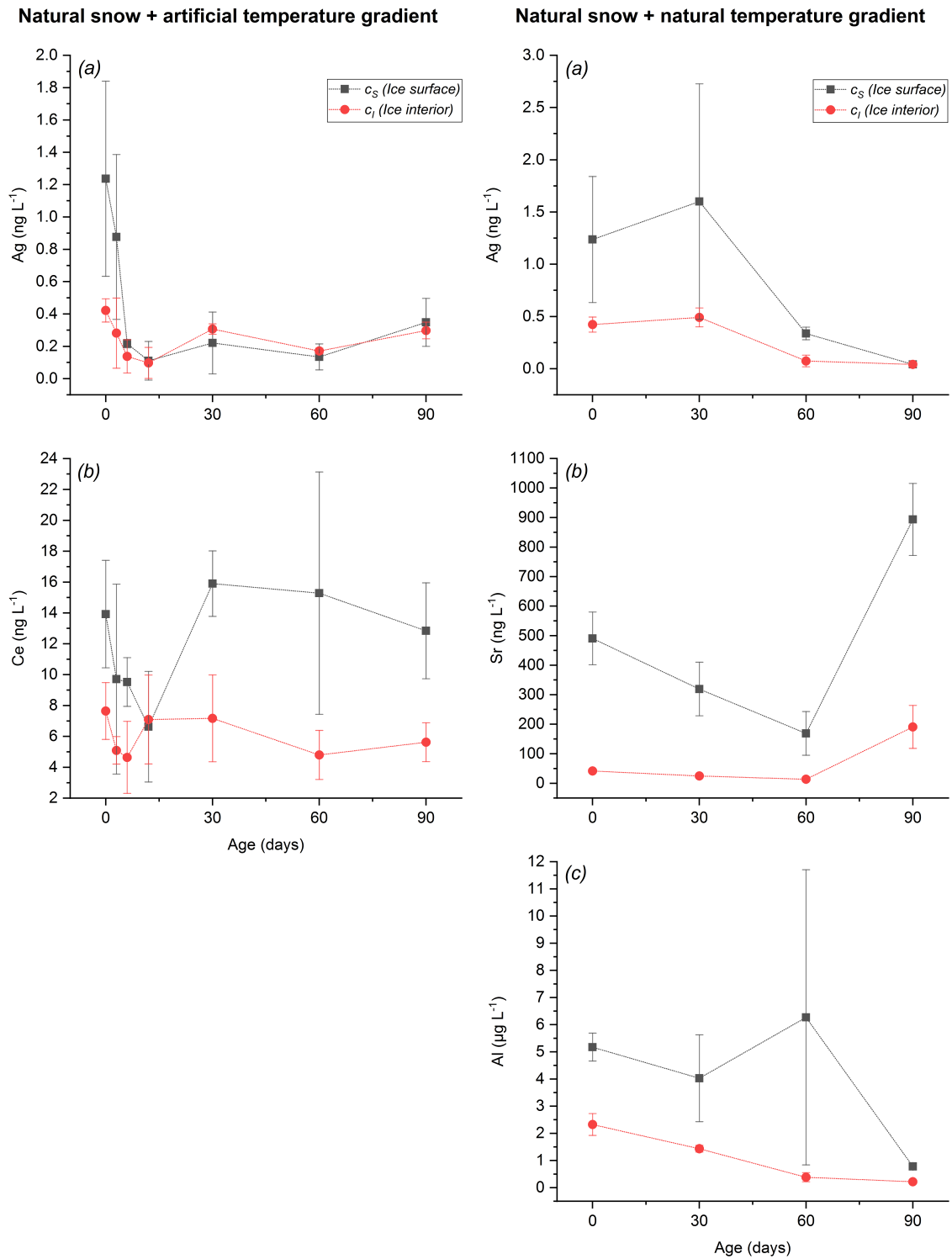


**Figure 5.9:** Temporal evolution of concentrations  $c_s$  at ice surfaces and  $c_i$  of the ice interiors of natural snow exposed to a artificial temperature gradient (left) and of natural snow pack samples (right), respectively, for selected TEs.

Figure 5.9):

- a Overall decreasing trend of  $c_S$  with a steep decline in ice surface concentration within the first 12 days of artificial temperature gradient exposure, as observed for Ag and Ni.
- b No clear trend of  $c_S$ ; initial decrease within the first 12 days of temperature exposure and subsequent increase with a stable concentration after 30 days, as observed for the majority of TEs (Al, Ba, Bi, Ca, Ce, Cd, Co, Cs, Cu, Eu, Fe, La, Li, Mg, Mn, Mo, Na, Nd, Pb, Pr, Rb, Sb, Sc, Sm, Sr, Th, Tl, U, V, W, Yb, Zn, Zr).

None of the TEs revealed a reverse trend for the concentrations  $c_I$  in the residual post-elution samples, representing the composition of the ice interiors, compared to  $c_S$ .

### 5.2.3.2 Snow pack samples

Three distinct patterns of the  $c_S$  concentration profile were also identified for the natural snow taken from different depths of the snow pack at Weissfluhjoch (type 3, Figure 5.9):

- a Decreasing trend of  $c_S$  within 0 and 90 days, as observed for Ag, Ba, Bi, Cs, Cd, Ce, Cu, Eu, Fe, La, Li, Mn, Mo, Na, Nd, Pb, Pr, Rb, Sb, Sc, Sm, Th, Tl, V, W, Yb, Zn, and Zr.
- b Decrease of  $c_S$  within the first 60 days, followed by a strong increase between 60 and 90 days, as observed for Mg, Sr, and U.
- c No clear trend of  $c_S$ , as observed for Al, Ca, Co, and Ni.

A reverse trend for the concentrations  $c_I$  compared to  $c_S$  was only observed for Na.

Apart from the TEs that revealed no clear trend (Al, Ca, Co), Ag is the only TE showing a consistent behavior both during artificial and natural temperature gradient exposure.

### 5.2.4 Discussion

The decrease in concentration with increasing volume of collected eluate aliquots (Figure 5.8) for all the individual batches of the two performed types of elution experiment and the fact, that the 9<sup>th</sup> and 10<sup>th</sup> aliquots of collected eluate were usually close or below the detection limit, indicates that the method of elution worked well and contamination of the samples did not occur.

### 5.2.4.1 Artificial metamorphism of natural snow

The general decrease in concentration of all TEs on the ice surfaces ( $c_S$ ) during the first 12 days of artificial temperature gradient exposure correlates with a decline in specific surface area (SSA) of  $\sim 12 \text{ m}^2 \text{ kg}^{-1}$  within the same time period (Figure 5.4). As explained above for the major ions, this SSA decrease reduces the active area available for chemical exchange processes between the ice surfaces and the content (gaseous and/or liquid) of the interstitial porous space.

For the period between 12 and 90 days of artificial temperature gradient exposure, Ag and Ni reveal a stable  $c_S$ , while the other TEs show an increasing  $c_S$ . According to the previous findings from the upper Grenzgletscher ice core segment TE analysis (Chapter 3) and the Weissfluhjoch snow pit study (Chapter 4), Al, Ba, Ca, Cd, Co, Fe, Mg, Mn, Na, Ni, Sr, Zn, Zr, and the rare-earth elements (Ce, Eu, La, Nd, Pr, Sc, Sm, Yb) are expected to be enriched on ice surfaces with progressing temperature gradient metamorphism. In contrast, Ag, Bi, Cs, Cu, Li, Mo, Pb, Rb, Sb, Th, Tl, U, V, and W should reveal an enrichment in the ice interiors. A matching trend for  $c_S$  was only identified for Ag, which is, however, not reflected in an inverse trend for  $c_I$ . According to Chapter 4, TEs in Alpine snow are either water-soluble or water-insoluble. As ultra-pure water was used as eluent, the water-insoluble fraction of TEs could not be eluted. As a result, the determination of  $c_S$  for the individual batches is non-quantitative (also reflected in large errors, Figure 5.9) and prohibits a monitoring of temporal changes of total TE concentrations at ice surfaces. As a consequence,  $c_I$  contains a mixture of the water-insoluble fraction of TEs that remained on the ice surface after elution and of the total TE composition in the ice interiors. This is likely to explain the fact that the remaining snow samples in the elution column revealed a higher concentration compared to the 9<sup>th</sup> and 10<sup>th</sup> aliquots of collected eluate. Due to this mixing, further interpretation of the temporal evolution of  $c_I$  would be inconclusive. For the same reason, a normalization of concentrations using the  $c_S/c_{\text{Bulk}}$  ratio, to compare the temporal evolution of different TEs, cannot be applied as  $c_{\text{Bulk}}$ , contrary to  $c_S$ , contains both the water-soluble and water-insoluble TE fraction. Using 0.2 M  $\text{HNO}_3$  as eluent may be a possibility to also collect water-insoluble TEs on ice surfaces by acid leaching, even though a full digestion of TE containing particles even with concentrated acids is unlikely [Uglietti *et al.*, 2014].

### 5.2.4.2 Snow pack samples

An enrichment of TEs on the ice surfaces ( $c_S$ ) after natural metamorphism exposure for 90 days was observed for Mg and Sr. Ag, Bi, Cs, Cu, Li, Mo, Pb, Rb, Sb, Th, Tl, V, and W revealed a decrease of  $c_S$ . These observations are in line with the findings described in Chapter 3 and Chapter 4. Nevertheless, as explained above,  $c_S$  is not representative of the total TE composition on the ice surfaces and an interpretation of the outcome of the elution experiment using natural snow pack samples in greater



detail is difficult. A matching opposed trend of  $c_1$  was not visible for the TEs, as  $c_1$  represents a mixture of the water-insoluble TE fraction on the ice surfaces and the TE concentration in the interior of the crystals. The fact, that the majority of TEs showed either not the expected or an indistinct  $c_3$  concentration evolution can also be attributed, as proposed for the major ions, to the heterogeneity of the snow samples from different depths of the snow pack.

### 5.2.5 Conclusion

The elution experiment designed for investigating the location of water-soluble major ions in snow was found to be not suitable for studying the distribution of TEs. TEs in high-Alpine snow and glacier ice have different solubilities in water. Therefore, an elution experiment with water (or acid solutions) as eluent is unfavorable to investigate a fractionation of TEs during snow metamorphism. An elution experiment focusing on TEs can only be performed with artificial snow doped with water-soluble TEs. Implementing the latter requires an elaborate adaption of the frozen droplet preparation procedure to prevent contamination on an ultra-trace level. In the future, methods that allow for surface sampling of bulk material on a microscopic scale, such as laser ablation ICP-MS (see Chapter 6), should be chosen to investigate redistribution processes of TEs during snow metamorphism. However, the applicability of laser ablation ICP-MS to a porous material like snow needs to be assessed beforehand.

### Bibliography

Uglietti, C., P. Gabrielli, J. W. Olesik, A. Lutton, L. G. Thompson, Large variability of trace element mass fractions determined by ICP-SFMS in ice core samples from worldwide high altitude glaciers, *Applied Geochemistry*, 47, 109–121, doi:10.1016/j.apgeochem.2014.05.019, 2014.



# 6 Development of a method for *in situ* trace element analysis with high spatial resolution of high-Alpine glacier ice

Sven Erik Avak<sup>a,b,c</sup>, Mario Birrer<sup>a</sup>, Andrés Laso<sup>a</sup>, Marcel Guillong<sup>d</sup>, Oscar Laurent<sup>d</sup>, Markus Wälle<sup>d</sup>, Thorsten Bartels-Rausch<sup>a</sup>, Margit Schwikowski<sup>a,b,c</sup>, and Anja Eichler<sup>a,c</sup>

<sup>a</sup>Laboratory of Environmental Chemistry, Paul Scherrer Institute, Villigen PSI, 5232, Switzerland

<sup>b</sup>Department of Chemistry and Biochemistry, University of Bern, Bern, 3012, Switzerland

<sup>c</sup>Oeschger Centre for Climate Change Research, University of Bern, Bern, 3012, Switzerland

<sup>d</sup>Institute of Geochemistry and Petrology, ETH Zurich, Zurich, 8092, Switzerland

## Abstract

Understanding the interplay between snow metamorphism and the redistribution of impurities is of considerable relevance for atmospheric chemistry, snow physics, and the reconstruction of past atmospheric conditions using glacier ice cores. Investigating the impact of snow metamorphism on the impurity location in glacier ice at a grain scale requires imaging chemical micro analysis with high spatial resolution and sensitivity. Here, we report on the development of an analytical method based on laser ablation inductively coupled plasma mass spectrometry allowing examining the location of trace elements in glacier ice. The development process comprised several steps: construction and consistent further development of a cooled sample holder (cryocell) featuring an automatic coolant leakage detection system and compatibility to a commercially available laser ablation system, choice of the optimal cooling medium, customization of the pre-existing laser ablation hardware and software, as well as development of additional equipment for both sample preparation and handling. Engineering an eminently suitable experimental setup went hand in hand with establishing the actual measurement procedure for glacier ice. Particular focus was set both on determining appropriate laser ablation parameters and setting up a calibration method to quantify signal intensities for glacier ice measurements. The availability of an internal standard in ice was evaluated and an approach to prepare matrix-matched ice standards for external calibration could be established. The acidity of multi-element solutions used to prepare ice standards and the time elapsed between freezing of the solution and measurement was observed to have the most significant impact on the ablation performance. The outcome of a first pilot study involving preliminary measurements of high-Alpine glacier ice samples from upper Grenzgletscher, Switzerland, finally demonstrates that a method for the *in situ* analysis of trace elements in glacier ice at a sub-millimeter resolution could be successfully developed. In agreement with two very recent studies on deep polar ice, samples with an overwhelming impurity abundance, mainly originating from mineral dust, revealed no evidence for a linkage between the distribution of trace elements and the grain boundary network, but rather a dispersion of trace elements on a micrometer scale. Minimizing the influence of dust particles on the fractionation of trace elements requires investigation of high-Alpine glacier ice exhibiting ultra low levels of trace elements and further background suppression of the developed method.

## 6.1 Introduction

### 6.1.1 Impurity location in glacier ice

Analyzing the location of impurities in glacier ice with high spatial resolution is challenging and has been subject to only a few studies. The first study of that

kind involved a combination of scanning electron microscopy (SEM) and energy-dispersive X-ray micro analysis (EDXMA) and allowed *Mulvaney et al.* [1988] to locate  $\text{H}_2\text{SO}_4$  in Antarctic ice. Concentrations at triple junctions in areas smaller than  $1 \mu\text{m}^2$  were found to be significantly higher ( $>1 \text{ M}$ ) than in the ice grain interiors ( $<5 \text{ nM}$ ). *Fukazawa et al.* [1998] also observed enrichment of  $\text{H}_2\text{SO}_4$  and  $\text{HNO}_3$  at triple junctions in polar ice from Antarctica using Raman spectroscopy. Detection limits (DL) could be significantly improved by utilizing low-vacuum SEM-EDXM which allowed to reveal enrichment of inorganic salts ( $\text{NaCl}$  and  $\text{MgSO}_4$ ) at grain boundaries in Greenland GISP2 ice [*Baker et al.*, 2003; *Cullen and Baker*, 2001]. However, artifacts are possible during the controlled sublimation of uncoated ice which is the procedure to obtain the concentrated impurities at grain boundaries and interiors [*Baker and Cullen*, 2003]. Recently, *Della Lunga et al.* [2014] did pioneering work in employing cryocell laser ablation inductively coupled plasma mass spectrometry (LA-ICP-MS) to analyze the distribution of trace elements (TEs) in glacier ice at a grain scale, which provided evidence that Al, Ca, Fe, Mg, Na, Pb, and Sr are enriched both at grain boundaries and junctions in clear bands of Greenland NGRIP deep ice. Until the beginning of this thesis, quantification of LA-ICP-MS signal intensities had not been established and first studies focused on Greenland ice, unfavorable for the analysis of many anthropogenic related TEs due to its remoteness from the respective emissions sources.

### 6.1.2 Laser Ablation ICP-MS

Around three decades ago, *Gray* [1985] coupled for the first time LA to ICP-MS. This fast and sensitive micro analytical method gained widespread usage in archeology, biology, chemistry forensics, geology, medicine, metallurgy, and environmental and materials sciences, as it allows direct sampling of solids to determine concentrations or isotope ratios of major, minor, and trace elements [*Durrant and Ward*, 2005; *Günther and Hattendorf*, 2005; *Koch and Günther*, 2011; *Lobo et al.*, 2018]. The operating principle of this elemental imaging technique is schematically shown in Figure 6.1. A laser serves as key component by emitting a pulsed beam (typically in the nanosecond range) which is focused onto the flat surface of a solid sample, located inside a gas-tight ablation chamber, and resulting in the release of tiny particles [*Sylvester and Jackson*, 2016]. The latter process is called “ablation”. Sample aerosols are transported by a carrier gas (typically argon or a mixture of argon and helium) to the ICP-MS for elemental analysis. After vaporization, atomization, and ionization in the plasma of the torch, ions are transferred to the mass analyzer, where they are separated according to their mass to charge ratio prior to quantification (counts per time unit) by a detector. Thus, spatial information is obtained by monitoring the position of the laser spot with a camera and elemental information is obtained by the coupling of the LA unit to a mass spectrometer. LA-ICP-MS is considered as *quasi* non-destructive method, because the volume of ablated target material is very small allowing the sample to be still available for replicate or further

analyses [Guillong and Günther, 2001]. The method's spatial resolution is principally confined by the laser spot size and the instrument detection limit. Spot sizes of a few micrometers are possible, but result in low sample quantities requiring high sensitivity of the ICP-MS. The ablation process is controlled by three parameters: the wavelength of the laser, the energy density on the target, also called “fluence” and usually specified in  $\text{J cm}^{-2}$ , and the repetition rate, defining the number of laser shots per time unit and usually specified in Hz. The latter two parameters can be adjusted, while the laser wavelength is system-specific and either in the UV or IR range.

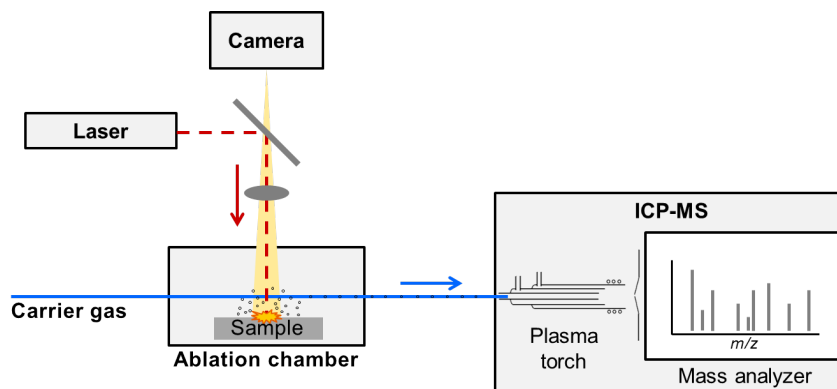


Figure 6.1: Schematic of LA-ICP-MS.

### 6.1.3 Overview of different cryocells

LA-ICP-MS is an analytical method that can principally be applied to solid samples of almost any kind. Frozen specimens require either the whole ablation chamber to be cooled or a cooled sample holder, the so-called cryocell, to maintain the sample below its melting point. Several cryocells have been developed to allow for the analysis of either frozen biological tissue samples [Feldmann *et al.*, 2002; Konz *et al.*, 2014; Zoriy *et al.*, 2005] or ice core samples [Müller *et al.*, 2011; Reinhardt *et al.*, 2001; Sneed *et al.*, 2015]. Two different types of design can be identified (Table 6.1): a cryocell can be either designed as separate sample holder customized to a pre-existing ablation chamber or as “all in one” system, where it also serves as ablation chamber. The latter can only be applied for small sample volumes. The wash-out time, the time required to remove the sample aerosol from the ablation chamber for subsequent elemental analysis, increases with the volume of the ablation cell and therefore particularly affects sensitivity [Arrowsmith and Hughes, 1988]. To be able to work with larger sample sizes while ensuring rapid washout times and high sensitivity, two-volume ablation chambers have been developed [Müller *et al.*, 2009; Sneed *et al.*, 2015], where a small, few cubic centimeters sized, volume hosts the actual ablation. The type of cooling system is another important parameter

**Table 6.1:** Key characteristics of different cryocells developed for LA-ICP-MS analysis of frozen samples.

	Type of design	Sample type	Sample volume	Cooling system	Operating temperature (°C)	Corpus material
<i>Reinhardt et al.</i> [2001]	Cryogenic ablation chamber	Ice core samples	~900 cm <sup>3</sup>	Circulation of coolant (silicon oil) & cooled carrier gas	-40	PTFE & copper
<i>Feldmann et al.</i> [2002]	Cryogenic ablation chamber	Biological tissue	60 cm <sup>3</sup>	Liquid nitrogen	-100 to -20	-
<i>Zoriy et al.</i> [2005]	Cryogenic ablation chamber	Biological tissue	-	Peltier elements	-15	PFA
<i>Müller et al.</i> [2011]	Cryocell compatible to commercially available ablation chamber	Ice core samples	3 x 8 cm <sup>3</sup>	Peltier elements	-25	Aluminum
<i>Konz et al.</i> [2014]	Cryogenic ablation chamber	Biological tissue	20 cm <sup>3</sup>	Peltier elements	-25	PA
<i>Sneed et al.</i> [2015]	Cryocell with small-volume (20 cm <sup>3</sup> ) ablation chamber attached	Ice core samples	~0.05 m <sup>3</sup>	Circulation of coolant	-25	PVC sandwich filled with spray foam

distinguishing the different cryocells (Table 6.1). Chilling of small-volume cryocells can be achieved by thermoelectric cooling (Peltier elements), while cooling of larger volumes needs to be implemented by circulation of coolant (e.g. liquid nitrogen, silicon oil, organic solvent) through a system of copper coils [*Sneed et al.*, 2015] or a channel system within the cryocell [*Kriews et al.*, 2001]. Which type of cooling principle is most appropriate is not only determined by the volume of the sample to be cooled, but also by the required refrigeration temperature. Temperatures < -25 °C can generally exclusively be achieved by circulation of a coolant. Finally, the corpus material is another important parameter (Table 6.1). Low-density polymers are often used due to excellent insulation properties. Hereafter, an overview on the applications of cryocell LA-ICP-MS (Table 6.1) to ice core analysis is provided.

### 6.1.4 Applications of cryocell LA-ICP-MS to ice core analysis

*Reinhardt et al.* [2001, 2003] were the first ones to pioneer in the application of LA-ICP-MS to ice core analyses. A cryogenic LA chamber (Table 6.1), designed to hold a sample with the size of 8.5 x 3.5 x 1 cm (length x width x thickness), was constructed and the respective LA-ICP-MS system, equipped with a 1064 nm IR laser, was optimized for the analysis of ice. Greenland ice core samples were analyzed with a spatial resolution of 4 mm to validate the method. The results revealed a good agreement to data obtained by conventional ICP-MS bulk analysis. A calibration procedure to obtain quantitative elemental information on a millimeter scale could also be established, where signals of up to eleven external ice standards ranging from 0.01 to 100  $\mu\text{g L}^{-1}$  were normalized to the signal of  $^{17}\text{OH}$ , used as internal standard. External standards were prepared by freezing multi-element standard solutions and allowed the quantification of 38 elements. This analytical method was further developed by *Müller et al.* [2011], who could achieve a significantly higher spatial resolution ( $< 300 \mu\text{m}$ ) using their 193 nm UV-LA-ICP-MS setup. Ice samples of 5 cm length, 1.3 cm width, and 1.2 cm thickness can be mounted onto the corresponding cryocell (Table 6.1). Based on the latter work, *Della Lunga et al.* [2014, 2017] could, for the first time, show concentration variations of TEs on a sub-millimeter scale in glacier ice from Greenland using a newly developed external calibration procedure. Another LA-ICP-MS setup using a 231 nm UV laser and dedicated to the analysis of glacier ice has been recently developed at the W. M. Keck Laser Ice Facility of the University of Maine Climate Change Institute [*Sneed et al.*, 2015; *Spaulding et al.*, 2017]. The corresponding custom-built cryocell (Table 6.1) is unique for its capability to hold and keep entire ice core sections of up to 1 m length frozen. The setup has been extensively used to identify small-scale variability in the chemical profiles of deep ice core sections from Greenland [*Mayewski et al.*, 2014], Antarctica [*Haines et al.*, 2016], and the Alps [*Bohleber et al.*, 2018; *More et al.*, 2017] that could not be resolved sufficiently by conventional ice core melting techniques so far.

Even though different types of lasers have been deployed by *Reinhardt et al.* [2001], *Sneed et al.* [2015], and *Della Lunga et al.* [2014], the output wavelength is very critical for the ablation of ice. *Warren* [1984] showed that the absorption coefficient of ice is wavelength dependent. The absorption coefficient determines the ablation efficiency, as the volume of ablated material increases with the absorption coefficient. It is approximately one order of magnitude higher at 1064 nm compared to 213 nm and 193 nm, respectively.

### 6.1.5 Motivation for this method development

A variety of atmospheric impurities is preserved in snow and glacier ice. The exact process leading to the embedding of impurities in snow and ice and whether post-depositional structural rearrangement of snow i.e., snow metamorphism causes a



relocation of impurities is not known so far [Bartels-Rausch, 2013]. Understanding those rearrangement processes occurring during snow metamorphism is relevant to avalanche research [Pinzer *et al.*, 2012; Schweizer, 2010] and they might also have an impact on the chemical reactivity of impurities [Bartels-Rausch *et al.*, 2014; Pratt *et al.*, 2013]. Moreover, the final embedding of impurities is also relevant for future reconstructions of past atmospheric conditions. Ice cores are important environmental archives to reconstruct historical changes of atmospheric pollution. The latter can be accomplished by analyzing TEs which were preserved in the ice of mountain glaciers over time and are therefore important reconstruction proxies in high-Alpine ice cores [Schwikowski *et al.*, 2004]. However, due to the current global temperature increase [Marcott *et al.*, 2013], ice core impurity records can be significantly altered if melting occurs. Eichler *et al.* [2001] reported strong evidence that the preservation of impurities with respect to relocation by meltwater is likely depending on their location in the ice crystal lattice. Impurities located at grain boundaries are prone to be eluted by meltwater, whereas impurities incorporated into the ice grain interior are more protected from meltwater-induced relocation. Several studies have been investigating possible relocation effects caused by melting on different sorts of reconstruction proxies, including TEs, in ice cores [Avak *et al.*, 2018; Eichler *et al.*, 2001; Ginot *et al.*, 2010; Müller-Tautges *et al.*, 2016; Pavlova *et al.*, 2015; Thompson *et al.*, 1993]. This knowledge is essential to further use them as environmental proxies to reconstruct natural and anthropogenic emissions to the atmosphere from ice core records affected by melting. However, in none of these studies the location of impurities in the crystal lattice of glacier ice could be directly determined. Cryocell LA-ICP-MS is the method of choice for the direct *in situ* chemical analysis of TEs at a sub-millimeter resolution in glacier ice [Della Lunga *et al.*, 2014; Sneed *et al.*, 2015].

As described in Section 6.1.1, until the beginning of this thesis, studies investigating the micro-scale distribution of TEs focused on glacier ice from Greenland and a quantification of LA-ICP-MS signal intensities was lacking. Here, we report on the development and preliminary application of cryocell LA-ICP-MS, enabling the investigation of TE location in high-Alpine glacier ice with high spatial resolution. Glacier ice from Alpine sites is expected due to the proximity to the emissions sources, to exhibit higher concentrations of many anthropogenic related TEs and therefore to possibly show a different micro-scale distribution pattern of TEs.

## 6.2 Materials and methods

### 6.2.1 Instrumentation

The LA-ICP-MS system consisted of a Resonetics Resolution S155 LA system (Australian Scientific Instruments, Fyshwick, Australia), equipped with a 193 nm ArF excimer gas laser and a two-volume ablation cell [Müller *et al.*, 2009], coupled to a

Thermo Element XR sector field ICP-MS (Thermo Fisher Scientific, Bremen, Germany) and located at the Institute of Geochemistry and Petrology, ETH Zurich. The LA-ICP-MS system was daily optimized as described in *Guillong et al.* [2014]. NIST Standard Reference Materials SRM<sup>®</sup> 610, 612, 614, or 616 (Trace elements in glass, National Institute of Standards and Technology, Gaithersburg MD, United States) served as reference materials where indicated and were ablated using 43  $\mu\text{m}$  laser spot size, 3 Hz repetition rate, 3.5 J  $\text{cm}^{-2}$  fluence, and 5  $\mu\text{m s}^{-1}$  scan speed. Concentrations reported by *Jochum et al.* [2011] were taken as reference. Ultra-pure water of 18 M  $\Omega$  cm quality (Milli-Q<sup>®</sup> Element system, Merck Millipore, Burlington MA, United States) was used where indicated. A chiller (C50P Phoenix refrigerated circulator, Thermo Haake, Karlsruhe, Germany) was employed to adjust the coolant to the desired temperature. All modifications and upgrades made to this commercially available setup to adapt it to the scope of this work are described in Section 6.3.1 and Section 6.3.2.

## 6.2.2 Sample preparation and processing

Samples with a cross section of  $\sim 1.4 \times 1.4$  cm and a length of  $\sim 8$  cm were cut with a band saw, fitted with a Teflon coated saw guide and table top, at  $-20$  °C in the cold room of the Paul Scherrer Institute. Blank ice samples were prepared by freezing ultra-pure water and cutting them to the same dimensions. Blank ice and ice core samples were transported in a cooling box, filled with dry ice, to the Institute of Geochemistry and Petrology, ETH Zurich, and stored in a freezer (KS 9807, Severin, Sundern, Germany) at  $-20$  °C until measurement. Ultra-clean plastic gloves (Semadeni, Ostermundigen, Switzerland) were worn during sample preparation or handling steps of any kind. Further sample preparation and handling procedures specifically developed within the scope of this work are described in Section 6.3.2.1 and Section 6.3.4.

## 6.3 Results and discussion

### 6.3.1 Development of the cryocell

The key part of this work consisted in the construction of a cryocell compatible to the commercially available Resonetics Resolution S155 LA setup. The design of the LA setup demanded the cryocell to fulfill four requirements:

1. The stationary laser requires any sample holder to be movable inside the ablation chamber.
2. The ablation chamber has two high precision linear slides whose range of motion needs to be unobstructed to allow for full navigation of the sample holder.

3. The maximum dimensions of the cryocell are determined by the limited space inside the ablation chamber (33.3 x 23.7 x 3.8 cm, length x width x height) and the size of the small aperture (16.8 x 3.8 cm) used for loading a sample holder into the ablation chamber. The limitation in space and the required movability of the cryocell are rather unfavorable for chilling with a coolant, which entails additional coolant hoses.
4. The ablation chamber is set under helium atmosphere during the LA process and is made of a massive metal body, requiring significant cooling capacity. The latter can only be met by chilling with a coolant. Peltier elements would most likely not have been powerful enough and their generated heat needs to be dissipated which is difficult inside a closed system with limited space available.

The cryocell designed within this work (Figure 6.2a) consists of a polyether ether ketone (PEEK) body. PEEK was chosen as corpus material as it exhibits good insulation properties, excellent abrasive resistance, and is suitable for high vacuum applications. The PEEK corpus holds a cooling block (Figure 6.2b) made of aluminum. The cooling block features three slots for sample and standard holders (Section 6.3.1.1) on the top and a helical channel system for the coolant at the bottom. A shell of hard foam between corpus and cooling block serves as insulation. The upper surface of the cooling block and hard foam insulation is covered with a 1 mm layer of Teflon to facilitate maintaining a clean surface of the cryocell. Additionally, two temperature sensors (Pt100) are located at the surface of the cryocell and within the cooling block for temperature control. A customized lid of the ablation chamber aperture provided ducts for the cooling tubes and connectors (LEMO, Éclubens, Switzerland) to power the temperature sensors (Note: one of them was later replaced by a capacitive sensor, Section 6.3.1.3).

### 6.3.1.1 Standard and sample holders

Sample and standard holders for ice samples of  $\sim 8$  cm length or for frozen calibration standards (Section 6.3.3.2) fitting into the slots of the cooling block were made of aluminum (Figure 6.3). Two different types of standard holders were developed: one with smaller pits (6 mm diameter, 3 mm depth) to comprise single frozen droplets ( $\sim 10 \mu\text{L}$ ), the other one with larger pits (8 mm diameter, 6 mm depth) to comprise several small volume layers of frozen standard solution. The holders were first Ematal coated (hard coat anodizing), which turned out to be not tight towards acid used for decontamination, and later with PFA ( $< 0.5$  mm) to achieve an easy-to-clean surface. For the latter reason, we also designed sample and standard holders both entirely made of PTFE and with the top 2 mm made of PTFE. However, as these holders showed an insufficient heat transfer in the cryocell, they were not further used.

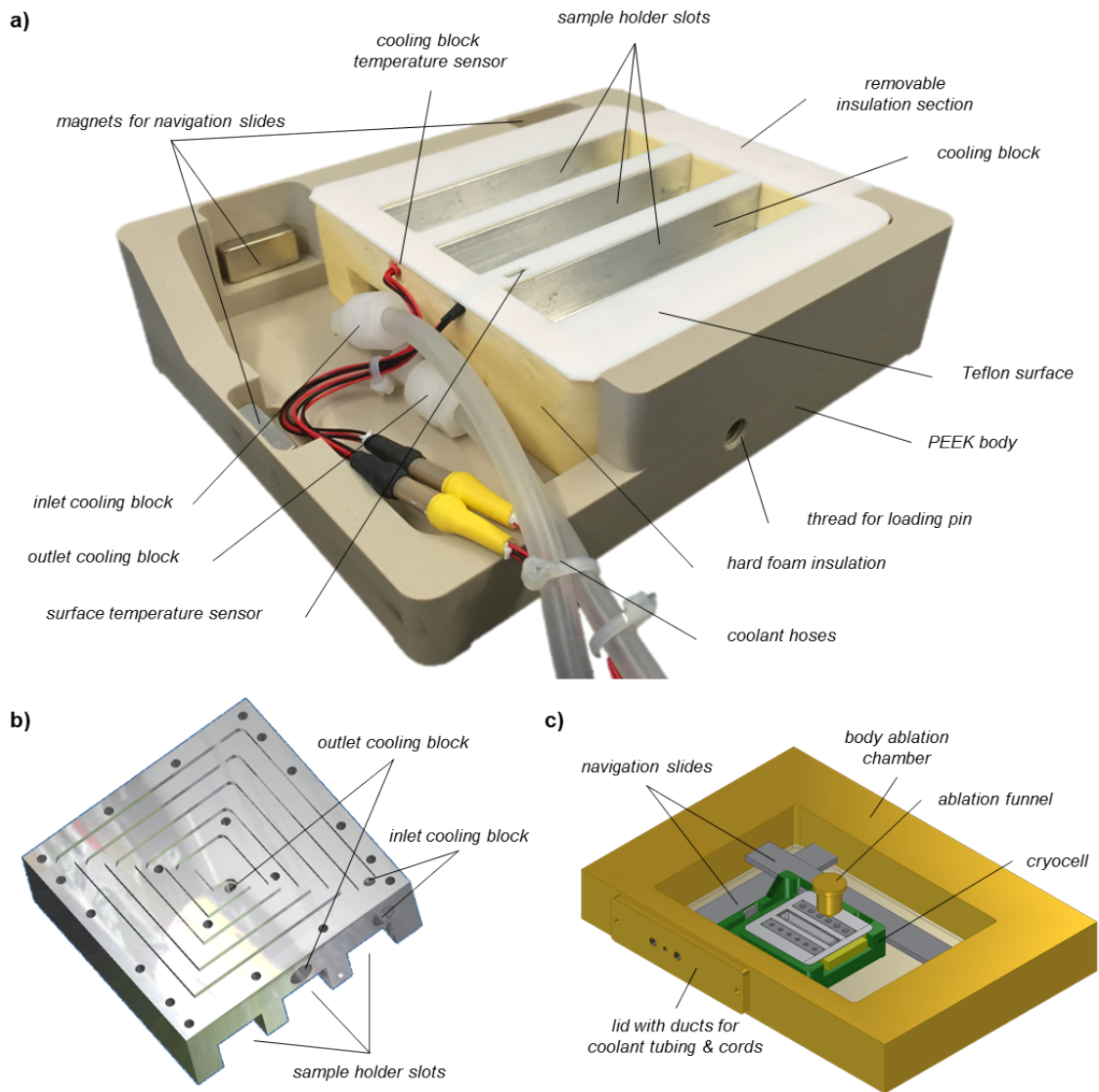


**Figure 6.2:** a) Sketch of the newly developed cryocell compatible to the Resonetics Resolution S155 laser ablation system. b) Sketch of the cooling block made of aluminum featuring a helical channel system for circulation of the coolant at the bottom. c) Sketch of the cryocell (depicted in green) inside the ablation chamber. Coolant hoses are not shown.

### 6.3.1.2 Coolant hoses

Finding appropriate hoses for the coolant was the most critical part during the construction and the consistent further development of the experimental hardware (Section 6.3.1.3) as they need to fulfill several demands almost contradicting themselves. The inner diameter needs to be large enough ( $>5$  mm) to ensure a sufficient high flow rate of the coolant to chill the aluminum core of the cryocell to a tempera-

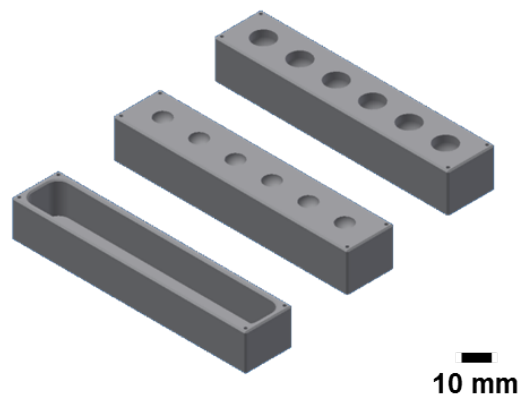


**Figure 6.3:** Sketch of the two types of standard holders and the sample holder for ice samples of 8 cm length.

ture of  $\leq -25$  °C. Reaching this temperature is impeded by the thick-walled body of the ablation chamber made from aluminum which effectively dissipates the supplied chillness. Nevertheless, as the cryocell needs to be movable inside the evacuated ablation chamber (Section 6.3.1), the coolant hoses need to be flexible and light due to the limited traction of the navigation slides, vacuum suitable, as well as resistant to temperatures down to  $-35$  °C and to pressures of several bars. Additionally, they need to exhibit limited permeability to prevent diffusion of coolant causing elevated ICP-MS backgrounds (Section 6.3.1.5). Many of these requirements were not apparent during the initial development process of the cryocell, but were figured out during the operational phase due to unexpected difficulties. The latest modification of deployed tubing representing the best compromise of all necessary requirements is described hereafter.

### 6.3.1.3 Further essential developments of the cryocell hardware

A severe flooding of the ablation chamber with cooling liquid due to a crack of a weld seam of the cooling hose next to the inlet into the cooling block demonstrated the need of further modifications of the cryocell to prevent another leakage of coolant. The tubing was replaced by a vacuum suitable, corrugated PTFE hose (CIMA KA, Zurich, Switzerland), with a wall thickness of 0.75 mm and an inner diameter of 8 mm. Compared to the hoses used before, it is made from one piece (no weld seams), it can be used within a temperature range from  $-200$  to  $260$  °C, and it exhibits a very good resistance towards organic solvents. The new tubing was extensively tested by exposure to ethanol at  $-35$  °C under maximum pressure for several hours. Simultaneous manual compression and dragging of the tubes, mimicking the mechanical stress during the sample exchange process of the LA system, showed their suitability for the intended use. Moreover, the power supply unit of the pump was replaced by a switching mode power supply (PeakTech 6095, PeakTech, Ahrensburg,

Germany) limiting the voltage supplied to the pump. This significantly lowered the maximum pressure delivered by the pump compared to the non-adjustable pressure delivered before and consequently exposed the tubing to less mechanical stress. The power supply was also coupled to the control unit of the chiller. The latter sets off an alarm in case the level of coolant gets too low (i.e., due to a leakage) and the respective output signal can be received by the power supply initiating a circuit break to the pump. This rather insensitive protective mechanism in the event of a coolant leakage was complemented with the installation of a capacitive sensor (SK1-8-34/16/8-P-b-ö, Sentronic, Busslingen, Switzerland) in proximity to the inlet and outlet of the cooling hoses to the cooling block (Figure 6.4). The sensor was coupled to the switching mode power supply of the pump to immediately stop filling of the ablation chamber with coolant in case of another leakage. The sensor is originally designed to detect water, but spattering of the sensor with ethanol under helium atmosphere, even though ethanol has a significantly lower conductivity, still caused a change in capacity large enough to make an output signal to the power supply, leading to an immediate power interruption of the pump.

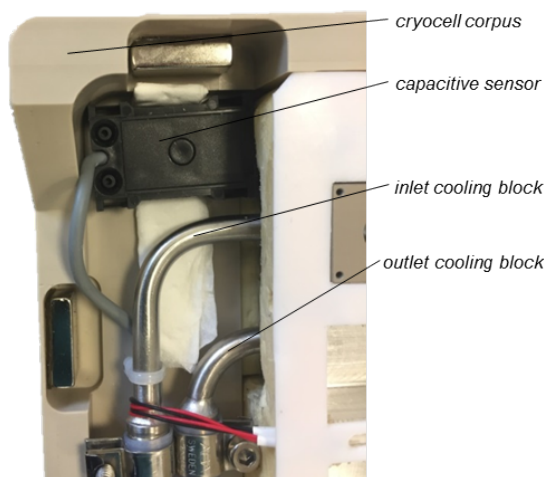


**Figure 6.4:** Capacitive sensor within the cryocell. A tissue placed underneath the sensor ensures absorption of a possible discharge of coolant and direct channeling to the detection field located at the bottom of the sensor.

#### 6.3.1.4 Adaptation of the laser ablation control software

The user interface of the LA system control software (GeoStar, NorrisSoftware, Oxford, United Kingdom) was modified to be able to navigate the cryocell. Therefore, a sketch showing the top view of the cryocell was added to the list of available S155 sample holders and mapped to the stage coordinates and the camera video image (Figure 6.5).

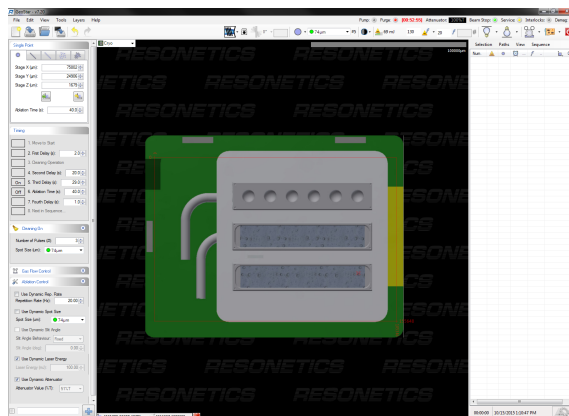


**Figure 6.5:** Modified user interface of the GeoStar LA control software allowing navigation of the cryocell developed in this thesis using the pre-existing LA system (sketch of the cryocell depicted in green).

### 6.3.1.5 Coolant

Following the construction of the cryocell, the optimal cooling liquid had to be selected. This phase of the development process ran parallel to the operational phase due to unforeseeable difficulties. Typical coolants for applications requiring temperatures below 0 °C include organic solvents, synthetic oils, or antifreeze solutions (mixture of water and a suitable organic compound) due to their high heat capacity, low viscosity, and being non-corrosive. Ethanol, silicon oil, and a mixture of water and ethylene glycol were tested for cooling of the cryocell. Ethanol exhibits the lowest viscosity at  $-35$  to  $-30$  °C which revealed to be advantageous due to the long and narrow channel system of the cryocell. However, as ethanol is very volatile, diffusion through the initial cooling hoses occurred. This caused (even with the optimized carrier gas flow pathway, Section 6.3.2.2) highly elevated background levels for many isotopes and various interferences typical for carbon (Figure 6.6). A similar difficulty was observed for silicon oil, which caused an elevated long-lived background for mass 28 u (Si) due to its high creeping capability (common lubricant). This was unfavorable for the silicon measurements in geological samples performed by our collaborators. Using a temperature-optimized 2:3 mixture of water and ethylene glycol [Cordray *et al.*, 1996] actually turned out to be the best compromise between non-significant increased background count rates and obtaining a constant cryocell temperature of  $-25$  °C. However, a severe flooding of the ablation chamber due to a crack of the cooling hose (Section 6.3.1.3) showed that antifreeze solutions are not suitable as coolants for the present setup, as they would leave behind significant damage to the LA system in case of reoccurring coolant leakage. Therefore, together with optimized coolant tubing (Section 6.3.1.3), ethanol was determined to be the most appropriate coolant.

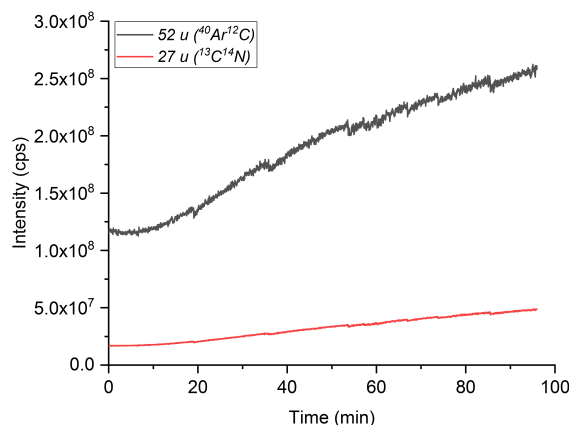


**Figure 6.6:** ICP-MS signal of the masses 27 u ( $^{13}\text{C}^{14}\text{N}$ ) and 52 u ( $^{40}\text{Ar}^{12}\text{C}$ ), susceptible to carbon induced interferences caused by diffusion of ethanol through the coolant hoses.

### 6.3.1.6 Characterization of the setup

**Definition of coolant temperature** Defining the optimal coolant temperature was one of the first steps during the commissioning of the cryocell to ensure an ice surface temperature of  $\leq -20$  °C throughout the entire measurement process. A small temperature sensor (Pt100) was frozen on the surface of a blank ice sample to monitor temperature changes during evacuation, helium purging, cryocell navigation, and ablation. The helium atmosphere and the ablation funnel, made of aluminum, were found to have the most significant effect and resulted in an increase of surface temperature by  $\sim 5$  and  $\sim 10$  °C, respectively, compared to ambient conditions. A new ablation funnel made from PTFE (Section 6.3.2.2) was subsequently used to eliminate heat transfer from the sample surface. Adjusting the temperature of the coolant in the chiller reservoir to  $-35$  °C allowed to maintain a surface temperature of the ice sample of at least  $-25$  to  $-20$  °C.

**Definition of laser ablation parameters** First tests using blank ice samples also included the determination of the optimal LA operating conditions to obtain a neat ablation of ice. We found that a fluence of  $3\text{--}4$  J  $\text{cm}^{-2}$  in combination with a repetition rate of 20 Hz are necessary to obtain clearly visible and nicely shaped craters using point ablations and  $6\text{--}7$  J  $\text{cm}^{-2}$  for ablations along a path with a scan speed of  $50$   $\mu\text{m s}^{-1}$ , respectively. These ablation parameters were also the basis for the analysis of high-Alpine glacier ice samples at a later stage of the method development phase (Section 6.3.4.2, Table 6.3). Similar conditions have been reported by *Della Lunga et al.* [2014, 2017]. However, the ablation behavior of ice appeared to have strong small-scale variability. Figure 6.7a shows point ablations using the mentioned LA operating conditions and a circular ( $163$   $\mu\text{m}$ ) laser spot. Even though the LA operating conditions are identical, crater formation differs. Crater 1 and



3 are located inside the same grain a few hundred micrometers apart from each other, but reflect the outcome of an uncontrolled and a controlled ablation, respectively. Grain boundaries or triple junctions do not necessarily have to obstruct a controlled ablation as visible for crater 2. The inhomogeneity of ice with varying density, different bubble content, and various grain sizes could be possible reasons causing this phenomenon. Moreover, even minimum unevenness of the surface despite of prior smoothing (Section 6.3.2.1) is likely to cause an inconsistency in LA performance. Perpetual sublimation during the measurement process can roughen the smoothed surface leading to a less controlled ablation behavior. Ablations were consequently performed on sites where the sample surface appeared to be smooth, indicated by an intense reflection of light. If not stated otherwise, in addition to the manual sample surface decontamination (Section 6.3.2.1), laser pre-cleaning of the ice surface using identical LA parameters, but a larger spot size, was performed prior to the actual ablation for sampling to remove possible debris from precedent ablations (Figure 6.7b).

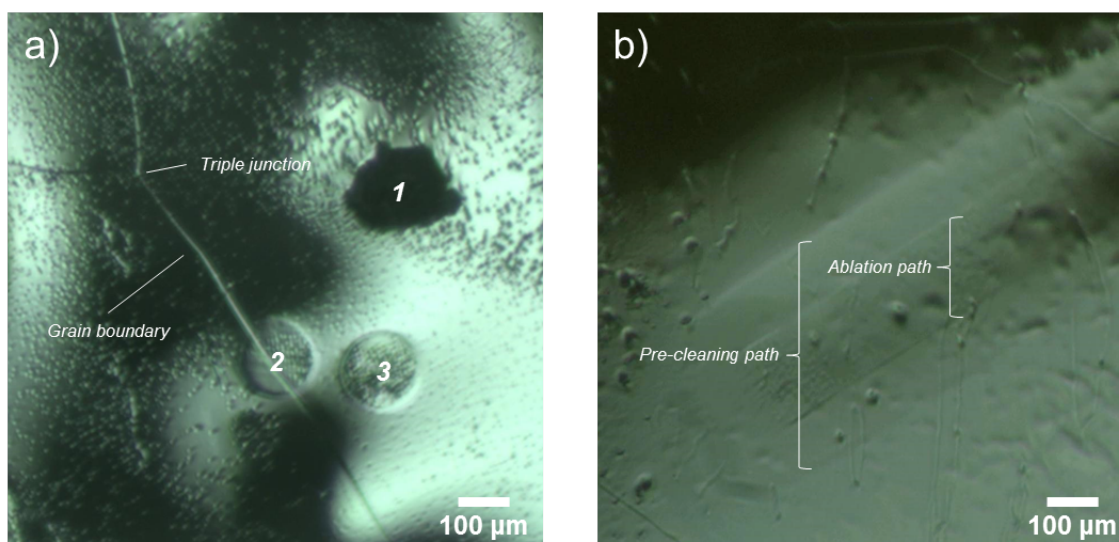


**Figure 6.7:** a) Threefold point ablation of an ice blank sample resulting in distinct crater formation and exhibiting the inconsistent ablation behavior of ice using identical LA conditions. b) Ablation passage for pre-cleaning of the (blank) ice surface performed prior to the actual ablation passage for sampling.

**Assessment of the cryocell LA-ICP-MS setup's sensitivity** The NIST standard reference material with the lowest TE concentrations available (SRM 616) was measured with the modified cryocell setup (Section 6.3.2.2) to determine the sensitivity of the setup and to select TEs principally detectable in glacier ice. Bi, Cd, Ce, Co, Cs, Cu, Dy, Eu, Gd, Hf, La, Li, Lu, Mn, Mo, Nb, Nd, Ni, Pr, Rb, Sm, Ta, Th, Tl, U, V, Y, Yb, and Zr occur in concentrations  $<1 \mu\text{g g}^{-1}$  in the SRM 616. During

ablation of the latter, Co, Gd, Hf, Mn, Nb, Nd, Ni, Li, Sm, V, and Yb did not show a background resolved signal indicating that these TEs are most probably not detectable in glacier ice where concentrations are far below  $1 \mu\text{g g}^{-1}$  (Section 6.3.4). For Al, Ca, K, and Na no statement can be made as they are part of the bulk glass matrix, nor for Ba, Mg, F, Pb, and Zn as they occur in concentrations  $>1 \mu\text{g g}^{-1}$  and therefore resulted in any case in a background resolved signal.

## 6.3.2 Development of additional experimental hardware

### 6.3.2.1 Ice plane

To remove contamination by metal residues after the sawing and for smoothing of the surface, an ice plane (Figure 6.8) was made out of PVDF and equipped with a height-adjustable ceramic  $\text{ZrO}_2$  blade (CX-3, American Cutting Edge, Centerville OH, United States). The ice plane is compatible to the dimensions of the cryocell sample holders. Mounting of the blade at an angle of  $\sim 20^\circ$  was found to ensure the best surface quality. A smooth sample surface is necessary for better visibility of the grain boundary network and to improve ablation performance (Della Lunga, 2015). Therefore, the time period between the smoothing and the ablation needs to be as short as possible as the roughness of the ice surface increases with time due to sublimation. 1 to 2 mm of the sample's surface were routinely removed in steps of  $\sim 0.5$  mm.

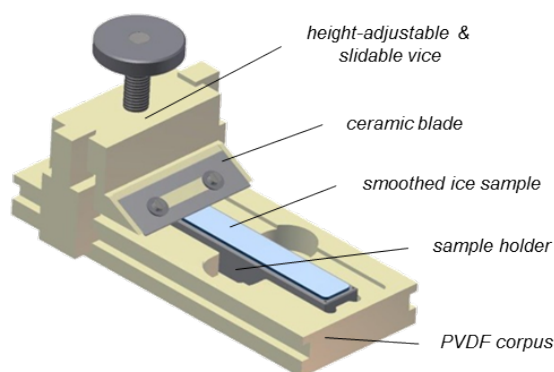


**Figure 6.8:** Sketch of the custom-built ice plane used for decontamination and smoothing of ice sample surfaces.

### 6.3.2.2 Optimization of the carrier gas flow pathway

By default the carrier gas (helium) is laterally introduced into the Laurin Technic two-volume LA chamber (Figure 6.9), flows through the interior of the chamber, and enters into the funnel-shaped smaller chamber, where the actual ablation takes

place, from both its top and bottom, before taking up the sample aerosol formed during ablation for further transport to the ICP-MS [Müller *et al.*, 2009]. This carrier gas flow pathway allows mixing of the helium introduced for entraining the sample aerosol with the “residual” helium atmosphere in the LA chamber. This is unfavorable as the atmosphere inside the chamber is presumably not as clean as the freshly introduced gas. Diffusion of coolant through the hoses (Figure 6.6), release of harvested air inside the porous hard foam insulation of the cryocell, or contamination on the inner surfaces of the ablation chamber and the sample aerosol transport system [Schlöglova *et al.*, 2017] due to previous analyses of minerals performed by other users of the LA-ICP-MS system, result in unfavorable elevated backgrounds of the ICP-MS. To minimize the contact time between the carrier gas and the atmosphere inside the chamber, a new ablation funnel was designed which, in contrast to the original funnel, introduces the carrier gas as a ring flow directly above the sampling spot (Figure 6.9 and Figure 6.10). As for the original funnel manufactured by Laurin Technic, this new funnel not only ensures an invariant gas flow around the ablation site, but also has the advantage of short signal washout times due to its similar inner funnel-shaped geometry and volume (1-2 cm<sup>3</sup>) [Müller *et al.*, 2009]. Additionally it is made of PTFE which has a lower thermal conductivity than aluminum reducing the dissipation of cold and therefore making the ice sample underneath less susceptible to surface melting Section 6.3.1.6. To test performance and suitability of the new ablation funnel compared to the original Laurin Technic funnel, intensities of 24 isotopes (<sup>85</sup>Rb, <sup>89</sup>Y, <sup>90</sup>Zr, <sup>93</sup>Nb, <sup>95</sup>Mo, <sup>97</sup>Mo, <sup>111</sup>Cd, <sup>133</sup>Cs, <sup>139</sup>La, <sup>140</sup>Ce, <sup>141</sup>Pr, <sup>146</sup>Nd, <sup>147</sup>Sm, <sup>153</sup>Eu, <sup>157</sup>Gd, <sup>163</sup>Dy, <sup>172</sup>Yb, <sup>175</sup>Lu, <sup>178</sup>Hf, <sup>181</sup>Ta, <sup>205</sup>Tl, <sup>209</sup>Bi, <sup>232</sup>Th, <sup>238</sup>U) in NIST SRMs 610, 612, and 614 were measured using both funnels and identical LA-ICP-MS operating conditions. Ratios of NIST SRM 610/614 and 612/614 intensities did not differ by more than 5% on average between the two funnels and the average deviations of the two ratios compared to the ratios of the corresponding reference values were smaller than 6%. This shows that the new ablation funnel, even though significantly changing the carrier gas flow pathway, ensures reproducible measurements. Moreover, the carrier gas blank was measured under identical conditions using both funnels (Figure 6.11). The new funnel of the LA setup yielded 90% lower background count rates on average most likely due to the minimized contact time between the helium serving as carrier gas and the helium atmosphere inside the ablation chamber.

### 6.3.2.3 Flow box for on-site sample handling and standard preparation

A flow box (Figure 6.12) was constructed to allow for on-site preparation of ice samples (Section 6.3.2.1), freezing of external calibration standards (Section 6.3.3.2), and loading of the cryocell under clean conditions. The flow box can be constantly flushed with nitrogen gas to prevent frosting of cold surfaces and to avoid permeation of outside air. The flow box’s working top is large enough to simultaneously hold the cryocell and a highly insulated pan of 1 L volume made from EVA foam

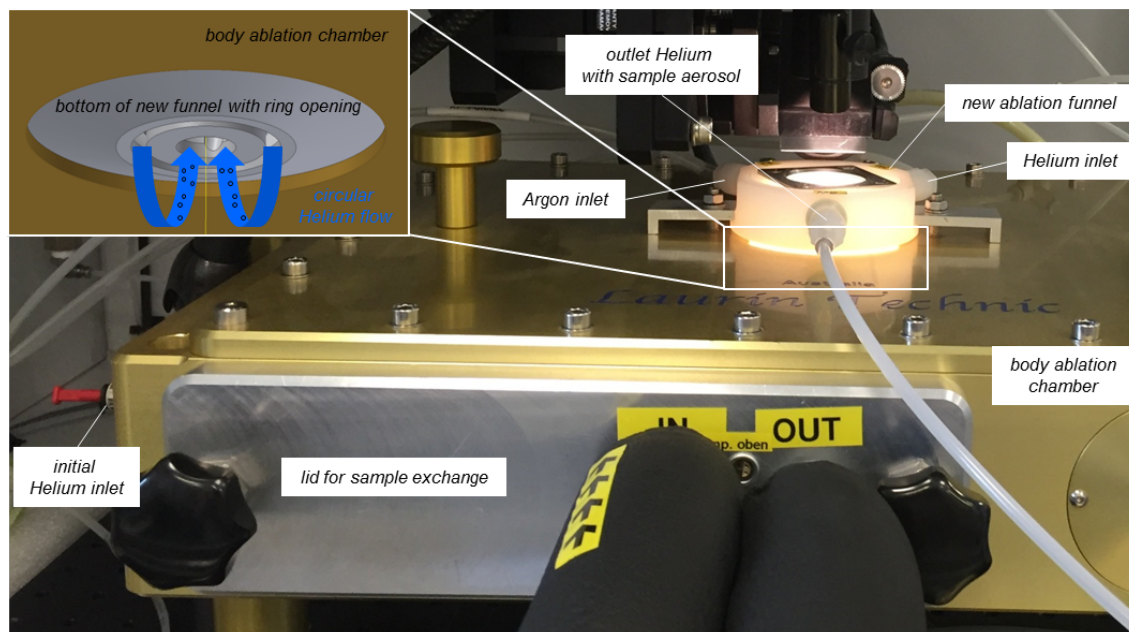


**Figure 6.9:** Frontal view on the modified Laurin Technic two-volume LA chamber. The sketch in the top left shows the ring opening on the bottom side of the new ablation funnel (Figure 6.10). This allows introduction of the helium carrier gas as a circular flow directly above the sampling spot for immediate uptake of the sample aerosol.

(Corning Inc., Corning NY, United States) serving as reservoir for liquid nitrogen. The pan was complemented with an exactly fitting and height-adjustable perforated aluminum rack for on-site smoothing of ice samples using the ice plane or ice standard preparation. For the latter purpose, the rack has a notch for the standard holders.

### 6.3.3 Development of a calibration procedure

A direct quantification of differences in TE concentrations between grain boundaries and interiors in glacier ice using cryocell LA-ICP-MS requires a calibration with, if feasible, internal, but certainly with matrix-matched external standards. The steps undertaken to assess the realization of an internal calibration for glacier ice measurements and the development of external calibration standards are described hereafter.

#### 6.3.3.1 Evaluation of internal standard availability

To ensure the precision of a quantitative chemical analysis, an internal standard is necessary to correct for possible losses of analyte during the measurement process

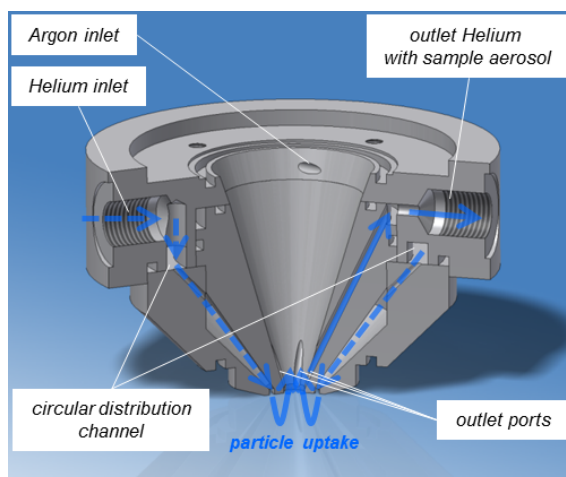


**Figure 6.10:** Cross-section of the new ablation funnel designed to minimize the contact time between the helium carrier gas and the inert atmosphere inside the ablation chamber and to reduce thermal flow. The flow pathway of the carrier gas is depicted in blue. Dashed and continuous arrows represent the flow pathway before and after sample particle uptake, respectively. Helium is laterally introduced into the funnel, distributed via a circular channel to escape as a circular flow for sample aerosol uptake at the bottom of the funnel. After mixing with the separately introduced argon, helium is transported via four small ports (only three visible in the sketch) at the bottom to the main outlet (signal washout).

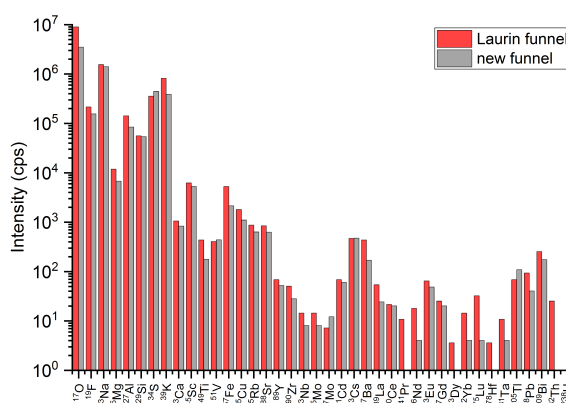


**Figure 6.11:** Comparison of isotopic ICP-MS backgrounds showing lower carrier gas blanks using the ablation funnel developed in this thesis.  $^{141}\text{Pr}$ ,  $^{163}\text{Dy}$ ,  $^{178}\text{Hf}$ ,  $^{232}\text{Th}$ , and  $^{238}\text{U}$ , revealed intensity values  $<1$  cps.

[Skoog and Leary, 1996]. In LA, the ablation behavior can significantly vary depending on sample properties such as density or surface roughness. Furthermore, variations in the transport of sample aerosol, changes in the plasma conditions, or instrumental drifts of the ICP-MS may be factors influencing the analytical signal.

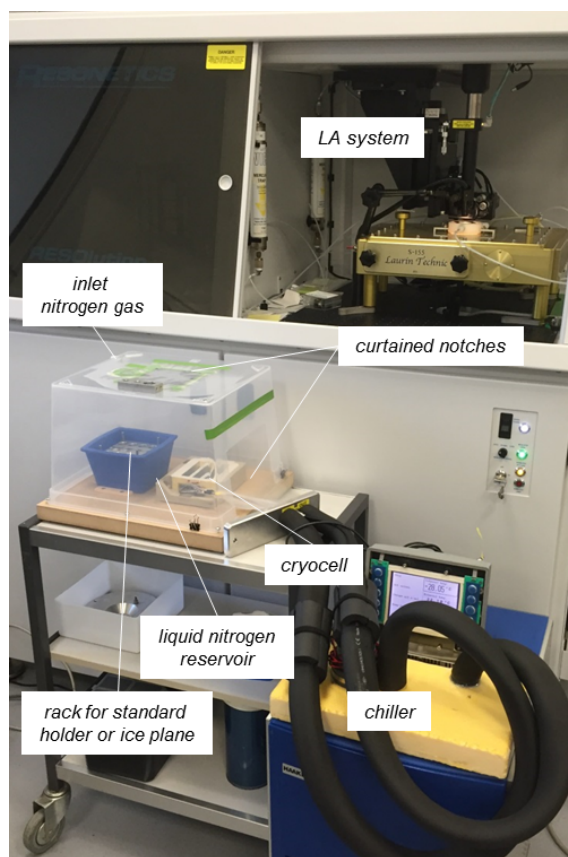


**Figure 6.12:** Custom-built flow box for multipurpose on-site sample preparation and handling.

A crucial part of this work was to assess the availability of an internal standard for glacier ice measurements. For solid materials such as ice, it is not possible to spike an internal standard prior to its measurement. However,  $\text{H}_2\text{O}$  is the main component of the ice matrix occurring in a constant concentration and thus offers several possibilities for an internal standard:  $^{17}\text{OH}$  ( $^{16}\text{O}^1\text{H}$ ),  $^{19}\text{OH}$  ( $^{18}\text{O}^1\text{H}$ ), and  $^{16}\text{O}^{18}\text{O}$ .  $^{17}\text{OH}$  and  $^{19}\text{OH}$  (Note: both of them are single positive charged molecular ions) have been previously used by *Reinhardt et al.* [2001, 2003] to normalize LA-ICP-MS signals of Greenland ice. Ablation of blank ice samples revealed that it is not feasible to use  $^{17}\text{OH}$  or  $^{19}\text{OH}$  as internal standards due the elevated background levels for mass 17 and 19, and insufficient sensitivity of the LA-ICP-MS system, respectively. This has also been observed by *Della Lunga et al.* [2014, 2017] and can be explained by a considerably lower amount of ablated material using a 193 nm UV laser compared to a 1064 nm IR laser [*Müller et al.*, 2011; *Warren*, 1984]. On the contrary, ablation of blank ice samples using the present setup exhibited a signal for mass 34. A medium resolution measurement revealed that the latter signal did not originate from the mixed oxygen isotope dimer  $^{16}\text{O}^{18}\text{O}$ , but from sulfur (Figure 13) even though there was no sulfur in the sample. *Guillong et al.* [2008] observed a sim-

ilar phenomenon when ablating quartz using a 193 nm UV laser and assumed that sulfur is released within the immediate ablation environment from slightly sulfur-contaminated interior surfaces of the ablation chamber that cannot be removed by normal means. They postulated that this is the result of a photo-chemically induced desorption reaction triggered either by the radiation emitted by the laser induced plasma at the ablation spot or directly by the laser light. This thorough assessment of internal standard availability in ice showed that no background-resolved signal for  $^{17}\text{OH}$ ,  $^{19}\text{OH}$ , and  $^{16}\text{O}^{18}\text{O}$  during UV-LA of ice could be obtained. To the best of our knowledge, there are no other isotopes that could possibly serve as internal standards in ice.

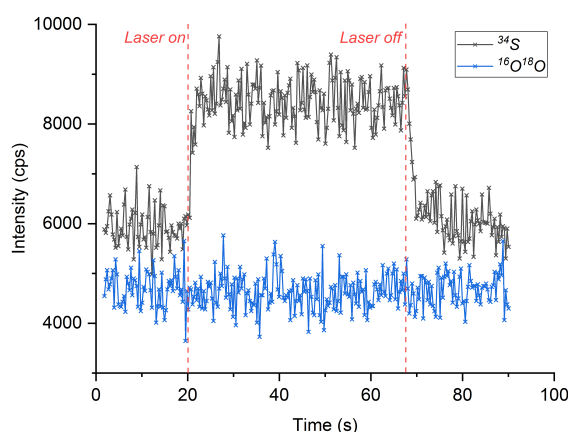


**Figure 6.13:** Signal acquisition of mass 34 in medium resolution revealing that the LA signal during the ablation of a blank ice sample does not originate from the mixed oxygen dimer  $^{16}\text{O}^{18}\text{O}$ , but from an unknown contamination of sulfur that cannot be eliminated by normal means.

### 6.3.3.2 Development of external ice standards

So-called matrix-matched external standards are necessary to calibrate LA-ICP-MS signal intensities for quantitative element data, especially if no internal standardization is available, as interferences, sensitivity drifts, elemental/isotopic fractionation, and matrix effects may limit accuracy and precision of the analysis [Lin *et al.*, 2016]. “Matrix-matched” means that both the external standard and the sample have the same matrix composition i.e., consist of the same bulk material. At the time when this study was initiated, external reference ice standards, homogeneous on a sub-millimeter scale, were reported to be lacking [Della Lunga *et al.*, 2014; Müller *et al.*, 2011]. Recently, Della Lunga *et al.* [2017] provided a procedure to prepare a set of external, homogenous ice standards for quantification of LA-ICP-MS signals acquired at 212  $\mu\text{m}$  resolution.

**Critical evaluation of the ice standard preparation procedure following Reinhardt et al. [2001]** The basic idea of how to prepare frozen ice standards to calibrate LA-ICP-MS signals on a millimeter scale has already been reported in 2001 by Reinhardt et al., where small volumes (5 mL) of acidified multi-element ICP-MS standard solutions ( $\sim 0.3$  M  $\text{HNO}_3$ ) were frozen at  $-30$  °C and showed relative standard deviations (RSDs) of the corresponding LA-ICP-MS signal in the range of 3-6%.

In a first attempt,  $\sim 10$   $\mu\text{L}$  droplets of a 1 ppm in-house multi-element ICP-MS standard solution ( $1 \text{ mg L}^{-1}$  of Al, Bi, Cd, Ce, Cu, Fe, La, Nd, Pb, Tl, and Zn in  $0.2$  M  $\text{HNO}_3$ ) were frozen directly in the standard holder pits (Figure 6.3) at  $-20$  °C in the cold room of the Paul Scherrer Institute one day prior to their measurement at ETH Zurich. A thin layer of liquid on the surface of the frozen droplet could be observed during ablation. This can be explained by a freezing process proceeding at a rate low enough that impurities, such as nitric acid, are expelled from the growing crystal to the surface during the freezing process, and additionally, by recrystallization processes occurring during the time between preparation and ablation. Locally limited and elevated nitric acid deposits on the surface increase the freezing point of ice identifiable as thin layer of liquid (brine). Point ablation of this inhomogeneous matrix probably resulted in simultaneous evaporation and removal of both liquid and solid material. This is certainly not in line with the idea of matrix-matched calibration standards even though the ICP-MS signal of the included elements appeared to be stable (RSD  $\sim 10\%$ ). A different ablation behavior was observed for ice standards prepared by freezing  $10$   $\mu\text{L}$  droplets of low ( $\leq 2 \cdot 10^{-3}$  M  $\text{HNO}_3$ , dilution of the 1 ppm in-house ICP-MS standard solution) and non-acidified ( $10$  ppm Ca, Mg, and Na in-house IC standard solution for ion chromatography) standard solutions. The ice standard droplets appeared to be completely frozen i.e., without a liquid layer, but only a transient ICP-MS signal for the included elements could be achieved when ablating at the same spot. The same observation was made when ablating standards prepared by freezing several layers of  $10$   $\mu\text{L}$  standard solution droplets. Ablation along a path (scanning mode,  $12 \mu\text{m s}^{-1}$ ) resulted in a continuous LA-ICP-MS signal. The transient signal for point ablations is most likely caused by the rapid decrease of ablated material as the energy density decreases when the laser penetrates deeper into the sample [Reinhardt et al., 2001] and, as already explained above, by fractionation processes during and after freezing which enrich impurities particularly at the surface. We found that a liquid layer on the surface of the ice standards is identifiable if nitric acid concentrations exceed  $2 \cdot 10^{-3}$  M. Freezing at a temperature of  $-80$  °C using dry ice revealed the same phenomena for ice standards prepared from acidified and low/non-acidified standard solutions indicating that this phenomenon has to be observed for standards frozen at  $-30$  °C. Reinhardt et al. [2001, 2003] were not able to observe this feature, occurring on a micrometer scale due to a large laser spot size ( $300 \mu\text{m}$ ) and more importantly, due to a LA system lacking a microscope to monitor the ablation process.

This examination of the ice standard preparation procedure by Reinhardt et al. [2001] demonstrated that when freezing the standards at  $-20$  °C, the acid concen-



tration needs to be  $\leq 2 \cdot 10^{-3}$  M to prevent formation of liquid pockets on the surface of the droplets resulting in a ablation behavior unsuitable for matrix-matched calibration. Moreover, ablation along a path produces a more continuous ICP-MS signal compared to point ablations which yield transient LA-ICP-MS signals.

**Influence of storage time on the recrystallization of ice standards** As already hypothesized above, the time between the preparation and the measurement i.e., the storage time of ice standards is likely to allow for fractionation processes in the ice, segregating impurities to grain surfaces. To verify this assumption, ice standards were, as described above, prepared by freezing droplets of standard solution both directly and one day prior to their measurement. The non-acidified 10 ppm IC standard solution was used to exclude any influence of acidity. Figure 6.14 shows that the storage time of the ice standards needs to be as short as possible in order to reduce the impact of intermediate recrystallization processes causing additional inhomogeneities in impurity distribution. A time delay of several hours already leads to a  $\sim 30\text{-}40\%$  more fluctuating LA-ICP-MS signal. Based on this finding, the ice standard preparation procedure was adapted by on-site freezing of the ice standards prior to their measurement in our custom-built flow box (Section 6.3.2.3) at  $-30$  °C in the pre-cooled cryocell. Hereafter, the influence of the freezing temperature on the homogeneity of the ice standard is discussed.

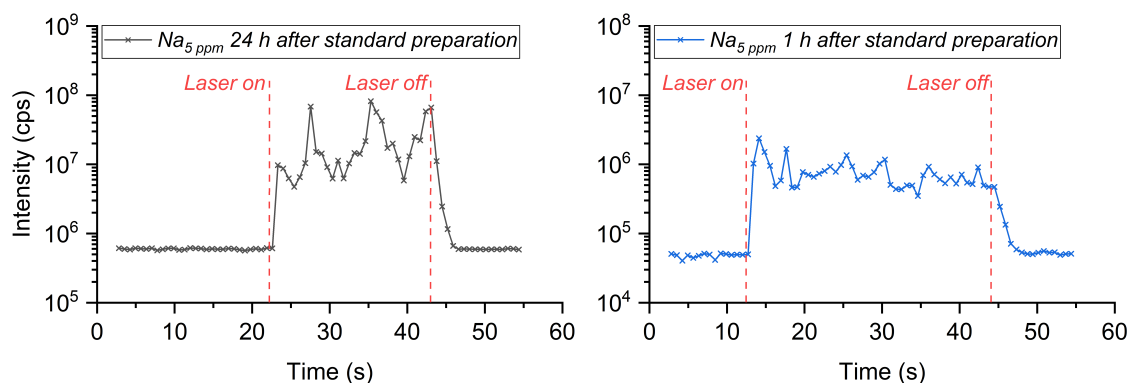


**Figure 6.14:** Comparison of the  $^{23}\text{Na}$  LA-ICP-MS signal between two equally concentrated frozen standards differing in the time between preparation and measurement (storage time). Note: Data was acquired on different days, which is evident in the different background levels that are a result of the daily gas blank variation.

**Standard preparation using liquid nitrogen** The storage time of an ice standard needs to be as short as possible to avoid intermediate recrystallization processes. As proposed above, a slow freezing of the standard solution is also likely to induce fractionation processes causing agglomeration of impurities from the standard

solution at the surface during the crystallization process. An instantaneous temperature drop (“shock-freezing”) leads to a sudden loss of internal energy of the system and is therefore likely to inhibit fractionation effects due to equilibrium processes in ice during freezing [Reinhardt, 2001]. To enable such shock-freezing conditions, droplets of standard solution were frozen at  $-196\text{ }^{\circ}\text{C}$  by placing the standard holder into the liquid nitrogen reservoir of our custom-built flow box (Section 6.3.2.3). A new in-house multi-element ICP-MS standard solution (2000  $\text{mg L}^{-1}$  of Al, Ba, Bi, Br, Ca, Cd, Ce, Co, Cu, Fe, K, La, Mg, Mn, Na, Nd, Pb, Sr, Ti, Tl, U and Zn in 0.2 M  $\text{HNO}_3$ ) enabled to prepare dilutions of five standards (5, 2, 1, 0.5, and 0.1  $\text{mg L}^{-1}$ ) of low acidity ( $<3\cdot 10^{-3}$  M  $\text{HNO}_3$ ) that were frozen both at  $-30$  and  $-196\text{ }^{\circ}\text{C}$ . Figure 6.15 indicates that for low/non-acidified ice standard comparable calibration curves can be obtained despite a differing freezing temperature. A procedure to successfully prepare ice standards using liquid nitrogen as freezing agent was simultaneously developed by Della Lunga *et al.* [2017].

As described above, Reinhardt *et al.* [2001, 2003] and later Della Lunga *et al.* [2017] used acidified standard solutions for ice standard preparation. However, the influence of ice standard acidity on the outcome of the calibration is not known so far and our initial attempts in preparing ice standards revealed a strong influence of acidity on the ablation performance. Multi-element standard solutions used for calibration of ICP-MS signals are generally acidified to a pH of 0-2 to prevent adsorption of its constituents on the walls of the storage container. Ablation of a series of five 10  $\mu\text{L}$  ice standards (5, 2, 1, 0.5, and 0.1  $\text{mg L}^{-1}$ ), prepared by diluting the 2000 ppm in-house ICP-MS standard solution with 0.2 M  $\text{HNO}_3$  and freezing at  $-196\text{ }^{\circ}\text{C}$ , revealed no liquid layer on their surface as observed for a freezing temperature of  $-20$  and  $-30\text{ }^{\circ}\text{C}$ , respectively. Formation of liquid acid pockets on the droplet surface can therefore be prevented by applying a very low freezing temperature. However, comparison to a calibration obtained by ablation of another ice standard series comprising equal concentrations, but of lower acidity ( $<3\cdot 10^{-3}$  M  $\text{HNO}_3$ ) due to dilution with ultra-pure water, showed a significant difference (Figure 6.15). Signal intensities (normalized to the daily ablation signal of a NIST SRM 610) of acidified standards were  $\sim 100$  times higher than for low-acidified standards indicating that the freezing process and therefore the homogeneity of the ice standards is clearly influenced by the acidity of the deployed standard solutions.

Replicative ablation on different locations of the highest concentrated (5  $\text{mg L}^{-1}$ ) ice standard generally showed deviations of 10-80% (Figure 6.15), strongly suggesting that the developed ice standard preparation procedure does not yet guarantee a sufficient reproducibility, which may have the following reasons:

1. Monitoring the consistency of the ablation performance of the frozen droplets was difficult because of an obscured camera image. The spherical shape of the frozen droplets together with the fact, that the design of the cryocell does not allow transmission of light through the specimen, cause a strong reflection of the camera light at the highest point of the sphere.
2. Spherical surfaces appeared to be unfavorable for LA in contrast to an even

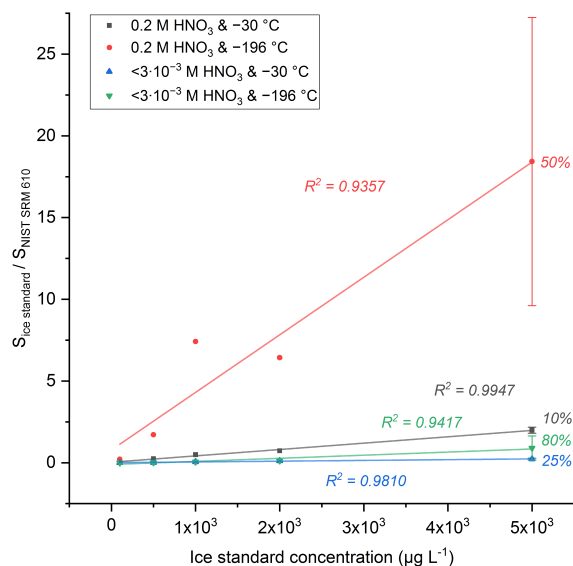


**Figure 6.15:** Exemplary calibration curves for  $^{208}\text{Pb}$  obtained by LA of ice standards prepared by freezing small amounts ( $\sim 10 \mu\text{L}$ ) of a dilution series (5, 2, 1, 0.5, 0.1  $\text{mg L}^{-1}$ ) of acidified (0.2 M  $\text{HNO}_3$ ) and low acidified ( $< 3 \cdot 10^{-3}$  M  $\text{HNO}_3$ ) standard solution at  $-30$  and  $-196$   $^\circ\text{C}$ , respectively.  $^{208}\text{Pb}$  generally showed the most continuous LA signal, making it a suitable isotope for the comparison of different ice standard freezing parameters. Signal intensities are normalized to the daily signal of  $^{208}\text{Pb}$ , obtained by ablating a NIST 610 SRM glass, as ice standards were prepared and measured on different days. Measurements of the highest concentrated standard were performed multiple times to assess the reproducibility of the ice standard preparation procedure.

and smoothed surface, as the laser is not entirely focused while ablating along a path. The latter causes a diminished ablation performance. The ice plane (Section 6.3.2.1) is not suitable to smooth the surface of millimeter sized frozen droplets.

3. The surface of the standard holders might not be smooth enough to ensure a uniform spread of standard solution yielding in a more homogenous shock freezing.

A procedure recently reported by *Della Lunga et al.* [2017] allows to prepare ice standards, large enough to be surface-cleaned and smoothed, by stepwise shock-freezing of standard solution onto an ultra-smooth, polished glass slide. RSDs were reported to range between  $\pm 10$ -15%. Therefore, it would be of great value to employ the latter procedure for the preparation of low/non-acidified ice standards and to unequivocally clarify whether the outcome of the calibration is influenced by the acidity. Additionally, it would enable to compare the reproducibility of preparing low acidified ice standards by shock-freezing.

To complement the previously described assessment of the setup's sensitivity (Sec-

tion 6.3.1.6), RSDs of shock-frozen ice standards in the range  $\pm 20\%$  would allow for an accurate estimation of DLs.

Matrix-matched external ice standards could be successfully prepared, although the RSDs for shock-frozen standards are still too large (50 and 80%) to obtain precise calibration curves. Our developmental work demonstrated that the acidity of the solution used for ice standard preparation, the type of ablation, the storage time of the ice standard, and the freezing temperature are the four parameters likely to substantially influence the quality of a matrix-matched external standardization. Freezing of standard solutions at  $-30\text{ }^{\circ}\text{C}$  causes the formation of liquid acid pockets on the ice standard surface if  $\text{HNO}_3$  concentrations exceed  $2 \cdot 10^{-3}\text{ M}$ . In general, high acidity has been observed to most probably bias an ice standard calibration. Strictly speaking, the use of acid is not adequate to the principle of matrix-matching as Alpine glacier ice is only slightly acidic with a pH of  $\sim 5\text{--}6$  [Legrand *et al.*, 2003]. Line ablations yield more steady LA-ICP-MS signals compared to point ablations and liquid nitrogen as freezing agent ensures instantaneous shock freezing. The storage time of ice standards should be kept as short as possible to restrict fractionation processes.

### 6.3.4 Pilot study for final method assessment

In a previous study we investigated the behavior of 35 TEs in a section affected by meltwater percolation in a 50 m high-Alpine ice core segment from upper Grenzgletscher, Switzerland (Chapter 3, Avak *et al.* [2018]). A fractionation was observed, where Ba, Ca, Cd Co, Mg, Mn, Na, Ni, Sr, and Zn revealed significant concentration depletion while Ag, Al, Bi, Cu, Cs, Fe, Li, Mo, Pb, Rb, Sb, Th, Tl, U, V, W, Zr, and the rare-earth elements (REEs) were well preserved. We explained this to be the result of TE location at the grain scale and their distinct mobilization during meltwater percolation. TEs present in insoluble minerals (Al, Fe, Zr, REEs) tend to be enriched at grain surfaces during snow metamorphism, but were mostly preserved because their insolubility in water results in immobility with meltwater. Water-soluble TEs were incorporated into the ice lattice depending on their concentration in the ice. We concluded that this tentative indirect assessment of TE location in glacier ice needs to be corroborated using a direct *in situ* technique with sub-millimeter resolution such as cryocell LA-ICP-MS.

#### 6.3.4.1 Ice core sample selection

To test whether the cryocell LA-ICP-MS setup is capable to analyze the spatial distribution of TEs at a grain scale, samples from the upper Grenzgletscher ice core segment were selected for preliminary analyses. The samples B81\_183 and B98\_42 were purposefully selected for two reasons:

**Table 6.2:** Mean concentrations of the TEs in the B81\_183 and B98\_42 upper Grenzgletscher ice core samples. The respective mean concentrations within the part of the ice core segment not affected by meltwater percolation (ice core averages) are listed for comparison. Concentrations (bulk) are given in  $\mu\text{g L}^{-1}$  and were measured with ICP-MS (Chapter 3).

Trace element	B81_183	B98_42	Ice core average
Al	78	340	19
Ba	9.2	9.5	0.58
Bi	0.029	<DL	0.003
Ca	200	940	140
Cd	0.032	0.077	0.011
Co	0.047	0.23	0.021
Cu	1.4	0.58	0.11
Fe	84	190	11
La	0.31	0.42	0.040
Li	0.064	0.16	0.018
Mg	29	99	16
Mn	2.6	14	1.3
Na	12	210	16
Ni	0.45	0.37	0.077
Pb	25	0.53	1.1
Zn	9.6	3.6	0.87

1. They originate from depths of 25.2 and 32.2 m w.eq., respectively, which belong to the ice part of the core situated below the meltwater-affected section. Ice samples are necessary, as samples from the firn part situated above the meltwater-affected section are likely to exhibit a very inhomogeneous ablation behavior due to their increased porosity. Selecting samples from the meltwater-affected section itself is not reasonable either, because pristine ice, where no meltwater percolation occurred, is required if possible TE distribution differences on a grain scale are to be investigated.
2. Both samples reveal, according to the previously performed discrete ICP-MS measurements (Chapter 3), elevated TE concentrations especially of Al, Ba, Ca, Cu, Fe, Mg, Mn, Na, Pb, and Zn (Table 6.2). In the case of B98\_42, high TE concentrations are most probably related to a well visible yellow mineral dust layer occurring at the same depth. Considering the purpose of this pilot study, the selection of “high concentration” samples is reasonable to exceed the background level of the cryocell LA-ICP-MS setup for as many TEs as possible.

For time reasons, the calibration procedure (Section 6.3.3) was not applied, but signal intensities of Al, Ba, Bi, Ca, Cd, Cu, Fe, La, Li Mg, Mn, Na, Ni, Pb, and Zn in B81\_183 and B98\_42 were analyzed using cryocell LA-ICP-MS to qualitatively investigate their distribution at a sub-millimeter resolution.

**Table 6.3:** LA-ICP-MS operating conditions used for the preliminary analysis of upper Grenzgletscher ice core samples.

He carrier gas flow	700 mL min <sup>-1</sup>
Monitored isotopes	<sup>7</sup> Li, <sup>23</sup> Na, <sup>24</sup> Mg, <sup>27</sup> Al, <sup>44</sup> Ca, <sup>55</sup> Mn, <sup>56</sup> Fe, <sup>59</sup> Co, <sup>62</sup> Ni, <sup>65</sup> Cu, <sup>66</sup> Zn, <sup>111</sup> Cd, <sup>138</sup> Ba, <sup>139</sup> La, <sup>208</sup> Pb, <sup>209</sup> Bi
Fluence	~6.5 J cm <sup>-2</sup>
Repetition rate	20 Hz
Laser spot size (circular)	163 μm
Laser acquisition mode	Continuous line tracks
Ablation speed	50 μs <sup>-1</sup>

### 6.3.4.2 Cryocell LA-ICP-MS analysis of upper Grenzgletscher ice core samples

LA measurements using the parameters listed in (Table 6.3) were performed on both samples at different locations where the grain boundary network was well visible. Ablation tracks were defined in a way that both grain interior and grain boundary material was continuously sampled to directly identify qualitative differences in signal intensities between both crystallographic features. An ablation passage of larger laser spot size preceding the actual sampling passage as described in Section 6.3.1.6 and by *Della Lunga et al.* [2014] could not be accomplished. Even after extensive testing of different LA parameters, ablation tracks appeared to be fringed and deeply penetrating into the ice, resulting in a significantly decreased amount of removed material during a subsequent second ablation passage. Minimal differences in the density of high-Alpine glacier ice, originating from a depth of ~30 m (0.900 g cm<sup>-3</sup>) and formed by the compaction of individual snow grains, compared to blank ice, formed by crystallization, or extremely compacted deep (~2700 m) Greenland ice, may be still large enough to cause a different ablation behavior (see also Figure 6.7a).

**Results** As the outcome of the individual measurements on both samples very much resembled each other, the results of a measurement on sample B98\_42 is exemplarily and extensively discussed here. Figure 6.16a shows a site on the smoothed surface of sample B98\_42 before LA. A section of the grain boundary network, consisting of three boundaries ending in a triple junction, is well visible. Furthermore, an air bubble (black spot) can be identified. Figure 6.16b shows the identical section after LA. The ablation track starts within the center of a grain (1), traverses the grain till it meets a boundary (2), follows the latter (3), before entering the opposite grain (4). Therefore, material from both the grain boundary region and the grain

interior was continuously sampled allowing investigating a possible partitioning of TEs between grain boundary regions and grain interiors.

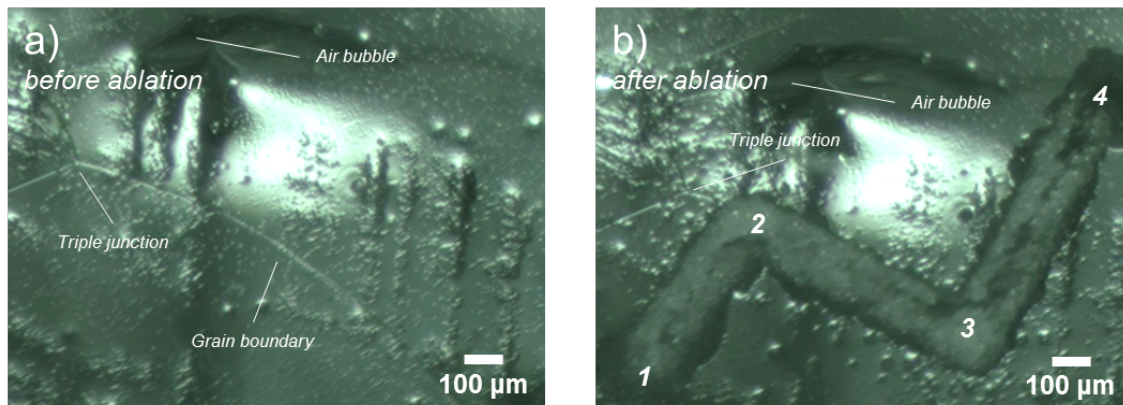


**Figure 6.16:** a) Smoothed surface of the sample B98\_42 from a depth of 32.3 m w.eq. (upper Grenzgletscher ice core section B98). Three grain boundaries joining a triple junction are visible. b) Same surface area after LA using a spot size of  $163\ \mu\text{m}$ . The sections of the ablation path from 1 to 2, and 3 to 4 are within the grain matrix whereas the path section between 2 and 3 follows a grain boundary.

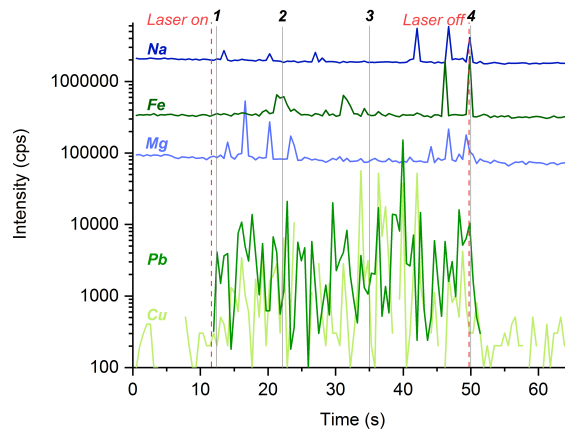


**Figure 6.17:** ICP-MS signal corresponding to the ablation of sample B98\_42 shown in Figure 6.16b. The time intervals from 1 to 2, and 3 to 4 correspond to the signal acquired within the grain matrix whereas the interval between 2 and 3 reflects the signal of an ablation along a grain boundary.

Figure 6.17 displays the corresponding ICP-MS signals for Cu, Fe, Mg, Na, and Pb. The data acquired for Al, Ba, Bi, Ca, Cd, Co, La, Li, Mn, Ni, and Zn is not shown for reasons of clarity. Ca, Cd, Co, La, Li, and Ni signals do not exceed the background signal. Only the signals of Cu, Pb, and Zn are fully background resolved,

whereas the data of Al, Ba, Bi, Fe, Mg, Mn, and Na consist of several spikes exceeding the background signal. As for Figure 6.16b, numbers from 1 to 4 indicate whether the signal corresponds to an ablation within a grain interior (1 to 2, and 3 to 4) or reflects an ablation following a grain boundary (2 to 3). The fully background resolved Cu, Pb, and Zn signals do not show a clear difference in intensity for the grain interior and grain boundary part. As for the “spiky” Al, Ba, Bi, Fe, Mg, Mn, and Na signals, no consistent accumulation of peaks can be attributed neither for the grain interior nor for the grain boundary part of the ablation path.

While Cu, Pb, and Zn signals are fully background resolved, the majority of measured isotopes exhibit either no background resolved signal, or a partially resolved signal, indicating gas blank levels limiting the analysis of impurities in glacier ice occurring in ultra-trace amounts. This is likely to be the result of, although considerably improved (Section 6.3.2.2), contamination introduced into the LA system by the cryocell such as release of ambient air by the cryocell’s insulation or by diffusion of coolant through the hoses. Beyond that, an influence of the LA system itself cannot be excluded. The LA-ICP-MS system housed at the Institute of Geochemistry and Petrology at ETH Zurich is mainly being employed for micro analysis of TE concentrations in various minerals occurring in the two to three-digit  $\text{mg L}^{-1}$  range or, even on a micrometer scale, in the two-digit  $\mu\text{g L}^{-1}$  range [Lechmann *et al.*, 2018]. Considering the average concentrations in the ice samples from upper Grenzgletscher on a centimeter scale (Table 6.2), it is possible that even little deposition and re-mobilization of previously ablated material on the surfaces of the ablation cell, on the walls of the sample aerosol transport tubing between the cell and the ICP-MS, and on the skimmer and sample cones of the ICP-MS [Schlöglova *et al.*, 2017] lead to a low level background contamination already sufficient to limit the analysis of TEs in glacier ice. Additionally, regular measurements of NIST 61x SRMs are known to significantly increase ICP-MS backgrounds of major elements such as Na [Jochum *et al.*, 2011].

**Interpretation** Taking into consideration the elevated TE concentrations in both samples, most probably originating from mineral dust, these results are in agreement with the work performed by Della Lunga *et al.* [2014] who neither observed a correlation between Al, Ca, Fe, Mg, Na, Pb, and Sr signal intensities and grain boundaries for cloudy bands (layers enriched in impurities) in deep Greenland ice. In contrast, strong correlation between TE signal intensities and the grain boundary network, with enrichments of up to 100 times compared to grain interiors, was identified within layers of interstadial ice less enriched in impurities. A very recent study by the same authors refined this picture of small-scale impurity variability and showed that, although still high impurity concentrated deep Greenland ice samples were investigated, TEs related to soluble impurities, such as Mg or Na, are higher concentrated in the proximity of boundaries and junctions, while TEs related to mineral dust, such as Al or Fe, are still less adjusted to boundaries and show an irregular dispersion in the matrix (Della Lunga *et al.* [2017], Figure 6.18).



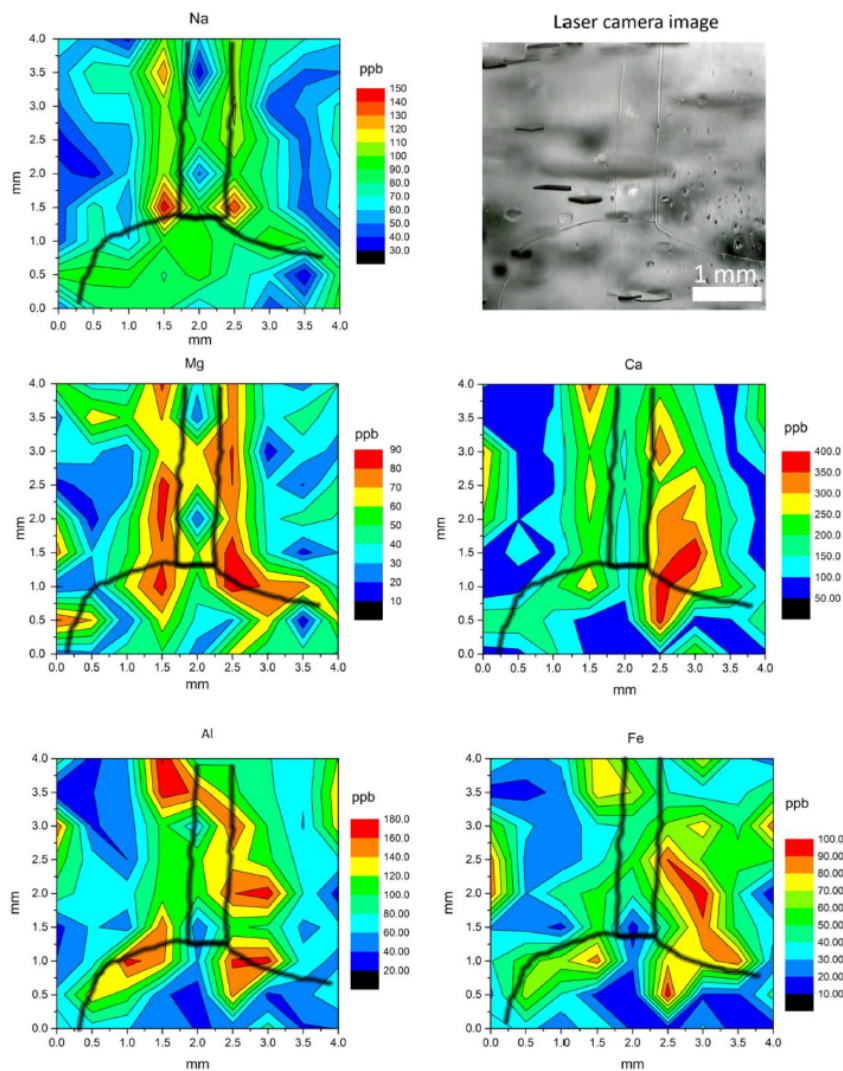


**Figure 6.18:** Two-dimensional TE concentrations maps (Al, Ca, Fe, Mg, Na) with, as observed in transmitted light (top right), the grain boundary network overlaid of deep Greenland (NGRIP) ice (from *Della Lunga et al.* [2017]).

The absence of a micro-scale fractionation of TEs in Alpine glacier ice samples with high concentrations in mineral dust is also in line with a recent study by *Eichler et al.* [2017]. Samples from Antarctic (EDML) and Greenland (NEEM) deep ice revealed that in the case of undissolved impurities, there is no evidence for correlation between grain boundary enrichment and their abundance in the ice.

According to the previously established indirect assessment of TE location in high-Alpine glacier ice (Chapter 3), Fe and Al are likely to originate from water-insoluble particles which are expected to be enriched at grain boundary regions. However, the cryocell LA-ICP-MS data does not exhibit an enrichment of Fe and Al at boundaries, but single peaks both in grain boundary and grain interior regions. Moreover,

if originating from water-soluble particles, Ba, Mg, Mn, Na, and Zn are expected to reveal an enrichment at grain boundaries, whereas Bi, Cu, and Pb should show a stronger distribution within grains. However, no enrichment at grain boundaries, nor in grain interiors, was observed for the latter TEs. These results indicate, that the hypothesis of TE location based on an indirect approach could not be confirmed by direct measurements. This can be explained as follows. Ba, Bi, Cu, Mg, Mn, Na, Pb, and Zn were proposed to be present as (low) water-soluble compounds and their incorporation into the ice lattice is mainly driven by low atmospheric concentrations. However, as samples B81\_183 and B98\_42 exhibit particularly elevated TE concentrations most likely originating from mineral dust (Note: B98\_42 corresponds a well visible yellow mineral dust layer), it is possible that exceeded solubility limits resulted in the exclusion of TEs to grain boundary regions, too. Therefore, a preferential location of certain TEs at grain boundaries or in grain interiors is most likely only present in low concentrations ranges (e.g., tens of  $\mu\text{g L}^{-1}$  as suggested by *Della Lunga* [2015]), while TEs seem to be evenly distributed between boundaries and interiors if concentrations are elevated (e.g., hundreds of  $\mu\text{g L}^{-1}$  as suggested by *Della Lunga* [2015]). Additionally, as proposed by *Eichler et al.* [2017] and *Della Lunga et al.* [2017], the “spiky” signal of Al, Ba, Bi, Fe, Mg, Mn, and Na can be particularly attributed to the non-uniform presence of single mineral dust particles.

This preliminary LA-ICP-MS analysis of samples from the upper Grenzgletscher ice core segment showed that our developed setup provides sufficient spatial resolution and technical capability to probe distribution differences of TEs in high-Alpine glacier ice at a grain scale. Samples with high TE concentrations, presumably due to elevated mineral dust content, revealed no correlation between high TE abundance and grain boundaries, respectively grain interiors. This is in agreement to recently reported observations in Greenland and Antarctic ice.

In contrast, an enrichment of certain TEs in the grain matrix compared to grain surfaces and contrariwise was proposed based on an indirect approach in Chapter 3. The incorporation of rather water-soluble TEs was shown to be concentration dependent with solubility limits likely to be in the low  $\text{ng L}^{-1}$  range. Contrary to the samples employed for this pilot study, corroborating this suggestion would require significantly lower concentrated samples. However, this implies a conflict of objectives as the cryocell LA-ICP-MS setup has too high background levels to analyze samples with such low concentrations. To measure a fractionation of TEs in lower concentrated samples, the current measurement conditions i.e., the sensitivity of the system needs to be further enhanced. Continuous flushing the LA system with carrier gas for several days might remove possible contamination caused by previous applications and is likely to result in reduced background levels. Moreover, the maximum sensitivity of the ICP-MS was fully exploited by increasing the laser spot size from  $163 \mu\text{m}$  to  $>200 \mu\text{m}$  and by performing ablations with separate spectral data acquisition for each TE/isotope of interest yielding an increased integration time per peak. Magnifying the spot size would require migration of the laser optics, while separate spectral data measurements would imply increased acquisition times.

## 6.4 Conclusion

The development and a preliminary application of cryocell LA-ICP-MS to *in situ* analyze TEs in glacier ice with high spatial resolution is presented here. A cryocell compatible to a commercially available LA system was successfully developed and installed. This involved both extensive testing and continuous adaption of experimental hardware and handling procedures. An assessment of possible internal calibration standard candidates in ice revealed that none of them is available if UV-LA is used. The method of preparing ice standards for external calibration was further refined. Standards should be prepared prior to their immediate measurement from only low acidified solutions to avoid a bias of the calibration. Glacier ice samples from upper Grenzgletscher exhibiting particularly elevated TE concentrations were investigated in the course of a preliminary test of the developed cryocell LA-ICP-MS setup's capabilities. Samples with high impurity content were found to show no correlation between TE abundance and the grain boundary network. This is in agreement with very recent studies on deep Antarctic and Greenland ice showing that for sections enriched in impurities, insoluble dust particles are rather dispersed on a micrometer scale. Investigation of high-Alpine glacier ice exhibiting low trace element concentrations would be necessary, to minimize the influence of dust particles. This requires future improvement of the developed method, such as stronger background suppression, to detect even trace elements in ultra trace levels in less dust-impacted samples and to directly corroborate the previous indirectly deduced TE fractionation between grain matrix and boundaries caused by redistribution processes during snow metamorphism.

## Acknowledgments

Funding by the Swiss National Science Foundation (SNSF, Grant No. 155999) is gratefully acknowledged. We also thank Dave Piguet for the construction of the ice plane and the workshop of the Department of Earth Sciences, ETH Zurich, for manufacturing a duplicate of the ablation chamber lid. Moreover, we are grateful to Damiano Della Lunga for his input and fruitful discussions, as well as to Silvia Köchli for preparing multi-element ICP-MS standard solutions.

## Bibliography

- Arrowsmith, P., and S. K. Hughes, Entrainment and Transport of Laser Ablated Plumes for Subsequent Elemental Analysis, *Applied Spectroscopy*, 42(7), 1231–1239, doi:10.1366/0003702884430100, 1988.
- Avak, S. E., M. Schwikowski, and A. Eichler, Impact and implications of meltwater percolation on trace element records observed in a high-Alpine ice core, *Journal of Glaciology*, 64(248), 877–886, doi:10.1017/jog.2018.74, 2018.

- Baker, I., and D. Cullen, SEM/EDS observations of impurities in polar ice: artifacts or not?, *Journal of Glaciology*, *49*(165), 184–190, doi:10.3189/172756503781830773, 2003.
- Baker, I., D. Cullen, and D. Iliescu, The microstructural location of impurities in ice, *Canadian Journal of Physics*, *81*(1-2), 1–9, doi:10.1139/p03-030, 2003.
- Bartels-Rausch, T., Ten things we need to know about ice and snow, *Nature*, *494*(7435), 27–29, doi:10.1038/494027a, 2013.
- Bartels-Rausch, T., et al., A review of air-ice chemical and physical interactions (AICI): liquids, quasi-liquids, and solids in snow, *Atmospheric Chemistry and Physics*, *14*(3), 1587–1633, doi:10.5194/acp-14-1587-2014, 2014.
- Bohleber, P., T. Erhardt, N. Spaulding, H. Hoffmann, H. Fischer, and P. Mayewski, Temperature and mineral dust variability recorded in two low-accumulation Alpine ice cores over the last millennium, *Climate of the Past*, *14*(1), 21–37, doi:10.5194/cp-14-21-2018, 2018.
- Cordray, D. R., L. R. Kaplan, P. M. Woyciesjes, and T. F. Kozak, Solid - liquid phase diagram for ethylene glycol + water, *Fluid Phase Equilibria*, *117*(1-2), 146–152, doi:10.1016/0378-3812(95)02947-8, 1996.
- Cullen, D., and I. Baker, Observation of impurities in ice, *Microscopy Research and Technique*, *55*(3), 198–207, doi:10.1002/jemt.10000, 2001.
- Della Lunga, D., Development and Application of Cryo-Cell - UV-Laser Ablation Mass Spectrometry (UV-LA-ICPMS) to Greenland Ice Cores: Implications for Abrupt Climate Change and Ice Physics, Ph.D. thesis, Royal Holloway University of London, 2015.
- Della Lunga, D., W. Müller, S. O. Rasmussen, and A. Svensson, Location of cation impurities in NGRIP deep ice revealed by cryo-cell UV-laser-ablation ICPMS, *Journal of Glaciology*, *60*(223), 970–988, doi:10.3189/2014JoG13J199, 2014.
- Della Lunga, D., W. Müller, S. O. Rasmussen, A. Svensson, and P. Vallelonga, Calibrated cryo-cell UV-LA-ICPMS elemental concentrations from the NGRIP ice core reveal abrupt, sub-annual variability in dust across the GI-21.2 interstadial period, *The Cryosphere*, *11*(3), 1297–1309, doi:10.5194/tc-11-1297-2017, 2017.
- Durrant, S. F., and N. I. Ward, Recent biological and environmental applications of laser ablation inductively coupled plasma mass spectrometry (LA-ICP-MS), *Journal of Analytical Atomic Spectrometry*, *20*(9), 821, doi:10.1039/b502206a, 2005.
- Eichler, A., M. Schwikowski, and H. W. Gäggeler, Meltwater-induced relocation of chemical species in Alpine firn, *Tellus B: Chemical and Physical Meteorology*, *53*(2), 192–203, doi:10.3402/tellusb.v53i2.16575, 2001.
- Eichler, J., I. Kleitz, M. Bayer-Giraldi, D. Jansen, S. Kipfstuhl, W. Shigeyama, C. Weikusat, and I. Weikusat, Location and distribution of micro-inclusions in the EDML and NEEM ice cores using optical microscopy and *in situ* Raman spectroscopy, *The Cryosphere*, *11*(3), 1075–1090, doi:10.5194/tc-11-1075-2017, 2017.
- Feldmann, J., A. Kindness, and P. Ek, Laser ablation of soft tissue using a cryogenically cooled ablation cell, *Journal of Analytical Atomic Spectrometry*, *17*(8), 813–818, doi:10.1039/b201960d, 2002.
- Fukazawa, H., K. Sugiyama, S. Mae, H. Narita, and T. Hondoh, Acid ions at triple junction of Antarctic ice observed by Raman scattering, *Geophysical Research Letters*, *25*(15), 2845–2848, doi:10.1029/98GL02178, 1998.
- Ginot, P., U. Schotterer, W. Stichler, M. A. Godoi, B. Francou, and M. Schwikowski, Influence of the Tungurahua eruption on the ice core records of Chimborazo, Ecuador, *The Cryosphere*, *4*(4), 561–568, doi:10.5194/tc-4-561-2010, 2010.

- Gray, A. L., Solid sample introduction by laser ablation for inductively coupled plasma source mass spectrometry, *The Analyst*, *110*(5), 551, doi:10.1039/an9851000551, 1985.
- Guillong, M., and D. Günther, Quasi 'non-destructive' laser ablation-inductively coupled plasma-mass spectrometry fingerprinting of sapphires, *Spectrochimica Acta Part B: Atomic Spectroscopy*, *56*(7), 1219–1231, doi:10.1016/S0584-8547(01)00185-9, 2001.
- Guillong, M., C. Latkoczy, J. H. Seo, D. Günther, and C. A. Heinrich, Determination of sulfur in fluid inclusions by laser ablation ICP-MS, *Journal of Analytical Atomic Spectrometry*, *23*(12), 1581, doi:10.1039/b807383j, 2008.
- Guillong, M., A. Von Quadt, S. Sakata, I. Peytcheva, and O. Bachmann, LA-ICP-MS Pb-U dating of young zircons from the Kos-Nisyros volcanic centre, SE Aegean arc, *Journal of Analytical Atomic Spectrometry*, *29*(6), 963–970, doi:10.1039/c4ja00009a, 2014.
- Günther, D., and B. Hattendorf, Solid sample analysis using laser ablation inductively coupled plasma mass spectrometry, *TrAC Trends in Analytical Chemistry*, *24*(3), 255–265, doi:10.1016/j.trac.2004.11.017, 2005.
- Haines, S. A., P. A. Mayewski, A. V. Kurbatov, K. A. Maasch, S. B. Sneed, N. E. Spaulding, D. A. Dixon, and P. D. Bohleber, Ultra-high resolution snapshots of three multi-decadal periods in an Antarctic ice core, *Journal of Glaciology*, *62*(231), 31–36, doi:10.1017/jog.2016.5, 2016.
- Jochum, K. P., et al., Determination of Reference Values for NIST SRM 610-617 Glasses Following ISO Guidelines, *Geostandards and Geoanalytical Research*, *35*(4), 397–429, doi:10.1111/j.1751-908X.2011.00120.x, 2011.
- Koch, J., and D. Günther, Review of the State-of-the-Art of Laser Ablation Inductively Coupled Plasma Mass Spectrometry, *Applied Spectroscopy*, *65*(5), 155–162, doi:10.1366/11-06255, 2011.
- Konz, I., B. Fernández, M. L. Fernández, R. Pereiro, and A. Sanz-Medel, Design and evaluation of a new Peltier-cooled laser ablation cell with on-sample temperature control, *Analytica Chimica Acta*, *809*, 88–96, doi:10.1016/j.aca.2013.11.040, 2014.
- Kriews, M., E. Dunker, H. Reinhardt, I. Beninga, E. Hoffmann, and C. Lüdke, Offenlegungsschrift DE 199 34 561 A1, 2001.
- Lechmann, A., J.-P. Burg, P. Ulmer, M. Guillong, and M. Faridi, Metasomatized mantle as the source of Mid-Miocene-Quaternary volcanism in NW-Iranian Azerbaijan: Geochronological and geochemical evidence, *Lithos*, *304-307*, 311–328, doi:10.1016/j.lithos.2018.01.030, 2018.
- Legrand, M., S. Preunkert, D. Wagenbach, H. Cachier, and H. Puxbaum, A historical record of formate and acetate from a high-elevation Alpine glacier: Implications for their natural versus anthropogenic budgets at the European scale, *Journal of Geophysical Research: Atmospheres*, *108*(D24), 1–15, doi:10.1029/2003JD003594, 2003.
- Lin, J., Y. Liu, Y. Yang, and Z. Hu, Calibration and correction of LA-ICP-MS and LA-MC-ICP-MS analyses for element contents and isotopic ratios, *Solid Earth Sciences*, *1*(1), 5–27, doi:10.1016/j.sesci.2016.04.002, 2016.
- Lobo, L., R. Pereiro, and B. Fernández, Opportunities and challenges of isotopic analysis by laser ablation ICP-MS in biological studies, *TrAC Trends in Analytical Chemistry*, *105*, 380–390, doi:10.1016/j.trac.2018.05.020, 2018.
- Marcott, S. A., J. D. Shakun, P. U. Clark, and A. C. Mix, A Reconstruction of Regional and Global Temperature for the Past 11,300 Years, *Science*, *339*(6124), 1198–1201, doi:10.1126/science.1228026, 2013.
- Mayewski, P. A., S. B. Sneed, S. D. Birkel, A. V. Kurbatov, and K. A. Maasch, Holocene warming marked by abrupt onset of longer summers and reduced storm frequency around Greenland, *Journal of Quaternary Science*, *29*(1), 99–104, doi:10.1002/jqs.2684, 2014.

- More, A. F., et al., Next-generation ice core technology reveals true minimum natural levels of lead (Pb) in the atmosphere: Insights from the Black Death, *GeoHealth*, 1(4), 211–219, doi:10.1002/2017GH000064, 2017.
- Müller, W., M. Shelley, P. Miller, and S. Broude, Initial performance metrics of a new custom-designed ArF excimer LA-ICPMS system coupled to a two-volume laser-ablation cell, *J. Anal. At. Spectrom.*, 24(2), 209–214, doi:10.1039/B805995K, 2009.
- Müller, W., J. M. G. Shelley, and S. O. Rasmussen, Direct chemical analysis of frozen ice cores by UV-laser ablation ICPMS, *Journal of Analytical Atomic Spectrometry*, 26(12), 2391, doi:10.1039/c1ja10242g, 2011.
- Müller-Tautges, C., A. Eichler, M. Schwikowski, G. B. Pezzatti, M. Conedera, and T. Hoffmann, Historic records of organic compounds from a high Alpine glacier: influences of biomass burning, anthropogenic emissions, and dust transport, *Atmospheric Chemistry and Physics*, 16(2), 1029–1043, doi:10.5194/acp-16-1029-2016, 2016.
- Mulvaney, R., E. W. Wolff, and K. Oates, Sulphuric acid at grain boundaries in Antarctic ice, *Nature*, 331(6153), 247–249, doi:10.1038/331247a0, 1988.
- Pavlova, P. A., T. M. Jenk, P. Schmid, C. Bogdal, C. Steinlin, and M. Schwikowski, Polychlorinated Biphenyls in a Temperate Alpine Glacier: 1. Effect of Percolating Meltwater on their Distribution in Glacier Ice, *Environmental Science & Technology*, 49(24), 14,085–14,091, doi:10.1021/acs.est.5b03303, 2015.
- Pinzer, B. R., M. Schneebeli, and T. U. Kaempfer, Vapor flux and recrystallization during dry snow metamorphism under a steady temperature gradient as observed by time-lapse microtomography, *The Cryosphere*, 6(5), 1141–1155, doi:10.5194/tc-6-1141-2012, 2012.
- Pratt, K. A., et al., Photochemical production of molecular bromine in Arctic surface snowpacks, *Nature Geoscience*, 6(5), 351–356, doi:10.1038/ngeo1779, 2013.
- Reinhardt, H., Development and application of a Laserablation ICP-MS technique for multielement analysis of atmospheric deposition in, Ph.D. thesis, Universität Bremen, 2001.
- Reinhardt, H., M. Kriews, H. Miller, O. Schrems, C. Lüdke, E. Hoffmann, and J. Skole, Laser ablation inductively coupled plasma mass spectrometry: a new tool for trace element analysis in ice cores, *Fresenius' Journal of Analytical Chemistry*, 370(5), 629–636, doi:10.1007/s002160100853, 2001.
- Reinhardt, H., M. Kriews, H. Miller, C. Lüdke, E. Hoffmann, and J. Skole, Application of LA-ICP-MS in polar ice core studies, *Analytical and Bioanalytical Chemistry*, 375(8), 1265–1275, doi:10.1007/s00216-003-1793-5, 2003.
- Schlöglöva, K., M. Wälle, and C. A. Heinrich, LA-ICP-MS analysis of fluid inclusions: Contamination effects challenging micro-analysis of elements close to their detection limit, *Journal of Analytical Atomic Spectrometry*, 32(5), 1052–1063, doi:10.1039/c7ja00022g, 2017.
- Schweizer, J., Applied snow and avalanche research, *Cold Regions Science and Technology*, 64(2), 69–72, doi:10.1016/j.coldregions.2010.09.001, 2010.
- Schwikowski, M., et al., Post-17th-Century Changes of European Lead Emissions Recorded in High-Altitude Alpine Snow and Ice, *Environmental Science & Technology*, 38(4), 957–964, doi:10.1021/es034715o, 2004.
- Skoog, D. A., and J. J. Leary, *Instrumentelle Analytik*, Springer-Lehrbuch, Springer Berlin Heidelberg, Berlin, Heidelberg, doi:10.1007/978-3-662-07916-4, 1996.
- Sneed, S. B., et al., New LA-ICP-MS cryocell and calibration technique for sub-millimeter analysis of ice cores, *Journal of Glaciology*, 61(226), 233–242, doi:10.3189/2015JoG14J139, 2015.

- Spaulding, N. E., S. B. Sneed, M. J. Handley, P. Bohleber, A. V. Kurbatov, N. J. Pearce, T. Erhardt, and P. A. Mayewski, A New Multielement Method for LA-ICP-MS Data Acquisition from Glacier Ice Cores, *Environmental Science & Technology*, 51(22), 13,282–13,287, doi:10.1021/acs.est.7b03950, 2017.
- Sylvester, P. J., and S. E. Jackson, A Brief History of Laser Ablation Inductively Coupled Plasma Mass Spectrometry (LA-ICP-MS), *Elements*, 12(5), 307–310, doi:10.2113/gselements.12.5.307, 2016.
- Thompson, L., E. Mosley-Thompson, M. Davis, P. Lin, T. Yao, M. Dyurgerov, and J. Dai, "Recent warming": ice core evidence from tropical ice cores with emphasis on Central Asia, *Global and Planetary Change*, 7(1-3), 145–156, doi:10.1016/0921-8181(93)90046-Q, 1993.
- Warren, S. G., Optical constants of ice from the ultraviolet to the microwave, *Applied Optics*, 23(8), 1206, doi:10.1364/AO.23.001206, 1984.
- Zoriy, M., M. Kayser, A. Izmer, C. Pickhardt, and J. Becker, Determination of uranium isotopic ratios in biological samples using laser ablation inductively coupled plasma double focusing sector field mass spectrometry with cooled ablation chamber, *International Journal of Mass Spectrometry*, 242(2-3), 297–302, doi:10.1016/j.ijms.2004.10.026, 2005.





## 7 Conclusion and outlook

This thesis provided for the first time a detailed monitoring and understanding of the behavior of an extensive set of TEs during melting of high-Alpine snow and glacier ice. It was shown that meltwater percolation leads to the preferential loss of certain TEs from high-Alpine snow and glacier ice. This was attributed to fractionation processes during snow metamorphism leading to a distinct spatial distribution of TEs. Water-insoluble TEs were found to be most likely segregated to grain surfaces during snow metamorphism. However, they remain immobile with meltwater due to their insolubility in water. Water-soluble TEs are incorporated into the ice matrix depending on their concentration and their solubility in ice. TEs exhibiting high abundance are assumed to exceed solubility limits and are therefore segregated to grain surfaces, exposing them to uptake and relocation with meltwater percolation. No influence of the size of the corresponding ions could be identified.

As the results from the two high-Alpine sites upper Grenzletscher and Weissfluhjoch largely matched each other, a set of meltwater-persistent proxies available for future paleo-atmospheric reconstructions using melt-affected ice core and snow pit records from the Alpine region was postulated for typical Central European atmospheric aerosol composition.

Post-depositional redistribution of atmospheric impurities in snow, also affecting their final embedding in glacier ice, was shown to be mainly driven by temperature gradient exposure of snow during metamorphism.

An analytical method for the direct *in situ* analysis of TEs at a grain scale in high-Alpine glacier ice was successfully developed. The analysis of samples from upper Grenzletscher finally demonstrated, in line with recently published observations in deep ice from Antarctica and Greenland, that the spatial distribution of TEs is not correlating with the presence of grain boundaries in sections where high impurity abundance prevails. The proposed preferential location of certain TEs at grain boundaries or in grain interiors is most likely present in low concentrations ranges, while TEs seem to be evenly distributed between boundaries and interiors if concentrations are elevated.

The findings made within this thesis may be extended with the following ideas:

- Future studies should involve extensive *in situ* analysis of high-Alpine glacier ice exhibiting ultra low levels of TE abundance to minimize the influence of mineral dust particles. The latter requires subsequent sensitivity enhancement of the cryocell LA-ICP-MS setup, likely to allow for detection of TE fractionation at a grain scale and for a corroboration of the indirect determination of TE

location in high-Alpine glacier ice. A sensitivity enhancement can be achieved by increasing the laser spot size, acquiring separate spectral data for each isotope of interest, and further background suppression of the LA-ICP-MS setup.

- In this thesis, investigation of the impact of melting on the preservation of TEs focused on snow and the firn part of high-Alpine glaciers. However, as meltwater percolation will in the future also affect deeper layers of glaciers, an understanding of how meltwater percolation proceeds in deep compact ice will be equally relevant. No information exists on the permeability of compact ice for meltwater so far.
- The statements made in this thesis concerning the proposed applicability of TEs as reconstruction proxies that are rather persistent to meltwater-induced relocation, have to be carefully reviewed for other regions of the world. High-mountain glaciers worldwide serving as invaluable environmental archives up to the present, such as in the Andes, in the North American Cordillera, or on the Tibetan Plateau, are increasingly affected by melting. Therefore, it is particularly necessary to examine whether site-specific variations in TE concentrations and mineralogy modify the established classification of meltwater-persistent TEs. For instance, glaciers in regions with higher mineral dust input favor the presence of water-insoluble TEs, that are less prone to meltwater-induced relocation.
- Experimentally determined solubility data of impurities in ice is only available for  $\text{Cl}^-$ ,  $\text{F}^-$ , and  $\text{NH}_4^+$ . Additionally, maximum solubilities were suggested for  $\text{SO}_4^{2-}$ ,  $\text{Na}^+$ , and  $\text{Ca}^{2+}$ . Solubilities in ice need to be determined for more atmospherically relevant impurities to unequivocally corroborate the proposed incorporation of TEs in snow and glacier ice.
- The studies at upper Grenzgletscher and Weissfluhjoch revealed that preferential runoff of atmospheric contaminants includes hazardous substances, such as Cd or Ni. The release of heavy metals from mountain glaciers into surface waters may have, even in low concentration ranges, harmful effects to the environment which has to be thoroughly scrutinized.
- Finally, investigating the impact of melting on the preservation of atmospheric impurities in high-Alpine glaciers needs to be expanded to other reconstruction proxies. No comprehensive examination has been accomplished for instance for mercury or black carbon, pollutants which have been significantly emitted to the atmosphere since the onset of industrialization. So far, no long-term record of Western European atmospheric mercury emissions from a high-Alpine ice core exists.

# List of abbreviations and symbols

AD	Anno Domini
Ag	Silver
Al	Aluminum
a.s.l.	Above sea level
Ba	Barium
Bi	Bismuth
C	Carbon
Ca	Calcium
Cd	Cadmium
Ce	Cerium
Cl	Chloride
Co	Cobalt
cps	Counts per second
Cs	Cesium
CT	Computer tomography
Cu	Copper
$\delta^{18}\text{O}$	Stable oxygen isotope ratio
DL	Detection limit
EDML	EPICA Dronning Maud Land
EDXMA	Energy-dispersive X-ray microanalysis
EPICA	European Project for Ice Coring in Antarctica
ETH	Swiss Federal Institute of Technology
Eu	Europium
EVA	Ethylene-vinyl acetate
F	Fluoride
Fe	Iron
GG	Upper Grenzgletscher
GISP	Greenland Ice Sheet Project
H	Hydrogen
IC	Ion chromatography

ICP	Inductively coupled plasma
I <sub>h</sub>	Hexagonal ice
IUPAC	International Union of Pure and Applied Chemistry
IR	Infrared
K	Potassium
LA	Laser ablation
La	Lanthanum
Li	Lithium
LR	Low resolution
Mg	Magnesium
MI	Major ion
MiSo	Microscale distribution of impurities in snow and glacier ice
Mn	Manganese
Mo	Molybdenum
MR	Medium resolution
MS	Mass spectrometry
<i>m/z</i>	Mass-to-charge ratio
N	Nitrogen
Na	Sodium
Nd	Neodymium
NEEM	North Greenland Eemian Ice Drilling
NGRIP	North Greenland Ice Core Project
Ni	Nickel
NIST	National Institute of Standards and Technology
O	Oxygen
PA	Polyamide
Pb	Lead
PEEK	Polyether ether ketone
PFA	Perfluoroalkoxy alkane
PP	Polypropylene
ppb	Parts per billion
ppm	Parts per million
ppt	Parts per trillion
Pr	Praseodymium
PSI	Paul Scherrer Institute
PTFE	Polytetrafluoroethylene

PVC	Polyvinyl chloride
PVDF	Polyvinylidene fluoride
REE	Rare-earth element
Rb	Rubidium
RSD	Relative standard deviation
S	Sulfur
SSA	Specific surface area
Sb	Antimony
Sc	Scandium
SEM	Scanning electron microscopy
SF	Sector-field
SLF	Snow and Avalanche Research Institute
Sm	Samarium
Sr	Strontium
SRM	Standard reference material
Tc	Capped trigonal site
TE	Trace element
Th	Thorium
Tl	Thallium
Tu	Uncapped trigonal site
U	Uranium
UV	Ultraviolet
V	Vanadium
W	Tungsten
w.eq.	Water equivalent
WFJ	Weissfluhjoch test site
WSI	Water stable isotopes
WSL	Swiss Federal Institute for Forest, Snow and Landscape Research
Yb	Ytterbium
Zn	Zinc
Zr	Zirconium



# List of Figures

1.1	Periodic table showing the most common trace elements analyzed in high-Alpine ice core and snow pit records. . . . .	4
1.2	Paleo concentration record of Pb from Colle Gnifetti, Switzerland, showing Western European pre-industrial and industrial Pb emissions to the atmosphere. . . . .	4
1.3	Cumulative land surface hypsometry of the European Alps, separated by the north-south weather divide. . . . .	6
1.4	Structural evolution of snow during snow metamorphism observed by using <i>in situ</i> time-lapse X-ray micro-tomography. . . . .	8
2.1	Location of the two study sites of this thesis in Switzerland. . . . .	15
2.2	View of the Grenzgletscher, a valley glacier located between the western part of Monte Rosa and the summit of Liskamm in the Southern Swiss Alps . . . . .	16
2.3	Scheme showing the suggested flow of meltwater at the drilling site of upper Grenzgletscher. . . . .	17
2.4	View of the Weissfluhjoch test site of the WSL Institute for Snow and Avalanche Research SLF at an elevation of 2536 m a.s.l. in the Plessur Alps, Switzerland. . . . .	18
2.5	Special precautions during the snow pit samplings to avoid contamination of the samples. . . . .	19
2.6	Scheme of a double-focusing ICP-SF-MS with inverse Nier-Johnson geometry. . . . .	20
2.7	Schematic of LA-ICP-MS. . . . .	22
3.1	Monthly mean concentration records of Ag, Cs, Pb, Eu, Tl, Na, and Cd measured in the ice core segment from upper Grenzgletscher. . . .	31
3.2	Rank of preservation plotted against the concentration ratio for each TE. . . . .	34
3.3	Hydrated and ionic radii in aqueous solution plotted against the concentration ratio of the corresponding TEs. . . . .	37
3.4	Mean concentration within the unaffected part of the ice core segment and atomic mass of the measured isotopes plotted against the concentration ratio of each TE. . . . .	39
4.1	Continuous air temperature and daily snow heights at the Weissfluhjoch test site, Swiss Alps, during the winter season of 2016/17. . .	51

4.2	During the sampling of April 17 <sup>th</sup> the snow pack was partly soaked with meltwater. . . . .	51
4.3	Snow pit sampling at the Weissfluhjoch test site. . . . .	52
4.4	Concentration profiles of $\delta^{18}\text{O}$ , $\text{NH}_4^+$ , $\text{Cl}^-$ , and $\text{Ca}^{2+}$ of the five snow pits taken at the Weissfluhjoch test site during winter/spring and early summer. . . . .	55
4.5	Time evolution of relative snow grain surface and interior accumulation of $\text{Na}^+$ , $\text{NH}_4^+$ , $\text{Ca}^{2+}$ , $\text{Cl}^-$ , and $\text{SO}_4^{2-}$ during snow metamorphism. . . . .	57
4.6	Concentration profiles of Co, Fe, Ce, Sb, Ca and Sr of the five snow pits taken at the Weissfluhjoch test site between winter/spring and early summer. . . . .	60
4.7	Rank of preservation plotted against the concentration ratio $c_{\text{wet}}/c_{\text{dry}}$ in the overlapping part (45-65 cm w.eq. depth) of the snow pits at the Weissfluhjoch test site for each TE classified into group 1 (retained concentration profile) or 2 (depleted concentration profile). . . . .	61
5.1	Scheme of the metamorphism box and the elution setup. . . . .	74
5.2	Structural development of the snow samples during metamorphism imaged by microCT. . . . .	77
5.3	Qualitative evolution of artificial and natural snow under an artificial temperature gradient of $40 \text{ K m}^{-1}$ imaged by microCT after 0 and 12 days. . . . .	78
5.4	SSA evolution of natural and artificial snow aged at the artificial temperature gradient of $40 \text{ K m}^{-1}$ . . . . .	79
5.5	Comparison of the $\text{NH}_4^+$ and $\text{Ca}^{2+}$ concentration in the 10 different aliquots and the molten residual snow during the elution of natural snow after 0 day and 30 days storage time. . . . .	80
5.6	Temporal evolution of normalized ion concentrations $c_{\text{S}}/c_{\text{Bulk}}$ at ice surfaces and $c_{\text{I}}/c_{\text{Bulk}}$ in the ice interior. . . . .	81
5.7	Concentration records of the individual ions in relation to $\text{NH}_4^+$ within the ice interior. . . . .	82
5.8	Exemplary elution curves of Cs and Sm for different artificial temperature gradient exposure times. . . . .	95
5.9	Temporal evolution of concentrations $c_{\text{S}}$ at ice surfaces and $c_{\text{I}}$ of the ice interiors of natural snow exposed to a artificial temperature gradient and of natural snow pack samples, respectively, for selected TEs. . . . .	96
6.1	Schematic of LA-ICP-MS. . . . .	104
6.2	The newly developed cryocell compatible to the Resonetics Resolution S155 laser ablation system. . . . .	110
6.3	Sketch of the two types of standard holders and the sample holder for ice samples. . . . .	111
6.4	Capacitive sensor within the cryocell. . . . .	112



6.5	Modified user interface of the GeoStar LA control software allowing navigation of the cryocell. . . . .	113
6.6	ICP-MS signal of the masses 27 u and 52 u, susceptible to carbon induced interferences caused by diffusion of ethanol through the coolant hoses. . . . .	114
6.7	Threefold point ablation of an ice blank sample resulting in distinct crater formation and laser pre-cleaning of the ice surface. . . . .	115
6.8	Sketch of the custom-built ice plane used for decontamination and smoothing of ice sample surfaces. . . . .	116
6.9	Frontal view on the modified Laurin Technic two-volume LA chamber.	118
6.10	Cross-section of the new ablation funnel. . . . .	119
6.11	Comparison of isotopic ICP-MS backgrounds showing lower carrier gas blanks using the new ablation funnel. . . . .	119
6.12	Custom-built flow box for multipurpose on-site sample preparation and handling. . . . .	120
6.13	Signal acquisition of mass 34 in medium resolution. . . . .	121
6.14	Comparison of the $^{23}\text{Na}$ LA-ICP-MS signal between two equally concentrated frozen standards differing in the storage time. . . . .	123
6.15	Exemplary calibration curves for $^{208}\text{Pb}$ obtained by LA of ice standards.	125
6.16	Smoothed surface of sample B98_42 from the upper Grenzgletscher ice core section B98 and the same surface area after laser ablation. . .	129
6.17	ICP-MS signal corresponding to the ablation of sample B98_42 shown in Figure 6.16. . . . .	129
6.18	Two-dimensional TE concentrations maps of deep Greenland (NGRIP) ice from <i>Della Lunga et al.</i> [2017]. . . . .	131



# List of Tables

- 3.1 Detection limits, procedural blank concentrations of the discrete ICP-SF-MS analysis, concentration ratios between the mean concentration of the meltwater-affected section and the unaffected sections, mean concentrations within the unaffected part of the ice core segment, ionic radii in aqueous solution, and hydrated radii of the investigated TEs. . . . . 32
  
- 4.1 Classification, concentration ratio, and mean concentration of the dry snow pits (Jan 25<sup>th</sup>, Feb 22<sup>nd</sup>, Mar 21<sup>st</sup>) of MIs and TEs investigated in the Weissfluhjoch snow pit study. . . . . 58
  
- 5.1 Comparison of the different bulk concentrations  $c_0$  in ppb. . . . . 73
- 5.2 Combinations of metamorphism type and snow examined in this study. 75
- 5.3 Compilation of published elution sequences. . . . . 89
  
- 6.1 Key characteristics of different cryocells developed for LA-ICP-MS analysis of frozen samples. . . . . 105
- 6.2 Mean concentrations of the TEs in the B81\_183 and B98\_42 upper Grenzletscher ice core samples. . . . . 127
- 6.3 LA-ICP-MS operating conditions used for the preliminary analysis of upper Grenzletscher ice core samples. . . . . 128



# Acknowledgments

This PhD thesis is the result of almost four years of intense and successful research work that could not have been realized without all the people who encouraged and supported me along the way. I would like to thank all those who contributed in many ways to this thesis:

First of all, I would like to thank Prof. Dr. Margit Schwikowski for supervising my PhD thesis in this fascinating research field, the important comments to this work, and all the fruitful discussions. I am also very grateful to Dr. Anja Eichler for her excellent direct supervision. This included great support throughout the doctorate, continuous exchange of ideas, very valuable help in compiling this thesis, teaching me all the “scientific skills”, and the trust in my abilities. Her huge expertise together with her enthusiastic and motivating manner made it exceptionally nice to work with her.

I very much appreciate the commitment of the two other exam committee members, Prof. Dr. Carlo Barbante from the Ca’ Foscari University of Venice, who reviewed the thesis, and Prof. Dr. Martin Grosjean from the University of Bern, who chaired the committee.

I am also indebted to Mario Birrer for his incredible support in designing the experimental hardware and David “Dave” Piguet for assisting therein. This was the foundation of many of our experiments. My thanks also go to Andrés Laso who took over Mario’s work and provided brilliant technical support, too.

It would not have been possible for me to perform all the trace element analyses so independently without the great instruction I received from Leonhard “Leo” Tobler at the beginning of the doctorate. I also greatly appreciate the assistance I obtained from Dr. Theo Jenk whenever help was needed due to a technical defect of the ICP-MS.

I would like to express my gratitude to our MiSo project members Dr. Thorsten Bartels-Rausch, who headed the project, and Dr. Martin Schneebeli for all the discussions during our meetings and the valuable inputs that made this collaboration so successful. I also very much enjoyed working and spending the evenings after endless elution sessions in the cold lab together with my MiSo mates Jürg Trachsel and Jacinta Edebeli. Special thanks to Jürg for housing us in Davos.

Further, special thanks go to our co-workers Dr. Marcel Guillong, Dr. Markus Wälle, and Dr. Oscar Laurent from the Institute of Geochemistry and Petrology at ETH Zurich for providing access to the LA-ICP-MS facility and their great technical support.

I am thankful to Sabina Brütsch for helping during the field campaigns at Weissfluhjoch and her technical assistance in the lab. The latter included measuring an enormous number of almost one thousand MiSo IC samples. My thanks also go to our other lab technician Silvia Köchli.

I very much enjoyed sharing the OFLB/102 office with all the people that came and left during my time at PSI, especially Alex Vogel, Anna Dal Farra, Chaomin Wang, Dimitri Osmont, and Ling Fang. I would like to thank all the current and previous members of the Laboratory of Environmental Chemistry for the particular nice work climate. I must not forget to mention our assistant Doris Bühler who helped in any non-research related aspect and organized all the fabulous team events.

I would not have been able to pursue this path without my parents who enabled me this access to education and supported me wherever possible. For that I am very thankful. I also thank my brother and my sister for being so supportive all the time. I am deeply grateful to Andrea for all her love, the moral support, and for taking the load off from me especially during the end of this doctorate.

Finally, I would like to acknowledge the Swiss National Science Foundation for funding my doctorate (grant no. 155999).

# Declaration of consent

on the basis of Article 30 of the RSL Phil.-nat. 18

Name/First Name: Avak, Sven Erik

Matrikelnummer: 08-935-017

Study program: Chemistry and Molecular Sciences  
Bachelor  Master  Dissertation

Title of the thesis: Impact and Implications of Melting on the Preservation of Trace Elements in High-Alpine Snow and Glacier Ice

Supervisor: Prof. Dr. Margit Schwikowski

I declare herewith that this thesis is my own work and that I have not used any sources other than those stated. I have indicated the adoption of quotations as well as thoughts taken from other authors as such in the thesis. I am aware that the Senate pursuant to Article 36 paragraph 1 litera r of the University Act of 5 September, 1996 is authorized to revoke the title awarded on the basis of this thesis. For the purposes of evaluation and verification of compliance with the declaration of originality and the regulations governing plagiarism, I hereby grant the University of Bern the right to process my personal data and to perform the acts of use this requires, in particular, to reproduce the written thesis and to store it permanently in a database, and to use said database, or to make said database available, to enable comparison with future theses submitted by others.

Villigen PSI, January 31<sup>st</sup>, 2019

  
Signature





# Curriculum vitae

Sven Erik Avak

Born on the 26<sup>th</sup> of June 1989

in Biberach an der Riss, Germany

German citizen

## Education

---

2015-2019 PhD student in Chemistry and Molecular Sciences at the Department of Chemistry and Biochemistry, University of Bern, Switzerland

Dissertation at the Laboratory of Environmental Chemistry, Paul Scherrer Institute, Villigen PSI, Switzerland

Title of the thesis: *Impact and Implications of Melting on the Preservation of Trace Elements in High-Alpine Snow and Glacier Ice*

Supervised by Prof. Dr. Margit Schwikowski and Dr. Anja Eichler

2010-2015 Bachelor and Master of Science in Chemistry, University of Zurich, Switzerland

Master thesis at the Department of Environmental Chemistry, Eawag, Dübendorf, Switzerland

Title of the thesis: *Identification of Micropollutant Transformation Products Formed during Wastewater Treatment Using LC-HR-MS/MS*

Supervised by Prof. Dr. Juliane Hollender

## Publications in peer-reviewed journals

---

Avak, S. E., M. Schwikowski, and A. Eichler, Impact and implications of meltwater percolation on trace element records observed in a high-Alpine ice core, *Journal of Glaciology*, 64(248), 877–886, doi:10.1017/jog.2018.72, 2018.

Schollée, J. E., E. L. Schymanski, S. E. Avak, M. Loos, and J. Hollender, Prioritizing Unknown Transformation Products from Biologically-Treated Wastewater Using High-Resolution Mass Spectrometry, Multivariate Statistics, and Metabolic Logic. *Analytical Chemistry*, 87(24), 12121–12129. doi:10.1021/acs.analchem.5b02905, 2015.

### Contribution to scientific conferences and seminars

---

2018 *Impact and Implications of Melting on the Preservation of Trace Elements in High-Alpine Snow and Glacier Ice* (Oral presentation), Seminar of the PSI Laboratory of Environmental Chemistry, Villigen PSI, Switzerland, Oct 26

*Investigating the Microscopic Location of Trace Elements in Glacier Ice* (Oral presentation), SCAR/IASC Open Science Conference, Davos, Switzerland, Jun 19-23

*Impact and Implications of Meltwater Percolation on Trace Element Records Observed in a High-Alpine Ice Core* (Poster presentation), 2<sup>nd</sup> Cross-Divisional Poster Event at PSI, Villigen PSI, Switzerland, Apr 26

*Investigating the Microscopic Location of Trace Elements in Glacier Ice* (Oral presentation), 14<sup>th</sup> International Conference on the Physics and Chemistry of Ice, Zurich, Switzerland, Jan 7-12

2017 *Grenzgletscher and Weissfluhjoch – Two Unique Sites in the Swiss Alps to Study the Microscopic Location of Trace Elements in Glacier Ice and Snow* (Oral presentation), Seminar of the PSI Laboratory of Environmental Chemistry, Villigen PSI, Switzerland, Sep 22

*Investigating the Microscopic Location of Trace Elements in High-Alpine Glacier Ice* (Poster presentation), 16<sup>th</sup> International Swiss Climate Summer School, Ascona, Switzerland, Sep 3-8

*Investigating the Microscopic Location of Trace Elements in High-Alpine Glacier Ice* (Poster presentation), European Geosciences Union General Assembly, Vienna, Austria, 23-28 April

2016 *Development of a Cryocell LA-ICP-MS Setup for Spatial Trace Element Analysis in High Alpine Glacier Ice* (Poster presentation), 14<sup>th</sup> Swiss Geoscience Meeting, Geneva, Switzerland, Nov 18-19

*Investigating the Microscopic Location of Trace Elements in High-Alpine Glacier Ice* (Oral presentation), Seminar of the PSI Laboratory of Environmental Chemistry, Villigen PSI, Switzerland, Oct 21

*Investigating the Microscopic Location of Trace Elements in High-Alpine Glacier Ice* (Oral presentation), DCB First Year Graduate Student Symposium, Bern, Switzerland, Sep 12

*Development of a Cryocell for High-Resolution Trace Element Analysis of Ice Cores* (Poster presentation), 2<sup>nd</sup> IPICS Open Science Conference, Hobart, Australia, Mar 7-11

2015 *Development of a Cryocell for High-Resolution Trace Element Analysis of Ice Cores Using LA-ICP-MS* (Poster presentation), 13<sup>th</sup> Swiss Geoscience Meeting, Basel, Switzerland, Nov 20-21

## Teaching and outreach

---

2016-2018 120 hours of teaching assistance per year in the laboratory course “Praktikum Allgemeine Chemie II” (1<sup>st</sup> year of Bachelor program in Chemistry, Biochemistry, & Pharmaceutical Sciences) at the Department of Chemistry and Biochemistry, University of Bern

Mar 2018 Behind-the-scenes tour of the PSI ultra-trace analysis laboratory for students from the Kantonsschule Thun

Dec 2017 Participation in a reportage about the MiSo project part of the SRF 1 television broadcast “Heimatland – Weisses Gold”

Nov 2016 Assistance in the demonstration of the ice core drilling equipment to visitors during the PSI public event “Forschung live erleben”

Oct 2015 Explanation of experiments to visitors during the PSI open day “Am Puls der Forschung”

## Scientific field work

---

Rhône Glacier, Swiss Alps, 2400 m a.s.l.: 1 day in Aug 2017, ice core deep drilling

Weissfluhjoch test site, Swiss Alps, 2540 m a.s.l.: several one-day campaigns between Jan and Apr 2017, surface snow and snow pit sampling

Plaine Morte Glacier, Swiss Alps, 2700 m a.s.l.: 2 days in Aug 2015, cryoconite sampling and albedo measurements

